

APPENDICES



Published Articles

I.-2; II.-1; II.-2; III.-1; III.-2; III.-3

Distribution of elements among minerals of a single (muscovite-) biotite granite sample — an optimal approach and general implications

VOJTĚCH JANOUŠEK^{1,2}✉, TOMÁŠ NAVRÁTIL³, JAKUB TRUBAČ^{1,2}, LADISLAV STRNAD⁴, FRANTIŠEK LAUFEK¹ and LUDEK MINAŘÍK³

¹Czech Geological Survey, Klárov 3/131, 118 21 Prague 1, Czech Republic;

✉vojtech.janousek@geology.cz; jakub.trubac@geology.cz; frantisek.laufek@geology.cz

²Institute of Petrology and Structural Geology, Charles University in Prague, Albertov 6, 128 43 Prague 2, Czech Republic

³Institute of Geology, Academy of Science, Rozvojová 269, 165 00 Prague 6, Czech Republic; navratil@gli.cas.cz; alex@gli.cas.cz

⁴Laboratories of the Geological Institutes, Charles University in Prague, Albertov 6, 128 43 Prague 2, Czech Republic; ladislav.strnad@natur.cuni.cz

(Manuscript received January 17 2014; accepted in revised form June 5, 2014)

Abstract: The petrography and mineral chemistry of the coarse-grained, weakly porphyritic (muscovite-) biotite Říčany granite (Variscan Central Bohemian Plutonic Complex, Bohemian Massif) were studied in order to assess the distribution of major and trace elements among its minerals, with consequences for granite petrogenesis and availability of geochemical species during supergene processes. It is demonstrated that chemistry-based approaches are the best suited for modal analyses of granites, especially methods taking into account compositions of whole-rock samples as well as their mineral constituents, such as constrained least-squares algorithm. They smooth out any local variations (mineral zoning, presence of phenocrysts, schlieren...) and are robust in respect to the presence of phenocrysts or fabrics. The study confirms the notion that the accessory phases play a key role in incorporation of many elements during crystallization of granitic magmas. Especially the REE seem of little value in petrogenetic modelling, unless the role of accessories is properly assessed and saturation models for apatite, zircon, monazite±rutile carefully considered. At the same time, the presence of several P-, Zr- and LREE-bearing phases may have some important consequences for saturation thermometry of apatite, zircon and monazite.

Key words: modal analyses, trace-element residence, ICP-MS, Central Bohemian Plutonic Complex, Říčany granite.

Introduction

The distribution of chemical elements among minerals in a single granite specimen represents a fundamental and intriguing problem, which, however, has attracted surprisingly little attention in the current literature (e.g. Gromet & Silver 1983; Sawka 1988; Evans & Hanson 1993; Wark & Miller 1993; Bea 1996). Still, a good understanding of the net contributions of individual phases to the whole-rock chemical budget is a necessary prerequisite should any relevant petrogenetic modelling be undertaken. Moreover, particular host minerals show variable resistance to alteration and/or weathering, thus controlling the degree to which the given element could be mobilized into the environment.

For such studies, reliable and precise concentration data in small sample volumes are crucial. The data must be sufficient to minimize the effects of inhomogeneities in the analysed material (for individual minerals it could be the presence of zoning, inclusions, alteration zones...). The required precision is often far beyond the limits of the electron microprobe microanalysis (EMPA); the prohibitive cost effectively rules out the ion probe as well. Fortunately the ICP-MS technique enables a reliable determination of sub-ppm amounts of elements both in the solution (dissolved whole-rock powders or monomineralic separates) and *in situ*, using the laser-ablation (LA) apparatus.

In addition, an accurate estimate of the mineral modal proportions has to be made. Theoretically this should pose no problem, given that the modal analyses have provided a basis for classification of holocrystalline igneous rocks for over eighty years (Niggli 1931; Johannsen 1932, 1937, 1938, 1939; Streckeisen 1974; Le Maitre 2002).

The classical technique relies on counting of individual mineral grains over a regular grid, either in a standard thin section or a polished rock slab. More sophisticated alternatives include computer-aided image analysis, powder X-ray diffraction (P-XRD) and chemistry-based mathematical approaches (normative recalculations or statistical methods employing the chemistry of the bulk rock and its mineral constituents).

The current paper initially focuses on methodological issues connected with obtaining a modal analysis representative of a large, coarse-grained granite sample. The various methods are compared and the most trustworthy approach/modal data chosen (Appendix 1*). Then, using a combination of EMPA with (LA) ICP-MS data, an attempt is made to identify the principal mineral hosts for individual elements, evaluating the relative contributions of each of them to the whole-rock budget. Finally we discuss the general implications for obtaining modal analyses of coarse-grained rocks, modelling of igneous processes, obtaining reliable whole-rock trace-element analyses and saturation thermometry.

Our case study concentrates on the Lower Carboniferous (Mississippian) Říčany (muscovite-) biotite granite pluton from the Central Bohemian Plutonic Complex (CBPC), Czech Republic (Fig. 1a). This small body is relatively well known, as it has been, over the years, a subject of numerous studies concerned with its geology, composition and genesis (e.g. Katzer 1888; Orlov 1933; Němec 1978; Palivcová et al. 1992; Janoušek et al. 1997; Trubač et al. 2009). Moreover, even more extensive research was done on element mobility during the weathering, mass fluxes, cycling and balance of elements within the model forest ecosystem (Minařík & Houdková 1986; Minařík & Kvidová 1986; Minařík et al. 1998, 2003; Navrátil et al. 2002, 2004, 2007). For both types of studies, detailed assessment of the elemental distribution among individual mineral phases has clearly been long overdue.

Geological setting

The CBPC is one of the largest composite granitoid complexes in the Central European Variscides (Fig. 1a). The individual petrographic types can be grouped into several suites, based on petrography, age, whole-rock and mineral geochemistry (Holub et al. 1997; Janoušek et al. 2000b; Žák et al. (2014) and references therein) (Fig. 1b). The oldest among them is the normal calc-alkaline *Sázava suite* (~355 Ma) forming much of the north-eastern CBPC. The most common in the central-southern CBPC are ~346 Ma old, K-rich calc-alkaline granodiorites to granites of the *Blatná suite* with minor basic bodies. The (ultra-) potassic *Čertovo břemeno suite* (~337 Ma) is formed by K-Mg-rich melagranites and melasyenites, the most basic types correspond-

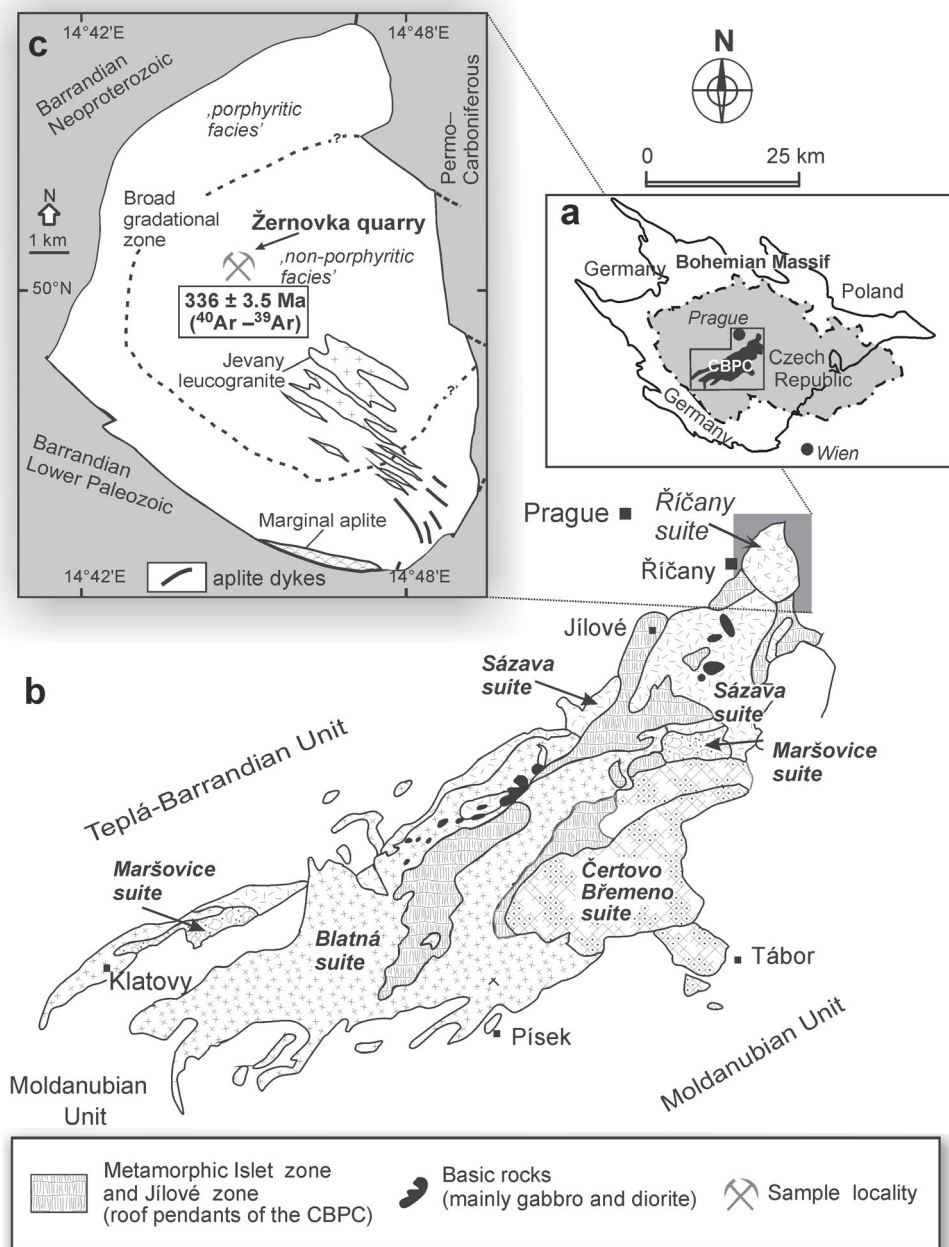


Fig. 1. a — Location of the Variscan Central Bohemian Plutonic Complex (CBPC) within the Bohemian Massif. b — Sketch of the CBPC with the main granitoid suites after Janoušek et al. (2000b) (normal calc-alkaline Sázava, high-K calc-alkaline Blatná, peraluminous Maršovice and (ultra-) potassic Čertovo břemeno). c — Geological outline of the Říčany Pluton and the surrounding units (after Janoušek et al. 1997). The position of the sampled locality, the working Žernovka quarry, is also indicated.

ing to the so-called durbachites. Strongly peraluminous Mu-Bt granodiorites (often Crd-bearing) of the *Maršovice suite* are regionally rather insignificant.

The Řičany Pluton (Fig. 1c), the main representative of the namesake suite, is a late (post-tectonic), shallow-level granitic body that has intruded the boundary between low-grade Upper Proterozoic to Lower Paleozoic metasediments of the Teplá-Barrandian Unit and dominantly high-grade metasediments of the Moldanubian Unit. Its eastern margin is obscured by Permo-Carboniferous sediments. The only modern geochronological information available is the ^{40}Ar - ^{39}Ar biotite age of 336 ± 3.5 Ma (unpublished data of H. Maluski, cited in Janoušek et al. 1997).

The intrusion has a roughly elliptical outline (13×9 km) and is mainly made up of two distinct granite varieties. The outer, 'strongly porphyritic' one contains more abundant K-feldspar phenocrysts, whereas in the central, 'weakly porphyritic' facies, the phenocrysts are scarce (Katzner 1888) (Fig. 1c). The granite encloses numerous large biotite-rich mafic enclaves and less common metasedimentary xenoliths. The Pluton is cut by many pegmatite and aplite dykes. The

central part has been intruded by several small bodies of fine-grained, equigranular, two-mica Jevany leucogranite and the southern exocontact is rimmed by the so-called Marginal aplite (Němec 1978).

Petrology and mineral chemistry

The studied rock comes from the central, 'weakly porphyritic' facies. It is relatively fresh, with the plagioclase showing limited argillitization along the cleavage planes (Fig. 2a). The scarce small K-feldspar phenocrysts are however slightly kaolinized and the biotite suffered incipient chloritization. The average grain size of the groundmass is 1-5 mm and rare phenocrysts may attain up to 3-5 cm. A completely unweathered sample of the granite was not available due to nowadays only limited quarry activity and widespread surface kaolinization of the pluton (Pivec 1969).

The *K-feldspar* phenocrysts are strongly perthitic and many show pronounced cross-hatched twinning; Carlsbad twins are also common. They contain numerous inclusions

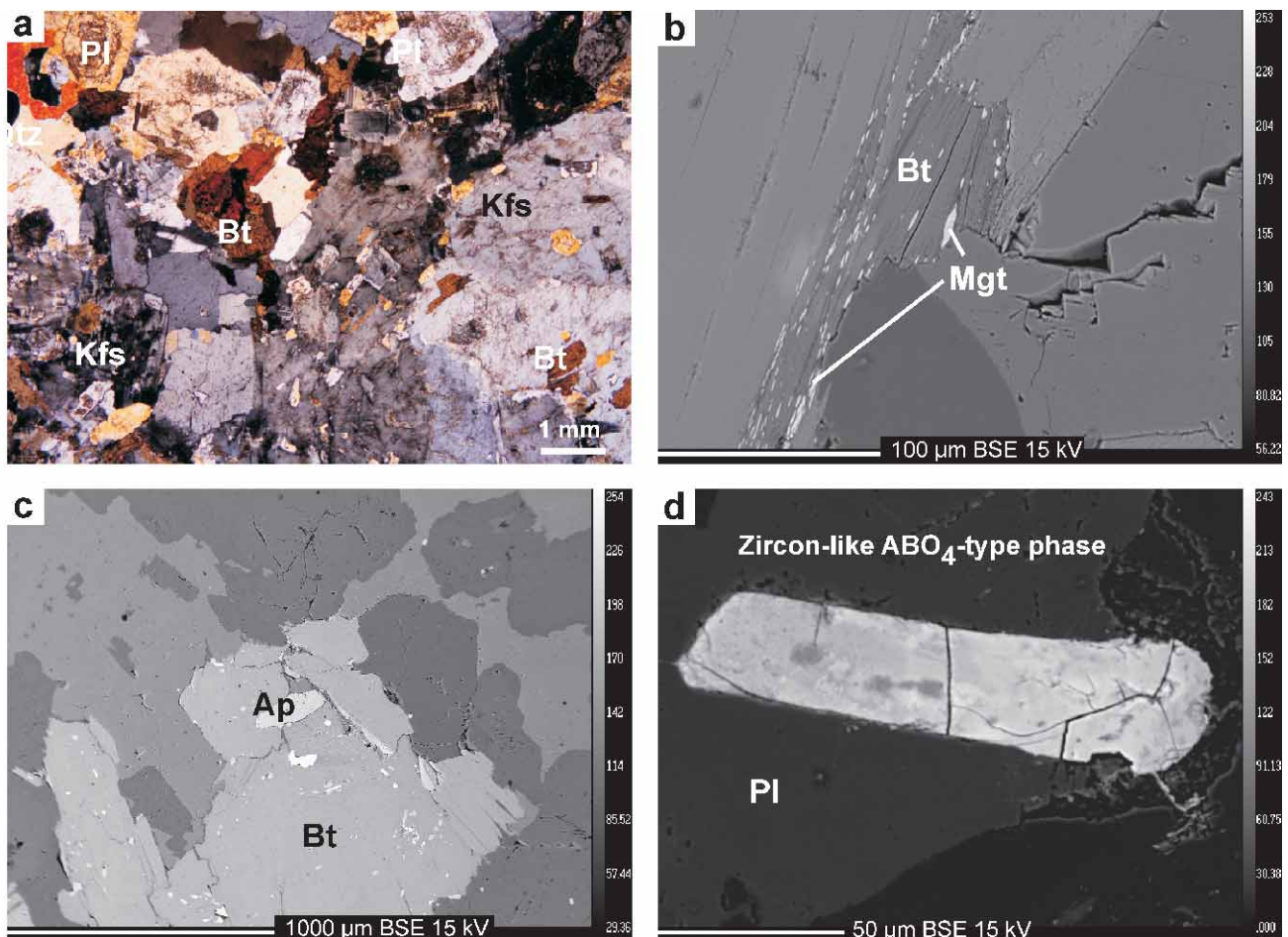


Fig. 2. Photomicrographs of the studied weakly porphyritic (muscovite-) biotite Řičany granite Žer-1. **a** — Photomicrograph of the typical magmatic texture at a rim of a small K-feldspar phenocryst with characteristic cross-hatched twinning. Crystals of the main rock-forming minerals exhibit no effects of solid-state deformation and are only slightly altered (plagioclase cores). Crossed polars. **b** — Back-scattered electron (BSE) image of micro-inclusions of magnetite in, and around, larger biotite flake. **c** — Typical BSE image of biotite, rich in apatite inclusions of variable shape and size. **d** — BSE image of the zircon-like ABO_4 -type phase enclosed in plagioclase.

of biotite, quartz and oligoclase (an 'hourglass' texture of Pivec 1970).

Plagioclase occurs as subhedral prismatic crystals with common albite law twin lamellae, on average 1.2–2.0 mm across. Apart from those enclosed within the K-feldspar, they are of uniform oligoclase composition (An_{11–19}; Appendix 2) and are usually chemically unzoned.

Biotite forms subhedral flakes on average 0.5–0.75 mm (up to 1.2 mm) across, with a strong pleochroism: X — straw yellow, Y=Z — dark rusty-brown. Pleochroic haloes around submicroscopic inclusions are very distinct and common. Biotite is often associated with grains of magnetite (Fig. 2b).

Anhedral *quartz* grains with weak undulose extinction are up to 2 mm across.

The biotite may also be overgrown by scarce primary *muscovite* (up to 0.2 mm across). Also the plagioclase encloses some small (0.1–0.2 mm) flakes of muscovite, at least some of which appear to be of primary magmatic origin.

According to our microscopic and EPMA study and previous work of Kodymová & Vejnár (1974), the granite contains significant proportions of *rutile* (0.1 mm). Small *apatite* (0.1–0.2 mm) prisms or needles are often enclosed by biotite (Fig. 2c). Euhedral crystals of *titanite* (0.1 mm), brown to reddish in colour, and euhedral dipyrnidal crystals of *zircon* (0.2 mm), pink to pale brown are less common accessories. *Monazite* (0.2 mm) usually occurs in forms aggregates of spherical grains. *Magnetite* (0.1 mm) occurs mostly in anhedral fragments, only rarely forming octahedra, up to 0.5 mm across. *Ilmenite* (0.1 mm) forms black opaque grains of non-metallic lustre, sometimes lamellated. Subangular hedral *zircon-like ABO₄-type phase* (up to 0.1 mm across) represents a newly encountered, rather rare accessory mineral. It occurs in plagioclase, very often together with monazite (Fig. 2d).

Modal proportions

Petrographic approaches

In the present case, both the conventional point counting and image analysis of the stained slab (Fig. 3a–b; see Appendix 1 for full analytical details on all methods used) were taken to approximate well the mineral proportions in the studied sample's matrix, as no sizeable K-feldspar phenocrysts are present in the hand specimen. The results do not differ greatly (Table 1). The image analysis (Fig. 3c–e) indicates somewhat higher amounts of biotite (9.0 vs. 7.3 vol. %: image analysis vs. conventional point counting, plagioclase (31.2 vs. 27.1 vol. %) and quartz (38.1 vs. 32.8 vol. %), at the expense of the K-feldspar (21.8 vs. 25.0 vol. %). Unfortunately the contents of kaolinite could not be determined by the image analysis. This mineral largely resisted staining and was thus counted, at least in part, as plagioclase.

Chemical methods

For sample Žer-1, the following mesonormative composition ('Improved Granite Mesonorm' of Mielke & Winkler 1979) is obtained (wt. %): Or 29.1, Pl (Ab+An) 36.8,

Table 1: Estimates of modal percentages (vol. % and wt. %, original data in bold) of the individual minerals in the Řičány granite Žer-1.

| Mineral phase | Ideal formula | Density ¹ (g·cm ⁻³) | Point counting ² (4890 points) | | Image analysis | | Granite mesonorm ³ | | Constrained least-squares | | X-ray diffraction (P-XRD) | |
|-----------------------------------|--|---|--|---------|----------------|---------|-------------------------------|-------------|------------------------------|---------|------------------------------|---------|
| | | | (vol. %) | (wt. %) | (vol. %) | (wt. %) | (vol. %) | (wt. %) | (vol. %) | (wt. %) | (vol. %) | (wt. %) |
| Main rock-forming minerals | | | | | | | | | | | | |
| orthoclase | KAlSi ₃ O ₈ | 2.570 | 25.0 | 24.4 | 21.8 | 21.2 | 30.0 | 29.1 | 28.7 | 29.6 | 30.4 | |
| plagioclase (albite) | NaAlSi ₃ O ₈ | 2.620 | 27.1 | 26.9 | 31.2 | 30.9 | 37.2 | 36.8 | 36.3 | 25.0 | 25.1 | |
| kaolinite | Al ₂ Si ₂ O ₅ (OH) ₄ | 2.594 | 7.5 | 7.4 | | | | | | 1.2 | 1.2 | |
| biotite (F-phlogopite) | KMg ₃ [AlSi ₃ O ₁₀]F ₂ | 2.878 | 7.3 | 7.9 | 9.0 | 9.8 | 5.3 | 5.8 | 10.2 | 10.4 | 9.5 | |
| quartz | SiO ₂ | 2.648 | 32.8 | 33.0 | 38.0 | 38.1 | 25.2 | 25.2 | 24.8 | 33.8 | 33.8 | |
| muscovite | KAl ₂ [AlSi ₃ O ₁₀](OH) ₂ | 2.831 | 0.2 | 0.2 | | | | | | | | |
| whole-rock | | 2.630 | | | | | | | | | | |
| Accessories | | | | | | | | | | | | |
| ilmenite | FeTiO ₃ | 4.788 | 0.1 | 0.1 | | | | | | | | |
| apatite | Ca ₅ (PO ₄) ₃ F | 3.200 | | | | | 0.2 | 0.3 | | | | |
| magnetite | Fe ₃ O ₄ | 5.200 | | | | | 0.3 | 0.3 | | | | |
| sum | | | 100.0 | 99.9 | 100.0 | 100.0 | 98.7 | 98.4 | 99.8 | 100.0 | 100.0 | |

¹—Data on mineral densities used in recalculation of wt. % to vol. % (or vice versa) are from Robie et al. (1967), whole-rock density of the Řičány granite from Hejtmán (1948). Original data are in bold.

²—For explanation of the individual methods (point-counting, image analysis, least-squares calculation and XRD), see text. For more detailed outcome of the constrained least-squares method, see **Table 3**.

³—'Improved Granite Mesonorm' of Mielke & Winkler (1979).

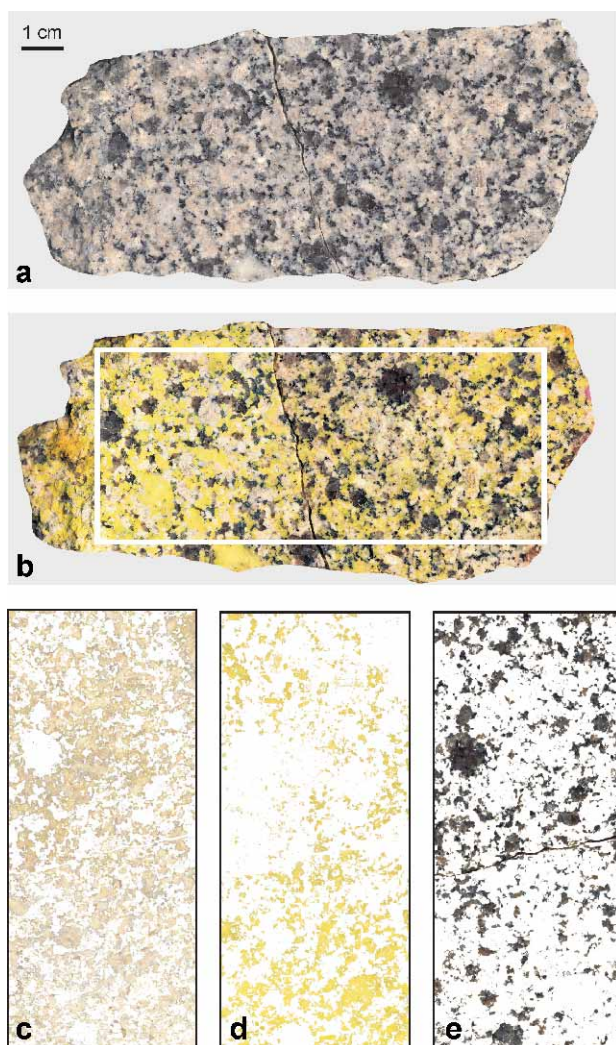


Fig. 3. Photograph of the polished hand specimen of the sample Žer-1, of natural appearance (a) and stained (b). The remaining images are separated colour components corresponding to the plagioclase (c) K-feldspar (d) and quartz with biotite (e). Box in figure (b) indicates the area used for image analysis (c–e).

Qtz 25.2, Bt 5.8, Ap 0.34, Mgt 0.9, Ilm 0.34, Cal 0.14 and Crn 0.54 (Table 1). The negligible proportion of normative corundum is in line with the subaluminous nature of the sample ($A/CNK \sim 1.0$ — Table 2). Normative calcite and corundum were further not considered as they do not correspond to mineral phases present in the rock.

The approximate proportions of the main rock-forming minerals (wt. %) were also obtained by the constrained least-squares (LSQ) method (Albarède 1995) implemented in the *GCDkit*. The whole-rock chemical composition and typical EMP analyses of the main rock-forming minerals served as an input (Table 3). Phosphorus, not present in appreciable amounts in any of the main phases but representing an essential structural component in two common accessories, apatite and monazite, was disregarded. The low sum of squared residuals ($R^2=0.071$) indicates an excellent fit. The proportions of K-feldspar (29.4 wt. %) and plagioclase (36.6 wt. %) are closely comparable to the mesonorm; but the quartz per-

| | |
|------------------------------------|--------|
| SiO ₂ | 70.34 |
| TiO ₂ | 0.36 |
| Al ₂ O ₃ | 14.64 |
| Fe ₂ O ₃ | 0.62 |
| FeO | 0.94 |
| MgO | 1.14 |
| MnO | 0.024 |
| CaO | 1.36 |
| SrO | 0.046 |
| BaO | 0.126 |
| Li ₂ O | 0.015 |
| Na ₂ O | 3.71 |
| K ₂ O | 5.55 |
| P ₂ O ₅ | 0.145 |
| F | 0.153 |
| CO ₂ | 0.06 |
| C | 0.016 |
| S tot | <0.005 |
| H ₂ O ⁺ | 0.51 |
| H ₂ O ⁻ | <0.05 |
| F(ekv) | -0.064 |
| S(ekv) | -0.001 |
| Total | 99.69 |
| A/CNK | 1.00 |
| K ₂ O/Na ₂ O | 1.50 |

Table 2: Whole-rock major- and minor-element analysis of the studied sample (wt. %).

$A/CNK =$
 $= \text{molar Al}_2\text{O}_3 / (\text{CaO} + \text{Na}_2\text{O} + \text{K}_2\text{O})$
 uncorrected for apatite.
 $\text{K}_2\text{O}/\text{Na}_2\text{O}$ ratio is given by weight.
 For whole-rock trace-element composition, see Appendix 4.

Table 3: Constrained least-squares approximation to the modal composition (wt. %).

| | Plagioclase ¹ Pl14 | K-feldspar Kfs1 | Biotite Bt14 | Quartz | Whole rock ² | | Residual | Squared residual |
|--------------------------------|-------------------------------|-----------------|--------------|--------|-------------------------|-----------|----------|--------------------|
| | | | | | Real | Estimated | | |
| SiO ₂ | 64.05 | 64.16 | 37.50 | 99.86 | 70.34 | 70.44 | -0.10 | 0.010 |
| TiO ₂ | 0.00 | 0.00 | 3.33 | 0.00 | 0.36 | 0.31 | 0.05 | 0.002 |
| Al ₂ O ₃ | 21.76 | 18.47 | 14.80 | 0.02 | 14.64 | 14.78 | -0.14 | 0.019 |
| FeOt | 0.04 | 0.03 | 17.26 | 0.00 | 1.50 | 1.64 | -0.14 | 0.018 |
| MnO | 0.05 | 0.03 | 0.24 | 0.00 | 0.02 | 0.05 | -0.02 | 0.001 |
| MgO | 0.00 | 0.00 | 13.35 | 0.00 | 1.14 | 1.25 | -0.11 | 0.011 |
| CaO | 3.87 | 0.01 | 0.04 | 0.00 | 1.36 | 1.42 | -0.06 | 0.004 |
| Na ₂ O | 9.42 | 0.96 | 0.14 | 0.00 | 3.71 | 3.75 | -0.04 | 0.001 |
| K ₂ O | 0.40 | 15.61 | 9.47 | 0.00 | 5.55 | 5.61 | -0.06 | 0.004 |
| wt. % | 36.6 % | 29.4 % | 9.3 % | 24.7 % | | | R sqr | 0.071 ³ |

¹ — Shown are real electron microprobe analyses of the main rock-forming minerals (see Appendix 2).

² — The observed whole-rock concentrations (Table 2) and the best estimate by the constrained least-squares method, with the corresponding differences (residuals).

³ — The sum of squared residuals indicating a goodness of fit.

centage (24.7 wt. %) is somewhat lower (Table 1). The amount of biotite, however, is nearly double (9.3 wt. %) but much closer to estimates by point counting and image analysis (if recast to wt. %).

Powder X-ray diffraction (P-XRD)

The results of Rietveld quantitative phase analysis (Appendix 1) are summarized in Table 1 and Fig. 4. Compared

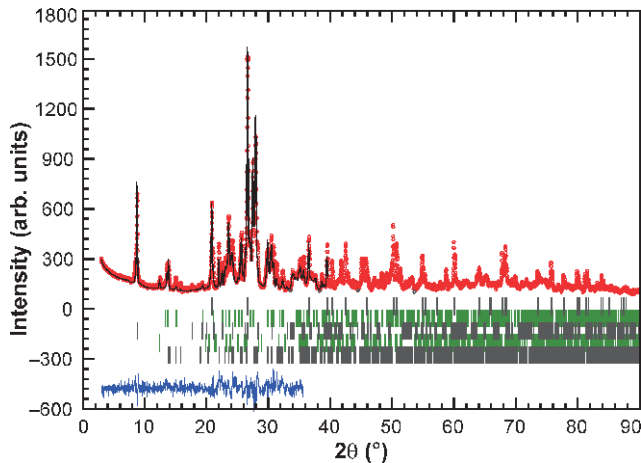


Fig. 4. Observed (circles), calculated (solid line) and difference Rietveld profiles for the studied sample. Markers of the peak positions (five rows of the vertical line segments) are for (from top to bottom) quartz, orthoclase, biotite, kaolinite and plagioclase.

with other methods, the plagioclase content is significantly underestimated (25.1 wt. %). The reason may be the complex preferred orientation of plagioclase, which shows two cleavage plane systems, namely [001] and [010], while only one correction for preferred orientation (for [001] direction) was applied in the Rietveld fit. The amount of K-feldspar (30.4 wt. %) is in agreement with the results of constrained LSQ (29.4 wt. %) and mesonorm (29.1 wt. %); while the quartz content is slightly higher (33.8 wt. %). The estimate of biotite (9.5 wt. %) is in line with other methods, except for the mesonorm. Clearly, the correction for preferred orientation in the [001] works sufficiently in this case. The content of kaolinite (1.2 wt. %) is significantly lower than that obtained by point counting (7.4 wt. %).

Mineral chemistry

The compositions of individual minerals were analysed by a combination of three methods (Appendix 1), EMPA (see averages and typical analyses in Appendix 2), *in situ* LA ICP-MS and ICP-MS analyses of dissolved monomineralic separates (Appendix 3, summarized in Appendix 4). Laser-ablation analyses were preferred for mineral separates in which the presence of minor admixture of phases/inclusions with contrasting chemistry was of particular concern (quartz, plagioclase and biotite). On the other hand, wet analysis was chosen for K-feldspar, minimizing the problem of the small-scale heterogeneity (abundance of perthite lamellae). Fig. 5 shows selected trace-element patterns normalized by the whole-rock (WR) contents and Fig. 6 illustrates the chondrite-normalized REE patterns.

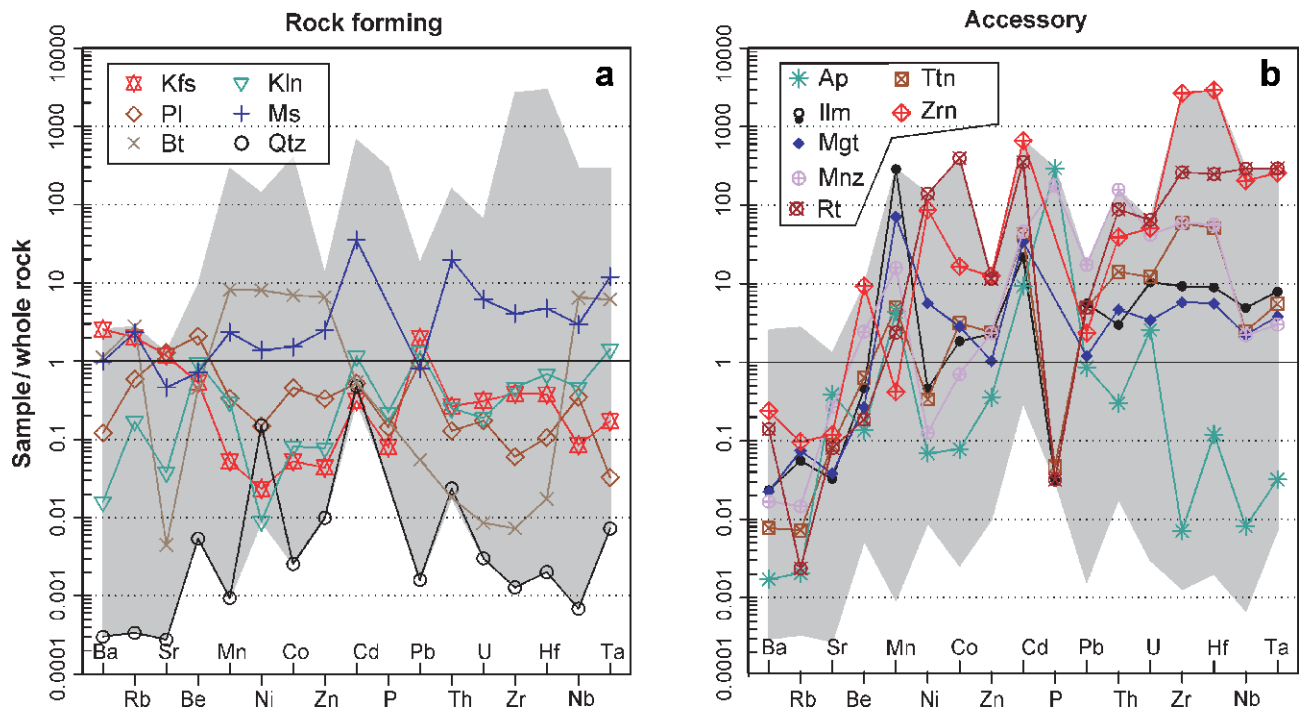


Fig. 5. Whole rock-normalized trace-element patterns for individual rock-forming (a) and accessory (b) minerals. Mineral abbreviations after Kretz (1983). Grey field denotes the total variation in the dataset.

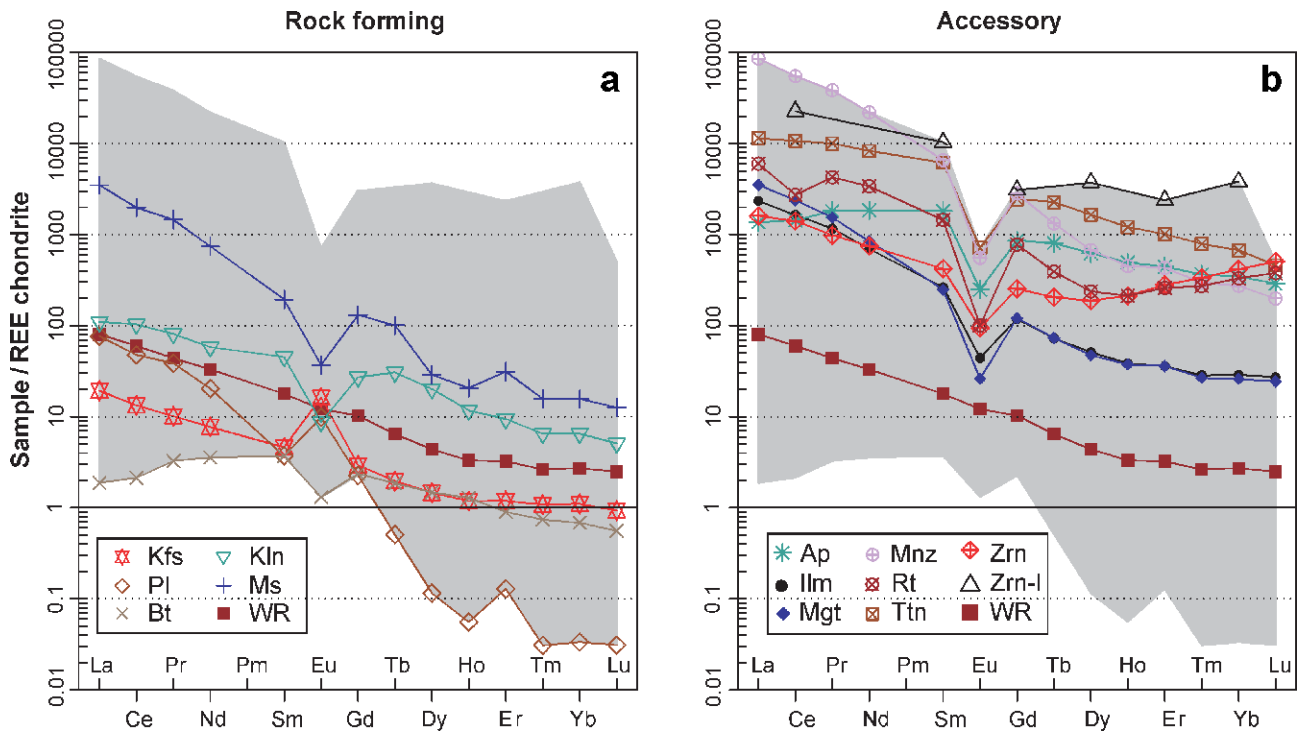


Fig. 6. Chondrite (Boynnton 1984)-normalized REE spiderplots for the individual minerals. Zrn-l = zircon-like ABO_4 -type phase. Grey field denotes the total variation in the dataset.

Feldspars and kaolinite

K-feldspar is characterized by roughly double enrichment of Ba, Rb and Pb over the whole-rock abundances; also Sr is slightly elevated (Fig. 5a). The *plagioclase* contains rather high Sr and Be (see Navrátil et al. 2002; Navrátil 2003). On the other hand, concentrations of transition metals and high field strength elements (HFSE) in both feldspars are very low. The *kaolinite* is stripped of much of the original *K-feldspars*' large-ion lithophile (LILE) budget, and contains only Cd, Pb and Ta in amounts exceeding those in the whole rock.

The *plagioclase* contains more than twice as much REE as the *K-feldspar* (81.3 vs. 26.6 ppm). Still the patterns are of similar shape, featuring a high degree of LREE over HREE enrichment and sizeable positive Eu anomalies (Fig. 6a). The feldspars share normalized Eu contents nearly identical to the whole rock but the concentrations of the remaining REE are significantly lower. The limited REE mobility in course of weathering of feldspars resulted in significantly higher apparent concentrations in the residual *kaolinite* ($\Sigma\text{REE} \sim 191$ ppm). Only Eu contents approach those of the host rock and thus the Eu anomaly turns to a strongly negative one.

Biotite and muscovite

The biotite is classified as phlogopite with 13.7–17.2 wt. % total Al_2O_3 (Al^{IV} 1.10–1.18 and Al^{VI} 0.16–0.27 apfu) and is relatively Mg-rich ($Mg/(Fe^T+Mg)=0.57$ –0.59). The content of Al_2O_3 for muscovite is 31.3 wt. % total (Al^{IV} 1.44 and Al^{VI} 3.44 apfu). Both micas are slightly enriched in Rb, Mn (see Navrátil et al. 2007), Ni, Co, Zn, Nb and Ta. Elevated

contents of Cd, Th, U, Zr and Hf are also characteristic of muscovite. The main differences lie in the total REE contents (7.3 ppm for biotite vs. 3396 ppm for muscovite). The muscovite REE pattern is steep, with a much higher degree of LREE/HREE enrichment compared to biotite (Fig. 6a). The Eu anomaly is negative in both cases.

Accessory minerals

Apatite: As shown by EMPA, the main minor constituents in apatite are Mn, Fe and Cl. It is further characterized by an enrichment of Mn, Cd and U (Fig. 5b). The Pb contents are close to those in the whole rock. Apatite is rich in REE, and the MREE in particular ($\Sigma\text{REE}=3962$ ppm; Fig. 6b). A negative Eu anomaly is characteristic.

Zircon: This mineral is rather Hf poor (0.01–0.02 apfu) but contains high concentrations of other HFSE, such as Nb and Ta. Zircon is a major Cd, Zn, Ni and Co bearing-phase. High concentrations of U with Th are typical, as well as high ΣREE (2615 ppm) and parabolic, convex-up chondrite-normalized pattern with elevated HREE contents (Fig. 6b). While the Eu anomaly is negative, the Ce anomaly, typical of most igneous zircons (Hoskin & Schaltegger 2003), is absent. This, together with a rather low degree of HREE enrichment, might reflect the presence of inclusions (see fig. 1 in Hoskin & Schaltegger op. cit.) or an admixture of the zircon-like (Zrn-l) phase.

Monazite: Monazite shows large concentrations of P, Zr and Hf. Enrichment in radioactive elements is characteristic, with Th prevailing over U. Pb contents are also high. This mineral is enriched in REE, and especially LREE, with Ce

being the most abundant ($\Sigma\text{REE}=91,205$ ppm; Fig. 6b). A deep negative Eu anomaly is characteristic.

Rutile: Rutile ($\text{TiO}_2 > 98$ wt. %) is a major transition metal-bearing phase (Ni, Co and Cd); it displays elevated U and Th contents. High HFSE concentrations (Zr, Hf, Nb and Ta) are also typical. It is a REE-rich mineral ($\Sigma\text{REE}=7358$ ppm) with a fair degree of LREE/HREE fractionation and a deep negative Eu anomaly.

Ilmenite and magnetite: Both minerals are characterized by high contents of metals (Mn and Cd, less enriched Pb, Zn, Co and Ni) as well as HFSE. The U and Th contents are also somewhat elevated (Fig. 5b). The minerals are enriched in REE (ΣREE for ilmenite is 2735 ppm, for magnetite 3818 ppm), and the LREE in particular (Fig. 6b). The Eu anomaly is deeply negative in both cases.

Titanite: Titanite shows low Al (0.09–0.11 apfu) and Fe (0.03–0.03 apfu) contents. It is enriched in HFSE (Zr, Hf, Th and U, less so Nb and Ta). Elevated Cd contents are also typical. On the other hand, the LILE (Ba, Rb and Sr) are depleted compared to the whole rock (Fig. 5b). The ΣREE is high (21,314 ppm) and the REE pattern relatively steep (Fig. 6b) with a pronounced negative Eu anomaly.

Zircon-like ABO_4 -type phase: The results of the EMPA of the zircon-like ABO_4 -type phase are summarized in Appendix 5. Because of the relatively high Th contents, crystals are metamict and altered, and yield low analytical totals. The analysed phase appears to be a member of the zircon–thorite solid solution series (0.27–0.33 apfu Th, 0.49–0.55 apfu Zr), with substitution of Si by P (0.22–0.24 apfu) in the tetrahedral position B. The phase is highly enriched in Fe (0.03–0.23 apfu) and Ca (0.20–0.22 apfu). The Fe and Ca atoms, which probably enter the crystal structure during self-amorphization and interactions with circulating fluids, could be positioned in

channels running parallel to the c axis of the crystal structure (Geisler et al. 2002, 2003). Silica removal accompanied by a hydration by post-magmatic, low-T fluids is also very probable.

Discussion

Modal analysis

Main rock-forming minerals

The choice of the most appropriate method for estimating modal abundances of the main rock-forming minerals was governed by comparison of the observed and calculated model whole-rock contents of the major- and minor-element oxides, as well as the most common among the LILE (Ba, Rb and Sr, which are hosted in granites mostly by feldspars and micas — Hanson 1978). Examining Fig. 7, it is clearly seen that the constrained LSQ method provides the most accurate estimate. As this approach does not give good assessments of contents of minor phases, no muscovite was included in the calculation and 0.2 wt. % of this mineral was added on the basis of the point counting. The ‘best’ modal proportions of the main rock-forming minerals are thus estimated to be: 0.365 Pl, 0.293 Kfs, 0.247 Qtz, 0.093 Bt and 0.002 Ms.

As for the rock classification in the QAP triangle (Fig. 8) (here essentially the vol. % of Kfs, Pl and Qtz recast to 1), the modal estimates by all methods yield comparable results and the studied rock classifies consistently as monzogranite. Still, the image analysis and, to some extent, point counting tend to overestimate somewhat the *Q* proportion, whereas the P-XRD approach results in a slightly lower $100^*P/(A+P)$ ratio of 47 % (other methods giving 55–59 %).

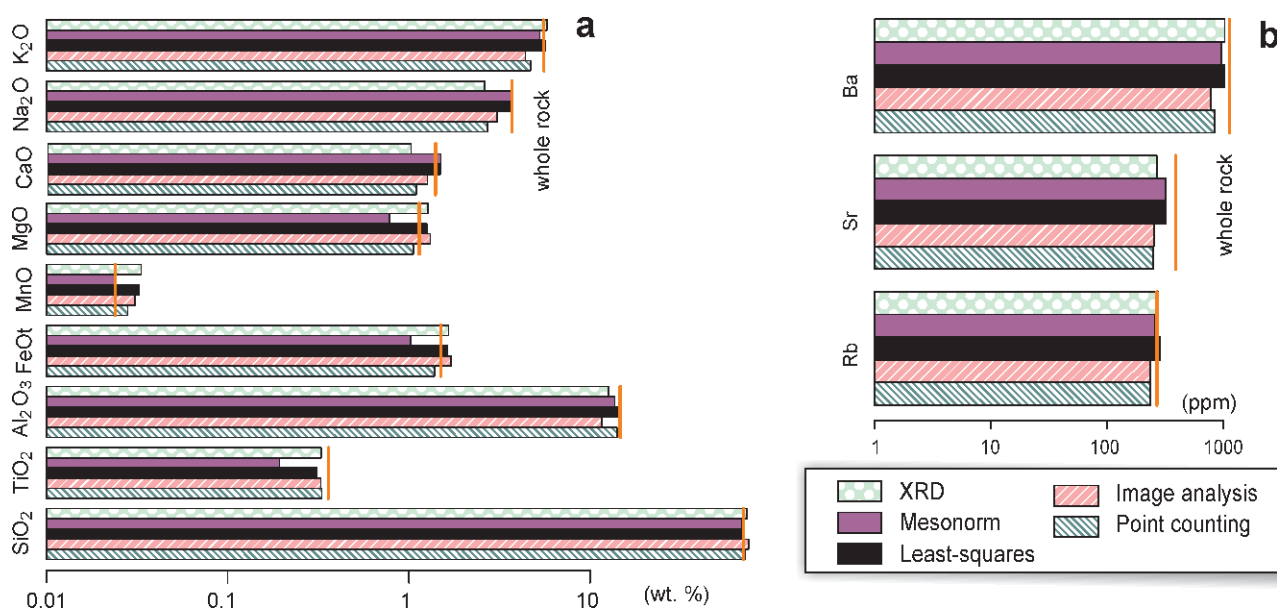


Fig. 7. Bar plots of calculated whole-rock contents of major- and minor-element oxides (a) and selected LILE (Rb, Sr and Ba) (b) calculated from representative mineral analyses (Appendices 2 and 4) and modal abundances estimated on the basis of the P-XRD, granite mesonorm, constrained least-squares (LSQ), image analysis of the stained thin slab and point counting of a standard thin section (Table 1). The best agreement with the whole-rock contents (vertical orange lines) is achieved by the LSQ method.

Accessory phases

After subtracting the elements hosted by the main rock-forming minerals (not only hosted incorporated in the lattice,

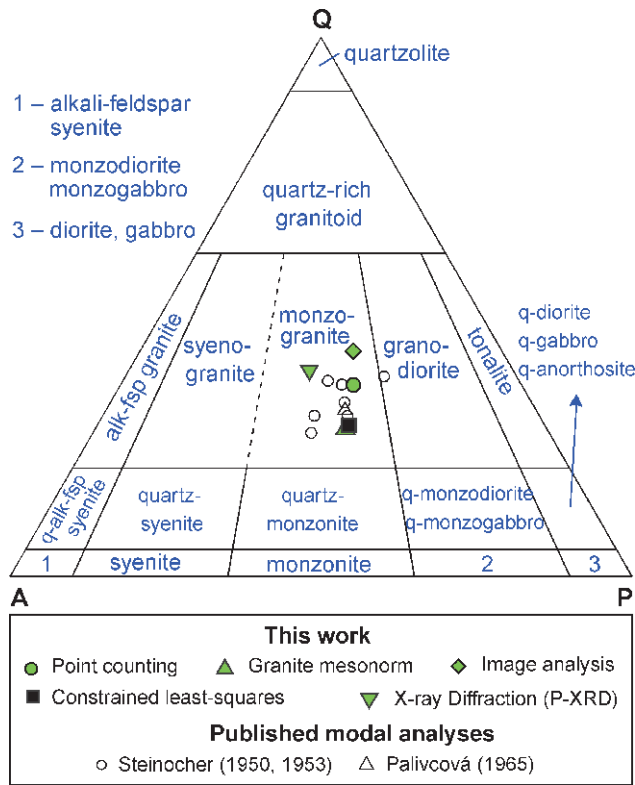


Fig. 8. QAP (quartz, K-feldspar, plagioclase) triangle of Streckeisen (1974) comparing previous modal analyses of the Řičany granite (Steinocher 1950, 1953; Palivcová 1965) with those obtained for sample Žer-1 in course of the present study by various methods. If necessary, the results were recast to vol. %.

Table 4: Maximum contents of selected accessory minerals (wt. %).

| | Zr | Nb | La | Nd | Eu | Yb | Y | P | wt. % |
|-----|--------------|--------------|--------------|-------|--------|-------|--------------|--------------|-------|
| Ap | | | 2.875 | 1.166 | 1.431 | 0.661 | 0.473 | 0.314 | 0.314 |
| Mnz | 1.442 | 10.761 | 0.046 | 0.098 | 0.641 | 0.838 | 0.661 | 0.524 | 0.046 |
| Zrn | 0.032 | 0.116 | 2.459 | 2.882 | 3.780 | 0.550 | 1.240 | | 0.032 |
| Rt | 0.327 | 0.081 | 0.655 | 0.634 | 3.543 | 0.691 | 1.391 | | 0.081 |
| Mgt | 14.835 | 10.647 | 1.121 | 2.544 | 13.639 | 8.811 | 7.978 | | 1.121 |
| Ttn | 1.443 | 9.563 | 0.343 | 0.260 | 0.498 | 0.340 | 0.255 | | 0.255 |

but also contained in small inclusions, fluid inclusions or sorbed at grain boundaries, interfacial films etc.), the rest of the whole-rock chemical inventory has to be accounted for by the accessories. A crude estimate of a maximum modal abundance can be made using trace-element characteristics of the individual minerals. Assuming that such a phase accommodates the entire whole-rock inventory of the given element, these are as follows (Table 4, elements in brackets being the most restrictive ones): apatite <0.314 wt. % (P), monazite <0.046 wt. % (La), zircon <0.032 wt. % (Zr), rutile <0.081 wt. % (Nb), magnetite <1.121 wt. % (La) and titanite <0.255 wt. % (Y).

For some minerals, these constraints should approach the real modal abundances; the others contain no unique essential structural component, and instead share their trace-element load with other mineral phase(s). For instance, the maximal apatite content is likely to be overestimated, as part of P resides in monazite. Likewise, the LREE hosted in minerals other than monazite can hardly be neglected.

Regarding the opaque phases, ilmenite and magnetite are the possible carriers of the ferromagnetic properties in the granite. It is worth stressing that the mean magnetic susceptibility of the Řičany granite is low ($13.13-105.3 \times 10^{-6}$ [SI]; Trubač et al. 2009) and thus the rock must contain only a very limited amount of ferromagnetic component. Moreover, in the constrained LSQ calculation, the whole-rock Fe budget is exhausted by biotite and residual TiO_2 is as low as 0.05 wt. % (Table 3). According to petrographic investigation (Kodymová & Vejnar 1974), rutile seems to be the most important Ti-bearing accessory. Ilmenite, magnetite and titanite were therefore not taken into further consideration, in accordance with the microscopic and electron-microprobe studies showing all three phases to be rather rare. The modal abundance of the zircon-like ABO_4 phase remains unknown as the complete trace-element data are not available.

In order to assess the abundances of the remaining accessory minerals (Ap, Mnz, Zrn and Rt), the *unconstrained* LSQ method was applied to the outstanding trace-element inven-

Estimates are based on an assumption that the given mineral contains the full whole-rock inventory of the individual elements, after subtracting those hosted by the main phases (0.365 Pl, 0.293 Kfs, 0.247 Qz, 0.093 Bt and 0.02 Ms). Minima for each mineral are shown in bold; these represent maximum possible contents of each phase (last column).

Table 5: Modal percentages of the most abundant accessories (wt. %) estimated by the unconstrained least-squares method.

| (ppm) | Ap ¹ | Mnz | Zrn | Rt | Real ² | Calc. ⁴ |
|--|-----------------|----------|----------|---------|-------------------|--------------------|
| Zr | 1.2 | 10086.7 | 453122.0 | 44550.4 | 145.5 | 145.5 |
| Nb | 0.1 | 35.3 | 3288.9 | 4675.2 | 3.8 | 4.6 |
| La | 424.5 | 26574.3 | 496.4 | 1861.8 | 12.2 | 13.5 |
| Nd | 1105.0 | 13148.3 | 446.9 | 2031.7 | 12.9 | 10.2 |
| Eu | 18.3 | 40.8 | 6.9 | 7.4 | 0.3 | 0.1 |
| Yb | 72.2 | 57.0 | 86.9 | 69.1 | 0.5 | 0.3 |
| Y | 1173.8 | 839.3 | 447.3 | 398.7 | 5.5 | 4.2 |
| P | 186228.0 | 111734.2 | 0.0 | 17.5 | 585.4 | 585.4 |
| Estimated modal proportions (wt. %) ³ | 0.290 % | 0.040 % | 0.023 % | 0.082 % | | |

¹ — Real mineral analyses are summarized in the **Appendix 2.**
² — The whole-rock composition not accounted for by the main rock-forming minerals. See text for discussion.
³ — Estimated modal percentages obtained by the least-squares approach.
⁴ — Composition of a mixture (ppm) calculated using these mineral proportions.

| wt. % | Or | Pl | Qtz | Bt | Ms | Ap | Mnz | Zrn | Rt | wt. % |
|--------------------------------|--------|--------|--------|--------|-------|-------|-------|--------|-------|---------|
| | 29.178 | 36.379 | 24.527 | 9.285 | 0.199 | 0.289 | 0.04 | 0.023 | 0.081 | |
| SiO ₂ | 18.72 | 22.91 | 24.49 | 3.48 | 0.1 | | | 0.01 | | 69.71 |
| TiO ₂ | | | | 0.31 | | | | | 0.08 | 0.39 |
| Al ₂ O ₃ | 5.39 | 7.8 | | 1.37 | 0.06 | | | | | 14.12 |
| FeOt | 0.01 | | | 1.6 | 0.01 | | | | | 1.62 |
| MnO | 0.01 | | | 0.02 | | | | | | 0.03 |
| MgO | | | | 1.24 | | | | | | 1.24 |
| CaO | | 1.44 | | | | 0.16 | | | | 1.60 |
| Na ₂ O | 0.28 | 3.35 | | 0.01 | | | | | | 3.64 |
| K ₂ O | 4.55 | 0.16 | | 0.88 | 0.02 | | | | | 5.61 |
| P ₂ O ₅ | | 0.01 | | | | 0.12 | 0.01 | | | 0.14 |
| ppm | | | | | | | | | | |
| Rb | 156.56 | 57.2 | 0.02 | 68.64 | 1.23 | | | 0.01 | | 283.66 |
| Sr | 133.84 | 181.91 | 0.03 | 0.16 | 0.36 | 0.43 | 0.04 | 0.01 | 0.02 | 316.80 |
| Ba | 832.34 | 49.31 | 0.08 | 116.33 | 2.21 | 0.01 | 0.01 | 0.06 | 0.13 | 1000.48 |
| Ni | 0.1 | 0.77 | 0.53 | 10.72 | 0.04 | | | 0.29 | 1.63 | 14.08 |
| Co | 0.05 | 0.58 | | 2.28 | 0.01 | | | 0.01 | 1.13 | 4.08 |
| Zn | 0.5 | 4.75 | 0.1 | 24.14 | 0.2 | 0.04 | 0.04 | 0.12 | 0.37 | 30.26 |
| Cd | 0.01 | 0.02 | 0.01 | 0.01 | 0.01 | | | 0.02 | 0.03 | 0.11 |
| Be | 1.61 | 7.88 | 0.01 | 0.44 | 0.02 | | 0.01 | 0.02 | | 9.99 |
| Pb | 36.39 | 21.95 | 0.02 | 0.32 | 0.1 | 0.16 | 0.44 | 0.04 | 0.26 | 59.68 |
| Th | 1.88 | 1.14 | 0.14 | 0.04 | 0.96 | 0.02 | 1.62 | 0.22 | 1.75 | 7.67 |
| U | 0.87 | 0.6 | 0.01 | 0.01 | 0.12 | 0.07 | 0.16 | 0.11 | 0.5 | 2.45 |
| La | 1.74 | 8.63 | | 0.05 | 2.14 | 1.23 | 10.54 | 0.11 | 1.51 | 25.95 |
| Ce | 3.13 | 1.4 | | 0.16 | 3.17 | 3.34 | 17.55 | 0.26 | 1.79 | 43.40 |
| Pr | 0.36 | 1.71 | | 0.04 | 0.35 | 0.64 | 1.85 | 0.03 | 0.42 | 5.40 |
| Nd | 1.35 | 4.45 | | 0.2 | 0.89 | 3.19 | 5.21 | 0.1 | 1.65 | 17.04 |
| Sm | 0.26 | 0.26 | | 0.07 | 0.08 | 1.02 | 0.51 | 0.02 | 0.23 | 2.45 |
| Eu | 0.35 | 0.26 | | 0.01 | | 0.05 | 0.02 | | 0.01 | 0.70 |
| Gd | 0.22 | 0.21 | | 0.06 | 0.07 | 0.64 | 0.29 | 0.02 | 0.16 | 1.67 |
| Tb | 0.03 | 0.01 | | 0.01 | 0.01 | 0.1 | 0.02 | | 0.02 | 0.21 |
| Dy | 0.14 | 0.01 | | 0.04 | 0.02 | 0.33 | 0.09 | 0.01 | 0.06 | 0.95 |
| Ho | 0.02 | | | 0.01 | | 0.1 | 0.01 | | 0.01 | 0.15 |
| Er | 0.07 | 0.01 | | 0.02 | 0.01 | 0.27 | 0.04 | 0.01 | 0.04 | 0.47 |
| Tm | 0.01 | | | | | 0.03 | | | 0.01 | 0.05 |
| Yb | 0.07 | | | 0.01 | 0.01 | 0.21 | 0.02 | 0.02 | 0.06 | 0.40 |
| Lu | 0.01 | | | | | 0.03 | | | 0.05 | 0.01 |
| Y | 0.71 | 0.05 | | 0.26 | 0.07 | 3.39 | 0.33 | 0.1 | 0.32 | 5.23 |
| Nb | 0.4 | 2.02 | | 9.65 | 0.09 | | 0.01 | 0.76 | 3.8 | 16.73 |
| Ta | 0.08 | 0.02 | | 0.94 | 0.04 | | | 0.1 | 0.39 | 1.57 |
| Zr | 19.01 | 3.71 | 0.05 | 0.12 | 1.37 | | 4 | 104.38 | 36.21 | 168.83 |
| Hf | 0.6 | 0.21 | | 0.01 | 0.05 | | 0.12 | 3.69 | 1.11 | 5.79 |

Fig. 9. Balloon plot (Jain & Warnes 2006) expressing the balance of individual elements in the studied granite sample. The relative contributions of individual minerals are expressed by the colour and size of circles plotted. Each number was obtained by multiplication of the particular element/oxide concentration within the given mineral and the best estimate of its modal abundance. The goodness of fit could be assessed comparing row totals with the real whole-rock analyses.

tory. Trace elements which often represent their essential structural components (Zr, Nb, La, Nd, Eu, Yb, Y and P) were selected. In the solution (Table 5), Ap dominates (0.29 wt. %) over Rt (0.082 %), Mnz (0.04 %) and Zrn (0.023 %). The results are feasible as all obey the upper limits (Table 4) and the residuals for all modelled elements are satisfactory.

Whole-rock geochemical budget

Total balance

The overall balance of individual elements in the studied sample is illustrated by means of the balloon plot (Jain & Warnes 2006). This diagram conveys important aspects of tabular data without obscuring the exact numerical values (Fig. 9, see caption for explanation of the principle). For the trace elements, the final balance is also presented as an upper continental crust (Taylor & McLennan 1995) normalized spiderplot (Fig. 10). Here, both the real concentrations and computed abundances match rather well. Only middle-heavy REE and, most notably, Th and U are strongly underestimated, suggesting the presence of an additional, U,Th, HREE-rich phase not accounted for in our model. The obvious candidate is the zircon-like ABO₄ mineral (Appendix 5; Fig. 6b), the role of which could not be quantified as we do not have information on its modal percentage and most of the trace-element signature. Its mean concentrations of Th, U and Yb nevertheless correspond to ~27,000, >3500 and >350× those found in the upper continental crust (Taylor & McLennan 1995).

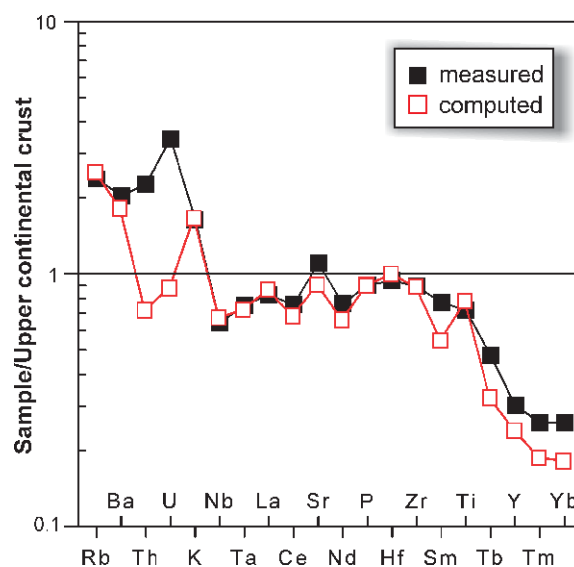


Fig. 10. Spiderplot of trace-element concentrations observed in the whole-rock sample Žer-1 (filled squares) and calculated (empty squares), normalized by abundances in the average upper continental crust (Taylor & McLennan 1995). The calculation was made for all the minerals present in Fig. 9.

Residence in individual minerals

Returning to Fig. 9, one can examine the residence of particular elements in detail. Silica is hosted almost equally by quartz (35 wt. % of its whole-rock abundance), plagioclase (33 %), and somewhat less by K-feldspar (27 %). Bulk Ti, Fe and Mg are held by biotite, whereby rutile contains a fifth of the whole-rock TiO₂. Much of the MnO is also accounted for by biotite but almost a third is hosted by K-feldspar. As expected, the main reservoirs for Al₂O₃ are the feldspars (Pl: 52 %, Kfs: 38 %). Surprisingly little Al, however, resides in biotite (10 %), owing to its small modal abundance. Most of the CaO and Na₂O are bound to plagioclase (~90 %); only 10 % of the former is stored in apatite and 8 % of the latter in K-feldspar. Part of the Na₂O contents in K-feldspar is to be ascribed to small plagioclase inclusions observed during petrographic studies. For K₂O, K-feldspar is clearly the key host (81 %), biotite accounting for a mere 16 % of the whole-rock budget. The main reservoir for P is apatite; monazite's contribution is small, close to 7 %.

Concerning the LILE, Rb is accumulated by K-feldspar (55 %), biotite comes second (24 %) and plagioclase third (20 %). The two feldspars represent almost equally important Sr reservoirs (Pl: 57 %, Kfs: 42 %). The bulk of Ba is concentrated in K-feldspar (83 %); both biotite (12 %) and plagioclase (5 %) are rather unimportant. The overwhelming majority of Be (79 %) is located in plagioclase; K-feldspar and biotite share the rest. Lead is another element for which the feldspars are the main hosts (Kfs: 61 %, Pl: 37 %).

The most important LREE reservoirs are monazite (41 % La) and plagioclase (33 % La), while muscovite, K-feldspar, rutile and apatite seem to be much less significant. The bulk of Eu is accounted for by the feldspars (Kfs: 50 % and Pl: 38 %); the apatite contribution represents a mere 8 %. On the other hand, apatite is the most important host for the middle and heavy REE as well as Y. Less significant HREE-bearing phase is rutile. Surprisingly, zircon and monazite do not rank among important sinks for HREE, owing to their scarcity.

Regarding the radioactive elements, both feldspars seem to incorporate much U (Kfs: 35 and Pl: 25 %). Among accessories, rutile accounts for over 20 % of both Th and U. Almost equally significant for Th are K-feldspar, monazite and rutile, less so plagioclase (15 %) and muscovite (13 %). Minerals such as zircon and apatite play only marginal roles in hosting the radioactive elements, unlike probably the newly recognized zircon-like ABO₄ phase, even though its role cannot be quantified.

Among the HFSE, the zircon contains only ~70 % of the total Zr and Hf; with rutile accounting for the rest. About 60 % of the Nb and Ta budget are hosted by biotite. We can only speculate that this may be in the form of submicroscopic inclusions; for rutile remains approximately one fifth of the whole-rock inventory.

General implications

Modal analysis

Petrographic techniques: In studies of granitic rocks, unstained thin sections are best suited for most textural obser-

vations, as well as description of optical properties and identification of mafic minerals. In many cases, however, it is difficult to determine some of the colourless phases, particularly if the feldspars are not twinned or their grains are small. One way out is to use cold-stage cathodoluminescence (CL), in which the (mostly) blue K-feldspars are easily distinguished from ochre-yellow plagioclases and almost non-luminescent quartz (Marshall 1988; Janoušek et al. 2000a, 2004). CL also facilitates rapid determination and mapping of some accessory phases, such as of apatite, monazite and zircon. Nowadays largely neglected, staining turns K-feldspars yellow and plagioclase white, also facilitating point counting (Gabriel & Cox 1929; Hollocher 2013).

Obtaining a statistically valid modal analysis by point counting of a standard thin section can be troublesome, especially for coarse-grained or porphyritic rocks (Chayes & Fairbairn 1951; Chayes 1954, 1965; Hutchison 1974). In order to maximize the counted area in these cases, it was proposed to use rock slabs or point count directly on the outcrop (e.g. Hutchison 1974) — but such methods are cumbersome and seldom used. Clearly, the situation becomes even more complicated when the rock possesses a fabric, as one deals essentially with a 2D section of a three-dimensional anisotropic body.

In our case, the approach using the stained polished slab is superior, as it represents an area larger than the standard section (ca. 119 vs. 6 cm²). The current work confirms that the tedious point-counting of the stained sample can be successfully replaced by computer-aided image analysis. However, this method also brings about some new problems, for example, some degree of ambiguity caused by alteration of the feldspar.

P-XRD: The Rietveld method has been widely used for quantitative phase analysis of various geological materials and industrial products (Madsen & Scarlett 2009 and references therein). This full-pattern profile fitting method has several advantages over other diffraction approaches to quantitative phase analysis using at most a few of the strongest reflections from each phase in the mixture (Bish & Post 1989). Nevertheless, the application of the Rietveld method to geological materials still poses significant problems. The most pronounced difficulties are micro-absorption effects, complex preferred orientation, various chemical substitutions in minerals and also the presence of structural defects.

Our estimate of modal composition obtained by P-XRD is probably biased by the defective structure of kaolinite, which is affected by planar disorder. Considering the complexity of the diffraction pattern, the large number of reflections and presence of significant preferred orientation, the results from P-XRD are reasonable, in other words they are comparable to other approaches. The advantage of the P-XRD method over standard petrographic techniques is that it represents, like the chemical approaches, the whole volume of the homogenized sample.

Chemical methods: For the sample Žer-1, the bulk-rock analysis represents ~30 kg, or over 11,000 cm³ of the rock, and thus should be robust to the presence of fabrics, phenocrysts and local inhomogeneities such as schlieren. Major-element or norm-based schemes (Streckeisen & Le Maitre

1979; De La Roche et al. 1980; Debon & Le Fort 1988) have been preferred by many authors for classification purposes. However, some normative recalculations involve minerals not encountered in common felsic plutonites and thus their use is not straightforward (e.g. CIPW and Catanorm — Hutchison 1975). For this reason, Mielke & Winkler (1979) developed their 'Improved Mesonorm', designed specifically for granitic rocks.

With the spread of personal computers, mathematical methods became popular. They attempt to find the best estimate of modal proportions based on major- and minor-element analyses of the large whole-rock sample and its typical mineral constituents. As usually the number of chemical components exceeds that of the mineral phases, there is no unique solution and the algorithms rely on the least-squares or linear programming approaches (e.g. Wright & Doherty 1970; Le Maitre 1981; Laube et al. 1996; Paktunc 1998; Janoušek et al. 2006). Potential pitfalls could lie in the choice of typical mineral compositions and/or the weathering/alteration effects. The methods are also rather insensitive to the presence of minor/or accessory phases, whose contents have to be assessed separately.

Here the results obtained by mesonormative and LSQ approaches are closely comparable for felsic minerals (Fig. 8). The amount of biotite, however, is nearly half (5.8 vs. 9.3 wt. %, respectively), and much lower also than estimates by the remaining methods. The reason probably lies in the fact that the mesonorm also estimates the proportion of magnetite and ilmenite, whereby in the LSQ calculation the sole iron-bearing phase is biotite. The normative contents of the opaque phases seem overestimated by the mesonormative algorithm, especially that of magnetite (0.9 %).

Taken together, several of the methods employed here to estimate the modal proportions of the main rock-forming minerals have yielded comparable results. It is necessary to stress that the current case is a particularly favourable one, as no significant zoning of mineral phases, not even of plagioclase, has been observed in the Řičany Pluton. Moreover, K-feldspar phenocrysts in the studied sample are small and sparse. Still, the constrained LSQ method (Albarède 1995) was found superior to all other approaches. The obtained percentages of the main rock-forming minerals compare well with the modal analyses determined previously by conventional point counting (Steinöcher 1950, 1953; Palivcová 1965) (Fig. 8).

Petrogenetic modelling

Collectively, the four accessories, apatite, monazite, zircon and rutile host more than half of the total LREE and over three quarters of the HREE + Y, Zr and Hf of the studied granite sample. The cases of Th, U, Ti, Ni, Co, Nb and Ta are similar, albeit not so extreme. This confirms the notion that the accessories are often crucial in controlling the behaviour of many elements in granitic systems (e.g. Mittlefehldt & Miller 1983; Miller & Mittlefehldt 1984; Bea 1996). Particularly the REE are of little value in petrogenetic modelling of fractional crystallization of the main rock-forming minerals, unless the role of accessories is properly assessed.

Determination of the whole-rock trace-element abundances

Some 10–30 % of the whole-rock HREE, U, Th, Nb, Ta, Ti, Cd, Co and Ni, and even more of Zr and Hf, are contained in the resistant accessories, zircon and rutile. Thus the pressure bomb or sample fusion are absolutely essential in sample decomposition, if these elements are to be determined quantitatively (e.g. Potts 1987; García de Madinabeitia et al. 2008 and references therein). Using a combined HF, HCl and HNO₃ attack is clearly inadequate and will induce low total REE contents and artificially increased degrees of LREE/HREE fractionation. Alas such cases are by no means rare — for instance, the acid decomposition casts serious doubts on some of the results by Minařík et al. (1998).

Saturation thermometry

Our study provides some interesting implications for the accessory phase saturation thermometry commonly used in the granite studies (see Janoušek 2006 and Anderson et al. 2008 for review). As in Řičany phosphorus is hosted nearly exclusively by apatite (86 % of the whole-rock contents), the saturation thermometry involving this mineral should apply be applicable. Indeed the temperature calculated for the uncorrected whole-rock P₂O₅ content and that based on apatite-hosted P₂O₅ are both mutually closely comparable (946 vs. 931 °C according to the model of Harrison & Watson 1984). The fact that they are unrealistically high for a granitic magma can be related to the sensitivity of the algorithm to exact determinations of P₂O₅ contents, as the isotherms converge rapidly for increasingly acidic compositions (see fig. 3a in Janoušek 2006).

Zircon incorporates a mere 62 % of the whole-rock Zr budget (Fig. 9), the rest being hosted by other phases, most importantly the early crystallizing rutile. The zircon saturation thermometry (Watson & Harrison 1983) thus yields a liquidus temperature estimate (784 °C) ca. 40 °C higher than that calculated for the corrected Zr concentration.

The case of monazite is more complex, though. The model of Montel (1993) includes additional parameters apart from the temperature, major-element and LREE contents of the magma. One is the fraction of REE phosphates in the monazite but this can be directly measured (the average for Řičany monazite is 89.5 mol %). More difficult to constrain are the water contents of the magma. Fortunately, the effect is not great (738 °C is obtained for 3 wt. % H₂O; 761–724 °C for 1–5 wt. % H₂O).

Plagioclase represents an important sink for LREE, with monazite containing some 21–41 % of the whole-rock inventory. This brings problems for the LREE-based monazite thermometry. While the uncorrected LREE content yields 738 °C, the corrected content gives barely 668 °C, that is about 70 °C less (for 3 wt. % H₂O in the magma melt). Such a corrected temperature seems to be too low for a granitic magma. However, one should take into account the petrological evidence indicating that the monazite saturation level was probably reached early, prior to the onset of the plagioclase crystallization. Thus using the uncorrected temperature seems more justifiable here.

Conclusions

The study of the petrography and mineral chemistry of a single large sample of coarse-grained, weakly porphyritic (muscovite-) biotite granite from the Říčany intrusion (Czech Republic) has yielded the following conclusions:

1. The methods taking into account the whole-rock composition as well as the true mineral chemistries (linear programming or constrained least squares) are particularly suitable for modal analyses of granitic rocks. The modes then represent a large volume of sample and thus (i) smooth out any local variations, such as small-scale crystal accumulation, (ii) account for the presence of phenocrysts, and (iii) are insensitive to shaped-preferred orientation/fabric.

2. Accessory phases control the behaviour of many trace elements in differentiation of felsic granitic systems. Clearly the REE are of little value in petrogenetic modelling of the main rock-forming minerals fractionation, unless the role of accessories is properly assessed and existing saturation models for apatite, zircon, monazite ± rutile are carefully considered.

The fact that many of the essential structural components (P, Zr, LREE) used in apatite, zircon and monazite saturation thermometry are incorporated into other minerals may lead to significant overestimation of the liquidus temperatures. In the present case, the saturation temperatures for zircon would be overestimated as ca. 40 °C due to significant contents of Zr in the early crystallized rutile. However, the correction for monazite (–70 °C) probably should not be applied as most of the extra LREE are hosted by plagioclase, a relatively late mineral.

In the studied sample, over 80 % of the whole-rock Zr and Hf and ca. 10–30 % of HREE, U, Th, Nb, Ta, Ti, Cd, Co and Ni are contained in resistant accessory phases Zrn and Rt. Thus the pressure vessel or sample fusion — and not merely a combined acid attack — are absolutely essential in sample decomposition if these elements are to be determined quantitatively.

Acknowledgments: This manuscript benefited from insightful comments by I. Broska, an anonymous reviewer and handling editor I. Petrik, as well as from careful editing by E. Petriková. The authors are indebted to Z. Korbelová for assistance at the electron microprobe and J.K. Novák (both Geological Institute, Czech Academy of Sciences, Prague — GLI) who carried out the point counting analysis. V. Sedláček (GLI) did the mineral separations, P. Hasalová (Czech Geological Survey) helped with staining of feldspars. Janoušek and Trubač acknowledge the support by the Grant Agency of the Czech Republic (GAČR, No. P210/11/1168) and Czech Ministry of Education, Youth and Sports (Project LK 11202); Minařík and Navrátil were supported from institutional Project No. RVO67985831. This study is a part of the Ph.D. research of Jakub Trubač.

References

- Albarède F. 1995: Introduction to geochemical modeling. *Cambridge University Press*, Cambridge, 1–543.
- Anderson J.L., Barth A.P., Wooden J.L. & Mazdab F. 2008: Thermometers and thermobarometers in granitic systems. In: Putirka K.D. & Tepley III F.J. (Eds.): Minerals, inclusions and volcanic processes. *Mineral. Soc. Amer.; Geochem. Soc. Rev. Miner. Geochem.*, Washington 69, 121–142.
- Bea F. 1996: Residence of REE, Y, Th and U in granites and crustal protoliths; implications for the chemistry of crustal melts. *J. Petrology* 37, 521–552.
- Bish D.L. & Post J.E. 1989: Modern powder diffraction. *Mineral. Soc. Amer. Rev. Miner.*, Washington 20, 1–369.
- Boynton W.V. 1984: Cosmochemistry of the rare earth elements: meteorite studies. In: Henderson P. (Ed.): Rare earth element geochemistry. *Elsevier*, Amsterdam, 63–114.
- Chayes F. 1954: The theory of thin-section analysis. *J. Geol.* 62, 92–101.
- Chayes F. 1965: Reliability of point counting results. *Amer. J. Sci.* 263, 719–724.
- Chayes F. & Fairbairn H.W. 1951: A test of the precision of thin-section analysis by point counter. *Amer. Mineralogist* 36, 704–712.
- Debon F. & Le Fort P. 1988: A cationic classification of common plutonic rocks and their magmatic associations: principles, method, applications. *Bull. Minéral.* 111, 493–510.
- De La Roche H., Leterrier J., Grandclaude P. & Marchal M. 1980: A classification of volcanic and plutonic rocks using R₁R₂-diagram and major element analyses — its relationships with current nomenclature. *Chem. Geol.* 29, 183–210.
- Evans O.C. & Hanson G.N. 1993: Accessory-mineral fractionation of rare-earth element (REE) abundances in granitoid rocks. *Chem. Geol.* 110, 69–93.
- Gabriel A. & Cox E.P. 1929: A staining method for the quantitative determination of certain rock minerals. *Amer. Mineralogist* 14, 290–292.
- García de Madinabeitia S., Sánchez Lorda M.E. & Gil Ibarguchi J.I. 2008: Simultaneous determination of major to ultratrace elements in geological samples by fusion-dissolution and inductively coupled plasma mass spectrometry techniques. *Anal. Chim. Acta* 625, 117–130.
- Geisler T., Pidgeon R.T., van Bronswijk W. & Kurtz R. 2002: Transport of uranium, thorium, and lead in metamict zircon under low-temperature hydrothermal conditions. *Chem. Geol.* 191, 141–154.
- Geisler T., Pidgeon R.T., Kurtz R., van Bronswijk W. & Schleicher H. 2003: Experimental hydrothermal alteration of partially metamict zircon. *Amer. Mineralogist* 88, 1496–1513.
- Gromet L.P. & Silver L.T. 1983: Rare earth element distribution among minerals in a granodiorite and their petrogenetic implications. *Geochim. Cosmochim. Acta* 47, 925–939.
- Hanson G.N. 1978: The application of trace elements to the petrogenesis of igneous rocks of granitic composition. *Earth Planet. Sci. Lett.* 38, 26–43.
- Harrison T.M. & Watson E.B. 1984: The behavior of apatite during crustal anatexis: equilibrium and kinetic considerations. *Geochim. Cosmochim. Acta* 48, 1467–1477.
- Hejtman B. 1948: Directory of quarries in Czechoslovakia, No. 26, Český Brod. [Soupis lomů ČSR, č. 26, okres Český Brod.] *SGÚ ČSR*, Praha, 1–71 (in Czech).
- Hollocher K. 2013: Staining feldspars in thin section. Accessed on 23 December 2013 at http://minerva.union.edu/hollochkc_petrology/staining_feldspars.htm
- Holub F.V., Machart J. & Manová M. 1997: The Central Bohemian Plutonic Complex: geology, chemical composition and genetic interpretation. *Sbor. Geol. Věd, ložisk. Geol. Mineral.* 31, 27–50.
- Hoskin P.W.O. & Schaltegger U. 2003: The composition of zircon and igneous and metamorphic petrogenesis. In: Hancher J.M. & Hoskin P.W.O. (Eds.): Zircon. *Mineral. Soc. Amer.; Geochem. Soc. Rev. Miner. Geochem.*, Washington 53, 27–62.

- Hutchison C.S. 1974: Laboratory handbook of petrographic techniques. *John Wiley & Sons*, New York, 1-527.
- Hutchison C.S. 1975: The norm, its variations, their calculation and relationships. *Schweiz. Mineral. Petrogr. Mitt.* 55, 243-256.
- Jain N. & Warnes G.R. 2006: Ballon plot. *R News* 6, 35-38.
- Janoušek V. 2006: *Saturnin*, R language script for application of accessory-mineral saturation models in igneous geochemistry. *Geol. Carpathica* 57, 131-142.
- Janoušek V., Farrow C.M. & Erban V. 2006: Interpretation of whole-rock geochemical data in igneous geochemistry: introducing Geochemical Data Toolkit (GCDkit). *J. Petrology* 47, 1255-1259.
- Janoušek V., Rogers G., Bowes D.R. & Vaňková V. 1997: Cryptic trace-element variation as an indicator of reverse zoning in a granitic pluton: the Říčany granite, Czech Republic. *J. Geol. Soc., London* 154, 807-815.
- Janoušek V., Bowes D.R., Braithwaite C.J.R. & Rogers G. 2000a: Microstructural and mineralogical evidence for limited involvement of magma mixing in the petrogenesis of a Hercynian high-K calc-alkaline intrusion: the Kozárovice granodiorite, Central Bohemian Pluton, Czech Republic. *Trans. Roy. Soc. Edinb., Earth Sci.* 91, 15-26.
- Janoušek V., Bowes D.R., Rogers G., Farrow C.M. & Jelinek E. 2000b: Modelling diverse processes in the petrogenesis of a composite batholith: the Central Bohemian Pluton, Central European Hercynides. *J. Petrology* 41, 511-543.
- Janoušek V., Braithwaite C.J.R., Bowes D.R. & Gerdes A. 2004: Magma-mixing in the genesis of Hercynian calc-alkaline granitoids: an integrated petrographic and geochemical study of the Sázava intrusion, Central Bohemian Pluton, Czech Republic. *Lithos* 78, 67-99.
- Johannsen A. 1932, 1937, 1938, 1939: A descriptive petrography of the igneous rocks. *University of Chicago Press*.
- Katzer F. 1888: Geologische Beschreibung der Umgebung von Řičan. *Jb. Geol. Reichsanst.* 38, 355-417.
- Kodymová A. & Vejnar Z. 1974: Accessory heavy minerals in plutonic rocks of the Central Bohemian Pluton. [Akcesorické těžké minerály v hlubinných horninách středoečeského plutonu.] *Sbor. Geol. Věd, ložisk. Geol. Mineral.* 16, 89-128 (in Czech).
- Kretz R. 1983: Symbols for rock-forming minerals. *Amer. Mineralogist* 68, 277-279.
- Laube N., Hergarten S. & Neugebauer H.J. 1996: MODUSCALC — a computer program to calculate mode from a geochemical rock analysis. *Comput. and Geosci.* 22, 631-637.
- Le Maitre R.W. 1981: GENMIX — a generalized petrological mixing model program. *Comput. and Geosci.* 7, 229-247.
- Le Maitre R.W. 2002: Igneous rocks: a classification and glossary of terms: recommendations of the International Union of Geological Sciences, subcommission on the systematics of igneous rocks. *Cambridge University Press*, 1-236.
- Madsen I.C. & Scarlett N.V.Y. 2009: Quantitative phase analysis. In: Dinnebier R.E. & Bilinge S.J.J. (Eds.): Powder diffraction: Theory and practise. *RCS Publishing*, Cambridge, 298-331.
- Marshall D.J. 1988: Cathodoluminescence of geological materials. *Unwin Hyman*, Boston, 1-145.
- Mielke P. & Winkler H.G.F. 1979: Eine bessere Berechnung der Mesonorm für granitische Gesteine. *Neu. Jb. Mineral., Mh.*, 471-480.
- Miller C.F. & Mittlefehldt D.W. 1984: Extreme fractionation in felsic magma chambers; a product of liquid-state diffusion or fractional crystallization? *Earth Planet. Sci. Lett.* 68, 151-158.
- Minařík L. & Houdková Z. 1986: Element distribution during the weathering of granitic rocks and formation of soils in the area of the massif of Říčany. [Distribuce prvků při zvětrávání hornin a tvorbě půd v oblasti říčanského masívu.] *Acta Montana* 74, 59-78 (in Czech, with English summary).
- Minařík L. & Kvidová O. 1986: Fractionation of rare earth elements during weathering of rocks. [Frakcionace vzácných zemin při zvětrávání hornin.] *Acta Montana* 72, 63-74 (in Czech, with English summary).
- Minařík L., Žigová A., Bendl J., Skřivan P. & Štastný M. 1998: The behaviour of rare-earth elements and Y during the rock weathering and soil formation in the Říčany granite massif, Central Bohemia. *Sci. Total Environ.* 215, 101-111.
- Minařík L., Skřivan P., Novák J.K., Fottová D. & Navrátil T. 2003: Distribution, cycling and impact of selected inorganic contaminants in ecosystem of the Lesní potok catchment, the Czech Republic. *Ekologia*, Bratislava 22, 305-322.
- Mittlefehldt D.W. & Miller C.F. 1983: Geochemistry of the Sweetwater Wash Pluton, California; implications for "anomalous" trace element behavior during differentiation of felsic magmas. *Geochim. Cosmochim. Acta* 47, 109-124.
- Montel J.M. 1993: A model for monazite/melt equilibrium and application to the generation of granitic magmas. *Chem. Geol.* 110, 127-146.
- Navrátil T. 2003: Biogeochemistry of the II.A group elements in a forested catchment. *Unpublished Ph.D. Thesis, Charles University in Prague*, 1-113.
- Navrátil T., Skřivan P., Minařík L. & Žigová A. 2002: Beryllium geochemistry in the Lesní Potok Catchment (Czech Republic), 7 years of systematic study. *Aquat. Geochem.* 8, 121-133.
- Navrátil T., Vach M., Skřivan P., Mihaljevič M. & Dobešová I. 2004: Deposition and fate of lead in a forested catchment, Lesní potok, Central Czech Republic. *Water Air Soil Poll., Focus* 4, 619-630.
- Navrátil T., Shanley J.B., Skřivan P., Krám P., Mihaljevič M. & Drahota P. 2007: Manganese biogeochemistry in a Central Czech Republic catchment. *Water Air Soil Poll.* 186, 149-165.
- Němec D. 1978: Genesis of aplite in the Říčany massif, central Bohemia. *Neu. Jb. Mineral., Abh.* 132, 322-339.
- Niggli P. 1931: Die quantitative mineralogische Klassifikation der Eruptivgesteine. *Schweiz. Mineral. Petrogr. Mitt.* 11, 296-364.
- Orlov A. 1933: Contribution to the petrography of the Central Bohemian Granite Massif (the Říčany-Benešov-Milevsko-Pisek region). [Příspěvek k petrografii středoečeského žulového masívu (Říčansko-Benešovsko-Milevsko-Pisecko).] *Věst. St. Geol. Úst. Čs. Repl.* 9, 135-144 (in Czech).
- Paktunc A.D. 1998: MODAN: an interactive computer program for estimating mineral quantities based on bulk composition. *Comput. and Geosci.* 24, 425-431.
- Palivcová M. 1965: The Central Bohemian Pluton — a petrographic review and an attempt at a new genetic interpretation. *Krystalinikum* 3, 99-131.
- Palivcová M., Waldhausrová J., Ledvinková V. & Fatková J. 1992: Říčany granite (Central Bohemian Pluton) and its ocelli- and ovoids-bearing mafic enclaves. *Krystalinikum* 21, 33-66.
- Pivec E. 1970: On the origin of phenocrysts of potassium feldspars in some granitic rocks of the Central Bohemian Pluton. *Acta Univ. Carol., Geol.* 1970, 11-25.
- Pivec E. 1969: Residues of surface kaolinization in granite of Říčany. [Relikty povrchové kaolinizace v říčanské žule.] *Čas. Mineral. Geol.* 14, 61-67 (in Czech, with English summary).
- Potts P.J. 1987: A handbook of silicate rock analysis. *Blackie & Son Ltd.*, Glasgow and London, 1-622.
- Robie R.A., Bethke P.M. & Beardsley K.M. 1967: Selected X-ray crystallographic data, molar volumes, and densities of minerals and related substances. *U.S. Geol. Surv. Bull.* 1248, Washington, 1-87.
- Sawka W.N. 1988: REE and trace element variations in accessory minerals and hornblende from the strongly zoned McMurry Meadows Pluton, California. *Trans. Roy. Soc. Edinb., Earth Sci.* 79, 157-168.

- Steinöcher V. 1950: The position of some plutonic and dike rocks of the plutonic mass of Central Bohemia in P. Niggli's quantitative mineralogical and chemical system. Part I. *Sbor. St. Geol. Úst. Čs. Rep., Odd. Geol.* 17, 721–764.
- Steinöcher V. 1953: The position of some plutonic and dyke rocks of the Pluton of Central Bohemia in P. Niggli's quantitative mineralogical and chemical system. Part II. *Sbor. Ústř. Úst. Geol., Odd. Geol.* 20, 241–288.
- Streckeisen A. 1974: Classification and nomenclature of plutonic rocks. *Geol. Rdsch.* 63, 773–786.
- Streckeisen A. & Le Maitre R.W. 1979: A chemical approximation to the modal QAPF classification of the igneous rocks. *Neu. Jb. Mineral., Abh.* 136, 169–206.
- Taylor S.R. & McLennan S.M. 1995: The geochemical evolution of the continental crust. *Rev. Geophys.* 33, 241–265.
- Trubač J., Žák J., Chlupáčová M. & Janoušek V. 2009: Magnetic fabric of the Říčany granite, Bohemian Massif: a record of helical magma flow? *J. Volcanol. Geotherm. Res.* 181, 25–34.
- Wark D.A. & Miller C.F. 1993: Accessory mineral behavior during differentiation of a granite suite: monazite, xenotime and zircon in the Sweetwater Wash pluton, southeastern California, U.S.A. *Chem. Geol.* 110, 49–67.
- Watson E.B. & Harrison T.M. 1983: Zircon saturation revisited: temperature and composition effects in a variety of crustal magma types. *Earth Planet. Sci. Lett.* 64, 295–304.
- Wright T.L. & Doherty P.C. 1970: A linear programming and least squares computer method for solving petrologic mixing problems. *Geol. Soc. Amer. Bull.* 81, 1995–2008.
- Žák J., Verner K., Janoušek V., Holub F.V., Kachlík V., Finger F., Hajná J., Tomek F., Vondrovic L. & Trubač J. (2014): A plate-kinematic model for the assembly of the Bohemian Massif constrained by structural relationships around granitoid plutons. In: Schulmann K., Martínez Catalán J.R., Lardeaux J.M., Janoušek V. & Oggiano G. (Eds.): The Variscan orogeny: Extent, timescale and the formation of the European Crust. *Geol. Soc. London, Spec. Publ.* 405, 169–196. Doi: 10.1144/SP405.9

Electronic supplement

JANOŠEK et al.: Distribution of elements among minerals of a single (muscovite-) biotite granite sample — an optimal approach and general implications

Appendix 1

Analytical techniques

Sampling

The whole-rock sample Žer-1 (~30 kg) was collected in the Žernovka quarry, ca. 850 m NNW of the namesake village off the pluton's center (Fig. 1c, GPS 50°0' 22.64" N; 14°44' 56.13" E). Its bulk was crushed by a steel jaw crusher, homogenized and ground in an agate mill at the Laboratories of the Institute of Geology, Czech Academy of Sciences, v.v.i. (CAS).

Mineral separation

The crushed material (<500 μm) was floated on a Wilfley shaking table. The heavy fraction was filtered on glass frit, rinsed with ethanol and air dried. The light fraction was dried at 105 °C and was used for separation of the main rock-forming minerals. The fraction between 63 and 250 μm thereof served for magnetic separation of biotite. The biotite separate was finally cleaned in acetylene tetrabromide with density of 2.54 kg·m⁻³.

The quartz separate was obtained after biotite separation by flotation using ANP1 (amino nitro paraffin) agent. K-feldspar was separated in bromoform solution (2.59 kg·m⁻³). The material with density greater than 2.54 kg·m⁻³ was plagioclase. Following the separation of quartz and orthoclase, muscovite separation was achieved in bromoform with density 2.74–2.84 kg·m⁻³. Kaolinite was isolated by centrifugation of the fine fraction (<25 μm) in bromoform.

The dried heavy fraction from the shaking table was sieved on a 315 μm nylon sieve. The fine fraction was used for separation of heavy minerals — zircon and monazite. Apatite was recovered from the heavy fraction by centrifugation in methyl-eniodide with density 3.18–3.25 kg·m⁻³. Magnetite was obtained from the dark part of the heavy fraction by magnetic separation with the intensity of magnetic field set to 0.2 A.

Electron microprobe and BSE imaging

The analyses of the major rock-forming and selected accessory minerals were done with a fully automated CAMECA SX-100 electron microprobe, employing $\Phi(\rho z)$ correction procedure (Merlet 1992) at the CAS. All analyses were performed at an acceleration voltage of 15 kV but with different beam currents and spot sizes chosen according to the mineral type. Thus 20–40 nA and a spot size of 10 μm were employed for analyses of apatite, titanite, rutile, monazite, magnetite, ilmenite and zircon-thorite solid solution. For feldspars, micas

and quartz, the beam current was 10–15 nA and spot size 2 μm. Minor-element interferences have been checked routinely and corrected for by measuring the corresponding standards. All the mineral abbreviations are after Kretz (1983).

Whole-rock major- and minor-element analyses

The major-element whole-rock analysis of the whole-rock sample was undertaken by wet chemistry in the laboratories of the Czech Geological Survey, Prague — Barrandov. Further analytical details are given in Dempířová (2010); the relative 2 σ uncertainties were better than 1 % (SiO₂), 2 % (FeO), 5 % (Al₂O₃, K₂O and Na₂O), 7 % (TiO₂, MnO, CaO), 6 % (MgO) and 10 % (Fe₂O₃, P₂O₅). Interpretation and plotting of the whole-rock geochemical data was done by the R-language package *GCDkit* (Janoušek et al. 2006).

Trace-element analyses

Solution ICP-MS analyses

The trace-element analyses of mineral separates and whole-rock samples were carried out after modified total digestion in mineral acids (HF+HClO₄) and borate fusion (Na₂CO₃+Na₂B₄O₇) in Pt crucibles followed by solution nebulization ICP-MS PQ3 VG Elemental at Charles University in Prague. All the chemicals involved were reagent grade (Merck, Germany) and the acids were double distilled. Deionized water from a Millipore system (Milli-Q Academic, USA) was used for all dilutions.

The measured data were processed on-line using VG PlasmaLab software, applying corrections for instrumental drift. The analytical precision for all the elements analysed ranged from 0.5 to 5 % relative. The accuracy of this analytical method was checked using the G-2 and BCR-2 reference materials (USGS, USA). Trace-element ICP-MS analyses followed the methods of Strnad et al. (2005).

In-situ laser ablation analyses

In-situ trace-element analyses were performed on a quadrupole-based ICP-MS Thermo Fisher X-Series II (Charles University) coupled to a NewWave UP 213 laser microprobe (NewWave Research; USA) operating at output wavelength of 213 nm. All samples were prepared as polished thin sections. The data were acquired in the time-resolved and peak jumping mode with one point measured per mass peak and processed off-line by Thermo Fisher PlasmaLab software 2.5.11 321. The raster pattern was linear, approximately

80×400 µm. External calibration of the laser-ablation analyses was done using standards NIST 610 and 612 (Pearce et al. 1997). For internal standardization ²⁹Si concentrations based on electron microprobe measurements were applied. Data reduction included correction for the gas blank, the internal standard and a calibration check; the data were processed off-line in a MS Excel spreadsheet-based program. For details on analytical protocol and correction strategy see Strnad et al. (2005).

Modal analyses

Point counting

Point counting was done on a thin section 3×2 cm using a standard optical microscope. The total number of points counted was 4890.

Image analysis of stained rock slab

The rock sample was stained according to the method of Gabriel & Cox (1929). The polished sample surface was exposed to fumes of HF for about 15 min., then treated with a concentrated solution of sodium cobaltinitrite for another 10 min., rinsed and dried. This reaction forms a yellow coating on K-feldspar and white on plagioclase; quartz remains unaffected.

The image analysis was performed on a scanned stained polished rock slab (ca. 17×7 cm). The abundance of mineral phases was estimated on the basis of pixel colour analysis by Quick Photo Micro 2.2 software. Dark-black areas were attributed to biotite, grey and greyish glassy-like colour to quartz, white to plagioclase and yellow to K-feldspar.

Powder X-ray diffraction

A powder sample was prepared by grinding in an agate mill and, subsequently, in an agate mortar. The powder X-ray diffraction pattern was collected in a conventional Bragg-Brentano geometry on the Philips X'Pert diffractometer equipped with graphite secondary monochromator. The CuK_α radiation was used. To minimize the background, the sample was placed on a flat low-background silicon wafer. Data were acquired in the angular range 3–90° 2θ, with a step interval of 0.02° and a step-counting time of 9 s. A divergence slit of 0.5° and a receiving slit of 0.1 mm were used.

The quantitative phase analysis of the sample was performed using the Rietveld method (Young 2000). Refinement was done by minimizing the sum of the weighted squared differences between observed and calculated intensities at every 2θ step in a powder diffraction pattern (Bish & Post 1993). Quartz, orthoclase, plagioclase (albite), biotite and kaolinite were detected in the P-XRD pattern. The Rietveld refinement was performed using the FullProf program (Rodríguez-Carvajal 2006). The structure models used in the refinement were as follows: quartz (Le Page & Donnay 1976), orthoclase (Prince et al. 1973), albite (Ferguson et al. 1958), biotite (Brigatti & Davoli 1990) and kaolinite (Bish & Von Dreele 1989). The structural model of oligoclase instead of albite was

also tested in Rietveld refinements, however the differences in the profile agreement factors between both Rietveld fits were insignificant. The differences in the estimated modal composition were below 0.1 wt. %. The background was determined by linear interpolation between consecutive break-points in the powder pattern. The pseudo-Voigt function was employed to generate the line shape of the diffraction peaks. The refinement involved the scale factor for each phase, unit-cell parameters for each phase except albite, peak-width parameters for each phase, two asymmetry parameters for biotite and 2θ zero error. Atomic coordinates, overall isotropic displacement factors, and site occupancy parameters were fixed during the refinement for all phases. The unit-cell parameters of albite were also fixed, since their refinement caused divergence of the fit. The March-Dollase correction for preferred orientation was applied. The [001] direction was used for biotite, kaolinite, feldspar and plagioclase. The refinement converged to the values of the profile agreement factors $R_p = 8.9\%$ and $R_{wp} = 11.4\%$.

Principles of the least-squares calculations

The least-squares method is employed to solve an overdetermined set of linear algebraic equations, which occur where there are more independent equations than variables (Bryan et al. 1969). Given a matrix A and a vector y , we want to know the vector x that fulfils.

$$y = Ax \quad 1$$

Our estimate of the vector x should also be chosen so that the computed and real elements of the vector y differ as little as possible.

$$y' = Ax' \quad 2$$

The squares of these differences are commonly minimized (so-called least-squares method: Bryan et al. 1969; Albarède 1995):

$$R^2 = |y' - y|^2 \quad 3$$

$$R^2 = \min \quad 4$$

and the sum of squared residuals is taken as the measure of the goodness of fit. Albarède (1995) discussed in a detail all the necessary mathematical apparatus that is behind the solution. Moreover, Janoušek & Moyon (in print) provide examples of various types of calculations (including normative calculations using real mineral compositions by the least-squares method) and their implementation into the freeware R language.

In geochemistry we very often examine variables that sum up, for instance, to a unity or 100 %. The least-squares method generally does not produce normalized solutions, in the form of vectors whose components would sum up to a given number. We can define the Lagrange multiplier λ as (Albarède (1995):

$$\lambda = \frac{1 - J^T x}{J^T (A^T A)^{-1} J} \quad 5$$

where x stands for an ordinary least-squares solution and J is a vector, all elements of which are equal to 1. The constrained least-squares solution is then given by:

$$\hat{x} = x + \lambda (A^T A)^{-1} J \quad 6$$

References

- Albarède F. 1995: Introduction to geochemical modeling. *Cambridge University Press*, Cambridge, 1–543.
- Bish D.L. & Post J.E. 1993: Quantitative mineralogical analysis using the Rietveld full-pattern fitting method. *Amer. Mineralogist* 78, 932–940.
- Bish D.L. & Von Dreele R.B. 1989: Rietveld refinement of non-hydrogen atomic positions in kaolinite. *Clays and Clay Miner.* 37, 4, 289–296.
- Brigatti M.F. & Davoli P. 1990: Crystal-structure refinements of 1 M plutonic biotites. *Amer. Mineralogist* 75, 305–313.
- Bryan W.B., Finger L.W. & Chayes F. 1969: Estimating proportions in petrographic mixing equations by least-squares approximation. *Science* 163, 926–927.
- Dempírová L. 2010: Evaluation of SiO₂, Na₂O, MgO, K₂O determinations in silicate samples by z-score obtained from nineteen interlaboratory tests. [Zhodnocení stanovení SiO₂, Na₂O, MgO a K₂O v silikátových vzorcích pomocí z-skóre získaných z devatenácti mezilaboratorních porovnávání.] *Zpr. Geol. Výzk. v roce 2009*, 323–326 (in Czech with English summary).
- Ferguson R.B., Traill R.J. & Taylor W.H. 1958: The crystal structures of low-temperature and high-temperature albites. *Acta Crystallogr.* 11, 331–348.
- Gabriel A. & Cox E.P. 1929: A staining method for the quantitative determination of certain rock minerals. *Amer. Mineralogist* 14, 290–292.
- Janoušek V. & Moyen J.F. (in print): Mass balance modelling of magmatic processes in *GCDkit*. In: Kumar S. & Singh R.N. (Eds.): Modelling of magmatic and allied processes. *Soc. Earth Sci., Ser. 83, Springer*, Berlin, 225–238.
Doi: 10.1007/978-3-319-06471-0_11
- Janoušek V., Farrow C.M. & Erban V. 2006: Interpretation of whole-rock geochemical data in igneous geochemistry: introducing Geochemical Data Toolkit (GCDkit). *J. Petrology* 47, 1255–1259.
- Kretz R. 1983: Symbols for rock-forming minerals. *Amer. Mineralogist* 68, 277–279.
- Le Page Y. & Donnay G. 1976: Refinement of the crystal structure of low-quartz. *Acta Crystallogr., Sect. B* 32, 2456–2459.
- Merlet C. 1992: Accurate description of surface ionization in electron probe microanalysis: an improved formulation. *X-RAY Spectrom.* 21, 229–238.
- Pearce N.J.G., Perkins W.T., Westgate J.A., Gorton M.P., Jackson S.E., Neal C.R. & Chenery S.P. 1997: A compilation of new and published major and trace element data for NIST SRM 610 and NIST SRM 612 glass reference materials. *Geostand. Newsl.* 21, 115–144.
- Prince E., Donnay G. & Martin R.F. 1973: Neutron diffraction refinement of an ordered orthoclase structure. *Amer. Mineralogist* 58, 500–507.
- Rodríguez-Carvajal J. 2006: Full Prof .2k Rietveld profile matching & integrated intensities refinement of X-ray and/or neutron data (powder and/or single-crystal). *Laboratoire Léon Brillouin, Centre d'Etudes de Saclay, Gif-sur-Yvette Cedex, France.*
- Strnad L., Mihaljevič M. & Šebek O. 2005: Laser ablation and solution ICP-MS determination of rare earth elements in USGS BIR-1G, BHVO-2G and BCR-2G glass reference materials. *Geost. Geoanal. Res.* 29, 303–314.
- Young R.A. 2000: The Rietveld method. *Oxford University Press*, Oxford, 1–312.

Appendix 2

Electron microprobe analyses.

a — Average electron-microprobe data used in mass-balance calculations (wt. %).

| | SiO ₂ | TiO ₂ | Al ₂ O ₃ | FeOt | MnO | MgO | CaO | Na ₂ O | K ₂ O | P ₂ O ₅ |
|------------|------------------|------------------|--------------------------------|-------|-------|-------|-------|-------------------|------------------|-------------------------------|
| WR | 70.34 | 0.36 | 14.64 | 1.5 | 0.024 | 1.14 | 1.36 | 3.71 | 5.55 | 0.15 |
| Qtz | 99.86 | n.d. | 0.02 | n.d. | n.d. | n.d. | n.d. | n.d. | n.d. | n.d. |
| Or | 64.16 | n.d. | 18.47 | 0.03 | 0.034 | n.d. | 0.01 | 0.96 | 15.61 | 0.01 |
| Pl | 62.97 | n.d. | 20.07 | n.d. | n.d. | 0.01 | 3.95 | 9.2 | 0.44 | 0.02 |
| Bt | 37.5 | 3.33 | 14.8 | 17.26 | 0.24 | 13.35 | 0.04 | 0.14 | 9.47 | n.d. |
| Ms | 49.38 | 0.27 | 31.26 | 3.72 | 0.05 | 0.98 | 0.12 | 0.27 | 9.79 | n.d. |
| Kln | 45.59 | 0.91 | 39.84 | 0.02 | 0.01 | n.d. | n.d. | n.d. | n.d. | 0.03 |
| Ilm | 0.01 | 50.32 | n.d. | 42.71 | 3.091 | n.d. | n.d. | n.d. | n.d. | 0.01 |
| Ttn | 30.49 | 35.77 | 2.79 | 1.11 | 0.092 | n.d. | 27.58 | n.d. | n.d. | 0.01 |
| Ap | 0.04 | 0.01 | n.d. | 0.03 | 0.161 | n.d. | 55.98 | n.d. | n.d. | 42.68 |
| Mgt | n.d. | n.d. | n.d. | n.d. | 0.233 | n.d. | n.d. | n.d. | n.d. | n.d. |
| Mnz | 2.42 | n.d. | n.d. | 0.04 | n.d. | n.d. | 0.37 | n.d. | n.d. | 25.61 |
| Zrn | 31.1 | n.d. | 0.29 | 0.44 | 0.006 | n.d. | 0.14 | n.d. | n.d. | n.d. |
| Rt | 0.28 | 97.35 | n.d. | 1.59 | 0.031 | n.d. | 0.08 | n.d. | n.d. | n.d. |

n.d. — not detected.

b — Typical analyses for the main and accessory minerals (wt. % and apfu).

| ID | Feldspars | | | Biotite | | Magnetite | |
|--------------------------------|-----------|--------|-------|--------------------------------|-------|--------------------------------|-------|
| | Plg15T | Plg19T | 16T | ID | Bt14 | ID | Mgt1 |
| SiO ₂ | 63.75 | 66.44 | 64.26 | SiO ₂ | 37.50 | SiO ₂ | 0.03 |
| TiO ₂ | n.d. | 0.01 | n.d. | TiO ₂ | 3.33 | TiO ₂ | 0.01 |
| Al ₂ O ₃ | 22.00 | 20.33 | 18.29 | Al ₂ O ₃ | 14.80 | Al ₂ O ₃ | 0.04 |
| FeOt | n.d. | n.d. | 0.02 | FeOt | 16.95 | FeOt | 95.55 |
| MnO | 0.02 | n.d. | n.d. | MnO | 0.24 | MnO | 1.17 |
| MgO | 0.009 | n.d. | 0.01 | MgO | 13.35 | MgO | n.d. |
| CaO | 3.59 | 1.72 | 0.03 | CaO | 0.04 | CaO | 0.01 |
| Na ₂ O | 9.72 | 10.84 | 1.30 | Na ₂ O | 0.14 | Na ₂ O | n.d. |
| K ₂ O | 0.38 | 0.21 | 15.48 | K ₂ O | 9.47 | K ₂ O | n.d. |
| P ₂ O ₅ | 0.013 | 0.009 | 0.008 | H ₂ O+ | 2.44 | P ₂ O ₅ | n.d. |
| Total | 99.46 | 99.61 | 99.39 | F | 1.66 | ThO ₂ | n.d. |
| Si apfu | 2.834 | 2.930 | 2.987 | Total | 99.92 | U ₂ O ₃ | n.d. |
| Ti | 0.000 | 0.000 | 0.000 | Si apfu | 2.812 | Y ₂ O ₃ | n.d. |
| Al | 1.153 | 1.057 | 1.002 | Al(IV) | 1.188 | TR ₂ O ₃ | n.d. |
| Fe | 0.000 | 0.000 | 0.001 | Σ | 4.000 | Total | 96.81 |
| Mn | 0.001 | 0.000 | 0.000 | Al(VI) | 0.121 | Si apfu | 0.004 |
| Mg | 0.001 | 0.000 | 0.001 | Ti | 0.188 | Ti | 0.001 |
| Ca | 0.171 | 0.081 | 0.002 | Fe | 1.063 | Al | 0.005 |
| Na | 0.838 | 0.927 | 0.117 | Mn | 0.015 | Fe ²⁺ | 0.964 |
| K | 0.021 | 0.012 | 0.918 | Mg | 1.492 | Fe ³⁺ | 1.995 |
| P | 0.000 | 0.000 | 0.000 | Σ | 2.879 | Mn | 0.037 |
| O | 8.000 | 8.000 | 8.000 | Ca | 0.003 | Mg | 0.000 |
| An mol. % | 16.6 | 8.0 | 0.1 | Na | 0.020 | Ca | 0.000 |
| Ab | 81.3 | 90.9 | 8.5 | K | 0.906 | Na | 0.000 |
| Or | 2.1 | 1.2 | 91.4 | Σ | 0.930 | K | 0.000 |
| | | | | F | 0.394 | P | 0.000 |
| | | | | OH* | 1.606 | Th | 0.000 |
| | | | | XMg | 0.58 | U | 0.000 |
| | | | | XFe | 0.42 | Y | 0.000 |

n.d. — not detected, n.a. — not analysed.

| ID | Zircon | | | Monazite | | Rutile | Titanite |
|--------------------------------|--------------|--------------|--------------|----------------|----------------|----------------|--------------|
| | Zrn5 | Zrn7 | Zrn10 | Mnz8 | Mnz9 | Rt1 | Ttn4 |
| SiO ₂ | 32.08 | 31.10 | 32.27 | 1.89 | 2.42 | 0.51 | 30.30 |
| TiO ₂ | 0.02 | n.d. | n.d. | 0.01 | 0.00 | 98.82 | 36.32 |
| Al ₂ O ₃ | 0.06 | 0.29 | n.d. | n.d. | n.d. | 0.01 | 2.44 |
| P ₂ O ₅ | n.d. | n.d. | n.d. | 26.61 | 25.61 | 0.00 | 0.02 |
| FeO | 0.14 | 0.44 | 0.05 | 0.00 | 0.04 | 0.46 | n.a. |
| Fe ₂ O ₃ | n.a. | n.a. | n.a. | n.a. | n.a. | n.a. | 1.08 |
| MnO | n.d. | 0.01 | n.d. | 0.12 | n.d. | n.d. | 0.11 |
| CaO | 0.02 | 0.14 | n.d. | 0.41 | 0.37 | 0.10 | 27.23 |
| Y ₂ O ₃ | n.d. | 0.39 | 0.11 | 0.55 | 0.40 | 0.06 | 0.36 |
| ZrO ₂ | 63.28 | 61.21 | 62.89 | n.a. | n.a. | n.a. | n.a. |
| HfO ₂ | 1.87 | 1.89 | 1.30 | n.a. | n.a. | n.a. | n.a. |
| Ce ₂ O ₃ | n.d. | n.d. | 0.04 | 32.74 | 32.78 | 0.14 | 0.50 |
| La ₂ O ₃ | 0.13 | 0.07 | n.d. | 15.07 | 14.51 | n.d. | 0.07 |
| Nd ₂ O ₃ | n.d. | n.d. | 0.08 | 9.35 | 8.66 | n.d. | 0.60 |
| Pr ₂ O ₃ | 0.12 | 0.10 | n.d. | 2.87 | 2.86 | 0.04 | 0.23 |
| Sm ₂ O ₃ | 0.00 | 0.09 | 0.04 | 1.07 | 1.18 | 0.00 | 0.02 |
| Eu ₂ O ₃ | 0.01 | 0.02 | 0.01 | n.d. | n.d. | 0.05 | n.d. |
| Gd ₂ O ₃ | 0.02 | 0.04 | 0.01 | 0.48 | 0.37 | n.d. | 0.15 |
| Tb ₂ O ₃ | n.d. | n.d. | n.d. | 0.08 | 0.03 | n.d. | 0.08 |
| Dy ₂ O ₃ | 0.01 | 0.01 | 0.04 | 0.04 | n.d. | 0.01 | 0.08 |
| Ho ₂ O ₃ | n.d. | 0.01 | 0.03 | 0.01 | 0.01 | 0.04 | 0.02 |
| Er ₂ O ₃ | 0.00 | 0.02 | 0.00 | 0.05 | 0.02 | 0.00 | 0.03 |
| Tm ₂ O ₃ | n.d. | n.d. | n.d. | 0.08 | 0.09 | 0.02 | 0.02 |
| Yb ₂ O ₃ | n.d. | n.d. | 0.04 | n.d. | 0.03 | 0.02 | 0.01 |
| Lu ₂ O ₃ | n.d. | n.d. | n.d. | n.d. | n.d. | 0.00 | n.d. |
| ThO ₂ | 0.13 | 0.17 | 0.03 | 8.18 | 10.42 | 0.02 | 0.02 |
| U ₂ O ₃ | 0.18 | 0.20 | 0.60 | 0.50 | 0.37 | 0.03 | 0.01 |
| Total | 98.05 | 96.19 | 97.54 | 100.110 | 100.144 | 100.322 | 99.66 |
| Si apfu | 1.007 | 0.998 | 1.015 | 0.077 | 0.099 | 0.007 | 1.001 |
| Ti | 0.000 | 0.000 | 0.000 | 0.000 | 0.000 | 0.988 | 0.903 |
| Al | 0.002 | 0.011 | 0.000 | 0.000 | 0.000 | 0.000 | 0.095 |
| P | 0.000 | 0.000 | 0.000 | 0.912 | 0.887 | 0.000 | 0.001 |
| Fe ²⁺ | 0.004 | 0.012 | 0.001 | 0.000 | 0.001 | 0.005 | n.a. |
| Fe ³⁺ | n.a. | n.a. | n.a. | n.a. | n.a. | n.a. | 0.027 |
| Mn | 0.000 | 0.000 | 0.000 | 0.004 | 0.000 | 0.000 | 0.003 |
| Ca | 0.001 | 0.005 | 0.000 | 0.018 | 0.016 | 0.001 | 0.964 |
| Y | 0.000 | 0.007 | 0.002 | 0.012 | 0.009 | 0.000 | 0.006 |
| Zr | 0.968 | 0.958 | 0.965 | n.a. | n.a. | n.a. | n.a. |
| Hf | 0.017 | 0.017 | 0.012 | n.a. | n.a. | n.a. | n.a. |
| Ce | 0.000 | 0.000 | 0.000 | 0.485 | 0.491 | 0.001 | 0.006 |
| La | 0.001 | 0.001 | 0.000 | 0.225 | 0.219 | 0.000 | 0.001 |
| Nd | 0.000 | 0.000 | 0.001 | 0.135 | 0.127 | 0.000 | 0.007 |
| Pr | 0.001 | 0.001 | 0.000 | 0.042 | 0.043 | 0.000 | 0.003 |
| Sm | 0.000 | 0.001 | 0.000 | 0.015 | 0.017 | 0.000 | 0.000 |
| Eu | 0.000 | 0.000 | 0.000 | 0.000 | 0.000 | 0.000 | 0.000 |
| Gd | 0.000 | 0.000 | 0.000 | 0.006 | 0.005 | 0.000 | 0.002 |
| Tb | 0.000 | 0.000 | 0.000 | 0.001 | 0.000 | 0.000 | 0.001 |
| Dy | 0.000 | 0.000 | 0.000 | 0.000 | 0.000 | 0.000 | 0.001 |
| Ho | 0.000 | 0.000 | 0.000 | 0.000 | 0.000 | 0.000 | 0.000 |
| Er | 0.000 | 0.000 | 0.000 | 0.001 | 0.000 | 0.000 | 0.000 |
| Tm | 0.000 | 0.000 | 0.000 | 0.001 | 0.001 | 0.000 | 0.000 |
| Yb | 0.000 | 0.000 | 0.000 | 0.000 | 0.000 | 0.000 | 0.000 |
| Lu | 0.000 | 0.000 | 0.000 | 0.000 | 0.000 | 0.000 | 0.000 |
| Th | 0.001 | 0.001 | 0.000 | 0.075 | 0.097 | 0.000 | 0.000 |
| U | 0.001 | 0.001 | 0.004 | 0.005 | 0.003 | 0.000 | 0.000 |
| A | 0.995 | 1.005 | 0.988 | 1.020 | 1.024 | | |
| B | 1.009 | 1.009 | 1.015 | 0.988 | 0.986 | | |
| Sum cat. | 2.004 | 2.014 | 2.003 | 2.015 | 2.016 | 1.004 | 3.021 |

Appendix 3: Laser-ablation ICP-MS data for the main rock forming minerals (ppm).

| LA ICP-MS | | Quartz | | | | | | | | | | |
|-----------|-----|--------|-------|-------|-------|-------|------|------|------|------|-------|------|
| DL (LA) | ppm | q1 | q2 | q3 | q4 | q1 | q2 | q3 | q4 | q1 | Avg | SD |
| 0.01 | Be | 0.08 | 0.11 | | 0.17 | 0.03 | 0.00 | 0.05 | 0.00 | 0.00 | 0.06 | 0.06 |
| 0.35 | Mn | 0.12 | 0.12 | 0.16 | 0.10 | 0.09 | 0.21 | 0.22 | 0.20 | 0.20 | 0.16 | 0.05 |
| 0.095 | Co | 0.01 | 0.01 | 0.00 | 0.01 | 0.01 | 0.01 | 0.03 | 0.00 | 0.01 | 0.01 | 0.01 |
| 1.15 | Ni | 1.97 | 1.77 | 0.94 | 1.27 | 2.29 | 2.17 | 3.02 | 2.93 | 3.12 | 2.16 | 0.77 |
| 0.48 | Zn | 0.10 | 0.22 | 0.26 | 0.19 | 0.11 | 0.64 | 0.69 | 0.69 | 0.65 | 0.39 | 0.26 |
| 0.26 | Rb | 0.03 | 0.05 | 0.05 | 0.05 | 0.35 | 0.08 | 0.07 | 0.05 | 0.09 | 0.09 | 0.10 |
| 0.085 | Sr | 0.10 | 0.16 | 0.09 | 0.06 | 0.12 | 0.13 | 0.07 | 0.13 | 0.12 | 0.11 | 0.03 |
| 0.045 | Y | 0.00 | 0.00 | 0.01 | 0.05 | 0.00 | 0.00 | 0.00 | 0.00 | 0.00 | 0.01 | 0.02 |
| 0.25 | Zr | 0.05 | 0.03 | 1.31 | | 0.09 | 0.14 | 0.06 | 0.04 | 0.03 | 0.22 | 0.44 |
| 0.05 | Nb | 0.01 | 0.00 | 0.00 | | 0.00 | | 0.04 | | 0.01 | 0.01 | 0.01 |
| 0.23 | Cd | 0.16 | 0.08 | 0.02 | 0.01 | 0.11 | 0.05 | 0.01 | 0.01 | 0.03 | 0.05 | 0.05 |
| 0.085 | Ba | 0.19 | 0.28 | 0.12 | 0.13 | 0.80 | 0.39 | 0.36 | 0.38 | 0.38 | 0.34 | 0.20 |
| 0.020 | La | 0.001 | 0.009 | 0.003 | 0.007 | 0.001 | 0.01 | 0.00 | 0.00 | 0.00 | 0.004 | 0.00 |
| 0.028 | Ce | 0.008 | 0.013 | 0.007 | 0.021 | 0.011 | 0.03 | 0.00 | 0.01 | 0.00 | 0.012 | 0.01 |
| 0.008 | Pr | 0.000 | 0.000 | 0.000 | 0.003 | 0.000 | 0.00 | 0.00 | 0.00 | 0.00 | 0.001 | 0.00 |
| 0.083 | Nd | 0.000 | 0.000 | 0.007 | 0.004 | 0.003 | 0.01 | 0.00 | 0.00 | 0.00 | 0.003 | 0.00 |
| 0.097 | Sm | 0.000 | 0.000 | 0.000 | 0.000 | 0.000 | 0.00 | 0.00 | 0.00 | 0.00 | 0.000 | 0.00 |
| 0.008 | Eu | 0.000 | 0.000 | 0.000 | 0.000 | 0.000 | 0.00 | 0.00 | 0.00 | 0.00 | 0.000 | 0.00 |
| 0.032 | Gd | 0.000 | 0.000 | 0.000 | 0.000 | 0.000 | 0.00 | 0.00 | 0.00 | 0.00 | 0.000 | 0.00 |
| 0.009 | Tb | 0.000 | 0.000 | 0.000 | 0.000 | 0.000 | 0.00 | 0.00 | 0.00 | 0.00 | 0.000 | 0.00 |
| 0.030 | Dy | 0.000 | 0.000 | 0.000 | 0.001 | 0.000 | 0.00 | 0.00 | 0.00 | 0.00 | 0.000 | 0.00 |
| 0.004 | Ho | 0.000 | 0.000 | 0.001 | 0.001 | 0.000 | 0.00 | 0.00 | 0.00 | 0.00 | 0.000 | 0.00 |
| 0.012 | Er | 0.000 | 0.000 | 0.003 | 0.005 | 0.000 | 0.00 | 0.00 | 0.00 | 0.00 | 0.001 | 0.00 |
| 0.002 | Tm | 0.000 | 0.000 | 0.000 | 0.001 | 0.000 | 0.00 | 0.00 | 0.00 | 0.00 | 0.000 | 0.00 |
| 0.022 | Yb | 0.000 | 0.000 | 0.000 | 0.002 | 0.000 | 0.00 | 0.00 | 0.00 | 0.00 | 0.000 | 0.00 |
| 0.003 | Lu | 0.000 | 0.000 | 0.000 | 0.000 | 0.000 | 0.00 | 0.00 | 0.00 | 0.00 | 0.000 | 0.00 |
| 0.03 | Hf | 0.00 | 0.00 | 0.08 | | 0.00 | 0.01 | 0.00 | 0.00 | 0.00 | 0.01 | 0.03 |
| 0.05 | Ta | 0.01 | 0.01 | 0.01 | | 0.01 | | 0.02 | 0.02 | 0.02 | 0.01 | 0.01 |
| 0.21 | Pb | 0.08 | 0.07 | 0.07 | 0.08 | 0.11 | 0.15 | 0.13 | 0.12 | 0.11 | 0.10 | 0.03 |
| 0.02 | Th | 0.66 | 1.01 | 0.11 | 0.04 | 0.35 | 0.97 | 0.31 | | 1.13 | 0.57 | 0.43 |
| 0.011 | U | 0.01 | 0.01 | 0.04 | 0.11 | 0.01 | 0.02 | 0.02 | 0.02 | 0.02 | 0.03 | 0.03 |

DL = detection limit.

| | K-feldspar | | | | Avg | SD |
|----|------------|---------|---------|---------|---------|---------|
| | k1 | k2 | k3 | k4 | | |
| Be | 0.58 | 0.85 | 2.15 | 1.77 | 1.34 | 0.74 |
| Mn | 2.15 | 2.44 | 1.33 | 1.72 | 1.91 | 0.49 |
| Co | 0.04 | 0.07 | 0.03 | 0.01 | 0.04 | 0.02 |
| Ni | 0.60 | 0.65 | 0.54 | 0.19 | 0.49 | 0.21 |
| Zn | 1.28 | 1.18 | 0.97 | 0.29 | 0.93 | 0.45 |
| Rb | 323.07 | 328.94 | 342.18 | 337.47 | 332.91 | 8.55 |
| Sr | 529.10 | 458.50 | 390.70 | 325.38 | 425.92 | 87.67 |
| Y | 0.07 | 0.56 | 0.14 | 0.10 | 0.21 | 0.23 |
| Zr | 2.05 | 5.52 | 5.23 | 1.16 | 3.49 | 2.21 |
| Nb | 0.10 | 0.13 | 0.04 | 0.05 | 0.08 | 0.04 |
| Cd | 0.06 | 0.04 | 0.02 | 0.04 | 0.04 | 0.02 |
| Ba | 4104.54 | 3186.51 | 1552.54 | 1134.56 | 2494.54 | 1391.38 |
| La | 1.76 | 1.77 | 1.58 | 1.49 | 1.65 | 0.14 |
| Ce | 1.41 | 2.07 | 2.61 | 1.26 | 1.84 | 0.62 |
| Pr | 0.07 | 0.17 | 0.12 | 0.12 | 0.12 | 0.04 |
| Nd | 0.14 | 0.72 | 0.46 | 0.44 | 0.44 | 0.24 |
| Sm | 0.02 | 0.17 | 0.08 | 0.06 | 0.08 | 0.06 |
| Eu | 1.21 | 1.07 | 0.93 | 0.75 | 0.99 | 0.19 |
| Gd | 0.02 | 0.14 | 0.05 | 0.04 | 0.06 | 0.05 |
| Tb | 0.00 | 0.02 | 0.00 | 0.00 | 0.01 | 0.01 |
| Dy | 0.01 | 0.09 | 0.02 | 0.02 | 0.03 | 0.04 |
| Ho | 0.00 | 0.01 | 0.00 | 0.00 | 0.00 | 0.01 |
| Er | 0.00 | 0.04 | 0.02 | 0.00 | 0.02 | 0.02 |
| Tm | 0.00 | 0.01 | 0.00 | 0.00 | 0.00 | 0.00 |
| Yb | 0.00 | 0.03 | 0.02 | 0.01 | 0.01 | 0.01 |
| Lu | 0.00 | 0.01 | 0.00 | 0.00 | 0.00 | 0.00 |
| Hf | 0.09 | 0.13 | 0.14 | 0.03 | 0.10 | 0.05 |
| Ta | 0.04 | 0.04 | 0.03 | 0.03 | 0.04 | 0.01 |
| Pb | 121.45 | 107.57 | 121.25 | 115.96 | 116.56 | 6.51 |
| Th | 0.14 | 0.16 | 0.23 | 0.07 | 0.15 | 0.07 |
| U | 0.10 | 0.28 | 0.25 | 0.83 | 0.36 | 0.32 |

| | Plagioclase | | | | Excluded from calculation | | |
|----|-------------|--------|--------|--------|---------------------------|--------|--------|
| | p1 | p2 | Avg | SD | p3 | p4 | p5 |
| Be | 19.66 | 23.66 | 21.66 | 2.83 | 17.25 | 18.36 | 22.67 |
| Mn | 77.23 | 33.80 | 55.52 | 30.71 | 47.62 | 40.88 | 56.09 |
| Co | 2.29 | 0.92 | 1.61 | 0.97 | 1.28 | 0.77 | 1.54 |
| Ni | 2.90 | 1.35 | 2.12 | 1.10 | 3.29 | 2.22 | 2.33 |
| Zn | 18.12 | 7.98 | 13.05 | 7.17 | 10.68 | 6.73 | 12.87 |
| Rb | 268.20 | 46.29 | 157.25 | 156.91 | 154.30 | 101.40 | 90.50 |
| Sr | 499.30 | 500.80 | 500.05 | 1.06 | 524.90 | 606.90 | 512.70 |
| Y | 0.13 | 0.16 | 0.15 | 0.02 | 0.66 | 0.57 | 5.25 |
| Zr | 16.53 | 3.90 | 10.21 | 8.93 | 14.43 | 6.36 | 293.40 |
| Nb | 9.51 | 1.60 | 5.55 | 5.59 | 0.24 | 1.77 | 1.47 |
| Cd | 0.07 | 0.04 | 0.06 | 0.02 | 0.10 | 0.03 | 0.11 |
| Ba | 213.10 | 57.97 | 135.54 | 109.69 | 104.40 | 111.10 | 72.53 |
| La | 20.43 | 27.00 | 23.72 | 4.65 | 213.50 | 326.80 | 54.60 |
| Ce | 36.29 | 40.69 | 38.49 | 3.11 | 283.30 | 356.50 | 129.40 |
| Pr | 3.94 | 5.47 | 4.71 | 1.09 | 40.92 | 51.38 | 10.52 |
| Nd | 11.22 | 13.24 | 12.23 | 1.43 | 125.50 | 159.00 | 34.09 |
| Sm | 0.57 | 0.88 | 0.73 | 0.22 | 6.80 | 8.76 | 3.22 |
| Eu | 0.60 | 0.84 | 0.72 | 0.17 | 1.12 | 1.32 | 1.05 |
| Gd | 0.59 | 0.57 | 0.58 | 0.01 | 4.45 | 5.88 | 2.33 |
| Tb | 0.02 | 0.03 | 0.024 | 0.01 | 0.18 | 0.25 | 0.22 |
| Dy | 0.03 | 0.05 | 0.037 | 0.01 | 0.27 | 0.28 | 1.05 |
| Ho | 0.00 | 0.00 | 0.004 | 0.00 | 0.03 | 0.03 | 0.21 |
| Er | 0.03 | 0.03 | 0.027 | 0.00 | 0.17 | 0.25 | 0.61 |
| Tm | 0.00 | 0.00 | 0.001 | 0.00 | 0.01 | 0.01 | 0.10 |
| Yb | 0.01 | 0.00 | 0.007 | 0.01 | 0.03 | 0.03 | 0.80 |
| Lu | 0.00 | 0.00 | 0.001 | 0.00 | 0.00 | 0.00 | 0.12 |
| Hf | 0.95 | 0.20 | 0.58 | 0.53 | 0.63 | 0.19 | 7.68 |
| Ta | 0.09 | 0.02 | 0.05 | 0.05 | 0.02 | 0.18 | 0.03 |
| Pb | 62.66 | 58.04 | 60.35 | 3.27 | 78.75 | 78.32 | 76.86 |
| Th | 4.90 | 1.34 | 3.12 | 2.52 | 14.98 | 8.14 | 21.04 |
| U | 1.97 | 1.35 | 1.66 | 0.44 | 10.26 | 10.11 | 8.87 |

inclusions of Mnz, Ap?

| | Biotite | | | Avg | SD |
|----|----------|----------|----------|---------|--------|
| | B1 | B2 | B3 | | |
| Be | 4.481 | 5.162 | 4.468 | 4.70 | 0.40 |
| Mn | 1357.579 | 1380.579 | 1358.579 | 1365.58 | 13.00 |
| Co | 24.955 | 24.765 | 23.835 | 24.52 | 0.60 |
| Ni | 109.12 | 119.72 | 117.52 | 115.45 | 5.59 |
| Zn | 259.247 | 263.847 | 256.847 | 259.98 | 3.56 |
| Rb | 828.107 | 756.107 | 633.507 | 739.24 | 98.39 |
| Sr | 1.395 | 1.844 | 1.951 | 1.73 | 0.30 |
| Y | 0.053 | 4.416 | 4.036 | 2.84 | 2.42 |
| Zr | 0.915 | 2.243 | 0.567 | 1.24 | 0.88 |
| Nb | 91.419 | 95.239 | 124.999 | 103.89 | 18.38 |
| Cd | 0.079 | 0.096 | 0.005 | 0.06 | 0.05 |
| Ba | 1114.197 | 1186.197 | 1458.197 | 1252.86 | 181.43 |
| La | 0.031 | 0.801 | 0.901 | 0.58 | 0.48 |
| Ce | 0.03 | 2.372 | 2.756 | 1.72 | 1.48 |
| Pr | 0.001 | 0.623 | 0.568 | 0.40 | 0.34 |
| Nd | 0.003 | 3.189 | 3.232 | 2.14 | 1.85 |
| Sm | 0.001 | 1.139 | 1.017 | 0.72 | 0.62 |
| Eu | 0.054 | 0.103 | 0.132 | 0.10 | 0.04 |
| Gd | 0 | 0.915 | 0.918 | 0.61 | 0.53 |
| Tb | 0 | 0.139 | 0.124 | 0.09 | 0.08 |
| Dy | 0.002 | 0.733 | 0.695 | 0.48 | 0.41 |
| Ho | 0.001 | 0.134 | 0.141 | 0.09 | 0.08 |
| Er | 0.004 | 0.281 | 0.282 | 0.19 | 0.16 |
| Tm | 0 | 0.037 | 0.034 | 0.02 | 0.02 |
| Yb | 0.001 | 0.243 | 0.186 | 0.14 | 0.13 |
| Lu | 0.001 | 0.028 | 0.025 | 0.02 | 0.01 |
| Hf | 0.115 | 0.141 | 0.028 | 0.09 | 0.06 |
| Ta | 6.912 | 9.562 | 14.066 | 10.18 | 3.62 |
| Pb | 2.832 | 3.554 | 3.959 | 3.45 | 0.57 |
| Th | 0.076 | 0.709 | 0.534 | 0.44 | 0.33 |
| U | 0.027 | 0.133 | 0.086 | 0.08 | 0.05 |

Appendix 4

Trace-element composition of the whole-rock, individual rock-forming and accessory minerals determined by the ICP-MS technique (ppm).

| ppm | WR | | Qtz | | Qtz | | Kfs | | Kfs | | Pl | | Pl | | Bt | | Bt | | Ms | | Kln | | Ilm | | Ttn | | Ap | | Mgt | | Mnz | | Zrn | | Rt | | | | |
|-----|------------------|-----------------|-------|---------|---------|--------|--------|---------|---------|---------|-------|---------|----------|---------|---------|----------|---------------------|----------|-----|----|-----|----|-----|----|-----|----|-----|----|-----|----|-----|----|-----|----|-----|----|--|--|--|
| | wet ¹ | LA ² | wet | LA | wet | LA | wet | LA | wet | LA | wet | LA | wet | LA | wet | LA | wet | LA | wet | LA | wet | LA | wet | LA | wet | LA | wet | LA | wet | LA | wet | LA | wet | LA | wet | LA | | | |
| Rb | 266.56 | 0.09 | 11.71 | 536.58 | 332.91 | 157.25 | 101.71 | 739.24 | 1179.96 | 617.99 | 45.16 | 14.78 | 1.92 | 0.55 | 19.75 | 3.88 | 25.72 | 0.63 | | | | | | | | | | | | | | | | | | | | | |
| Sr | 387.27 | 0.11 | 27.19 | 458.72 | 425.92 | 500.05 | 520.24 | 1.73 | 14.74 | 178.81 | 14.66 | 12.58 | 34.11 | 150.48 | 14.81 | 103.73 | 46.38 | 31.03 | | | | | | | | | | | | | | | | | | | | | |
| Ba | 1122.41 | 0.34 | 52.77 | 2852.66 | 2494.54 | 135.54 | 764.91 | 1252.86 | 1058.16 | 1114.74 | 17.83 | 26.17 | 8.63 | 1.93 | 25.01 | 18.74 | 267.48 | 157.93 | | | | | | | | | | | | | | | | | | | | | |
| Be | 10.38 | 0.06 | 1.08 | 5.53 | 1.34 | 21.66 | 21.35 | 4.70 | 5.50 | 7.40 | 9.90 | 4.81 | 6.61 | 1.40 | 2.76 | 25.40 | 97.00 | 1.92 | | | | | | | | | | | | | | | | | | | | | |
| U | 9.61 | 0.03 | 3.01 | 2.99 | 0.36 | 1.66 | 5.08 | 0.08 | 29.02 | 59.31 | 1.80 | 100.40 | 116.40 | 24.73 | 32.82 | 403.65 | 489.30 | 620.25 | | | | | | | | | | | | | | | | | | | | | |
| Th | 24.36 | 0.57 | 8.28 | 6.45 | 0.15 | 3.12 | 13.42 | 0.44 | 69.99 | 485.63 | 6.09 | 72.80 | 346.15 | 7.32 | 113.40 | 3836.40 | 950.53 | 2158.54 | | | | | | | | | | | | | | | | | | | | | |
| Pb | 63.28 | 0.10 | 5.59 | 124.73 | 116.56 | 60.35 | 56.10 | 3.45 | 23.41 | 50.69 | 84.00 | 352.15 | 315.93 | 54.30 | 75.60 | 1101.00 | 150.00 | 315.52 | | | | | | | | | | | | | | | | | | | | | |
| Zr | 169.91 | 0.22 | 56.83 | 65.16 | 3.49 | 10.21 | 96.48 | 1.24 | 647.91 | 687.74 | 78.37 | 1574.23 | 10081.73 | 1.20 | 980.73 | 10086.73 | 453122 ³ | 44550.43 | | | | | | | | | | | | | | | | | | | | | |
| Hf | 5.46 | 0.01 | 1.82 | 2.05 | 0.10 | 0.58 | 3.10 | 0.09 | 21.72 | 25.72 | 3.73 | 48.69 | 278.46 | 0.66 | 30.50 | 307.86 | 16010 ³ | 1361.33 | | | | | | | | | | | | | | | | | | | | | |
| Nb | 16.04 | 0.01 | 1.02 | 1.36 | 0.08 | 5.55 | 2.94 | 103.89 | 178.97 | 47.20 | 7.45 | 79.26 | 39.74 | 0.13 | 35.69 | 35.31 | 3288.90 | 4675.19 | | | | | | | | | | | | | | | | | | | | | |
| Ta | 1.66 | 0.01 | 0.10 | 0.28 | 0.04 | 0.05 | 0.61 | 10.18 | 18.18 | 19.83 | 2.36 | 13.08 | 9.09 | 0.05 | 6.32 | 4.97 | 425.15 | 484.02 | | | | | | | | | | | | | | | | | | | | | |
| La | 24.85 | 0.00 | 6.74 | 5.98 | 1.65 | 23.72 | 17.35 | 0.58 | 41.20 | 1078.53 | 34.07 | 726.72 | 3555.57 | 424.51 | 1088.71 | 26574.30 | 496.37 | 1861.82 | | | | | | | | | | | | | | | | | | | | | |
| Ce | 48.38 | 0.01 | 13.29 | 10.75 | 1.84 | 38.49 | 31.08 | 1.72 | 98.37 | 1593.25 | 83.38 | 1325.86 | 8572.95 | 1158.43 | 1918.03 | 44278.88 | 1138.86 | 2199.46 | | | | | | | | | | | | | | | | | | | | | |
| Pr | 5.37 | 0.00 | 1.47 | 1.23 | 0.12 | 4.71 | 3.20 | 0.40 | 12.36 | 177.72 | 9.92 | 141.69 | 1219.82 | 220.99 | 187.90 | 4676.15 | 120.19 | 519.95 | | | | | | | | | | | | | | | | | | | | | |
| Nd | 19.81 | 0.00 | 5.47 | 4.64 | 0.44 | 12.23 | 11.01 | 2.14 | 52.50 | 446.35 | 34.78 | 417.65 | 4961.41 | 1104.99 | 506.24 | 13148.31 | 446.92 | 2031.71 | | | | | | | | | | | | | | | | | | | | | |
| Sm | 3.47 | 0.00 | 0.98 | 0.90 | 0.08 | 0.73 | 1.67 | 0.72 | 12.06 | 37.75 | 8.84 | 51.27 | 1199.01 | 353.17 | 48.38 | 1278.54 | 82.09 | 282.37 | | | | | | | | | | | | | | | | | | | | | |
| Eu | 0.89 | 0.00 | 0.11 | 1.19 | 0.99 | 0.72 | 1.12 | 0.10 | 0.70 | 2.71 | 0.64 | 3.23 | 52.55 | 18.27 | 1.92 | 40.79 | 6.92 | 7.38 | | | | | | | | | | | | | | | | | | | | | |
| Gd | 2.66 | 0.00 | 0.79 | 0.76 | 0.06 | 0.58 | 1.46 | 0.61 | 9.37 | 33.80 | 7.03 | 30.68 | 633.40 | 221.64 | 31.35 | 732.12 | 65.78 | 201.21 | | | | | | | | | | | | | | | | | | | | | |
| Tb | 0.31 | 0.00 | 0.10 | 0.09 | 0.01 | 0.02 | 0.16 | 0.09 | 1.28 | 4.76 | 1.45 | 3.44 | 107.44 | 38.17 | 3.46 | 62.70 | 9.70 | 18.59 | | | | | | | | | | | | | | | | | | | | | |
| Dy | 1.41 | 0.00 | 0.50 | 0.47 | 0.03 | 0.04 | 0.73 | 0.48 | 6.63 | 9.27 | 6.48 | 16.46 | 531.87 | 200.26 | 15.20 | 217.73 | 60.58 | 76.40 | | | | | | | | | | | | | | | | | | | | | |
| Ho | 0.24 | 0.00 | 0.09 | 0.09 | 0.00 | 0.00 | 0.13 | 0.09 | 1.18 | 1.48 | 0.84 | 2.76 | 86.80 | 35.36 | 2.69 | 32.37 | 15.22 | 15.27 | | | | | | | | | | | | | | | | | | | | | |
| Er | 0.68 | 0.00 | 0.27 | 0.25 | 0.02 | 0.03 | 0.41 | 0.19 | 3.37 | 6.56 | 1.98 | 7.54 | 212.97 | 93.23 | 7.53 | 90.19 | 58.75 | 54.28 | | | | | | | | | | | | | | | | | | | | | |
| Tm | 0.09 | 0.00 | 0.04 | 0.04 | 0.00 | 0.00 | 0.05 | 0.02 | 0.46 | 0.51 | 0.21 | 0.92 | 25.52 | 11.83 | 0.87 | 9.66 | 10.83 | 8.78 | | | | | | | | | | | | | | | | | | | | | |
| Yb | 0.57 | 0.00 | 0.24 | 0.23 | 0.01 | 0.01 | 0.36 | 0.14 | 3.00 | 3.27 | 1.36 | 6.03 | 140.28 | 72.22 | 5.42 | 56.97 | 86.87 | 69.14 | | | | | | | | | | | | | | | | | | | | | |
| Lu | 0.08 | 0.00 | 0.04 | 0.03 | 0.00 | 0.00 | 0.05 | 0.02 | 0.41 | 0.41 | 0.16 | 0.87 | 14.81 | 9.30 | 0.79 | 6.37 | 16.32 | 12.16 | | | | | | | | | | | | | | | | | | | | | |
| Y | 6.65 | 0.01 | 2.46 | 2.43 | 0.21 | 0.15 | 3.76 | 2.84 | 33.98 | 33.32 | 16.61 | 78.31 | 2173.15 | 1173.80 | 69.54 | 839.34 | 447.34 | 398.70 | | | | | | | | | | | | | | | | | | | | | |
| Ni | 14.36 | 2.16 | 0.71 | 0.34 | 0.49 | 2.12 | 1.59 | 115.45 | 136.90 | 19.81 | 0.13 | 6.61 | 4.82 | 0.99 | 80.92 | 1.81 | 1252.13 | 2010.92 | | | | | | | | | | | | | | | | | | | | | |
| Zn | 39.69 | 0.39 | 0.53 | 1.73 | 0.93 | 13.05 | 6.19 | 259.98 | 471.14 | 99.10 | 3.08 | 90.73 | 95.48 | 14.21 | 40.96 | 92.83 | 497.63 | 458.62 | | | | | | | | | | | | | | | | | | | | | |
| Co | 3.52 | 0.01 | 0.13 | 0.19 | 0.04 | 1.61 | 0.50 | 24.52 | 32.95 | 5.34 | 0.29 | 6.49 | 11.05 | 0.27 | 10.01 | 2.47 | 58.26 | 1394.28 | | | | | | | | | | | | | | | | | | | | | |
| Cd | 0.11 | 0.05 | 0.05 | 0.04 | 0.04 | 0.06 | 0.08 | 0.06 | 0.57 | 4.00 | 0.13 | 2.47 | 4.73 | 1.05 | 3.83 | 5.21 | 75.11 | 40.01 | | | | | | | | | | | | | | | | | | | | | |

¹ – Mineral separates dissolved and analyzed in solution by ICP-MS technique. See text Appendix 1 for analytical details.

² – Averaged single-spot analyses as determined by the laser-ablation ICP-MS.

³ – Electron microprobe; too high to be determined by the ICP-MS.

In grey are shown analyses not taken into consideration. See text for discussion.

Appendix 5

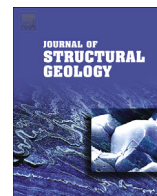
Typical electron-microprobe analyses of the zircon-like ABO₄-type phase (wt. % and apfu).

| | 1 | 2 | 3 | 4 | 5 | 6 |
|--------------------------------|---------------|---------------|---------------|---------------|---------------|---------------|
| SiO ₂ | 16.055 | 14.810 | 14.704 | 15.398 | 14.739 | 16.300 |
| TiO ₂ | 0.090 | n.d. | 0.087 | n.d. | 0.058 | 0.034 |
| Al ₂ O ₃ | 0.667 | 0.733 | 0.650 | 0.642 | 0.878 | 0.704 |
| FeO | 1.220 | 2.241 | 4.426 | 0.732 | 6.781 | 1.002 |
| MnO | 0.026 | 0.132 | 0.186 | 0.057 | 0.439 | 0.058 |
| MgO | 0.101 | 0.202 | 0.174 | 0.186 | 0.236 | 0.128 |
| CaO | 4.765 | 4.875 | 4.612 | 4.795 | 4.574 | 4.641 |
| K ₂ O | 0.137 | 0.091 | 0.098 | 0.086 | 0.095 | 0.218 |
| P ₂ O ₅ | 6.582 | 6.699 | 6.684 | 6.888 | 6.353 | 6.407 |
| SO ₂ | 0.149 | 0.241 | 0.202 | 0.188 | 0.198 | 0.172 |
| Sc ₂ O ₃ | 0.021 | 0.014 | 0.030 | 0.003 | 0.012 | 0.009 |
| As ₂ O ₃ | 0.479 | 0.332 | 0.285 | 0.264 | 0.362 | 0.483 |
| ZrO ₂ | 27.758 | 24.869 | 23.731 | 26.561 | 25.640 | 27.874 |
| HfO ₂ | 0.570 | 0.569 | 0.596 | 0.617 | 0.571 | 0.692 |
| Nb ₂ O ₅ | n.d. | 0.014 | 0.003 | 0.017 | n.d. | n.d. |
| SnO | 0.010 | n.d. | 0.029 | n.d. | 0.036 | 0.005 |
| PbO | 0.214 | 0.265 | 0.278 | 0.296 | 0.192 | 0.208 |
| UO ₂ | 1.278 | 1.106 | 1.179 | 1.208 | 1.240 | 1.033 |
| ThO ₂ | 31.947 | 32.353 | 31.751 | 35.250 | 29.028 | 31.265 |
| Ce ₂ O ₃ | 3.236 | 2.377 | 2.104 | 2.238 | 2.058 | 3.378 |
| SmO | 0.122 | 0.172 | 0.011 | 0.061 | 0.213 | 0.206 |
| Gd ₂ O ₃ | n.d. | n.d. | 0.169 | 0.210 | n.d. | 0.041 |
| Dy ₂ O ₃ | 0.170 | 0.119 | 0.042 | 0.067 | 0.371 | 0.181 |
| Er ₂ O ₃ | n.d. | n.d. | n.d. | n.d. | n.d. | n.d. |
| Yb ₂ O ₃ | 0.077 | 0.099 | n.d. | n.d. | n.d. | n.d. |
| Y ₂ O ₃ | 0.298 | 0.215 | 0.207 | 0.137 | 0.219 | 0.287 |
| F | 0.606 | 0.358 | 0.345 | 0.651 | 0.163 | 0.681 |
| Total | 96.578 | 92.886 | 92.583 | 96.552 | 94.456 | 96.007 |
| Si | 0.647 | 0.624 | 0.622 | 0.631 | 0.606 | 0.658 |
| Ti | 0.003 | 0.000 | 0.003 | 0.000 | 0.002 | 0.001 |
| Al | 0.032 | 0.036 | 0.032 | 0.031 | 0.043 | 0.034 |
| Fe | 0.041 | 0.079 | 0.156 | 0.025 | 0.233 | 0.034 |
| Mn | 0.001 | 0.005 | 0.007 | 0.002 | 0.015 | 0.002 |
| Mg | 0.006 | 0.013 | 0.011 | 0.011 | 0.014 | 0.008 |
| Ca | 0.206 | 0.220 | 0.209 | 0.210 | 0.201 | 0.201 |
| K | 0.007 | 0.005 | 0.005 | 0.004 | 0.005 | 0.011 |
| P | 0.225 | 0.239 | 0.239 | 0.239 | 0.221 | 0.219 |
| S | 0.006 | 0.010 | 0.008 | 0.007 | 0.008 | 0.007 |
| Sc | 0.001 | 0.001 | 0.001 | 0.000 | 0.000 | 0.000 |
| As | 0.012 | 0.008 | 0.007 | 0.007 | 0.009 | 0.012 |
| Zr | 0.546 | 0.511 | 0.489 | 0.530 | 0.514 | 0.549 |
| Hf | 0.007 | 0.007 | 0.007 | 0.007 | 0.007 | 0.008 |
| Nb | 0.000 | 0.000 | 0.000 | 0.000 | 0.000 | 0.000 |
| Sn | 0.000 | 0.000 | 0.001 | 0.000 | 0.001 | 0.000 |
| Pb | 0.002 | 0.003 | 0.003 | 0.003 | 0.002 | 0.002 |
| U | 0.011 | 0.010 | 0.011 | 0.011 | 0.011 | 0.009 |
| Th | 0.293 | 0.310 | 0.305 | 0.329 | 0.271 | 0.287 |
| Ce | 0.048 | 0.037 | 0.033 | 0.034 | 0.031 | 0.050 |
| Sm | 0.002 | 0.003 | 0.000 | 0.001 | 0.003 | 0.003 |
| Gd | 0.000 | 0.000 | 0.002 | 0.003 | 0.000 | 0.001 |
| Dy | 0.002 | 0.002 | 0.001 | 0.001 | 0.005 | 0.002 |
| Er | 0.000 | 0.000 | 0.000 | 0.000 | 0.000 | 0.000 |
| Yb | 0.001 | 0.001 | 0.000 | 0.000 | 0.000 | 0.000 |
| Y | 0.006 | 0.005 | 0.005 | 0.003 | 0.005 | 0.006 |
| F | 0.077 | 0.048 | 0.046 | 0.084 | 0.021 | 0.087 |
| site A | 0.921 | 0.917 | 0.909 | 0.914 | 0.886 | 0.929 |
| site B | 1.183 | 1.210 | 1.249 | 1.175 | 1.321 | 1.175 |

The EPMA results are recalculated on the basis of 4O *apfu*.

n.d. — not detected.

Site *B* includes Si, Al, P, As and S, the site *A* comprises all other elements (except F).



Magnetic fabric and modeled strain distribution in the head of a nested granite diapir, the Melechov pluton, Bohemian Massif



Jakub Trubač^{a, b, c, *}, Jiří Žák^d, Marta Chlupáčová^e, Vojtěch Janoušek^{a, b}

^a Czech Geological Survey, Klárov 3, Prague 11821, Czech Republic

^b Institute of Petrology and Structural Geology, Faculty of Science, Charles University, Albertov 6, Prague, 12843, Czech Republic

^c Institute of Geology, v.v.i., Academy of Sciences of the Czech Republic, Rozvojová 269, Prague, 16500, Czech Republic

^d Institute of Geology and Paleontology, Faculty of Science, Charles University, Albertov 6, Prague, 12843, Czech Republic

^e Boháčova 866, Prague, 14900, Czech Republic

ARTICLE INFO

Article history:

Received 15 January 2014

Received in revised form

14 May 2014

Accepted 26 May 2014

Available online 5 June 2014

Keywords:

Anisotropy of magnetic susceptibility (AMS)

Diapir

Emplacement

Fabric

Granite

Strain

ABSTRACT

The Melechov pluton, Bohemian Massif, is interpreted as a mid-crustal nested granitic diapir with an apical part exposed at the present-day erosion level. The diapir head exhibits a concentric structure defined by lithologic zoning and by the anisotropy of magnetic susceptibility (AMS). In concert with theoretical models, outward-dipping margin-parallel magnetic foliations are associated with oblate shapes of the susceptibility ellipsoids and higher degree of anisotropy, passing inward into weaker triaxial to prolate fabric. By contrast, magnetic fabric in an inner granite unit is in places oriented at a high angle to internal contacts and is interpreted as recording an internal diapir circulation. We use inverse modeling to calculate strain variations across the diapir from the AMS data. The magnetic fabric parameters and calculated strains are in agreement with strain distribution in heads of model Newtonian diapirs traveling a distance of two body radii and suggest granitic magma ascent as a crystal-poor suspension followed by crystallization of fabric markers and their response to strain near the final emplacement level. The intrusive fabric thus formed late but, though generally weak, was still capable of recording incremental strain gradient in the granite diapir.

© 2014 Elsevier Ltd. All rights reserved.

1. Introduction

Theoretical and analog models of salt, shale, and igneous diapirs have shown that their internal dynamics and strain patterns are largely governed by viscosity contrasts between the ascending fluid and its host, and by the travel distance of the diapir from its source region (e.g., Berner et al., 1972; Dixon, 1975; Marsh, 1982; Talbot and Jackson, 1987; Schmeling et al., 1988; Cruden, 1990; Weinberg and Podladchikov, 1994). These models have led to an idealized image of diapirs with predictions about their internal circulation, strain variations, and compositional zoning. A characteristic feature of the model diapirs is strain and associated fabric distribution where peripheral flattening in the diapir head passes inward to strongly constrictional diapir centers and tails (e.g., Bateman, 1984; Ramsay, 1989; England, 1990; Paterson and Fowler, 1993; Clemens, 1998; Kratinová et al., 2006). Natural examples,

however, may depart significantly from the theoretical models owing to rheological and temperature variations in the diapir and its host, multiple pulses of the ascending fluid passing through a single conduit, and variable imprint of tectonic deformation (e.g., Paterson and Vernon, 1995; Miller and Paterson, 1999).

One of the key issues for understanding the dynamics of diapiric intrusions in the Earth's crust is thus a quantitative comparison of theoretical models with the observed strain patterns. Unfortunately, natural diapirs lack reliable strain markers, as best exemplified by the rather problematic microgranular enclaves (see Paterson et al., 2004 for discussion), and exhibit mineral fabric that is a poor recorder of total strain experienced by the ascending fluid. Instead, granular and mineral fabrics in both salt and granites, respectively, are interpreted to record only late strain increments that postdate diapiric ascent (e.g., Talbot and Jackson, 1987; Paterson and Miller, 1998; Paterson et al., 1998). Still, a promising means for evaluating strain patterns in natural diapirs is the analysis of the anisotropy of magnetic susceptibility (AMS), allowing quantification of fabric parameters even in macroscopically isotropic rocks without strain markers.

* Corresponding author. Czech Geological Survey, Klárov 3, Prague, 11821, Czech Republic.

E-mail address: jakub.trubac@gmail.com (J. Trubač).

This paper explores the potential of the AMS technique for inferring strain patterns in granite diapirs (and in other types of intrusions as well) on the basis of data from the mid- to late-Carboniferous (Pennsylvanian) Melechov pluton, Bohemian Massif (Fig. 1), which is interpreted as a composite diapiric intrusion into mid-crustal migmatites. We first quantitatively characterize variations in magnetic fabric throughout the pluton and then use the AMS-to-strain inversion method of Ježek and Hrouda (2002, 2007) to infer the strain distribution in the proposed diapir head. Finally, we compare these data with theoretical models

for diapiric structures and discuss applicability of this method for strain analysis in granite plutons.

2. Geologic setting

2.1. Broader tectonic context

The Melechov pluton (radiometric age is poorly constrained between 318 ± 7 Ma and 313 ± 14 Ma, electron-microprobe (CHIME) U–Th–Pb dating on monazite; Breiter and Sulovský,

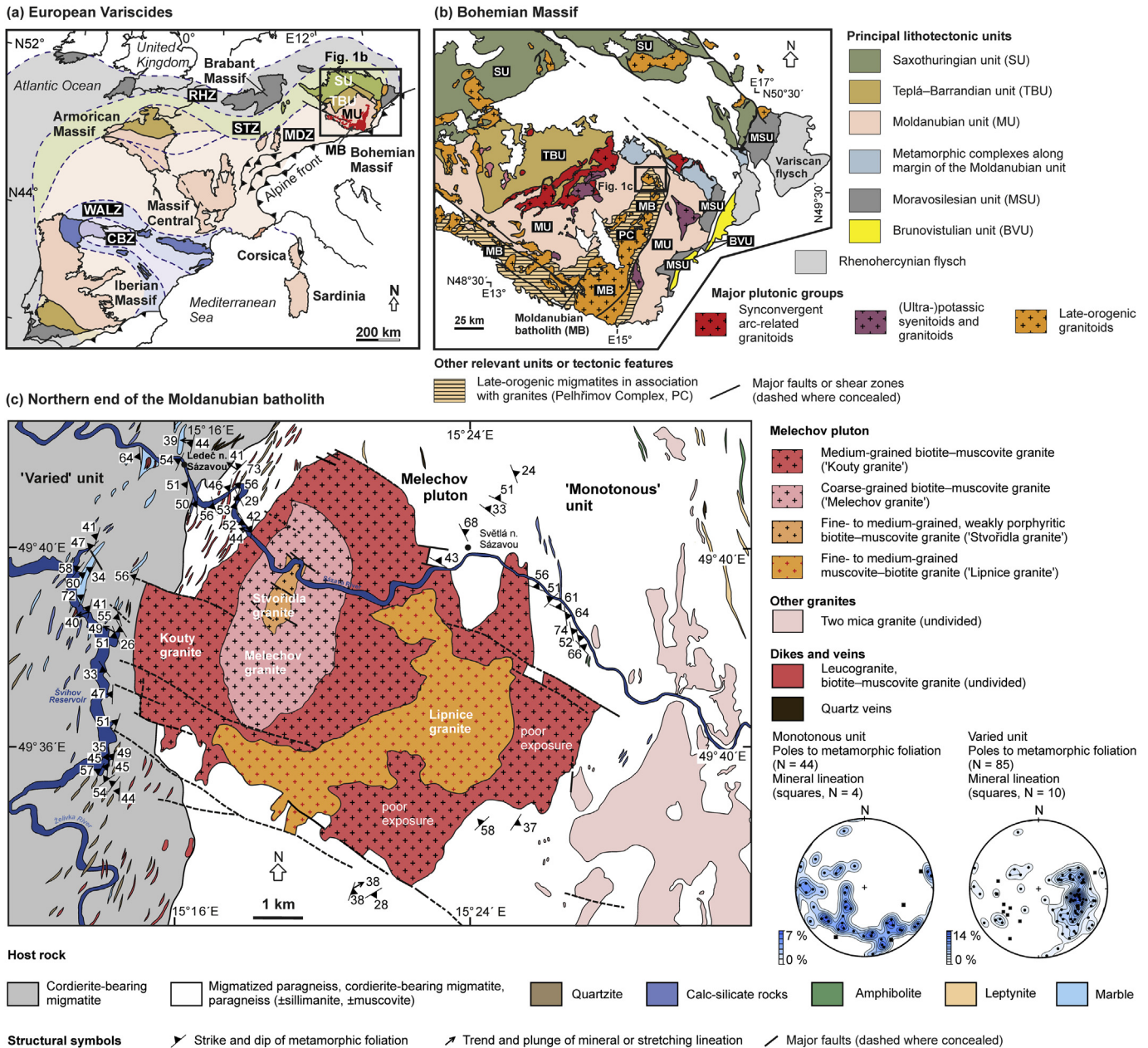


Fig. 1. (a) Geologic map showing basement outcrop areas and principal lithotectonic zones of the Variscan orogenic belt in Europe. Bohemian Massif is the easternmost inlier of the orogen, Moldanubian batholith (MB; highlighted in red) occupies its southern margin. Compiled from Winchester (2002), Asch (2003), and Martínez Catalán (2011). RHZ – Rhenohercynian Zone, STZ – Saxothuringian Zone, SU – Saxothuringian Unit, TBU – Teplá–Barrandian Unit, MDZ – Moldanubian Zone, MU – Moldanubian Unit, WALZ – West Asturian–Leonese Zone, CBZ – Cantabrian Zone. (b) Simplified geologic map of the interior Bohemian Massif emphasizing principal lithotectonic units and plutonic groups. The Pelhřimov core complex (PC) parallels the western edge of the underthrust Brunovistulian microplate. The Melechov pluton is the northernmost end of the complex. Compiled from Fušán et al. (1967) and Cháb et al. (2007). (c) Simplified geologic map of the Melechov pluton and its host rocks. Redrafted from Czech Geological Survey maps 1:50,000, sheets 23–12 Ledec nad Sázavou and 23–21 Havlíčkův Brod. Stereonets (equal area projection, lower hemisphere) show orientation of main structural elements. (For interpretation of the references to color in this figure legend, the reader is referred to the web version of this article.)

2005) makes up the northernmost end of the Moldanubian batholith (Fig. 1b), one of the largest granite complexes in the Variscan orogenic belt. The bulk of the eastern portion of the batholith formed during a short time span between ~330 and ~327 Ma (e.g., Gerdes et al., 2003; Bankwitz et al., 2004; Žák et al., 2011) and was recently interpreted as a NNE–SSW-elongated crustal-scale dome (Verner et al., 2014) that straddles along a side edge of an underthrust continental microplate (Schulmann et al., 2008). The dome consists of crustally-derived two mica granites in close association with migmatites and was interpreted as resulting from diapiric upwelling of hot and partially molten metapelitic middle crust (Verner et al., 2014; Žák et al., in press and references therein). In several locations along its axis, the granite–migmatite dome was pierced by smaller late-stage stocks, including the Melechov pluton (Fig. 1c), that are circular to weakly elliptical in plan view and vertically extensive as compared to the host granites and migmatites.

2.2. The three-dimensional shape of the Melechov pluton

In the map, the pluton has an irregular, weakly NW–SE-elongated outline, 14 × 10 km, that to some extent is modified by later brittle faults (Fig. 1c). The three-dimensional shape of the pluton at depth is fairly well constrained by a large body of existing geologic and gravimetric data (e.g., Procházka and Mlčoch, 1998; Breiter, 2007). On the Bouguer anomaly map, the pluton is associated with a pronounced gravity minimum as low as –44 mGal (Fig. 2), which is one of the most striking negative gravity anomalies in the Bohemian Massif (Blížkovský and Novotný, 1982). On the interpretive gravimetric cross-sections (Fig. 2b), the upper portion of the pluton is shown to dip outward at moderate angles, which is in agreement with Linsser indications (see Linsser, 1967; Šefara, 1973; Lenhardt et al., 2007 for principles of the method) pointing towards denser rocks and portraying strike and dip of the density boundaries down to a depth of 6 km (Fig. 2a). Deeper portions of the pluton are inferred as dipping steeply inward. Based on the gravity

data, the Melechov pluton can be traced to a depth of at least 14–16 km below the present-day erosion level (Mottlová, 1985; Hladík et al., 2006, Fig. 2b; c).

2.3. Internal zoning

The pluton consists of four granite units (Fig. 1c; Electronic Supplementary Material, Parts 1, 2), all peraluminous and derived from partial melting of a metasedimentary source with Sr–Nd isotopic signature similar to the Moldanubian paragneisses (Matějka and Janoušek, 1998; Harlov et al., 2008). The outer Kouty granite is medium-grained biotite–muscovite granite and is in contact with a southeasterly (off the pluton center) crescent-shaped body of the fine- to medium-grained muscovite–biotite Lipnice granite. In some places, the latter is foliated and rich in biotite schlieren and migmatite xenoliths (Staněk et al., 2013). The pluton center is occupied by an elliptical NE–SW-elongated body of the coarse-grained biotite–muscovite Melechov granite, which evolved separately from the remainder of the pluton (e.g., Mlčoch et al., 2000; Breiter and Sulovský, 2005) and encloses the innermost fine- to medium-grained, slightly porphyritic biotite–muscovite Stvořidla granite. Geochemical data suggest that the latter was derived from the Melechov granite through fractional crystallization (Mlčoch et al., 2000). Internal contacts are not exposed, thus the exact cross-cutting relations between component units remain unclear. Nevertheless, the overall concentric architecture of the pluton was also corroborated by previous unpublished structural and magnetic fabric studies (Schulmann et al., 1998; Blažiček, 2002; Staněk, 2013; unfortunately, values of the primary AMS data are not provided in these reports, precluding comparison with our new measurements).

2.4. Host rock

The host rock is dominated by metasedimentary rocks of the Moldanubian unit, a high-grade core of the Variscan orogen. The

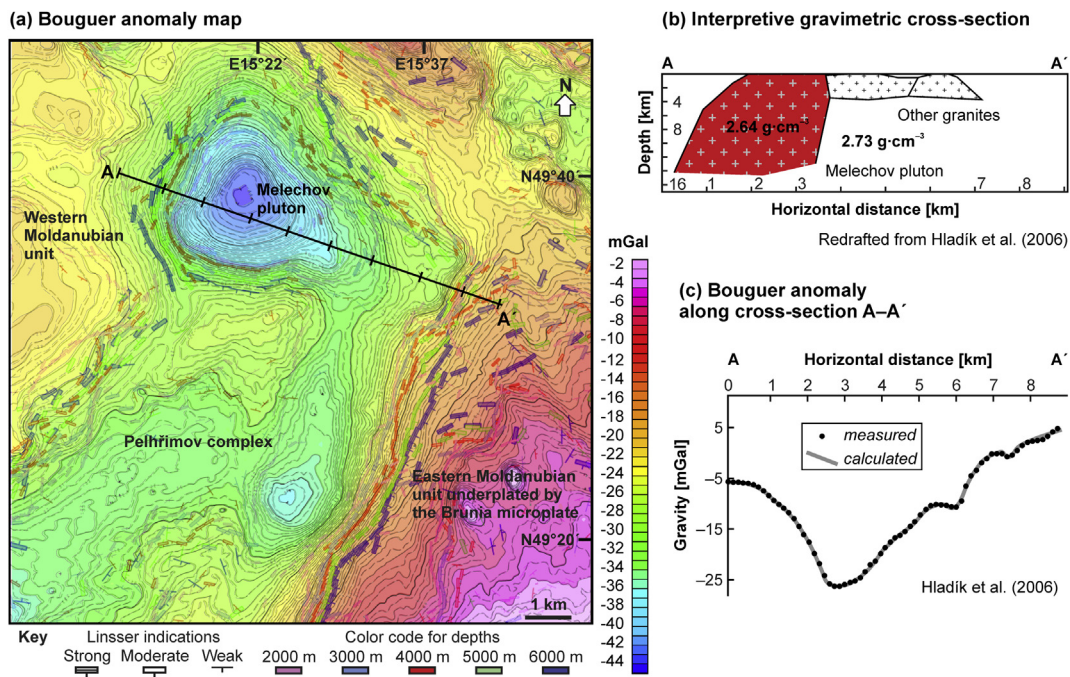


Fig. 2. (a) Bouguer gravity anomaly map of the Melechov pluton and its host rocks. Linsser indications portray principal density boundaries at different depths around the pluton and are consistent with its generally outward-dipping contacts. Map taken from Hladík et al. (2006), Linsser indications redrafted from Verner et al. (2014). (b) Gravimetric interpretation (cross-section) of the three-dimensional shape of the Melechov pluton at depth. (c) Measured and calculated Bouguer anomalies for each cross-section.

main portion of the pluton intruded variously migmatized paragneisses (\pm sillimanite, \pm muscovite) and cordierite-bearing migmatites with minor intercalations and lenses of quartzite and calc-silicate rocks, traditionally termed the 'Monotonous' unit (Fig. 1c). To the west, the pluton intruded cordierite-bearing migmatites which contain more abundant lenses of marble, calc-silicate rocks, amphibolites, and quartzites, collectively referred to as the 'Varied' unit (Fig. 1c). The existing pressure–temperature estimations from contact-metamorphic assemblages indicate temperature of about 670–750 °C at the pluton/host rock contact and pressure of about 0.5 GPa (Schulmann et al., 1998), which would correspond to mid-crustal emplacement at a depth of about 17–18 km.

The pluton/host rock contacts are generally poorly exposed, so their true attitude is difficult to determine. However, the dominant metamorphic foliation around the pluton (where exposed) exhibits a contact-parallel, outward-dipping pattern (Fig. 1c) which is in agreement with gravimetric data, and with Linsser indications in particular (Fig. 2a). In detail, the eastern and western portions of the pluton's structural aureole differ in intrusive geometries, fabric orientation and symmetry, structural style, and degree of partial melting and its temporal relation to deformation. To the east, the host rock is dominated by stromatic to nebulitic migmatites. Fabric is mostly oblate and defined by compositional banding in migmatites, suggesting deformation synchronous with anatexis. As the pluton is approached, the migmatites become intensely folded and commonly alternate with granite sheets (Fig. 3a) or even grade into

larger bodies of anatectic granites. In contrast, the western portion of the aureole shows a lesser degree of partial melting and is characterized by presumably sharp, non-sheeted granite/host contact. Fabric is mostly solid-state, consists of equally developed foliation and lineation (Fig. 3b, c), and exhibits more homogeneous orientation (Fig. 1c). Mineral and stretching lineation is typically down-dip or slightly dip-oblique (Fig. 3b). This fabric is also associated with normal, west-side-down, pluton-up kinematics defined by asymmetric quartz–feldspar aggregates, quartz boudins, S–C mylonites (Fig. 3c), and asymmetric s-shaped cascading folds (Fig. 3d).

3. Magnetic fabric of the pluton

3.1. Methodology

As mesoscopic fabric in the granites is mostly weak and difficult to discern with the exception of some portions of the Lipnice granite (see example fabrics in Electronic Supplementary Material, Parts 1, 2), the anisotropy of magnetic susceptibility (AMS) is used to quantitatively characterize the magnetic fabric and its gradients in the Melechov pluton. A total of 86 oriented cores were sampled using a hand-held drill at 41 stations across the four granites of the pluton (Fig. 4; Electronic Supplementary Material, Parts 3–5). After cutting, these samples yielded 553 standard specimens of 10 cm³ in volume. The AMS was measured in low field (450 Am⁻¹) with a MFK1-A Kappabridge in the Laboratory of Rock Magnetism,

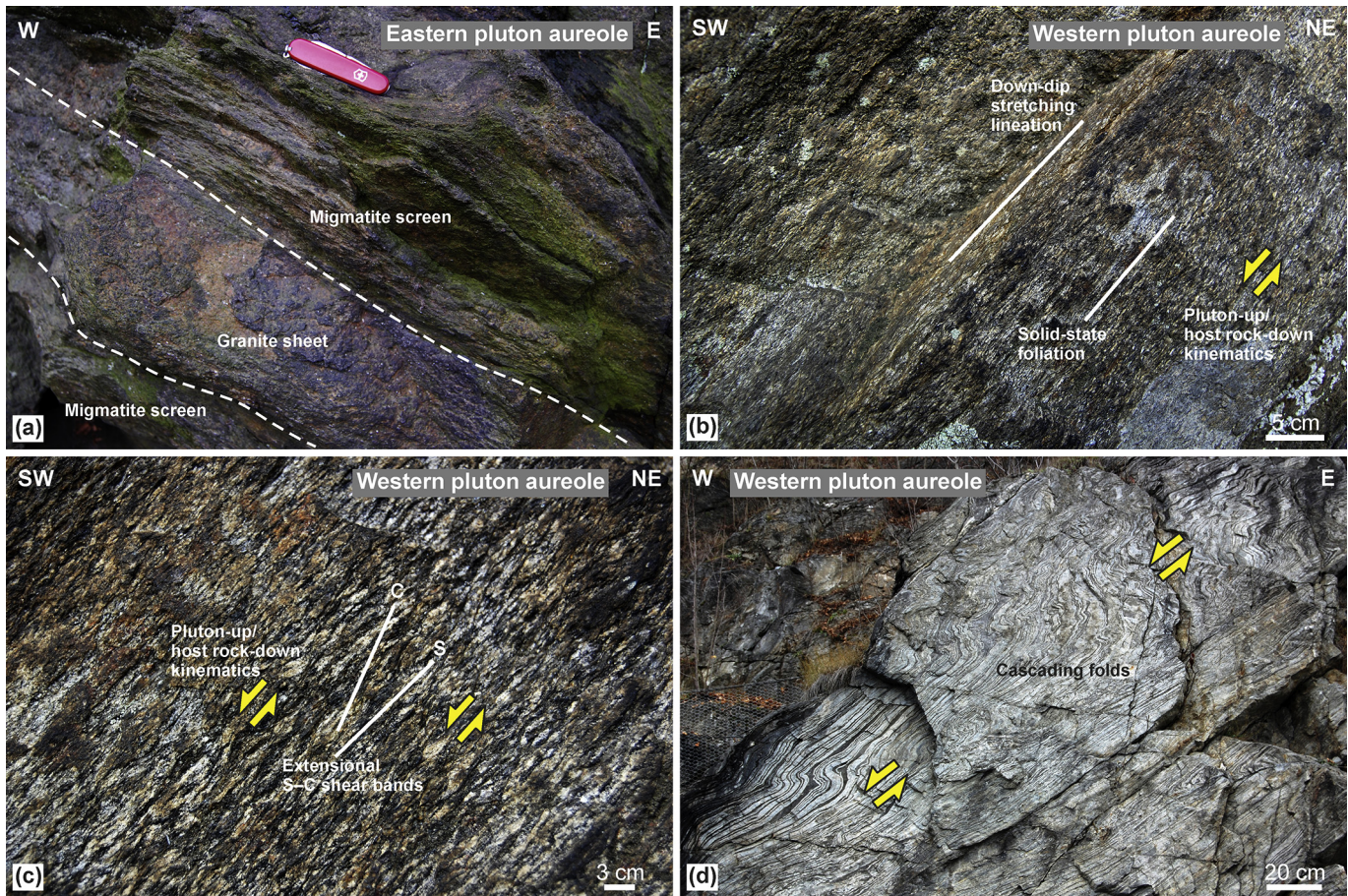


Fig. 3. Mesoscopic structures in the metamorphic host rocks around the Melechov pluton. (a) Close-up of an eastern contact of the pluton with outward-dipping granitic sheets intruding along banding in the host migmatites. Světlá nad Sázavou, GPS coordinates: N49°39.946', E15°23.510'. (b, c) Outward dipping solid-state fabric superposed on migmatized paragneiss and associated with pluton-up/host rock-down kinematics. South of Kozlí, GPS coordinates: N49°38.095', E15°14.947'. (d) Asymmetric minor folds in marbles, interpreted as cascading folds, consistent with pluton-up/host rock-down kinematics. Ledec nad Sázavou, GPS coordinates: N49°41.784', E15°16.868'.

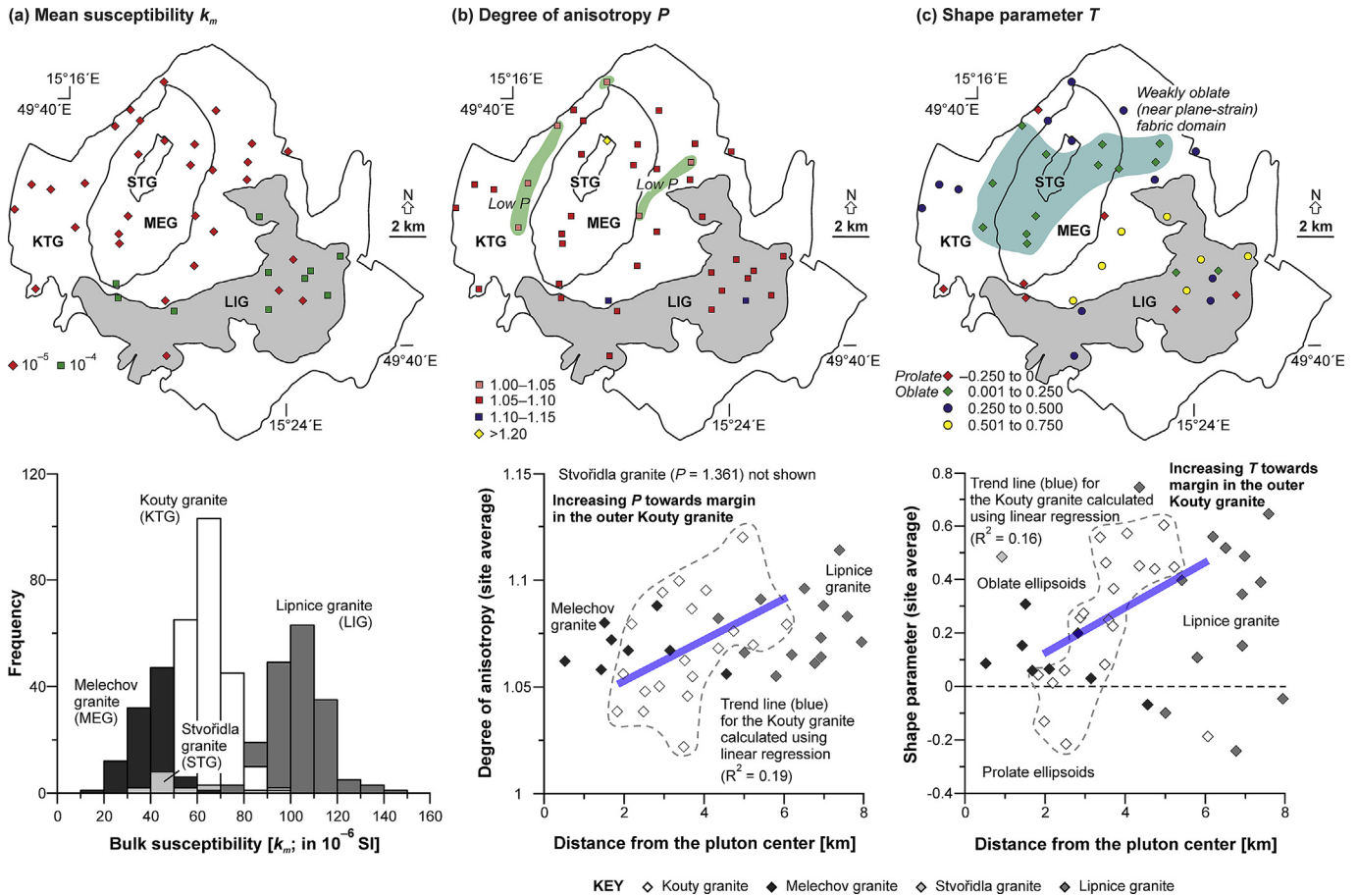


Fig. 4. Maps and graphs showing spatial distribution of the (a) mean susceptibility, (b) average degree of anisotropy, and (c) average shape parameter in the Melechov pluton. Gray lines (arrows) in the graphs show approximate spatial trends of magnetic fabric parameters in the outer Kouty granite. LIG – Lipnice granite, KTG – Kouty granite, MEG – Melechov granite, STG – Stvořidla granite.

Institute of Geology and Paleontology, Charles University in Prague. A statistical treatment and analysis of the AMS data was conducted using the ANISOFT 4.2 program package (www.agico.com). The measured data and parameters are presented in Figs. 4–7 and Electronic Supplementary Material (Parts 3–5).

The AMS data are represented by the k_m , P , and T parameters defined as follows: (1) $k_m = (k_1 + k_2 + k_3)/3$; (2) $P = k_1/k_3$; and (3) $T = 2\ln(k_2/k_3)/\ln(k_1/k_3) - 1$, where $k_1 \geq k_2 \geq k_3$ are the principal susceptibilities (e.g., Fig. 4). The parameter k_m represents the mean bulk magnetic susceptibility, which reflects the proportion and type of magnetic minerals in the analyzed rock. The parameter P (Nagata, 1961), called the degree of AMS, reflects the eccentricity of the AMS ellipsoid and may relate to the intensity of preferred orientation of magnetic minerals. The parameter T (Jelínek, 1981) characterizes the symmetry of the AMS ellipsoid. It varies from -1 (perfectly prolate ellipsoid) through 0 (triaxial ellipsoid) to $+1$ (perfectly oblate ellipsoid). In magnetic fabric studies, the maximum principal susceptibility (k_1) is referred to as the magnetic lineation and the minimum principal susceptibility (k_3) defines a pole to the magnetic foliation. Their orientations are presented in stereonets in the geographic (in situ) coordinate system and as locality mean values on the map.

3.2. Magnetic mineralogy

The bulk magnetic susceptibility of the measured specimens is on the order of 10^{-5} – 10^{-4} (Fig. 4a; SI units are used throughout this

paper), characteristic of paramagnetic granites (e.g., Hrouda and Kahan, 1991; Bouchez, 1997). A slight increase in the bulk susceptibility can be seen from the Melechov (19×10^{-6} – 67×10^{-6}) through Kouty (30×10^{-6} – 96×10^{-6}) to Lipnice granites (77×10^{-6} – 140×10^{-6} ; Fig. 4a). The bulk susceptibility of the Stvořidla granite is scattered and mostly overlaps with that of the other granites (39×10^{-6} – 7×10^{-6} ; Fig. 4a). These changes in bulk susceptibility for the different granites according to lithologic unit are also illustrated in the map of Fig. 4a.

To constrain the AMS carriers, we first calculated the maximum theoretical paramagnetic susceptibility (MTPS; Aydin et al., 2007; Hrouda, 2010) from representative analyses of Fe_2O_3 , FeO , and MnO (unpublished data of the authors) and then measured the variation of susceptibility with temperature (Fig. 5; Electronic Supplementary Material, Part 4). The calculated MTPS are 127×10^{-6} , 80×10^{-6} , and 74×10^{-6} for the Lipnice, Kouty, and Melechov granites, respectively. For the former two granites, the MTPS values correspond to the measured susceptibilities indicating that the AMS carriers are biotite and muscovite. For the Melechov granite, the MTPS is approximately two times higher than the measured susceptibility, indicating either the presence of a ferrimagnetic component (hematite–ilmenite) with greater Fe-content or greater proportion of diamagnetic quartz, decreasing the bulk susceptibility.

The variation of magnetic susceptibility with temperature was measured on 6 representative coarsely powdered specimens using a CS–3 Furnace and CS–L Cryostat instruments in the laboratory of Agico, Inc., Brno, Czech Republic. The magnetic susceptibility

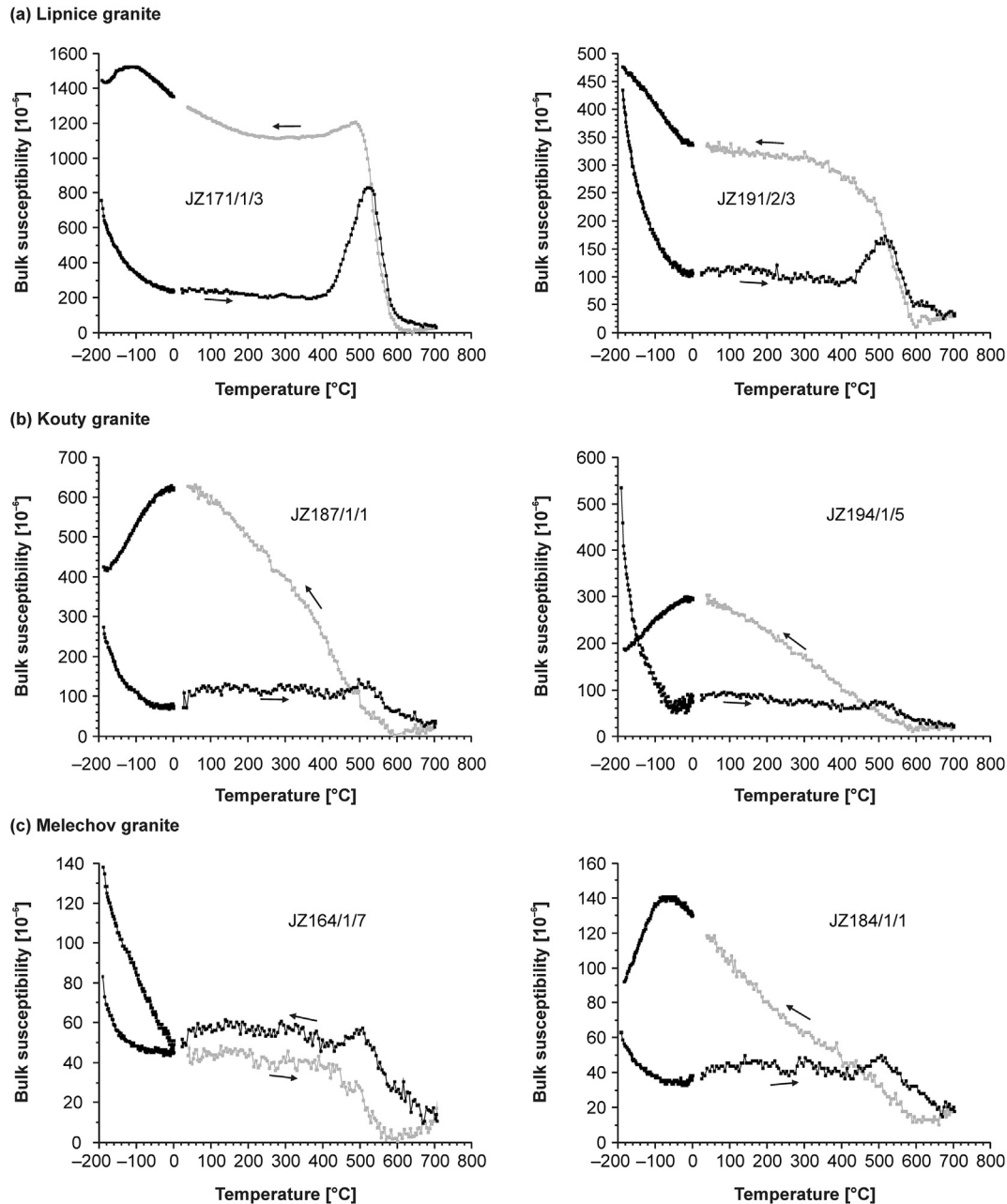


Fig. 5. Thermomagnetic curves for selected representative specimens from the Melechov pluton.

variations with temperature were measured in the temperature range of -196 °C to 0 °C and from room temperature to 700 °C (Fig. 5). Argon atmosphere was applied to avoid oxidation during heating, the heating rate was 10 °C per minute. The measured data were processed using the program Cureval8 (AGICO, Inc.).

In the temperature interval between -196 °C and 0 °C, the thermomagnetic curves are hyperbolic, which is typical of paramagnetic mineralogy (Fig. 5). At temperatures of 0 – 700 °C, however, the heating curves exhibit a susceptibility drop at around 550 – 580 °C and at 660 °C, indicating the presence of ferromagnetic admixtures. In detail, the shape of the heating curves also points to other complexities in magnetic mineralogy. The Lipnice granite (specimens JZ171/1/3, JZ191/2/2) differs from the other granites by a susceptibility increase above 400 °C, with a peak at around 500 °C and the T_C between 560 °C and 580 °C, suggesting growth of a

ferromagnetic mineral during heating. The variability in composition of ferromagnetic components can also be demonstrated for specimens JZ164/1/7 and JZ184/1/1 (the Melechov granite; Fig. 5c), which thermomagnetic curves show a susceptibility drop near room temperature that is consistent with the Morin transition of hematite.

The low-temperature k vs. T curves were measured twice. The first measurement was made prior to heating and the second was made after heating and cooling procedure. The second low-temperature measurement then reflects in some way new minerals created during heating and cooling. Without additional mineralogical analyses, however, it is difficult to determine the newly formed mineral species. Nevertheless, the lack of Verwey transition suggests that pure magnetite, except for the specimen JZ171/1/3, is not among the newly formed magnetic minerals.

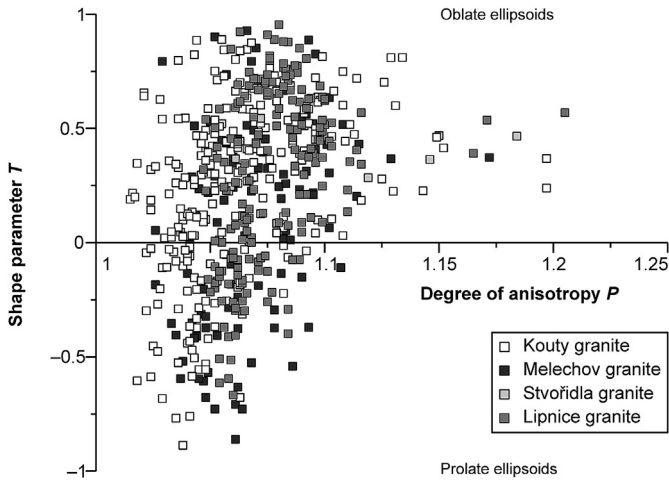


Fig. 6. Magnetic anisotropy P – T plot for all analyzed specimens from the Melechov pluton.

3.3. Magnetic fabric parameters and orientation

All four granites are characterized by low degree of anisotropy, not exceeding 1.2 (corresponding to 20% magnetic anisotropy) for most of the analyzed specimens (Fig. 6). The least anisotropic is the Kouty granite ($P = 1.015$ – 1.249 , two data outliers up to 1.495) with 40 % of the data having $P < 1.05$ (5% anisotropy) and most data not exceeding $P = 1.1$ (Fig. 6). Slightly more anisotropic is the Lipnice granite ($P = 1.047$ – 1.205 , 98 % of the data having $P > 1.05$; Fig. 6). The degree of anisotropy of the Melechov granite scatters more widely from 1.026 to 1.172 (Fig. 6). The greatest degree of anisotropy was measured in the Stvořidla granite ($P = 1.059$ – 1.361 , one outlier with $P = 5.101$). In contrast to the slight differences in the P parameter, the granites have similar

range of the shape parameter, which varies from highly prolate (T as low as -0.887) to highly oblate ($T = 0.955$ at most) and shows a distinct trend of increasing oblateness with increasing degree of anisotropy (Fig. 6).

Analysis of the map distribution of the P and T parameters in the pluton reveals that low-anisotropy, weakly oblate magnetic fabric occurs in domains along the internal contact between the Kouty and Melechov granites, passing outward into domains with slightly more anisotropic and strongly oblate fabric (Fig. 4b, c). Prolate fabrics are mostly localized near the outer pluton margin or internal contacts (Fig. 4c). The Lipnice granite exhibits less systematic spatial variations in the two parameters, with one domain of highly oblate fabrics in the north–central part of the intrusion (Fig. 4c).

In terms of orientation, the outer Kouty and Lipnice granites show margin-parallel magnetic foliations dipping outward at moderate to steep angles (Fig. 7a), well expressed on the stereonet as a broad circular band with several sub-maxima of foliation poles (k_3) about an vertical axis. On the map, both units display an ‘onion-skin’ foliation pattern (Fig. 7a). The exception to this overall trend are a few stations (JZ156, JZ173, JZ174, JZ177, JZ182, JZ187) with foliations at a high angle to the outer pluton margin or internal contacts (Fig. 7a). Magnetic lineations are mostly dip-oblique and follow a tangential pattern around the pluton (Fig. 7b). By contrast, only two stations (JZ164, JZ168) in the inner Melechov granite reveal margin-parallel, outward-dipping magnetic foliations, corresponding to the most prominent maximum of data points on the stereonet in Fig. 7, which are associated with variably oriented lineations (Fig. 7b). In the remainder of this granite, foliations are at a high angle to the internal contact, and display scattered maxima along the periphery of the stereonet (Fig. 7) and are associated with lineations plunging moderately from the south to the north (Fig. 7b). On the stereonet, the lineations thus define a girdle over ca. 180° of an arc (Fig. 7).

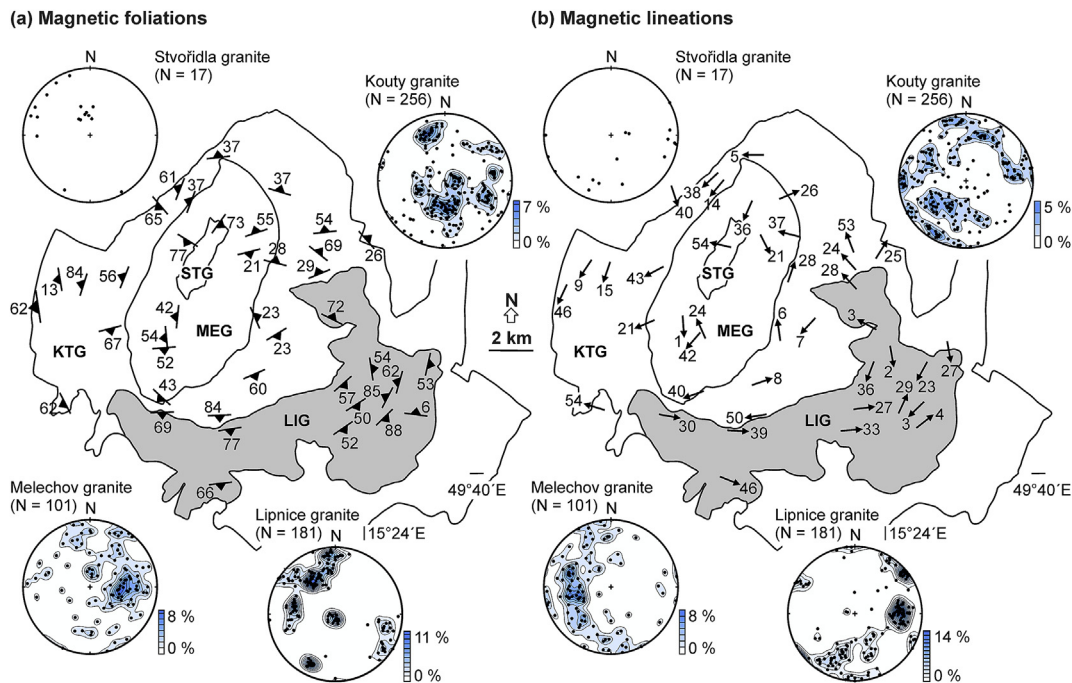


Fig. 7. Maps of (a) magnetic foliations and (b) magnetic lineations in the Melechov pluton. Stereonets (equal area, projection on lower hemisphere) show orientation of the minimum (k_3) and maximum (k_1) principal susceptibilities (i.e., poles to magnetic foliations and magnetic lineations, respectively). LIG – Lipnice granite, KTG – Kouty granite, MEG – Melechov granite, STG – Stvořidla granite.

4. Inverse strain calculation from magnetic fabric

To estimate strain recorded by the granitic magma and hence, determine strain distribution across the Melechov pluton, we used a method supported by a freely available Matlab program SUSIE developed by Ježek and Hrouda (2002, 2007), allowing an inverse strain calculation from the AMS data. This procedure yields the k and D parameters (Ramsay and Huber, 1983) at each station in the pluton. The k parameter reflects strain symmetry and is defined as $k = \ln(X/Y)/\ln(Y/Z)$, where X , Y , and Z represent the long, intermediate, and short semi-axes of the strain ellipsoid, respectively. For $0 < k < 1$ the strain is oblate (flattening), for $k = 1$ is triaxial, and for $1 < k < \infty$ is prolate (constrictional). The D parameter relates to strain intensity and is expressed as $D = \{[\ln(X/Y)]^2 + [\ln(Y/Z)]^2\}^{1/2}$.

The basic assumptions and input parameters for the modeling are: (1) The P and T parameters were taken as site-averaged values from the measured data (Electronic Supplementary Material, Part 3). (2) As the granites in question are paramagnetic and micas are the dominant carriers of the AMS, the modeled particle population consisted of biotite crystals with an axial ratio of 5, oblate magnetocrystalline anisotropy, and the P parameter of 1.3 (Zapletal, 1990; Martín-Hernández and Hirt, 2003). (3) The magmatic strains recorded by the AMS are assumed to be coaxial, which is in agreement with the lack of synmagmatic asymmetric structures associated with the measured fabrics. In addition, it should be noted that the differences in the k and D parameters for pure and simple shears are negligible for small strains (Ježek and Hrouda, 2007). (4) For each station in the pluton, we calculated three different models of initial particle orientation (Ježek and Hrouda, 2007): random (200 crystals), Sanderson–Marchini (156 crystals), and Ježek–Hrouda (160 crystals in most cases). The range of calculated values for the k and D parameters were small for all three types of initial particle orientation populations (Fig. 8c, d; Electronic Supplementary Material, Part 6). Given the similarity of the results, the analysis was then simplified to consider only the case for the random orientation population which is most consistent with undeformed rock fabric (Electronic Supplementary Material, Parts 1, 2).

Modeling the case with random orientations and considering the spatial distribution of the results across the granites of the pluton, the calculated k and D parameters (Electronic Supplementary Material, Part 6) reveal none or weak trends with respect to the distance from the pluton center (Fig. 8c, d, respectively), defined as the geometric center of the Stvořidla granite. However, a striking gradient in the k and D parameter emerges when only the outer and most voluminous Kouty granite, representing much of the pluton, is considered (Fig. 8e, f). In this granite, an outer zone near the pluton margin is characterized by stronger flattening strain ($k = 0.267–0.350$ for $D = 0.487–0.653$, respectively; Fig. 8), passing inward into a central domain of weak plane-strain to constriction ($k = 0.981–1.853$ for $D = 0.341–0.878$, respectively; Fig. 8). In the inner Melechov granite, the calculated strains are mostly constrictional, with the highest k (1.506–2.610) and D (0.483–0.623) parameters along the internal contact between the Melechov and Kouty granites and then decreasing inwards ($k = 0.959–1.262$ and $D = 0.448–0.560$; Fig. 8). The limited data set from the Stvořidla granite precludes a more rigorous assessment of the strain distribution. Nevertheless, the only analyzed station also corroborates overall constrictional strain in the pluton center ($k = 1.473$, $D = 3.010$; Fig. 8). In contrast, the Lipnice granite, forming a separate body off the pluton center, reveals more irregular variations in the calculated strains. This granite recorded predominantly oblate strains ($k = 0.103–0.727$) whereas plane-strain to constriction was calculated at several locations scattered across the granite ($k = 0.987–1.628$; Fig. 8). The

associated strain intensity D varies with no apparent spatial pattern from 0.408 to 0.861 (Fig. 8).

5. Discussion

5.1. Diapiric emplacement of the Melechov pluton

We favor diapiric emplacement of the Melechov pluton because: (1) An irregular, but more or less equant map outline in combination with the current gravimetric interpretation suggest a significant vertical extent and an overall inverted tear-drop shape of the pluton consisting of a cupola in the upper part, passing into a downward narrowing cone below ~5–6 km (Fig. 2b). (2) The crestal cupola is also defined by the generally outward-dipping pluton/host rock contacts and metamorphic foliation and compositional banding in the migmatites (Figs. 1c and 3). (3) The pluton reveals concentric compositional zoning (Fig. 1c), consistent with nested emplacement of at least three main magma batches, represented by the Kouty, Melechov, and Lipnice granites, completed by fractional crystallization of the innermost Stvořidla granite (Matějka and Janoušek, 1998; Mlčoch et al., 2000). (4) Widespread pluton-up/host rock-down kinematic indicators (Fig. 3c, d) are inferred to represent the structural result of downward return flow at the pluton aureole.

The measured AMS data are also inferred to lend a strong support to a model of diapiric emplacement. Below we first discuss the Kouty granite, which makes up the bulk of the pluton, and then the Lipnice and Melechov granites, which are smaller, 'second-order' intrusions inside the pluton (Fig. 1c). Foliations in the Kouty granite define a concentric, 'onion-skin' domal structure, suggesting that the present-day erosion surface intersects the head of the Melechov diapir. Assuming a simple AMS-to-strain relationship, the outward increasing degree of oblateness of the AMS ellipsoid in the Kouty granite (Fig. 4c) indicates syn-magmatic flattening of the pluton margin, passing into a broad central portion of the pluton that underwent near plane-strain (Fig. 4c). This transition in fabric symmetry is also linked to drop in the magnetic anisotropy from outer margin of the granite inward (Fig. 4b). Taken together, magnetic fabric orientation and spatial changes in fabric symmetry and intensity across the Kouty granite fit exceptionally well the theoretically predicted fabric parameters in igneous diapirs (e.g., Cruden, 1990).

Assuming model-consistent internal circulation driven by drag forces along the diapir margin, the theoretical models also postulate a characteristic evolution of internal compositional contacts from originally horizontal through vertical to increasingly complex geometries as a function of the diapir travel distance (e.g., Schmeling et al., 1988). In the Melechov pluton, examining fabric and internal contacts reveals two different kinds of relationship. First, the crescent-like shape of the off-center Lipnice granite generally parallels the concentric internal structure of the pluton (Fig. 1c). The same applies for magnetic fabric, which is roughly concordant with both the margin of this granite and with fabric in the adjacent Kouty granite (Fig. 7; Electronic Supplementary Material, Part 5). We interpret this fabric/contact relationship and the lack of fabric refraction as recording a single strain field during growth of the granite dome (diapir head).

Second, the inner Melechov granite shows a more complex fabric/contact relationship. Assuming that the granite pierced the center of the dome built by the Kouty granite as a steep-sided cylindrical intrusion (Mlčoch et al., 2000), one would expect significant strain in the surrounding magma and thus margin-parallel foliations both inside and outside the Melechov granite. This behavior should be theoretically accompanied by increasing degree of anisotropy in the Kouty host granite as the internal contact is

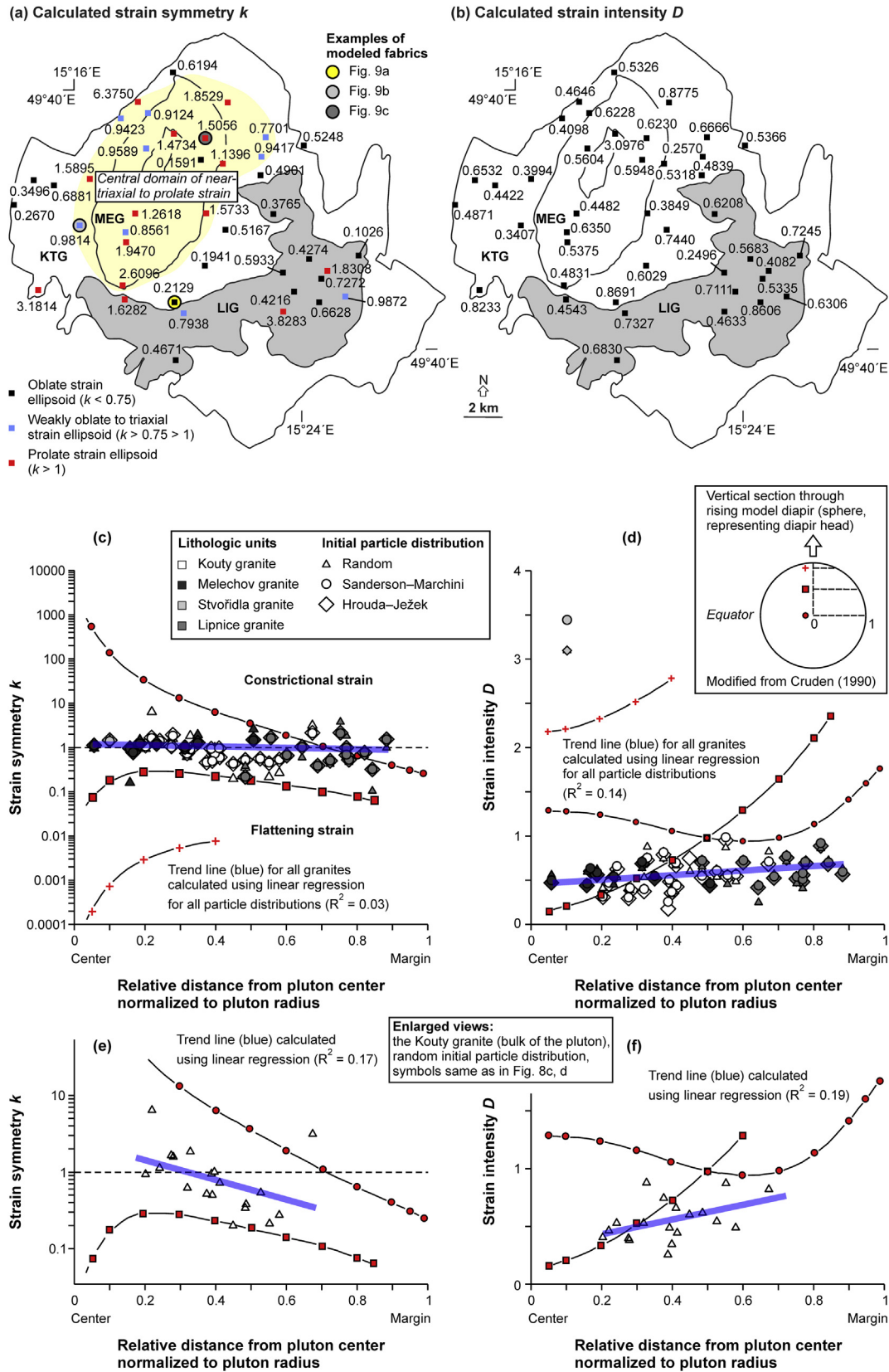


Fig. 8. Results of the inverse AMS-to-strain modeling using the Ježek–Hrouda method. Maps show spatial distribution of calculated (a) strain symmetry and (b) intensity at each station in the Melechov pluton (for random initial particle distribution). Graphs (c, d) show strain symmetry and intensity calculations from the Melechov pluton plotted against theoretically predicted values (red symbols) in an upper part of the model Newtonian diapir of Cruden (1990). Spatial trends in the calculated strain parameters in the outer Kouty granite highlighted by blue lines. Graphs (e, f) show highlighted symmetry and intensity calculations for random initial particle distribution (used in the interpretation). (For interpretation of the references to color in this figure legend, the reader is referred to the web version of this article.)

approached. Our AMS study reveals exactly the opposite, i.e., narrow zones of low-anisotropy (Fig. 4b) and fabrics oriented at a high angle to the internal contact in the Kouty granite (Fig. 7). An explanation for this disconnect between expectation and reality comes from understanding that fabrics oblique to or traversing internal boundaries are observed in many plutons and are interpreted to result from post-emplacement but still syn-magmatic tectonic overprint (e.g., Buddington, 1959; Cruden, 1990; Paterson and Vernon, 1995; Žák et al., 2007). However, for this explanation to apply, the fabric should be present in the pluton and the host rock, but for the Melechov granite, the fabric is confined to the granite, negating this explanation (Paterson et al., 1998). Another possible explanation for the fabric in the Melechov granite is provided from modeling by Cruden (1990) that showed that foliations may be discordant to internal contacts in central and lower parts of diapirs as a result of their internal fluid circulation.

5.2. Interpretation of strain gradients from the AMS

A striking feature of the granites in question is their weak magnetic anisotropy, mostly between 5 and 10% and decreasing to even less than 5% in two domains along the Kouty/Melechov internal contact (Figs. 4b and 6). Nevertheless, despite such small anisotropy magnitudes, the AMS mean directions are well defined on most stations (Electronic Supplementary Material, Part 5) and fabric parameters vary systematically across the pluton, particularly for the outer Kouty granite (Fig. 4). Furthermore, the trend of anisotropy decreasing inward is consistent with an inward strain decrease as predicted in theoretical models of diapirs (e.g., Ramsay, 1989; Cruden, 1990). The question thus arises of how to explain the small calculated magmatic strains in the context of the required large magnitude of magma flow and hence, expected large strains during diapiric ascent. We address this issue quantitatively using fabric-to-strain modeling based on the method of Ježek and Hrouda (2002) and, for the first time in the literature, we also explore the applicability of this method to strain estimation in granite plutons.

Though the thermomagnetic measurements indicate an admixture of Ti-hematite and hemoilmenite in the analyzed specimens, perhaps formed due to hydrothermal alteration and weathering (see also Procházka and Matějka, 2006), the AMS signal is clearly dominated by paramagnetic micas (Fig. 5). In the following, we thus consider micas as the primary particles defining the measured fabric pattern in the pluton.

The low fabric intensity observed in the Melechov pluton can be explained in two ways. First, the larger fraction ($\Phi = 20\text{--}50\%$) of mica crystals (either restitic from the source or newly grown) was already present in the melt before emplacement but fabric development was oscillatory as predicted by the Jeffery's theory of rigid particle rotation in viscous flow (e.g., Ježek et al., 1994; Arbaret et al., 2000; Jiang, 2007). In such a case, the flowing magma would go through transient periods of near-isotropic, low-intensity fabric periodically randomizing the earlier stronger fabric during ascent. However, we find this hypothesis unlikely because the magma would have to systematically freeze in the low-intensity fabric of the Jeffery's period across all the pluton without preserving any evidence for the high-intensity flow periods.

Alternatively, magma may have ascended a long distance as a crystal-poor, melt-dominated Newtonian suspension ($\Phi < 20\text{--}30\%$) and then crystallized near the final emplacement site, capturing only the latest strain increment at an inward-migrating crystallization front, and not the total strain. If the interpretation of the Newtonian crystal-poor magma is valid, the magmatic strains obtained from our fabric modeling can be directly compared with those modeled in the Newtonian diapirs, where strain is a function of position within the diapir and its travel

distance. Cruden (1990) examined diapirs traveling a distance of two, five, and ten body radii for a diapir/host viscosity contrast of 10^{-3} . Given that the diameter of the Melechov pluton is ~ 7 km, our strain estimations can be compared only with the first case (hereinafter referred to as the 'model diapir'; see also Fig. 4 in Cruden, 1990), corresponding to a feasible ~ 14 km travel distance through the crust.

Our AMS-to-strain calculations are consistent with Cruden's model, especially when the outer Kouty granite is considered and the random initial particle orientation distribution is assumed (Fig. 8e, f). The calculated strain symmetries (k) fall between those expected near the equator ($z = 0$) and those at a half ($z = 0.5$) of the upper hemisphere of the model diapir (Fig. 8c, e; note that the entire Cruden's sphere in fact represents a head of a diapir whereas what corresponds to a diapir tail is the region below the sphere). The same applies also for strain intensities (D) which increase towards the pluton margin (Fig. 8d, f). The D values, however, exhibit only a weak, approximately linear gradient and significantly smaller strain magnitudes at a distance of 0.3–0.7 body radii as compared to exponential gradient in the model diapir (Fig. 8d, f). All in all, these findings support the notion that magmatic fabrics in granites generally record (very) low magnitudes of late incremental strain (e.g., Benn, 1994; Paterson et al., 1998; Benn et al., 2001) but still may capture even subtle gradients in strain intensities and especially symmetries from the ascent stage.

5.3. Some methodological notes on strain estimation from fabric in granite plutons

As discussed above, the Ježek–Hrouda method is capable of determining intrusive strain variations even for very low degree of magnetic anisotropy ($P < 1.1$), which is a common feature of many paramagnetic granite plutons (e.g., Bouchez, 1997; Pueyo et al., 2004). Despite the differences in strain magnitude between the model diapir and values calculated from our AMS data (Fig. 8d, f), the approach of Ježek and Hrouda (2002) reveals an unexplored potential for estimation of strain gradients in granite plutons, which normally lack reliable strain markers (see, e.g., Hutton, 1988; Archanjo et al., 1995; Paterson et al., 2004; Sen et al., 2005; Sen and Mamtani, 2006 for discussions). Consequently, the method could be used in the future to discriminate among various pluton emplacement models and to quantify the relative contribution of magmatic and tectonic strains during emplacement.

On a grain-scale, the modeling also allows indirect estimation and visualization of the orientation distribution of mica crystals for various degrees of anisotropy and symmetries of the AMS and inferred strain ellipsoids (Fig. 9). The statistical characterization of the modeled grain populations is then included in the model through the P and T parameters, calculated from the magnetic susceptibility tensor which is directly related to the orientation tensor (e.g., Ježek and Hrouda, 2000, 2004). Importantly, the (pseudo-)hexagonal single mica crystals possess a highly oblate magnetocrystalline anisotropy, raising the question of how to directly relate the single-crystal AMS ellipsoid to the overall rock fabrics with different symmetries and low anisotropy. We consider our strain calculations from three stations to address this matter (Fig. 9). The stations were selected to illustrate the main end-member strain types across an ideal diapir from a strongly flattened margin to a vertically stretched center (e.g., Ramsay, 1989; Paterson and Fowler, 1993; Clemens, 1998). For a highly oblate rock fabric and inferred flattening strain (Fig. 9a), the modeled population of mica crystals with an initially random orientation distribution exhibits a clustered orientation distribution with the minimum susceptibility (k_3) axes laying close to the Z axis of the strain ellipsoid. As the strain symmetry moves towards the plane-

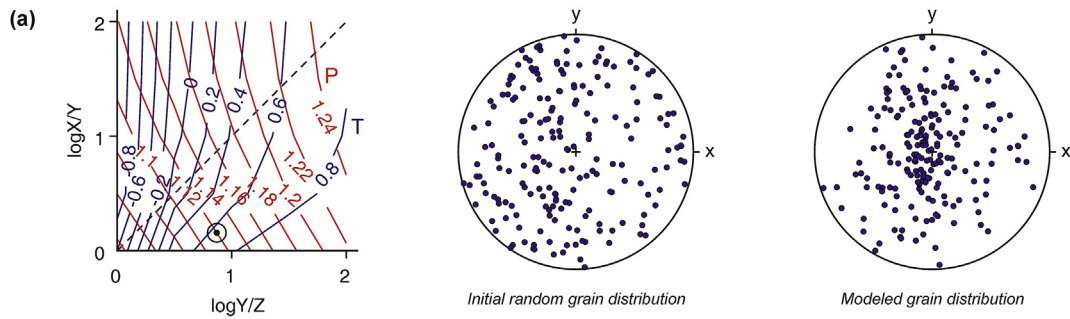
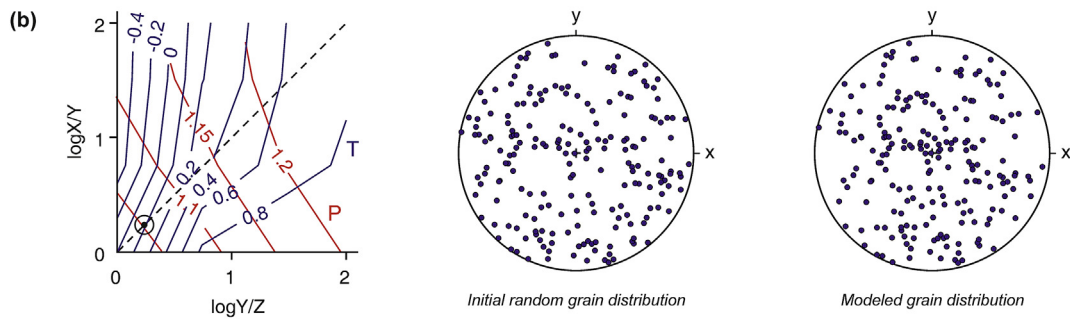
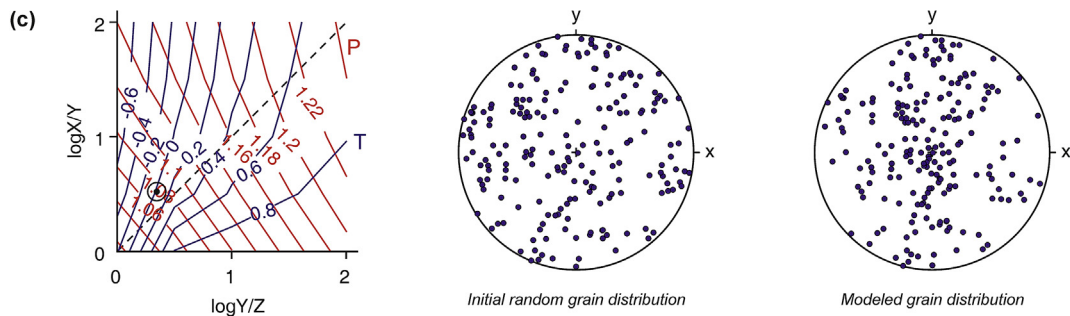
Flattening strain and modeled fabric near the pluton margin (Kouty granite, station JZ194)**Plane-strain and modeled fabric near the internal contact (Kouty granite, station JZ156)****Constrictional strain and modeled fabric in the pluton center (Melechov granite, station JZ186)**

Fig. 9. Examples of three crystal orientations modeled using the Ježek–Hrouda method for flattening strain (a), plane-strain (b), and constrictional strain (c). The modeled crystal orientations are calculated for random initial grain distribution and plotted on equal area, lower hemisphere stereonet. The coordinate system for the stereonet is the strain axes. Logarithmic Flinn plots show finite strains (circles) calculated for each example; X, Y, Z are semiaxes of the finite strain ellipsoid. Red and blue contours represent the degree of anisotropy (P) and shape parameter (T). (For interpretation of the references to color in this figure legend, the reader is referred to the web version of this article.)

strain and constrictional field, the crystals' orientation distribution evolves from scattered (Fig. 9b) to a girdle about the X axis of the strain ellipsoid (Fig. 9c). In other words, our modeling confirms that in regions where stretching dominates the crystallizing magma, such as in diapir centers and tails, particles with oblate magnetocrystalline anisotropy will reorient to define the overall prolate AMS ellipsoid and magnetic lineation (k_1) as the zone axis (Henry, 1997).

6. Conclusions

- (1) The Melechov pluton is interpreted as a mid-crustal vertically extensive granitic diapir with an apical part (diapir head) exposed at the present-day erosion level. The diapir head exhibits an overall concentric structure defined both by compositional zoning and magnetic fabric, and especially the latter is consistent with an idealized picture of igneous diapirs.
- (2) Margin-parallel, outward-dipping magnetic foliations are associated with oblate shapes of the susceptibility ellipsoids

and higher degree of anisotropy, passing inward into weaker triaxial to prolate fabric. Magnetic fabric of the inner Melechov granite, in places oriented at a high angle to the internal contacts and ductile host rock structures, is interpreted as recording the internal diapir circulation as predicted by theoretical models.

- (3) In terms of intensity and symmetry, the intrusive strain estimations from the AMS data using the Ježek–Hrouda method are in agreement with strain gradients in the heads of model Newtonian diapirs traveling a distance of two body radii, though magnitudes of the calculated strains are lower near the outer margin of the Melechov diapir. The low degree of anisotropy and calculated strain intensities across the diapir are consistent with granitic magma ascent as a dilute, crystal-poor suspension followed by crystallization of fabric markers and their response to strain near the final emplacement level. This mechanism explains why the generally weak intrusive fabrics may still be capable of recording the within-diapir strain gradient.

- (4) We conclude that the Ježek–Hrouda method has proven to be particularly useful for strain estimations from the AMS in granite plutons, which typically lack reliable strain markers. Future research could be directed towards comparing strain calculations against data obtained from microgranular enclaves or xenoliths, on comparing the modeled grain orientations with those of derived from some other independent method (e.g., image analysis, electron back-scatter diffraction), and examining strain variations for various pluton emplacement models.

Acknowledgments

We gratefully acknowledge two anonymous reviewers and Editor William M. Dunne for their detailed and constructive comments which helped to improve the original manuscript significantly. We also thank Josef Ježek, František Hrouda, Jan Švancara, Josef Šrámek, and Kryštof Verner for valuable discussions, and Jiří Sedlák for sharing gravimetric map of the pluton. Staff of the Hotel Stadion in Ledec nad Sázavou is thanked for hospitality during field work. This study is part of the Ph.D. research of Jakub Trubač. We acknowledge financial support from the Grant Agency of the Czech Republic through grants No. P210/11/1168 (to Jiří Žák) and from the Charles University in Prague Research Program PRVOUK P44.

Appendix A. Supplementary data

Supplementary data related to this article can be found at <http://dx.doi.org/10.1016/j.jsg.2014.05.015>.

References

- Arbaret, L., Fernandez, A., Ježek, J., Ildelfonse, B., Launeau, P., Diot, H., 2000. Analogue and numerical modelling of shape fabrics: application to strain and flow determination in magmas. *Trans. Royal Soc. Edinb. Earth Sci.* 90, 97–109.
- Archanjo, C.J., Launeau, P., Bouchez, J.L., 1995. Magnetic fabric vs. magnetite and biotite shape fabrics of the magnetite-bearing granite pluton of Gameleiras (Northeast Brazil). *Phys. Earth Planet. Inter.* 89, 63–75.
- Asch, K., 2003. The 1:5 Million International Geological Map of Europe and Adjacent Areas: Development and Implementation of a GIS-Enabled Concept. *Geologisches Jahrbuch, Sonderhefte*, A3. E. Schweizerbart'sche Verlagsbuchhandlung, Stuttgart.
- Aydın, A., Ferré, E.C., Aslan, Z., 2007. The magnetic susceptibility of granitic rocks as a proxy for geochemical differentiation: example from the Saruhan granitoids, NE Turkey. *Tectonophysics* 441, 85–95.
- Bankwitz, P., Bankwitz, E., Thomas, R., Wemmer, K., Kämpf, H., 2004. Age and depth evidence for pre-exhumation joints in granite plutons: fracturing during the early cooling stage of felsic rock. In: Cosgrove, J.W., Engelder, T. (Eds.), *The Initiation, Propagation, and Arrest of Joints and Other Fractures*, Geological Society, London, Special Publications, 231, pp. 25–47.
- Bateman, R., 1984. On the role of diapirism in the segregation, ascent and final emplacement of granitoid magmas. *Tectonophysics* 110, 211–231.
- Benn, K., 1994. Overprinting of magnetic fabrics in granites by small strains e numerical modeling. *Tectonophysics* 233, 153–162.
- Benn, K., Paterson, S.R., Lund, S.P., Pignotta, G.S., Kruse, S., 2001. Magmatic fabrics in batholiths as markers of regional strains and plate kinematics: example of the Cretaceous Mt. Stuart batholith. *Phys. Chem. Earth* 26, 343–354.
- Berner, H., Ramberg, H., Stephansson, O., 1972. Diapirism in theory and experiment. *Tectonophysics* 15, 197–218.
- Blažiček, M., 2002. Analysis of Fracture Networks and their Correlation with AMS Fabrics in the Melechov Massif. Diploma thesis. Charles University in Prague.
- Blížkovský, M., Novotný, A., 1982. Gravity Map of the Bohemian Massif. Geofyzika, Brno.
- Bouchez, J.L., 1997. Granite is never isotropic: an introduction to AMS studies of granitic rocks. In: Bouchez, J.L., Hutton, D.H.W., Stephens, W.E. (Eds.), *Granite: From Segregation of Melt to Emplacement Fabrics*. Kluwer Academic Publishers, pp. 95–112.
- Breiter, K., 2007. New results from geological investigation of the Melechov pluton. Geoscience Research Reports for 2006. Czech Geological Survey, Prague, pp. 202–205.
- Breiter, K., Sulovský, P., 2005. Geochronology of the Melechov Granite Massif. Geoscience Research Reports for 2004. Czech Geological Survey, Prague, pp. 16–19.
- Buddington, A.F., 1959. Granite emplacement with special reference to North America. *Geol. Soc. Am. Bull.* 70, 671–747.
- Cháb, J., Stráník, Z., Eliáš, M., 2007. Geological Map of the Czech Republic 1:500,000. Czech Geological Survey, Prague.
- Clemens, J.D., 1998. Observations on the origins and ascent mechanisms of granitic magmas. *J. Geol. Soc. London* 155, 843–851.
- Cruden, A.R., 1990. Flow and fabric development during the diapiric rise of magma. *J. Geol.* 98, 681–698.
- Dixon, J.M., 1975. Finite strain and progressive deformation in models of diapiric structures. *Tectonophysics* 28, 89–124.
- England, R.W., 1990. The identification of granitic diapirs. *J. Geol. Soc. London* 147, 931–933.
- Fusán, O., Kodým, O., Matějka, A., Urbánek, L., 1967. Geological Map of Czechoslovakia 1:500,000. Central Geological Survey, Prague.
- Gerdes, A., Friedl, G., Parrish, R.R., Finger, F., 2003. High-resolution geochronology of Variscan granite emplacement – the South Bohemian Batholith. *J. Czech Geol. Soc.* 48, 53–54.
- Harlov, D.E., Procházka, V., Förster, H.J., Matějka, D., 2008. Origin of monazite–xenotime–zircon–fluorapatite assemblages in the peraluminous Melechov granite massif, Czech Republic. *Mineral. Pet.* 94, 9–26.
- Henry, B., 1997. The magnetic zone axis: a new element of magnetic fabric for the interpretation of the magnetic lineation. *Tectonophysics* 271, 325–331.
- Hladík, V., Sedlák, J., Šrámek, J., Zabadal, S., 2006. Gravity Model of the Melechov Massif, 2nd Workshop on International Gravity Field Research (abstracts), Smolenice, Slovakia, pp. 40–44.
- Hrouda, F., Kahan, Š., 1991. The magnetic fabric relationship between sedimentary and basement nappes in the High Tatra Mountains, N. Slovakia. *J. Struct. Geol.* 13, 431–442.
- Hrouda, F., 2010. Modelling relationship between bulk susceptibility and AMS in rocks consisting of two magnetic fractions represented by ferromagnetic and paramagnetic minerals – implications for understanding magnetic fabrics in deformed rocks. *J. Geol. Soc. India* 75, 254–266.
- Hutton, D.H.W., 1988. Granite emplacement mechanisms and tectonic controls: inferences from deformation studies. *Trans. Royal Soc. Edinb. Earth Sci.* 79, 245–255.
- Jelínek, V., 1981. Characterization of the magnetic fabric of rocks. *Tectonophysics* 79, T63–T67.
- Ježek, J., Hrouda, F., 2000. The relationship between the Lisle orientation tensor and the susceptibility tensor. *Phys. Chem. Earth* 25, 469–474.
- Ježek, J., Hrouda, F., 2002. Software for modeling the magnetic anisotropy of strained rocks. *Comput. Geosci.* 28, 1061–1068.
- Ježek, J., Hrouda, F., 2004. Determination of the orientation of magnetic minerals from the anisotropy of magnetic susceptibility. In: Martín-Hernández, F., Lüneburg, C.M., Auborg, C., Jackson, M. (Eds.), *Magnetic Fabric: Methods and Application*. Geological Society, London, pp. 9–20. Special Publications 238.
- Ježek, J., Hrouda, F., 2007. SUSIE: a program for inverse strain estimation from magnetic susceptibility. *Comput. Geosci.* 33, 749–759.
- Ježek, J., Melka, R., Schulmann, K., Venera, Z., 1994. The behaviour of rigid triaxial ellipsoidal particles in viscous flows – modeling of fabric evolution in a multiparticle system. *Tectonophysics* 229, 165–180.
- Jiang, D., 2007. Numerical modeling of the motion of rigid ellipsoidal objects in slow viscous flows: a new approach. *J. Struct. Geol.* 29, 189–200.
- Kratinová, Z., Závada, P., Hrouda, F., Schulmann, K., 2006. Non-scaled analogue modelling of AMS development during viscous flow: a simulation on diapir-like structures. *Tectonophysics* 418, 51–61.
- Lenhardt, W.A., Švancara, J., Melichar, P., Pazdírková, J., Havíř, J., Sýkorová, Z., 2007. Seismic activity of the Alpine–Carpathian–Bohemian Massif region with regard to geological and potential field data. *Geol. Carpathica* 58, 397–412.
- Linsler, H., 1967. Investigation of tectonics by gravity detailing. *Geophys. Prospect.* 15, 480–515.
- Marsh, B.D., 1982. On the mechanics of diapirism, stoping, and zone melting. *Am. J. Sci.* 282, 808–855.
- Martínez Catalán, J.R., 2011. Are the oroclines of the Variscan belt related to late Variscan strike-slip tectonics? *Terra Nova* 23, 241–247.
- Martín-Hernández, F., Hirt, A.M., 2003. The anisotropy of magnetic susceptibility in biotite, muscovite and chlorite single crystals. *Tectonophysics* 367, 13–28.
- Matějka, D., Janoušek, V., 1998. Whole-rock geochemistry and petrogenesis of granites from the northern part of the Moldanubian batholith (Czech Republic). *Acta Univ. Carol. Geol.* 42, 73–79.
- Miller, R.B., Paterson, S.R., 1999. In defense of magmatic diapirs. *J. Struct. Geol.* 21, 1161–1173.
- Mlčoch, B., Breiter, K., Schulmannová, B., 2000. The Melechov Granite Massif. Geoscience Research Reports for 1999. Czech Geological Survey, Prague, pp. 91–93.
- Mottlová, L., 1985. The deep structure of the Central and Melechov massifs interpreted on the basis of alternative solutions of inverse gravity problems. *Bull. Central Geol. Surv.* 57, 351–363.
- Nagata, T., 1961. *Rock Magnetism*. Maruzen, Tokyo.
- Paterson, S.R., Fowler, T.K., 1993. Re-examining pluton emplacement processes. *J. Struct. Geol.* 15, 191–206.
- Paterson, S.R., Miller, R.B., 1998. Stopped blocks in plutons: paleo-plumb bobs, viscometers, or chronometers? *J. Struct. Geol.* 20, 1261–1272.
- Paterson, S.R., Vernon, R.H., 1995. Bursting the bubble of ballooning plutons: a return to nested diapirs emplaced by multiple processes. *Geol. Soc. Am. Bull.* 107, 1356–1380.

- Paterson, S.R., Fowler, T.K., Schmidt, K.L., Yoshinobu, A.S., Yuan, E.S., Miller, R.B., 1998. Interpreting magmatic fabric patterns in plutons. *Lithos* 44, 53–82.
- Paterson, S.R., Pignotta, G.S., Vernon, R.H., 2004. The significance of microgranitoid enclave shapes and orientations. *J. Struct. Geol.* 26, 1465–1481.
- Procházka, V., Matějka, D., 2006. Rock-forming accessory minerals in the granites of the Melečov Massif (Moldanubian Batholith, Bohemian Massif). *Acta Univ. Carol. Geol.* 48, 71–79.
- Procházka, J., Mlčoch, B., 1998. Complex geological survey of Melečov Massif (E-Bohemia). *Geoscience Research Reports for 1997. Czech Geological Survey, Prague*, pp. 31–37.
- Pueyo, E.L., Román-Berdiel, T.M., Bouchez, J.L., Casas, A.M., Larrasoana, J.C., 2004. Statistical significance of magnetic fabric data in studies of paramagnetic granites. In: Martín-Hernández, F., Lüneburg, C.M., Auborg, C., Jackson, M. (Eds.), *Magnetic Fabric: Methods and Application*. Geological Society, London, pp. 395–420. Special Publications 238.
- Ramsay, J.G., 1989. Emplacement kinematics of a granite diapir: the Chindamora batholith, Zimbabwe. *J. Struct. Geol.* 11, 191–209.
- Ramsay, J.G., Huber, M.I., 1983. *The Techniques of Modern Structural Geology. Volume 1: Strain Analysis*. Academic Press, London.
- Schmeling, H., Cruden, A.R., Marquart, G., 1988. Finite deformation in and around a fluid sphere moving through a viscous medium: implications for diapiric ascent. *Tectonophysics* 149, 17–34.
- Schulmann, K., Venera, Z., Konopásek, J., Lexa, O., 1998. Structural and Geological Investigation of the Melečov Massif. Unpublished report. Faculty of Science, Charles University, Prague.
- Schulmann, K., Lexa, O., Štípská, P., Racek, M., Tajčmanová, L., Konopásek, J., Edel, J.B., Peschler, A., Lehmann, J., 2008. Vertical extrusion and horizontal channel flow of orogenic lower crust: key exhumation mechanisms in large hot orogens? *J. Metamorph. Geol.* 26, 273–297.
- Šefara, J., 1973. Interpretation of vertical density interfaces using a map of gravity anomalies by means of digital computer. *J. Geol. Sci. Appl. Geophys.* 11, 19–29.
- Sen, K., Mamtani, M.A., 2006. Magnetic fabric, shape preferred orientation and regional strain in granitic rocks. *J. Struct. Geol.* 28, 1870–1882.
- Sen, K., Majumder, S., Mamtani, M.A., 2005. Degree of magnetic anisotropy as a strain intensity gauge in ferromagnetic granites. *J. Geol. Soc. London* 162, 583–586.
- Staněk, M., 2013. Structural and Petrophysical Characterisation of Granite Intended for Radioactive Waste Stocking. Ph.D. thesis. Charles University, Prague.
- Staněk, M., Géraud, Y., Lexa, O., Špaček, P., Ulrich, S., Diraison, M., 2013. Elastic anisotropy and pore space geometry of schlieren granite: direct 3-D measurements at high confining pressure combined with microfabric analysis. *Geophys. J. Int.* 194, 383–394.
- Talbot, C.J., Jackson, M.P.A., 1987. Internal kinematics of salt diapirs. *Am. Assoc. Pet. Geol. Bull.* 71, 1068–1093.
- Verner, K., Žák, J., Šrámek, J., Pačlíková, J., Závřelová, J., Machek, M., Finger, F., Johnson, K., 2014. Formation of elongated granite–migmatite domes as isostatic accommodation structures in collisional orogens. *J. Geodyn.* 73, 100–117.
- Weinberg, R.F., Podladchikov, Y., 1994. Diapiric ascent of magmas through power law crust and mantle. *J. Geophys. Res.* 99, 9543–9559.
- Winchester, J.A., 2002. Palaeozoic amalgamation of Central Europe: new results from recent geological and geophysical investigations. *Tectonophysics* 360, 5–21.
- Žák, J., Paterson, S.R., Memeti, V., 2007. Four magmatic fabrics in the Tuolumne batholith, central Sierra Nevada, California (USA): implications for interpreting fabric patterns in plutons and evolution of magma chambers in the upper crust. *Geol. Soc. Am. Bull.* 119, 184–201.
- Žák, J., Verner, K., Finger, F., Faryad, S.W., Chlupáčová, M., Veselovský, F., 2011. The generation of voluminous S-type granites in the Moldanubian unit, Bohemian Massif, by rapid isothermal exhumation of the metapelitic middle crust. *Lithos* 121, 25–40.
- Žák, J., Verner, K., Janoušek, V., Holub, F.V., Kachlík, V., Finger, F., Hajná, J., Tomek, F., Vondrovic, L., Trubač, J., 2014. A plate-kinematic model for the assembly of the Bohemian Massif constrained by structural relationships around granitoid plutons. In: Schulmann, K., Martínez Catalán, J.R., Lardeaux, J.M., Janoušek, V., Oggiano, G. (Eds.), *The Variscan Orogeny: Extent, Timescale and the Formation of the European Crust*. Geological Society, London. <http://dx.doi.org/10.1144/SP405.9>. Special Publications 405, in press.
- Zapletal, K., 1990. Low-field susceptibility anisotropy of some biotite crystals. *Phys. Earth Planet. Inter.* 63, 85–97.



Magnetic fabric of the Říčany granite, Bohemian Massif

J. TRUBAČ^{1,2,4*}, J. ŽÁK^{1,2} AND V. JANOUŠEK^{2,3}

¹*Institute of Geology and Paleontology, Faculty of Science, Charles University, Albertov 6, Prague, 128 43, Czech Republic.*

²*Czech Geological Survey, Klárov 3, Prague, 118 21, Czech Republic.*

³*Institute of Petrology and Structural Geology, Faculty of Science, Charles University, Albertov 6, Prague, 128 43, Czech Republic.*

⁴*Institute of Geochemistry, Mineralogy and Mineral Resources, Faculty of Science, Charles University, Albertov 6, Prague, 128 43, Czech Republic.*

*e-mail: jakub.trubac@gmail.com

Abstract: The Říčany pluton represents an elliptical shallow-level intrusion made up of outer, more fractionated, strongly porphyritic granite and inner, less evolved, weakly porphyritic granite. Mesoscopic foliation defines an onion-skin pattern and corresponds well to the magnetic (AMS) foliations. Magnetic lineation plunges shallowly (0-20°) and is subparallel to the contact in the outer part of the pluton, whereas in the pluton center lineation dips steeply (60-70°) with variable trends. We interpret the fabrics in the pluton as being a result of helical flow, whereby faster subvertical flow in the low-viscosity pluton center generated subhorizontal flow in the outer, higher-viscosity (phenocryst-rich) margin.

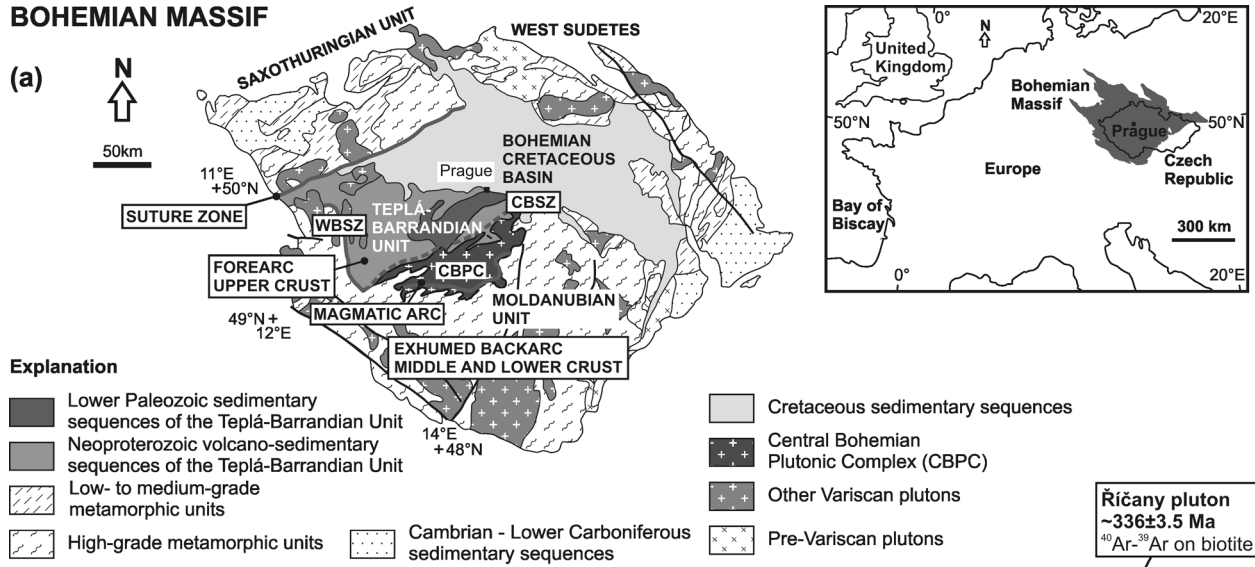
Keywords: anisotropy of magnetic susceptibility (AMS), Bohemian Massif, granite, magma flow, pluton.

Unravelling the geometrical patterns and the likely physical causes of magma flow in granitic magma chambers is one of the central aspects of understanding magma chamber dynamics. In many (or most?) cases, however, direct field evidence for chamber-wide flow or convection is completely erased from the rock record. Magmatic fabrics in plutons (i.e. foliations and lineations formed during the presence of a melt; Paterson *et al.*, 1989) commonly fail to provide unambiguous evidence for chamber-wide magma flow or convection. Instead, the preserved pluton fabrics are acquired late in magma chamber history along migrating crystallization fronts and are also easily reset by regional tectonic deformation, making infer-

ences on large-scale convection or flow patterns difficult or rather problematic (e.g. Paterson *et al.*, 1998).

In the present paper, we investigate an example of a post-tectonic pluton (the Říčany pluton, Bohemian Massif; figure 1) where the magmatic fabrics have not been overprinted by regional deformation and thus likely preserve a record of internal processes and magma flow. Below we present integrated structural, microstructural, and anisotropy of magnetic susceptibility (AMS) data, which revealed an unusual pattern of magmatic fabrics in the pluton. Subsequently, we discuss the significance of the observed fabrics and AMS and interpret these data to record a helical flow,

BOHEMIAN MASSIF



CENTRAL BOHEMIAN PLUTONIC COMPLEX

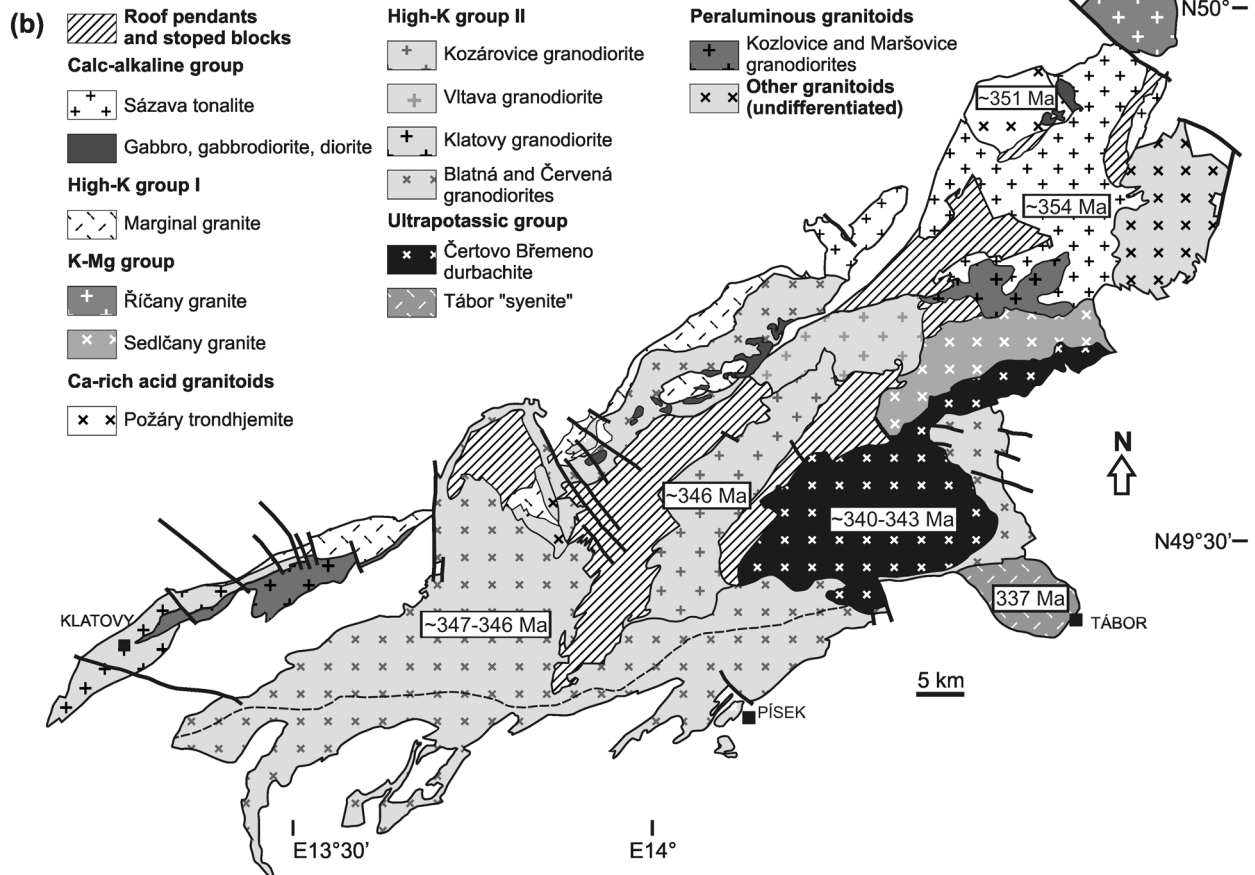


Figure 1. Simplified geological map of the Central Bohemian Plutonic Complex (b) and its position in the Bohemian Massif (a). The map is based on Czech Geological Survey 1:200 000 maps and Holub *et al.* (1997b). It shows the main intrusive units (or "types") with some recently published radiometric ages (Holub *et al.*, 1997a; Janoušek and Gerdes, 2003).

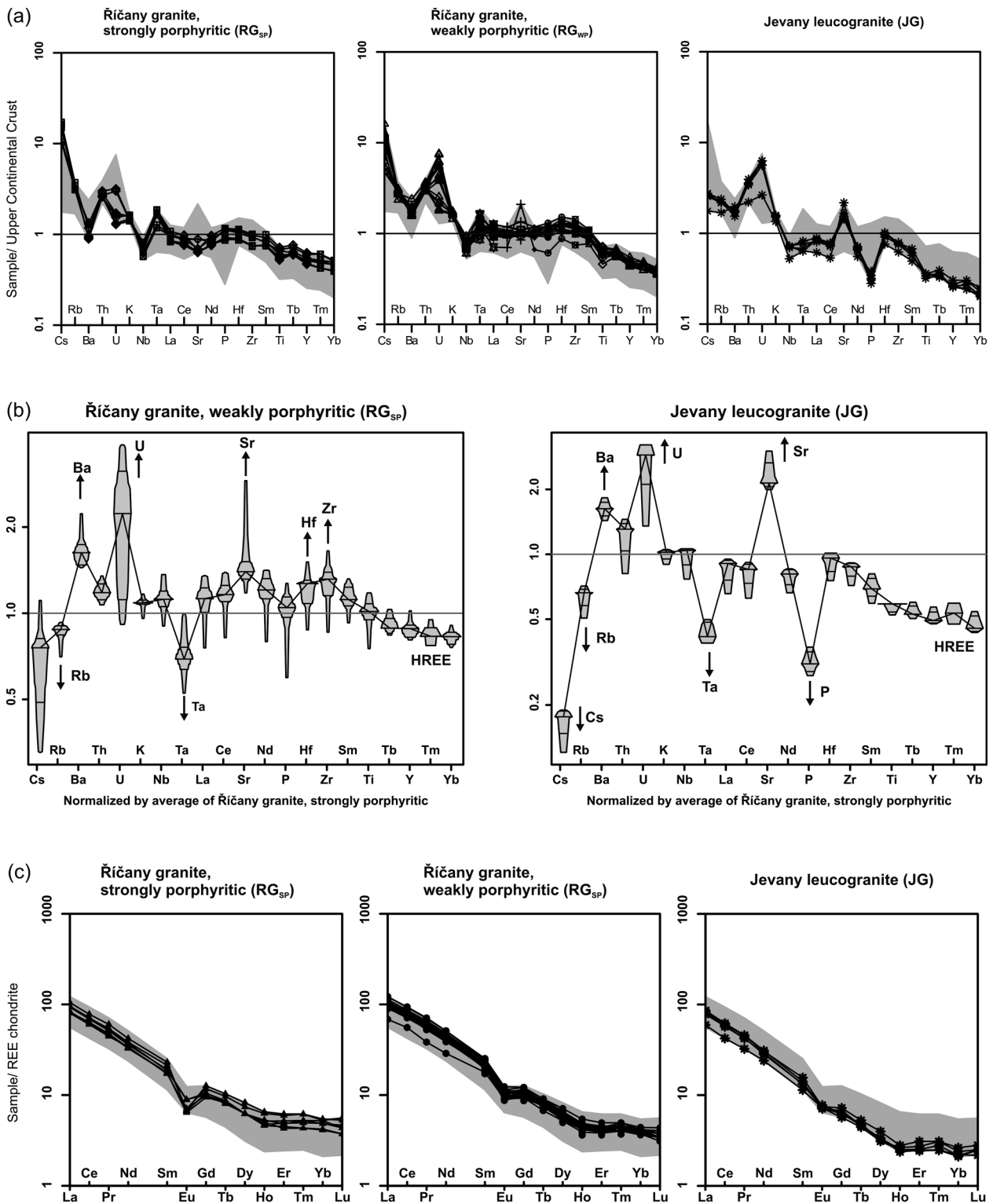


Figure 2. (a) Spider plots normalized by average composition of the upper crust (Taylor and McLennan, 1995) for the three main granite varieties of the Říčný pluton, (b) spider box and percentile plots (Janoušek and Holub, 2007) showing the statistical distribution of the trace-element abundances normalized by average contents in the outer, strongly porphyritic Říčný granite, (c) chondrite normalized (Boynton, 1984) REE patterns for the three main igneous pulses within the Říčný pluton.

a rarely documented flow mechanism in granitoid plutons.

Geological setting

The Říčany pluton of the Central Bohemian Plutonic Complex (Bohemian Massif; figure 1) represents a post-tectonic, shallow-level intrusion emplaced into low-grade Neoproterozoic and Lower Paleozoic siliciclastic rocks in Early Carboniferous times (figure 1; 336 ± 3.5 Ma, unpublished $^{40}\text{Ar}/^{39}\text{Ar}$ biotite data of H. Maluski, cited in Janoušek *et al.*, 1997). In map-view, the pluton has a roughly elliptical outline (13×9 km) and is made up of three distinct granite varieties: (i) outer, strongly porphyritic, (muscovite-) biotite Říčany granite, (ii) inner, weakly porphyritic, (muscovite-) biotite Říčany granite, and (iii) a small, poor-

ly exposed body of fine-grained, equigranular, two-mica Jevany leucogranite in the south-central part of the pluton. These granite varieties define a concentric pattern. The contact between the two porphyritic granites is gradational over several hundreds of meters; the nature of the outer contact of the Jevany leucogranite is unclear due to a poor exposure.

All varieties are fairly fractionated, peraluminous ($A/CNK = 1.01\text{--}1.13$), S-type granites enriched, if compared with average crustal composition (Taylor and McLennan, 1995), in Large Ion Lithophile Elements (LILE: Cs, Rb, Th, U, Sr) and depleted in some High Field Strength Elements (HFSE: Nb, Ti, HREE) (Fig. 2a). In general, the major-element compositions are comparable and do not vary greatly between the two facies of the Říčany granite.

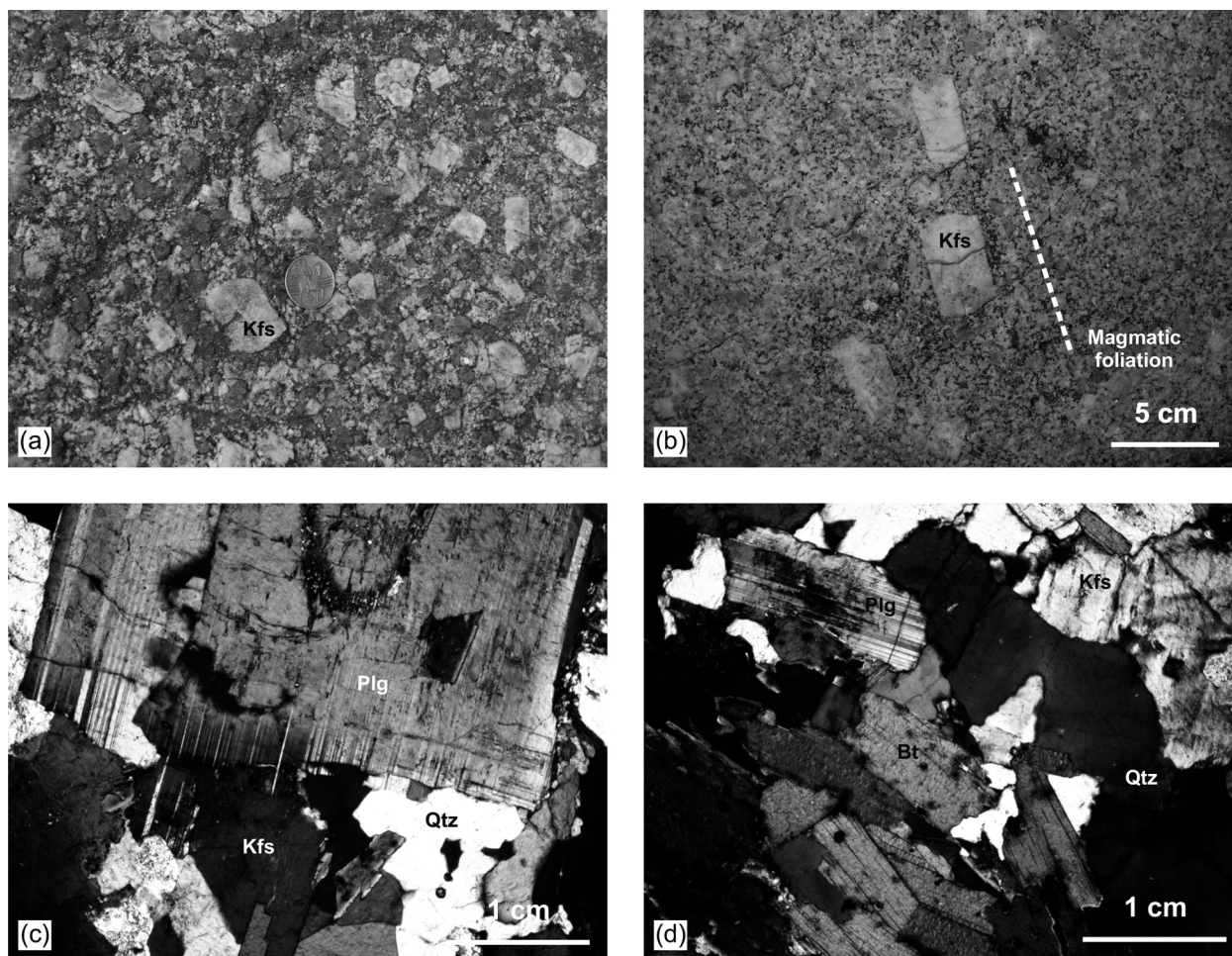


Figure 3. (a) K-feldspar phenocrysts (up to 4 cm in size) in the strongly porphyritic Říčany granite; coin for scale, (b) magmatic foliation defined by K-feldspar phenocrysts in the weakly porphyritic Říčany granite, (c) photomicrograph of a magmatic texture of strongly porphyritic muscovite-biotite Říčany granite, (d) photomicrograph of magmatic texture of weakly porphyritic muscovite-biotite Říčany granite. Crystals of main rock-forming minerals do not exhibit internal solid-state deformation. The magmatic textures are typical of all granite varieties in the Říčany pluton.

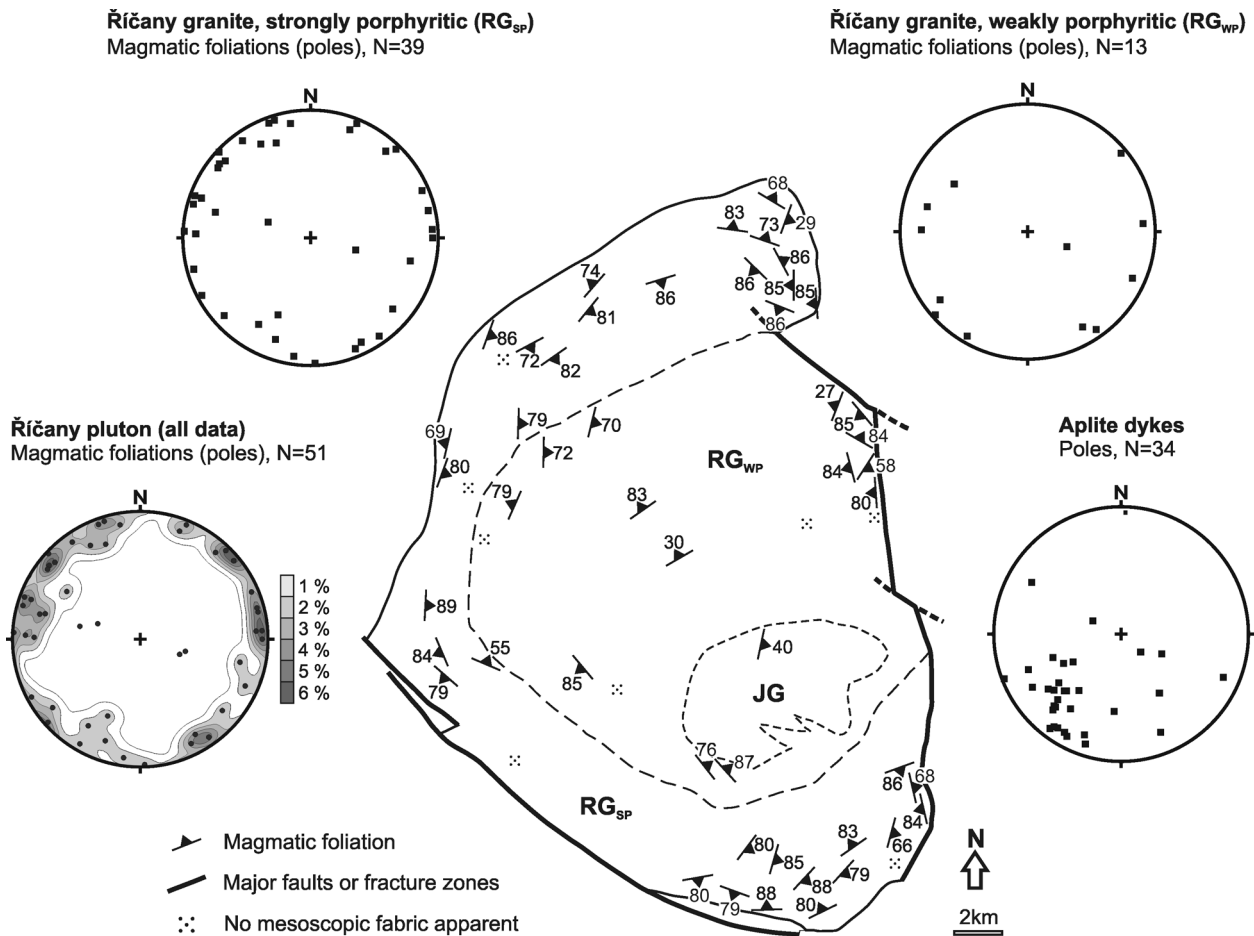


Figure 4. Structural map to show mesoscopic magmatic foliation pattern. Stereonets (lower hemisphere, equal area projection) show orientation of magmatic foliations in each granite variety.

However, there are some conspicuous differences in the trace-element signatures. For instance, the central, weakly porphyritic facies shows markedly lower Rb, Sr, Ta and HREE contents at elevated Ba, U, Sr, Hf and Zr if compared with the outer, strongly porphyritic facies (Fig. 2b). All the rocks are characterized by fractionated REE patterns with a high degree of LREE/HREE enrichment. Typical is also the presence of Eu anomalies, the magnitude of which increases outwards, reaching its maximum in the strongly porphyritic Říčný granite (Fig. 2c). The degree of fractionation decreases from the pluton margin inwards, the outer, strongly porphyritic granite being more evolved than the central, weakly porphyritic granite (Janoušek *et al.*, 1997). The position of the Jevany leucogranite is, to a large extent, independent and its genetic relationship to both the Říčný granite varieties still poorly constrained (Němec, 1978).

Magmatic fabric and anisotropy of magnetic susceptibility (AMS) of the granite

Mesoscopic foliation in the porphyritic granites is defined by a planar shape-preferred orientation of biotite and K-feldspar phenocrysts, lineation being mesoscopically indiscernible (Figs. 3a and 3b). At the micro-scale, no evidence for sub-solidus deformation was observed throughout the pluton (Figs. 3c and 3d). The foliation dips steeply (70–80°), is subparallel to the outer contact of the pluton and is thus clearly discordant with the regional host rock structures (Fig. 4).

We used the anisotropy of magnetic susceptibility (AMS) method to investigate the magnetic fabric of the Říčný pluton in order to corroborate the structural data and to quantify the fabric parameters in the pluton. 71 oriented samples were collected using a portable drill at 31 sampling sites. The AMS was measured with the KLY-4S Kappabridge apparatus

and statistical analysis of AMS data was performed using the ANISOFT package of programs.

The AMS data are represented by the k_m , P , and T parameters defined as follows $k_m = (k_1 + k_2 + k_3)/3$; $P = k_1/k_3$; $T = 2\ln(k_2/k_3)/\ln(k_1/k_3) - 1$. The k_m parameter represents the mean bulk magnetic susceptibility reflecting the qualitative and quantitative contents of magnetic minerals in the rock. The P parameter, called the degree of AMS, reflects the eccentricity of the AMS ellipsoid and thus indicates the intensity of the preferred orientation of the magnetic minerals in the rock. The higher the P parameter, the stronger the preferred orientation. The T parameter indicates the symmetry of the AMS ellipsoid. It varies from -1 (perfectly linear magnetic fabric) through 0 (transition between linear and planar magnetic fabric) to $+1$ (perfectly planar magnetic fabric). The orientations of the magnetic foliation poles and the magnetic lineations are presented either in a contour diagram in the geographic (*in situ*) coordinate system or as locality means in a map.

The mean bulk magnetic susceptibility of the analyzed samples is low, ranging from 13.13×10^{-6} (SI) to 10.53×10^{-6} (SI). Such a low susceptibility (in the order of 10^{-5}) is characteristic of paramagnetic granites (Bouchez, 1997), in which the main carriers of AMS are paramagnetic minerals. The degree of AMS (represented by parameter P) ranges from 1.009 to 1.149 in the strongly porphyritic granite and from 1.014 to 1.363 in the weakly porphyritic granite. The T parameter ranges from -0.754 to 0.904 in the strongly porphyritic granite and from -0.667 to

0.970 in the weakly porphyritic granite. No significant spatial variations in the degree of anisotropy or shape of the AMS ellipsoid were revealed in the pluton. In the Jevany leucogranite, the P parameter ranges from 1.07 to 1.27 and the T parameter ranges from 0.1 to 0.9.

The magnetic fabric pattern (AMS) of the Říčany pluton is characterized by margin-parallel, moderately to steeply dipping magnetic foliation (Fig. 5); its geometry is consistent with the orientation of mesoscopic magmatic foliation. Foliation poles tend to concentrate along the periphery of the stereonet (Fig. 5). Magnetic lineation steepens significantly as a function of distance from the pluton margin. In the outer part of the pluton, the lineation plunges shallowly ($0-20^\circ$) and is subparallel to the contact whereas in the center lineation dips steeply ($60-70^\circ$) with variable trends (Fig. 5).

Discussion and conclusions

Our structural and AMS data do not comply with existing models proposed for the emplacement of elliptical, onion-skin plutons (e.g. single-blob or nested diapirism, ballooning, laccolith-like emplacement). We interpret the mesoscopic and magnetic fabrics in the Říčany granite as a result of helical flow (as defined by Fowler, 1996). In our model, we consider the strongly and weakly porphyritic granites as two nested magma batches having different viscosities during emplacement. We envisage that the difference in K-feldspar phenocryst content in the two granites caused significant difference in their viscosities: the

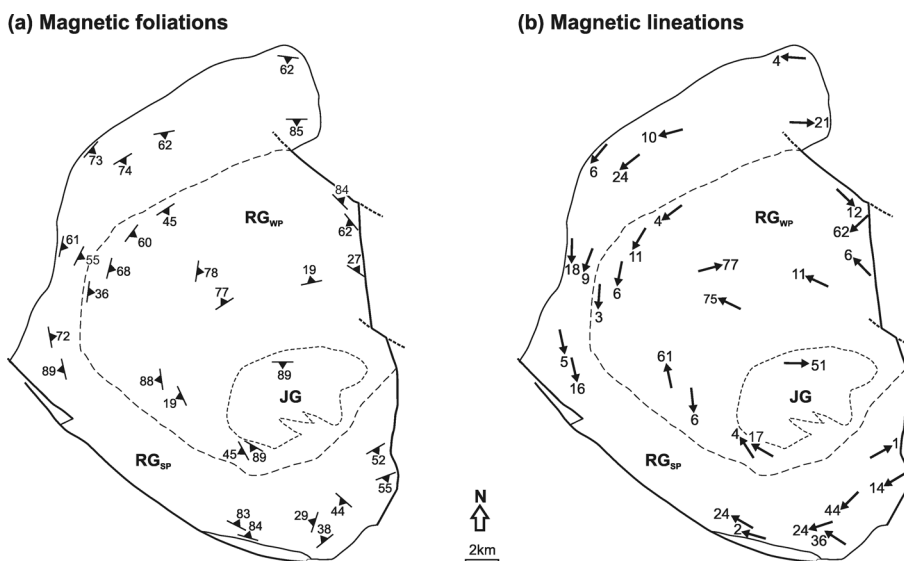


Figure 5. Map of magnetic foliations (a) and lineations (b) in the Říčany pluton (AMS).

outer, strongly porphyritic granite presumably had viscosity of a higher order of magnitude than the central, weakly porphyritic granite. This assumption is in agreement with an exponential increase in viscosity with crystal content as predicted by the Einstein-Roscoe equation for solid-liquid mixtures. Considering the Říčany pluton as a steep-sided cylindrical body, we can apply the Hagen-Poiseuille equation for fluid flow through a pipe to infer the flow mechanism within the pluton. Contrasting viscosities of the two magmas then would cause their different velocities during ascent. Consequently, faster subvertical flow of low-viscosity (phenocryst-poor) magma in the pluton center may have generated helical (subhorizontal) flow in the outer, high-viscosity and phe-

nocryst-rich layer. This two-layer model explains well the finite fabric pattern, with concentric, steep foliations and magnetic lineation being subhorizontal along the pluton margin and subvertical in the center. Taking into account the shallow emplacement level of the Říčany pluton, the pluton may be viewed as a conduit linking a deeper magma chamber with a volcanic system at the surface.

Acknowledgements

We would like to acknowledge comments by L. G. Corretgé which helped to improve the original version of the manuscript. This research is funded by a grant from the Grant Agency of Charles University in Prague (GAUK) No. 131607 (to J. Trubač).

References

- BOUCHEZ, J. L. (1997): Granite is never isotropic: an introduction to AMS studies of granitic rocks. In: J. L. BOUCHEZ, D. H. W. HUTTON and W. E. STEPHENS (eds): *Granite: From Segregation of Melt to Emplacement Fabrics*, Kluwer Academic Publishers, Amsterdam: 95-112.
- BOYNTON, W. V. (1984): Cosmochemistry of the rare earth elements: meteorite studies. In: P. HENDERSON (ed): *Rare Earth Element Geochemistry*, Elsevier, Amsterdam: 63-114.
- FOWLER, T. J. (1996): The properties and geological environments of helicoids: axially symmetric surfaces in torsional and non-torsional deformations. *J. Struct. Geol.*, 18: 505-517.
- HOLUB, F. V., COCHERIE, A. and ROSSI, P. (1997a): Radiometric dating of granitic rocks from the Central Bohemian Plutonic Complex: constraints on the chronology of thermal and tectonic events along the Barrandian-Moldanubian boundary. *C. R. Acad. Sci. II A*, 325: 19-26.
- HOLUB, F. V., MACHART, J. and MANOVÁ, M. (1997b): The Central Bohemian Plutonic Complex: geology, chemical composition and genetic interpretation. *Sborník Geologických Ved: Ložisková Geologie, Mineralogie - J. Geol. Sci. Econ. Geol., Mineral.*, 31: 27-50.
- JANOŮSEK, V., ROGERS, G., BOWES, D. R. and VAŇKOVÁ, V. (1997): Cryptic trace-element variation as an indicator of reverse zoning in a granitic pluton: the Říčany granite, Czech Republic. *J. Geol. Soc. London*, 154: 807-815.
- JANOŮSEK, V. and GERDES, A. (2003): Timing the magmatic activity within the Central Bohemian Pluton, Czech Republic: conventional U-Pb ages for the Sázava and Tábor intrusions and their geotectonic significance. *J. Czech Geol. Soc.*, 48, 1-2: 70-71.
- JANOŮSEK, V. and HOLUB, F. V. (2007): The causal link between HP-HT metamorphism and ultrapotassic magmatism in collisional orogens: case study from the Moldanubian Zone of the Bohemian Massif. *Proc. Geol. Assoc.*, 118: 75-86.
- NĚMEC, D. (1978): Genesis of aplite in the Říčany massif, central Bohemia. *Neues Jb. Miner. Abh.*, 132: 322-339.
- PATERSON, S. R., VERNON, R. H. and TOBISCH, O. T. (1989): A review of criteria for identification of magmatic and tectonic foliations in granitoids. *J. Struct. Geol.*, 11, 3: 349-363.
- PATERSON S. R., FOWLER T. K., SCHMIDT K. L., YOSHINOBU A. S., YUAN E. S. and MILLER R. B. (1998): Interpreting magmatic fabric patterns in plutons. *Lithos*, 44: 53-82.
- TAYLOR, S. R. and MCLENNAN, S. M. (1995): The geochemical evolution of the continental crust. *Rev. Geophys.*, 33: 241-265.

Structure, emplacement, and tectonic setting of Late Devonian granitoid plutons in the Teplá–Barrandian unit, Bohemian Massif

Jiří Žák · Zuzana Kratinová · Jakub Trubač ·
Vojtěch Janoušek · Jiří Sláma · Jan Mrlina

Received: 6 January 2010 / Accepted: 21 May 2010 / Published online: 12 June 2010
© Springer-Verlag 2010

Abstract The Štěnovice and Čistá granodiorite–tonalite plutons are small (~ 27 and ~ 38 km², respectively) intrusions that are largely discordant to regional ductile structures in the center of the upper-crustal Teplá–Barrandian unit, Bohemian Massif. Their whole-rock and trace-element compositions are consistent with medium-K calc-alkaline magma, generated above a subducted slab in a continental margin arc setting. The U–Pb zircon age of the Štěnovice pluton, newly determined at 375 ± 2 Ma using the laser ablation ICP-MS technique, is within the error of the previously published Pb–Pb age of 373 ± 1 Ma for the Čistá pluton. The two plutons also share other characteristics that are typical of concentrically expanded plutons (CEPs), such as elliptical cross-section in

plan view, steep contacts, inferred downward-narrowing conical shape, faint normal zoning, and margin-parallel magmatic foliation decoupled from the regional host-rock structures. We interpret the Štěnovice and Čistá plutons as representing the initial Late Devonian stage of much more voluminous early Carboniferous arc-related plutonism (represented most typically by the Central Bohemian Plutonic Complex) in the upper crust of the central Bohemian Massif. These two plutons are important tectonic elements in that they indicate an overall shift of the arc-related plutonic activity from the \sim NW to the \sim SE, accompanied with a general compositional trend of the magmas from medium-K calc-alkaline to shoshonitic/ultrapotassic. Such a pattern is compatible with SE-directed subduction of the Saxothuringian Ocean beneath the Teplá–Barrandian overriding plate as a cause of arc-related magmatism in this part of the Bohemian Massif.

Electronic supplementary material The online version of this article (doi:10.1007/s00531-010-0565-7) contains supplementary material, which is available to authorized users.

J. Žák (✉) · J. Trubač
Institute of Geology and Paleontology, Faculty of Science,
Charles University, Albertov 6, Prague 12843, Czech Republic
e-mail: jirizak@natur.cuni.cz

J. Žák
Czech Geological Survey, Klárov 3,
Prague 11821, Czech Republic

Z. Kratinová · J. Mrlina
Institute of Geophysics, Academy of Sciences of the Czech
Republic, Boční II/1401, Prague 14131, Czech Republic

Z. Kratinová
University of Lisbon and IDL, Edifício C8,
1749-016 Lisbon, Portugal

J. Trubač · V. Janoušek
Czech Geological Survey, Geologická 6,
Prague 15200, Czech Republic

V. Janoušek
Institute of Petrology and Structural Geology,
Faculty of Science, Charles University,
Albertov 6, Prague 12843, Czech Republic

J. Sláma
Centre for Geobiology and Department of Earth Science,
University of Bergen, Allegaten 41, 5007 Bergen, Norway

J. Sláma
Institute of Geology,
Academy of Sciences of the Czech Republic,
v.v.i., Rozvojová 135, Prague 6 16502, Czech Republic

Keywords Bohemian Massif · Granite · Pluton · Subduction · Teplá–Barrandian unit · Variscan orogeny

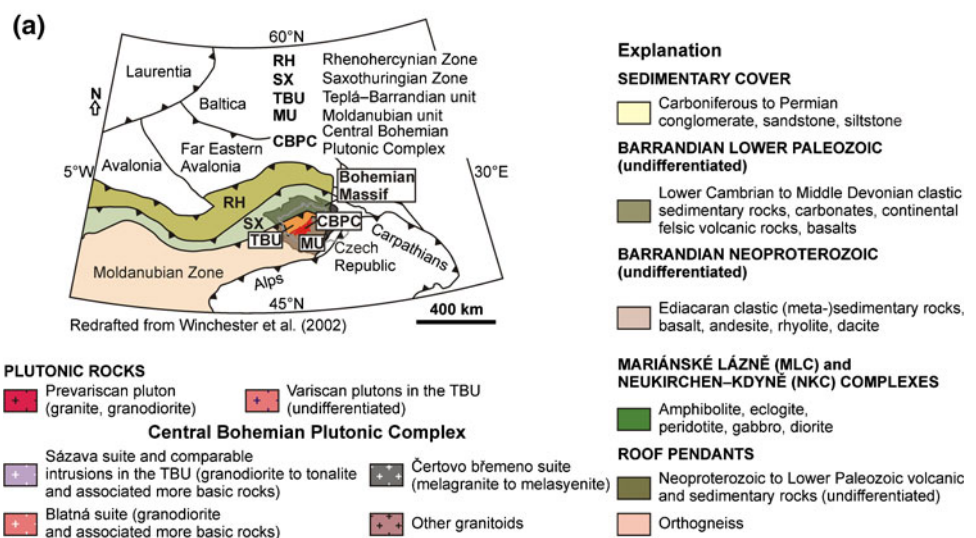
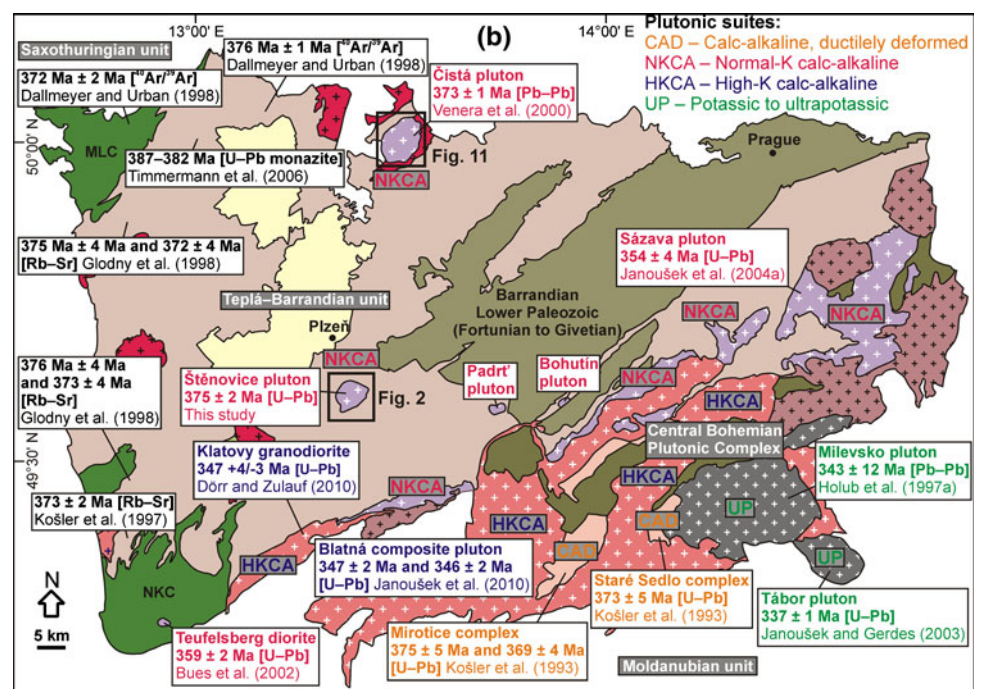
Introduction

The Variscan orogeny in the Bohemian Massif was accompanied by episodic granitoid plutonism throughout the development of the orogen, with several peaks of plutonic activity during Carboniferous that are now well characterized by a large body of geochemical and geochronologic data (e.g., Janoušek et al. 1995, 2000, 2004a; Finger et al. 1997, 2009; Holub et al. 1997a, b; Siebel et al. 1997, 1999, 2003, 2008; Gerdes et al. 2000a, b, 2003;

Gerdes 2001; Štemprok et al. 2003; Kovářková et al. 2007, 2010; Slaby and Martin 2008; Kusiak et al. 2010; Timmerman 2008; Dörr and Zulauf 2010; Kotková et al. 2010). On the contrary, the initial Late Devonian (Frasnian to Famennian) calc-alkaline plutonism has been poorly documented despite its potential key role for interpreting the timing and polarity of Variscan subductions and constraining the ages and loci of early orogenic deformation.

Compared to the voluminous Carboniferous plutonism, the Late Devonian granitoids and meta-granitoids are sparse, small intrusions localized in the upper-crustal Teplá–Barrandian unit (TBU) of the central Bohemian Massif (Fig. 1). The reported occurrences of the Late Devonian (meta-)granitoids include the ~380–365 Ma

Fig. 1 **a** Greatly simplified map of basement structure and Variscan lithotectonic zonation of Europe showing main units and suture zones in the Bohemian Massif as discussed in the text; modified after Winchester (2002). **b** Simplified geologic map of the Teplá–Barrandian unit (TBU) showing the arc-related plutons including the two Late Devonian plutons examined in this study (*bold rectangles*). The Ar–Ar (Bt), Rb–Sr (Bt), and U–Pb (monazite) ages indicating the Late Devonian cooling after tectonothermal activity in the western part of the TBU, while the U–Pb and Pb–Pb zircon ages of plutonic suites illustrate the Late Devonian to early Carboniferous shift of plutonism from the ~NW to the ~SE accompanied by a general compositional trend of the magmas from medium-K calc-alkaline to shoshonitic/ultrapotassic. Geology based on 1:500,000 Geologic map of the Czech Republic published by the Czech Geological Survey in 2007



Staré Sedlo and Mírotice orthogneiss complexes (Fig. 1b; Košler et al. 1993, 1995), the ~ 359 Ma Teufelsberg diorite pluton (Fig. 1b; Bues et al. 2002; Dörr and Zulauf 2010) near the present-day Teplá–Barrandian/Moldanubian boundary, and the ~ 373 Ma Čistá granodiorite pluton in the north-central TBU (Fig. 1b; Klomínský 1963; Chlupáčová et al. 1975; Kopecký et al. 1997; Venera et al. 2000). Another pluton, the previously largely unexplored Štěnovice granodiorite–tonalite, intruded the Neoproterozoic basement of the south-central TBU (Fig. 1b; Klomínský 1965). The age of the Štěnovice intrusion has not been determined before by modern geochronologic methods; however, many similarities in the field relations and composition with the Čistá pluton were noted as early as in the 1960s (Klomínský 1965; Bartošek et al. 1969).

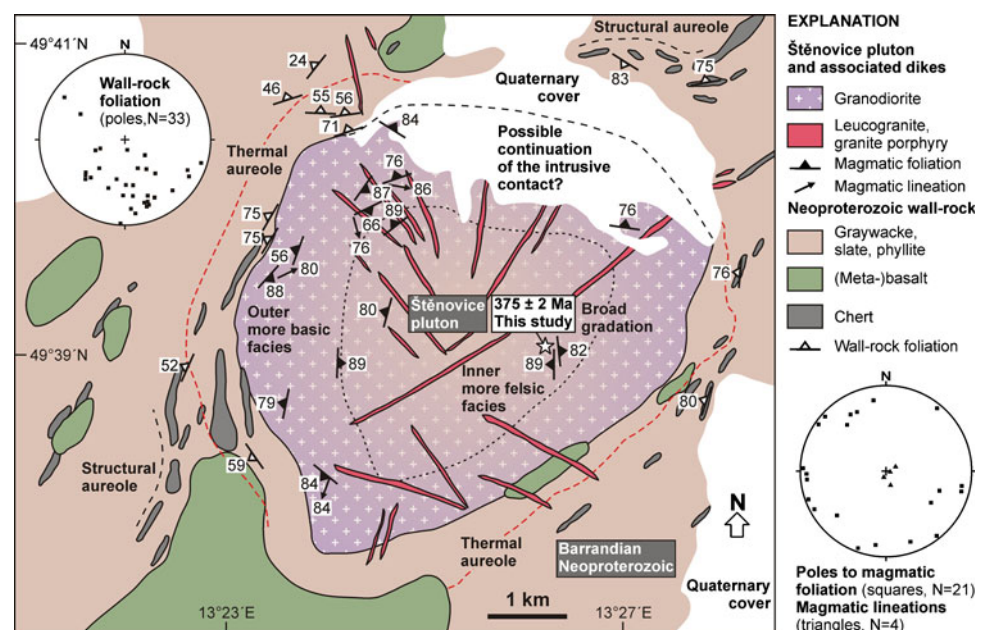
The goal of this paper is to provide an integrated overview of the principal field, geophysical, and geochemical characteristics of the Štěnovice and Čistá plutons (Fig. 1b). We first describe our new data from the Štěnovice pluton, including field observations, host-rock and pluton microstructures, gravimetry, whole-rock geochemistry, zircon geochronology, and anisotropy of magnetic susceptibility (AMS). To provide readers with a complete picture, the Čistá pluton is then briefly described utilizing our field observations and large existing data sets acquired by others. Finally, we interpret the structure and emplacement mode of these two plutons and discuss their tectonic significance for reconstructing the initial stages of the Variscan orogeny and polarity of subductions in the Bohemian Massif.

The Štěnovice pluton–field relationships and petrography

The Štěnovice pluton is weakly elliptical (5.5×5 km, ~ 27 km²) in plan view with its long axis oriented \sim NE–SW (Fig. 2). The pluton intruded the low-grade Neoproterozoic (Ediacaran) basement rocks of the TBU, represented here by prehnite–pumpellyite to lower greenschist facies slates and (meta-) graywackes enclosing lenses of chert and elongated to irregular bodies of metabasalt. Away from the pluton, the regional trend of lithologic contacts, cleavage, and large-scale folds is \sim NE–SW. The outer pluton/wall-rock contact, where not concealed by the Quaternary cover, is intrusive (sharp and non-sheeted), steep, or dips steeply to moderately (50 – 70°) outward along the northwestern pluton margin (Fig. 2).

The pluton has a well-developed thermal and structural aureole parallel to its outer margin. The thermal aureole, defined as a zone of detectable contact metamorphism around the pluton, is up to 600 m wide. The meta-graywackes in the contact aureole are characterized by spaced low-temperature pressure-solution cleavage, developed as short to continuous cleavage domains anastomosing around larger subangular detrital grains (Electronic Supplementary Material–ESM, Part 1a). During the contact metamorphism, irregular biotite aggregates grew preferentially along the cleavage domains but biotite also occurs as smaller grains in the fine-grained matrix (ESM, Part 1a). The cherts in the thermal aureole have locally a well-developed foliation and host folded quartz veins (ESM, Part 1b).

Fig. 2 Combined geologic and structural map of the Štěnovice pluton, associated dikes, and its Barrandian Neoproterozoic wall-rock. Stereonets (lower hemisphere, equal area projection) show orientations of wall-rock cleavage and of magmatic foliation and lineation in the pluton. *Star* indicates location of the geochronologic sample ZK-7. Geology based on Czech Geological Survey 1:50,000 map sheet 22-11 Přeštice



The structural aureole, defined as a zone where the background (regional) host-rock structures have been overprinted by emplacement-related deformation, can be clearly delimited near the northern and southern ends of the pluton where the intrusive contact is at an angle to the regional host-rock markers (foliation, lithologic contacts). Crossing the aureole boundary, the host-rock markers are deflected from their regional orientation (\sim NE–SW) toward parallelism with the pluton margin (Fig. 2). The structural aureole is \sim 1 km wide, that is, approximately 1/3 of pluton radius and almost twice as wide as the thermal aureole.

The pluton is composed of medium-grained (\sim 2–5 mm grain size) equigranular hornblende–biotite granodiorite to tonalite (ESM, Part 2a) and exhibits a faint normal compositional zoning defined by a more mafic outer facies grading into a more felsic center (Fig. 2; Klomínský 1965). The average modal composition of the granodiorite is 58% plagioclase (with normal oscillatory zoning), 20% quartz, 11% K-feldspar, 5% biotite, and 4% amphibole (Klomínský 1965). The modal proportion of plagioclase relative to K-feldspar decreases inward within the pluton (Klomínský 1965). Common accessories are apatite, zircon, titanite, and opaque minerals (chiefly magnetite).

Scattered decimeter-sized mafic microgranular enclaves composed mainly of diorite to quartz diorite (ESM, Part 2b–d), documenting multiple interactions between granodioritic and more mafic magmas (ESM, Part 2d; Vernon 1984; Didier and Barbarin 1991), occur throughout the pluton but are more common in the outer facies and sparse in the pluton center. Host-rock xenoliths (centimeter- to decimeter-sized) are rare. The pluton is cross-cut by more or less radially arranged leucogranite, aplite, and granite porphyry dikes (Fig. 2).

At the microscale, the textures are exclusively magmatic with no evidence for subsolidus deformation (defined using the criteria outlined in Paterson et al. 1989 and Vernon 2000); amphibole and feldspar grains have euhedral to subhedral shapes, and interstitial anhedral quartz is not recrystallized (ESM, Part 3a). Relatively abundant are microstructures indicative of material exchange/thermal disequilibrium due to the mixing between mafic and felsic magmas, such as mantled plagioclase, mixed acicular/equant apatite grain populations, and resorbed biotite flakes enclosed in large euhedral to subhedral amphibole crystals (ESM, Part 3b–d; e.g., Hibbard 1991, 1995; Janoušek et al. 2004a and references therein).

Gravimetric constraints on the Štěnovice pluton shape

In this study, gravity data are used to constrain approximately the overall shape and the minimum vertical

dimension of the Štěnovice pluton at depth. The gravity maps in Fig. 3a, b were constructed using the data owned by Geofond, Prague (Czech Republic), the gravity stations were positioned in a random grid and spaced 400–500 m apart (Fig. 3a, b).

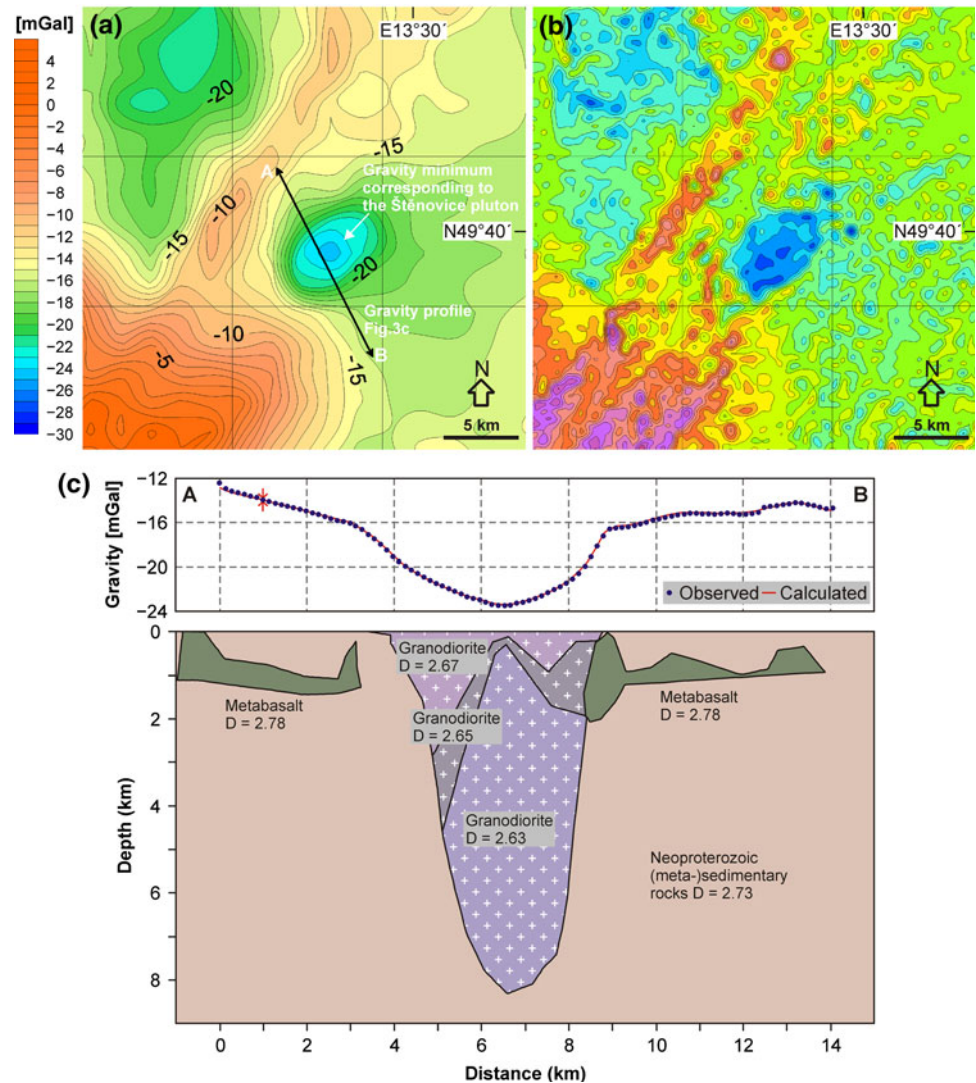
The principal feature in the central part of the gravity map is a positive anomaly corresponding to the Neoproterozoic metabasalts and a negative anomaly reflecting the Carboniferous cover to the NW. The pronounced gravity minimum of an elliptical, \sim NE–SW elongated shape (Fig. 3a) corresponds to the Štěnovice pluton. In order to better constrain the subsurface shape of the pluton, high-pass filtering was applied to construct the residual gravity map (Fig. 3b). This map also reveals an internal zoning within the pluton with the highest negative anomaly in the pluton center and along its southern margin (Fig. 3b).

The rock densities (defined as a bulk density with all pore space filled by water) used in the modeling are granodiorite $\rho = 2.67$ – 2.68 g cm $^{-3}$, Neoproterozoic (meta-)sedimentary rocks $\rho = 2.70$ – 2.75 g cm $^{-3}$, and metabasalts $\rho = 2.85$ – 2.95 g cm $^{-3}$. On the basis of simple modeling by Mrlina (1993) and our new 2.5D gravity modeling, the pluton seems to have a higher density in its upper part ($\rho = 2.65$ – 2.67 g cm $^{-3}$) and a lower density deeper section ($\rho = 2.63$ – 2.65 g cm $^{-3}$; Fig. 3c). The minimum vertical dimension of the pluton is estimated as \sim 6–8 km, and the pluton shape at depth is inferred as a steep-sided, downward-narrowing elliptical cone with its axis located close to the center of the gravity anomaly (Fig. 3c).

Whole-rock geochemistry

Six samples were taken in abandoned or active quarries to examine the whole-rock geochemical variations in the Štěnovice pluton (see Fig. 4 for sample locations, geographic coordinates are given in ESM, Part 4). The samples were analyzed for major- and trace-element whole-rock composition in the Activation Laboratories Ltd., Ontario, Canada (<http://www.actlabs.com>; using the 4Lithoresearch and Ultratrace-2 analytical packages). The samples were dissolved following the lithium metaborate/tetraborate fusion, analyses were carried out using ICP-MS/OES except for precious and base metals determined by aqua regia digestion and analyzed on ICP-MS. In addition, the new whole-rock analyses (ESM, Part 4) were supplemented by major-element data from the literature (Klomínský 1965; Breiter and Sokol 1997; Kopecký et al. 1997) and, for comparison, by the available analyses of the Čistá granodiorite (Klomínský 1965; Čadková et al. 1985; Breiter and Sokol 1997). All the data were then recalculated and plotted using the GCDkit software (Janoušek et al. 2006a).

Fig. 3 **a** Gravity map showing a pronounced negative gravity anomaly corresponding to the Štěnovice pluton. **b** Residual gravity map (high-pass filter) highlights the Neoproterozoic metabasalts (~NE–SW-trending clusters of local positive gravity anomalies) and a negative gravity anomaly of the Štěnovice pluton. **c** Gravity/density model of the Štěnovice pluton. D—density in g cm^{-3}



Major elements

Based on the newly obtained data, the granitoid rocks of the Štěnovice pluton are fairly acid ($\text{SiO}_2 = 66.6\text{--}69.7$ wt. %), corresponding to granodiorite–tonalite in the multicationic P–Q diagram of Debon and Le Fort (1983; Fig. 4a); several analyses published in the literature indicate intermediate, quartz dioritic to dioritic composition (Fig. 4a–b). The samples reveal a tendency to somewhat more felsic compositions in the pluton center compared to the margin. The Štěnovice pluton is made up of exclusively subalkaline rocks, as demonstrated by the TAS diagram (Fig. 4b), that define a calc-alkaline trend in the AFM plot (Fig. 4c; Irvine and Baragar 1971). All but one felsic sample ($\text{SiO}_2 > 65$ wt.%) can be characterized as medium-K rocks on the basis of the $\text{SiO}_2\text{--K}_2\text{O}$ diagram (Peccerillo and Taylor 1976; Fig. 4d). On the other hand, the more basic lithologies straddle the boundary with the adjacent low-K field. The Štěnovice granitoids are generally metaluminous, as

shown by the Shand's index A/CNK (molar $\text{Al}_2\text{O}_3/(\text{CaO} + \text{Na}_2\text{O} + \text{K}_2\text{O})$) ranging from 0.95 to 0.98 (Fig. 4e; ESM, Part 4); only a few samples are subaluminous having A/CNK up to 1.03. The mg number ($\text{mg}\# = \text{molar Mg}/(\text{Mg} + \text{Fet})$) of the newly collected samples varies only a little between 40 and 45, and sodium prevails significantly over potassium ($\text{K}_2\text{O}/\text{Na}_2\text{O} = 0.46\text{--}0.51$; ESM, Part 4).

Trace elements

The compositions of the newly collected samples were normalized by average normal mid-ocean ridge basalt (NMORB; Sun and McDonough 1989; Fig. 5a). The patterns are all enriched in LILE (Rb, Ba, Th, U, and K), starting at $>140 \times$ NMORB (Rb, Ba) and falling to less than $0.3 \times$ NMORB (Lu). All show superimposed peaks in Cs, Pb, and Sr; however, the most typical is a strong depletion in HFSE (troughs in Nb, P, and Ti).

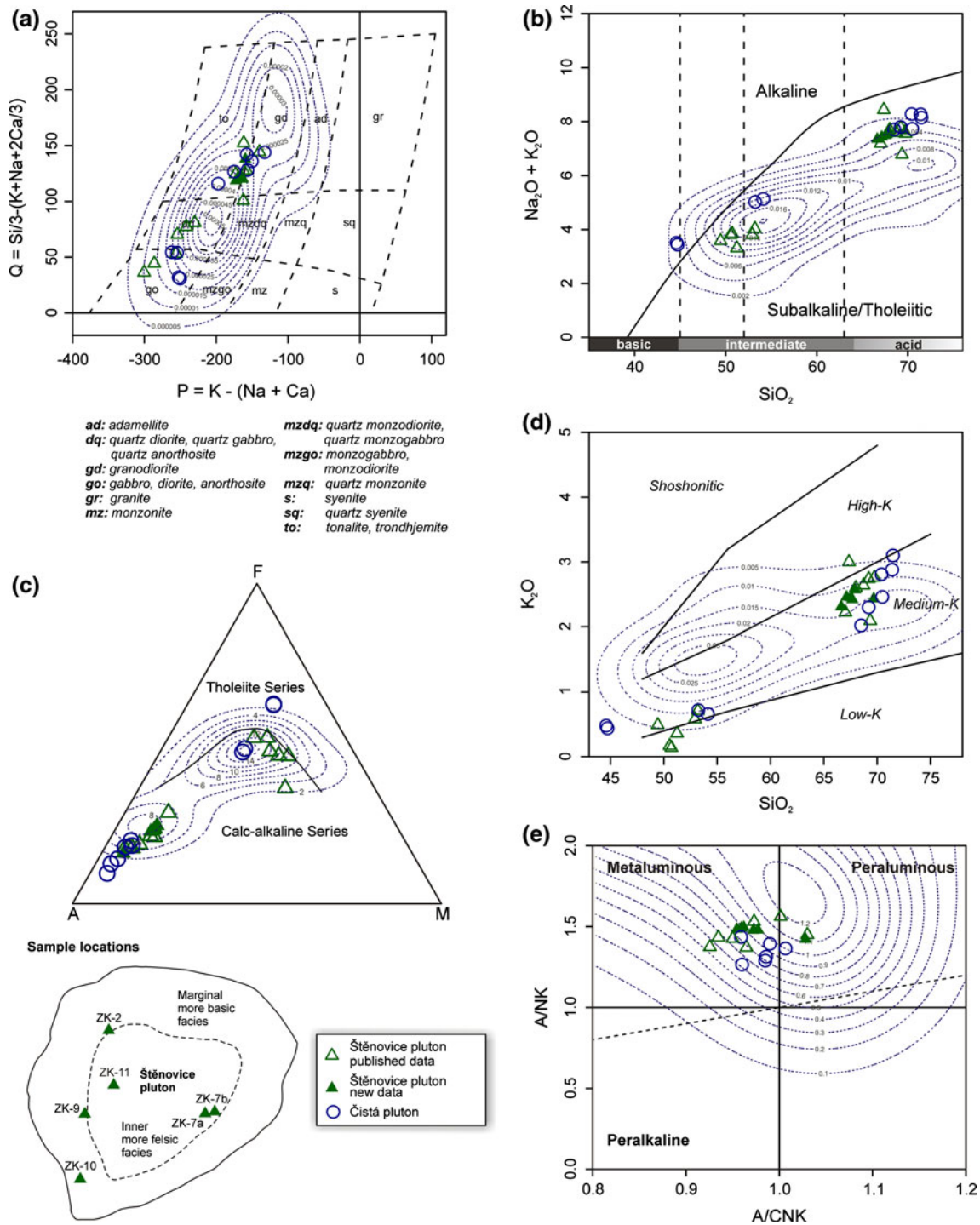


Fig. 4 Major-element-based classification of the Štěňovice and Čistá granitoids. The isolines as plotted by *GCDKit* (Janoušek et al. 2006a) portray the statistical distribution of the medium-K calc-alkaline Sázava suite, Central Bohemian Plutonic Complex (Janoušek et al. 2000, 2004a and unpublished data). **a** Multicationic P-Q plot (Debon and Le Fort 1983); P represents the proportion of K-feldspar to plagioclase and Q the quartz content. **b** SiO_2 - $\text{Na}_2\text{O} + \text{K}_2\text{O}$ (TAS) diagram with the discrimination boundary between the subalkaline and alkaline domains after Irvine and Baragar (1971). **c** AFM diagram (A = $\text{Na}_2\text{O} + \text{K}_2\text{O}$, F = FeO, M = MgO , all in wt. %; Irvine and

Baragar 1971). **d** SiO_2 - K_2O plot with the discrimination boundaries between the low-K, medium-K, high-K calc-alkaline, and shoshonitic rocks of Peccerillo and Taylor (1976). The more basic types correspond to low-K, whereas the acid rocks belong mostly to a medium-K association. **e** Molar $\text{Al}_2\text{O}_3/(\text{CaO} + \text{Na}_2\text{O} + \text{K}_2\text{O})$ vs $\text{Al}_2\text{O}_3/(\text{Na}_2\text{O} + \text{K}_2\text{O})$ (A/CNK vs A/NK, Shand 1943) plot of Maniar and Piccoli (1989) discriminating between metaluminous, peraluminous and peralkaline compositions. The plotted data points are metaluminous-subaluminous. Inset sketch map shows locations of geochemical samples

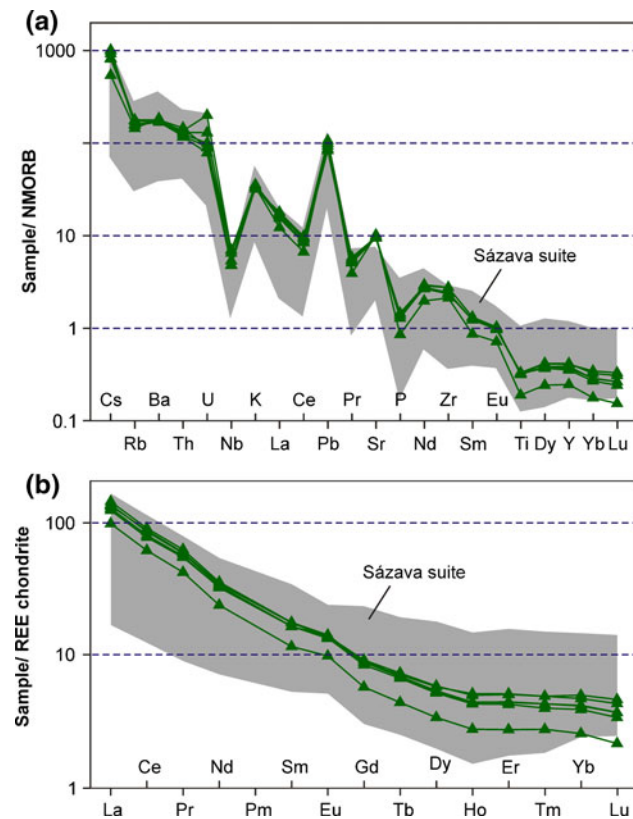


Fig. 5 Trace-element distribution in the studied granitoids of the Štěnovice pluton. **a** Normal Mid-Ocean Ridge Basalt (NMORB) normalized spider plots (Sun and McDonough 1989). **b** Chondrite-normalized (Boynton 1984) REE patterns. The shaded field denotes the range of compositions known from the medium-K calc-alkaline Sázava suite, Central Bohemian Plutonic Complex (Janoušek et al. 2000, 2004a and unpublished data)

The REE contents in the Štěnovice pluton do not vary significantly ($\Sigma\text{REE} = 107.6\text{--}159.1$; ESM, Part 4). The chondrite-normalized patterns have a slightly curved (convex down) shape with a fair degree of LREE/HREE enrichment ($\text{La}_N/\text{Yb}_N = 27.4\text{--}38.2$). They start at approximately $100\text{--}145 \times$ chondrite (La) and drop to $2.2\text{--}4.7 \times$ chondrite (Lu); typical is a weak positive Eu anomaly ($\text{Eu}/\text{Eu}^* = 1.1\text{--}1.2$; Fig. 5b).

The Zr concentrations broadly decreasing with silica indicate that saturation in zircon was reached, the occurrence of inheritance unlikely, and the zircon thermometry is applicable (Watson and Harrison 1983; Hoskin et al. 2000; Miller et al. 2003; Janoušek 2006). The calculated mean zircon saturation temperature is $783 \pm 14^\circ\text{C}$ (2σ , excluding the calibration and analytical errors).

Inferences on geotectonic setting of the Štěnovice pluton

In the NMORB-normalized spiderplots, the LILE/HFSE enrichments and deep troughs in HFSE of the analyzed

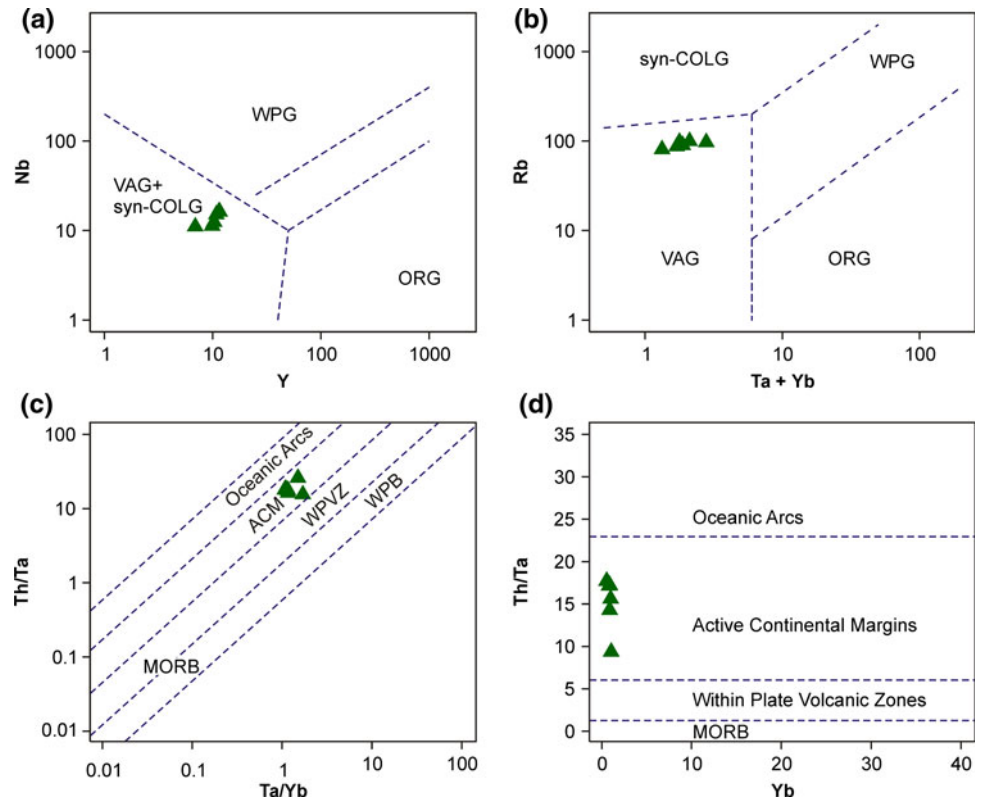
samples resemble those observed in K-rich basalts in the continental margin arc settings (e.g., Saunders et al. 1991; Pearce and Parkinson 1993; Tatsumi and Eggins 1995). The new data including those compiled from the literature (Čadková et al. 1985; Breiter and Sokol 1997) confirm such a notion (see selected diagrams in Fig. 6). For instance, in the Y vs. Nb and Ta + Yb vs. Rb plots after Pearce et al. (1984), all the samples fall into the Volcanic Arc Granites domain (VAG in Fig. 6a–b). Similarly, in the Ta/Yb vs. Th/Ta as well as Yb vs. Th/Ta diagrams (Schandl and Gorton 2002) the Štěnovice analyses occupy the Active Continental Margins field (ACM in Fig. 6c–d).

New zircon geochronology of the Štěnovice pluton

The sample for zircon dating (ZK-7) was taken in an active quarry near Štěnovický Borek ~ 1 km ESE of the pluton center (Fig. 2; WGS84 coordinates are $\text{N}49.64991032^\circ$, $\text{E}13.43986331^\circ$). The zircon grains were separated from the sample using the Wilfley shaking table and heavy liquids and were then mounted in epoxy-filled block and polished. Isotopic analysis of zircon by laser ablation ICP-MS followed the technique described in Košler et al. (2002) and in Košler and Sylvester (2003). A Thermo-Finnigan Element 2 sector field ICP-MS coupled to a 213 NdYAG laser (New Wave Research UP-213) at Bergen University, Norway, was used to measure Pb/U and Pb isotopic ratios in zircons. The sample introduction system was modified to enable simultaneous nebulization of a tracer solution and laser ablation of the solid sample (Horn et al. 2000). Natural Tl ($^{205}\text{Tl}/^{203}\text{Tl} = 2.3871$; Dunstan et al. 1980), ^{209}Bi and enriched ^{233}U and ^{237}Np ($>99\%$) were used in the tracer solution, which was aspirated to the plasma in an argon–helium carrier gas mixture through an Apex desolvation nebulizer (Elemental Scientific) and a T-piece tube attached to the back end of the plasma torch. A helium gas line carrying the sample from the laser cell to the plasma was also attached to the T-piece tube.

The laser was fired at a repetition rate of 10 Hz and energy of ca. $0.5 \text{ J}/\text{cm}^2$. Linear laser rasters (100 microns) were produced by repeated scanning of the laser beam at a speed of 10 microns/second across the zircon sample surface. Typical acquisitions consisted of 35 s measurement of blank with Tl–Bi–U–Np solution followed by measurement of U and Pb signals from the ablated zircon for another 110 s. The data were acquired in time resolved—peak jumping—pulse counting mode with 1 point measured per peak for masses 202 (flyback), 203 and 205 (Tl), 206 and 207 (Pb), 209 (Bi), 233 (U), 237 (Np), 238 (U), 249 (^{233}U oxide), 253 (^{237}Np oxide) and 254 (^{238}U oxide). Raw data were corrected for dead time of the electron multiplier and processed offline in a spreadsheet-based

Fig. 6 Geotectonic diagrams of Pearce et al. (1984): **a** Y vs. Nb plot, **b** Ta + Yb vs. Rb plot. The labeled fields are Volcanic Arc Granites (VAG), Within-Plate Granites (WPG), Syn-Collisional Granites (syn-COLG) and Ocean Ridge Granites (ORG). Geotectonic diagrams of Schandl and Gorton (2002) originally designed to decipher the geotectonic setting of felsic volcanic suites: **c** Ta/Yb vs. Th/Ta plot, **d** Yb vs. Th/Ta plot. The diagrams discriminate between rocks intruding in Oceanic Arcs, Active Continental Margins (ACM), and Within-Plate Volcanic Zones (WPVZ). Field of Mid-Oceanic Ridge Basalts (MORB) and Within-Plate Basalts (WPZ) is delineated for comparison



program (Lamdate; Košler et al. 2002). Data reduction included correction for gas blank, laser-induced elemental fractionation of Pb and U and instrument mass bias. Minor formation of oxides of U and Np was corrected for by adding signal intensities at masses 249, 253, and 254 to the intensities at masses 233, 237, and 238, respectively. No common Pb correction was applied to the data. Zircon reference material 91500 (1065 Ma; Wiedenbeck et al. 1995) was periodically analyzed during the measurement for quality control purposes.

From the sample of the Štěnovice granodiorite, 33 zircon grains with clear magmatic oscillatory zoning (Fig. 7a) yielded concordant U–Pb isotopic ages with the mean age of 375 ± 2 Ma (2σ ; Fig. 7b; ESM, Part 5); this is interpreted as the age of the crystallization of the Štěnovice pluton.

Structure and magnetic fabric of the Štěnovice pluton

Magmatic foliations and lineations

Magmatic (hypersolidus) foliations and lineations are macroscopically discernible planar and linear shape-preferred orientations of mineral grains (also referred to as the mineral fabric), respectively, acquired during the presence of a melt and showing no evidence of subsolidus deformation (Paterson et al. 1989, 1998; Vernon 2000). In the

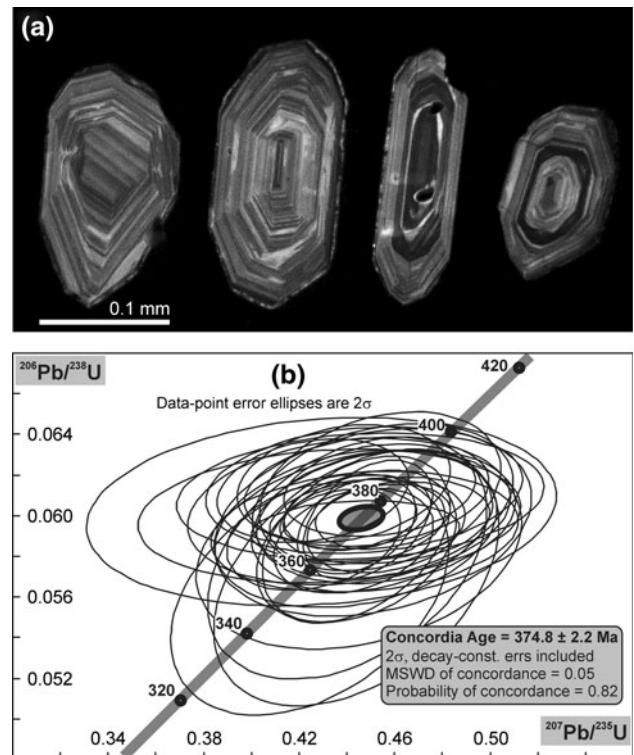
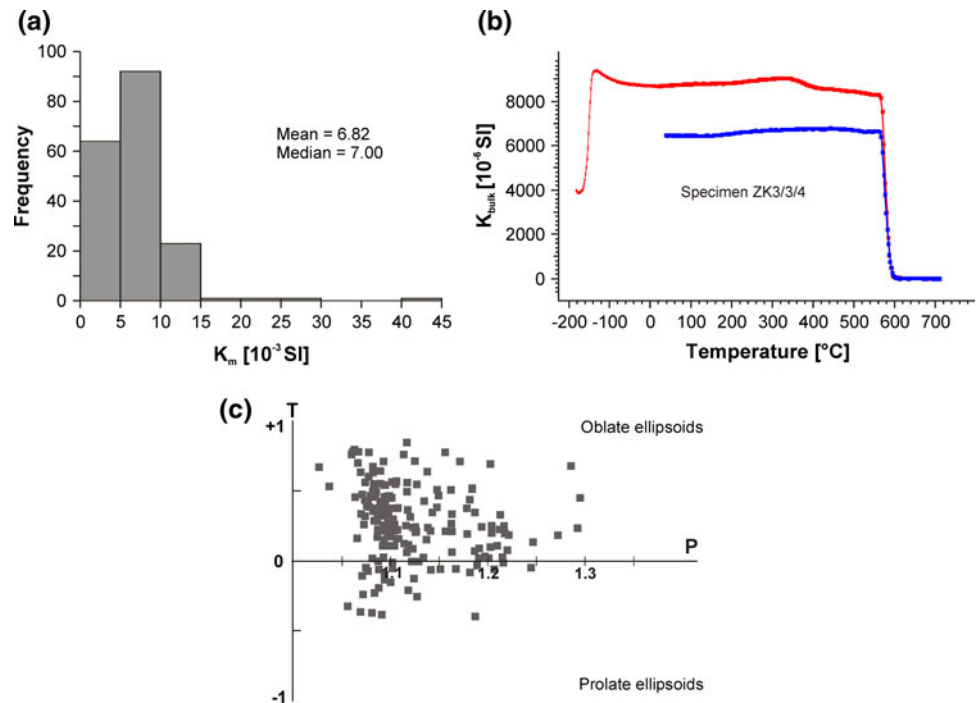


Fig. 7 **a** Representative cathodoluminescence images of analyzed magmatic zircon grains from the sample of Štěnovice granodiorite (ZK-7). **b** U–Pb Concordia diagram for zircons from the Štěnovice granodiorite (33 analyses in total). All data are plotted with 2σ uncertainties

Fig. 8 **a** Histogram of the bulk susceptibility distribution for all specimens from the Štěnovice pluton. **b** Heating magnetic susceptibility vs. temperature curve for one representative specimen of the granodiorite (ZK3/3/4), the shape of the curve and Curie temperature of about 580°C (drop in bulk susceptibility to zero) proves magnetite as the main carrier of the AMS. **c** Magnetic anisotropy P–T plot summarizing all data from the Štěnovice pluton. The AMS ellipsoid is mostly oblate ($T > 0$) and the degree of anisotropy (P) is low to moderate, clustering between 1.06 and 1.22



Štěnovice pluton, the magmatic lineation is defined by the alignment of euhedral hornblende crystals, and the magmatic (mineral) foliation is defined by biotite flakes, plagioclase, and K-feldspar grains (ESM, Part 2a). The intensity of the mineral fabric decreases from the pluton/wall-rock contact inward, and the fabric ellipsoid is typically oblate throughout the pluton, i.e., the mineral foliation is more intensely developed than the lineation. Near the pluton margins where the mineral foliation is stronger, the flattened microgranular enclaves are oriented subparallel to this foliation (ESM, Part 2b). The lineation is subvertical (plunge is 80–90°), the foliation also dips steeply (70–90°) and strikes subparallel to the outer pluton margin (Fig. 2). Magmatic foliation in the pluton thus defines a concentric, “onion-skin” pattern decoupled from the regional host-rock structures.

Anisotropy of magnetic susceptibility (AMS)

The anisotropy of magnetic susceptibility (AMS) was used to quantitatively characterize the magnetic fabric and its gradients in the pluton. A total of 183 oriented specimens were taken using a portable drill at 13 stations throughout the pluton. The AMS was measured with a KLY-4S Kappabridge apparatus at the Institute of Geophysics, Academy of Sciences of the Czech Republic. A statistical analysis of the AMS data was carried out using the ANISOFT package of programs (written by M. Chadima and V. Jelínek; www.agico.com). The measured AMS data and

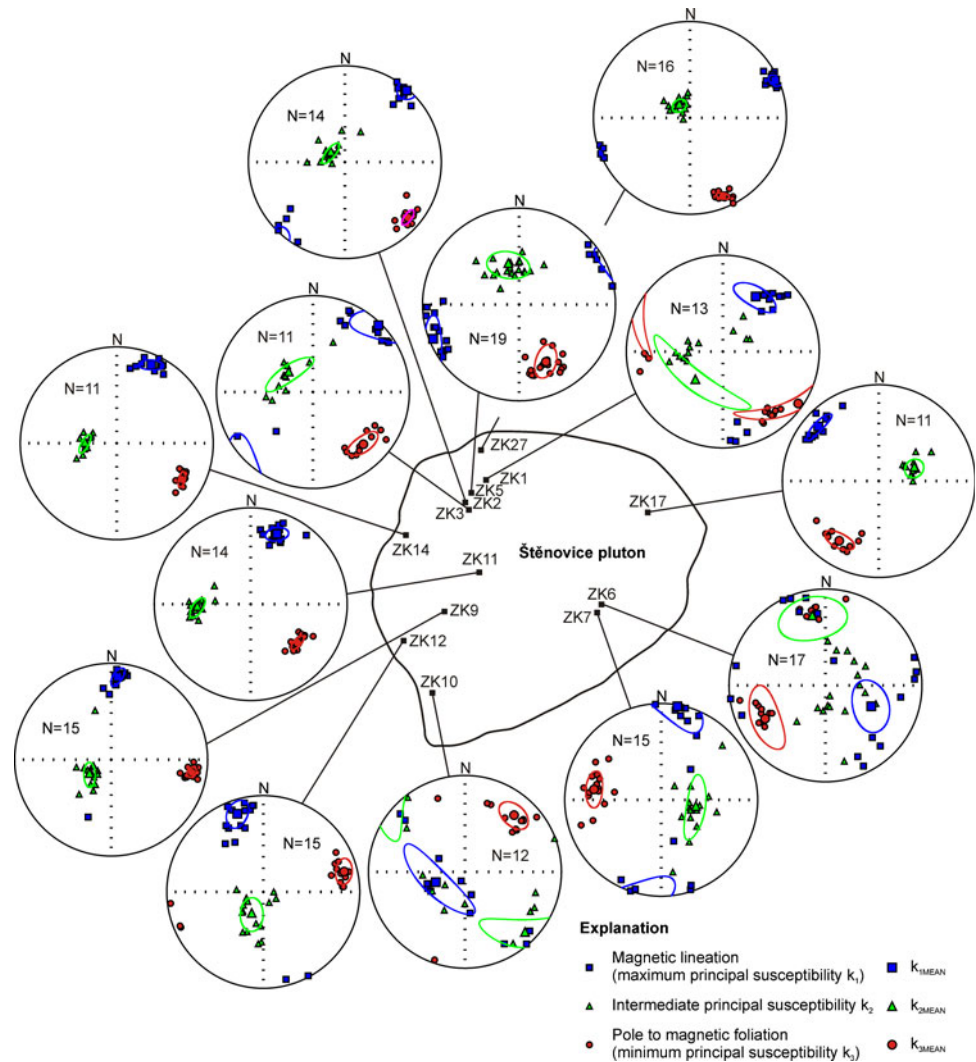
parameters are listed in the Electronic Supplementary Material (Part 6).

The AMS data are represented by the k_m , P , and T parameters defined as follows: (1) $k_m = (k_1 + k_2 + k_3)/3$; (2) $P = k_1/k_3$; and (3) $T = 2\ln(k_2/k_3)/\ln(k_1/k_3) - 1$; where $k_1 \geq k_2 \geq k_3$ are the principal susceptibilities. The parameter k_m represents the mean magnetic susceptibility, which reflects the qualitative and quantitative content of magnetic minerals in the rock. The parameter P (Nagata 1961), called the degree of AMS, reflects the eccentricity of the AMS ellipsoid and thus indicates the intensity of the preferred orientation of the magnetic minerals in the rock. The parameter T (Jelínek 1981) characterizes the symmetry of the AMS ellipsoid; it varies from -1 (perfectly linear magnetic fabric) through 0 (transition between linear and planar magnetic fabric) to $+1$ (perfectly planar magnetic fabric). In fabric studies, the maximum principal susceptibility (k_1) is referred to as the magnetic lineation, and the minimum principal susceptibility (k_3) defines a pole to the magnetic foliation; their orientations are presented in stereograms in the geographic (in situ) coordinate system and as locality mean values on the map.

Magnetic mineralogy

The mean magnetic susceptibility of the analyzed samples is in the order of 10^{-3} – 10^{-2} [SI]; the frequency distribution of the bulk susceptibility of the samples is shown in Fig. 8a. Such a high susceptibility is typical of ferromagnetic

Fig. 9 Simplified map of the Štěnovice pluton (bold outline) showing stereographic projections (equal area, lower hemisphere) of principal susceptibilities at each station, including their mean orientations and confidence ellipses



granites (e.g., Bouchez 1997) and indicates the presence of a ferromagnetic fraction that controls the rock susceptibility.

In order to specify the ferromagnetic carriers, the temperature variation of susceptibility was investigated on one specimen (ZK3/3/4) using the KLY-4S Kappabridge, CS-3 Furnace and CS-L Cryostat apparatus at the Institute of Geophysics, Academy of Sciences of the Czech Republic. The measured data were processed using the computer code Cureval (AGICO, Inc.). The susceptibility variations with temperature were measured in the temperature range of -196°C to 5°C where no changes in mineralogy appear and then in the interval from room temperature to 700°C .

The measurements of the magnetic susceptibility variation with temperature are presented in Fig. 8b. A clear Verwey transition exists in the low-temperature part of the curve (between -165°C and -150°C) as well as an abrupt decrease in susceptibility around 580°C (T_C ; the Curie temperature of magnetite), both proving that magnetite,

which is a common accessory phase, is the main carrier of the AMS in the Štěnovice pluton.

Magnetic fabric parameters and orientation

The degree of magnetic anisotropy (P) varies from 1.027 to 1.295 with the majority of specimens between $P = 1.060$ and $P = 1.150$ (Fig. 8c). The shape parameter (T) ranges from -0.396 to 0.844, indicating both prolate (16% specimens) but predominantly oblate (84% specimens) shapes of the AMS ellipsoid (Fig. 8c). On the map, the average values of P and T (calculated as arithmetic mean at each locality) exhibit no significant spatial variations within the pluton except for P being higher at some stations near the pluton margin (mean value is $P = 1.3$) compared to the center (mean value is $P = 1.08$; ESM, Part 7).

Magnetic foliations are generally steep (dip ranges from 48° to 89°) and margin-parallel throughout the pluton (Figs. 9, 10), corresponding to the mesoscopic (magmatic)

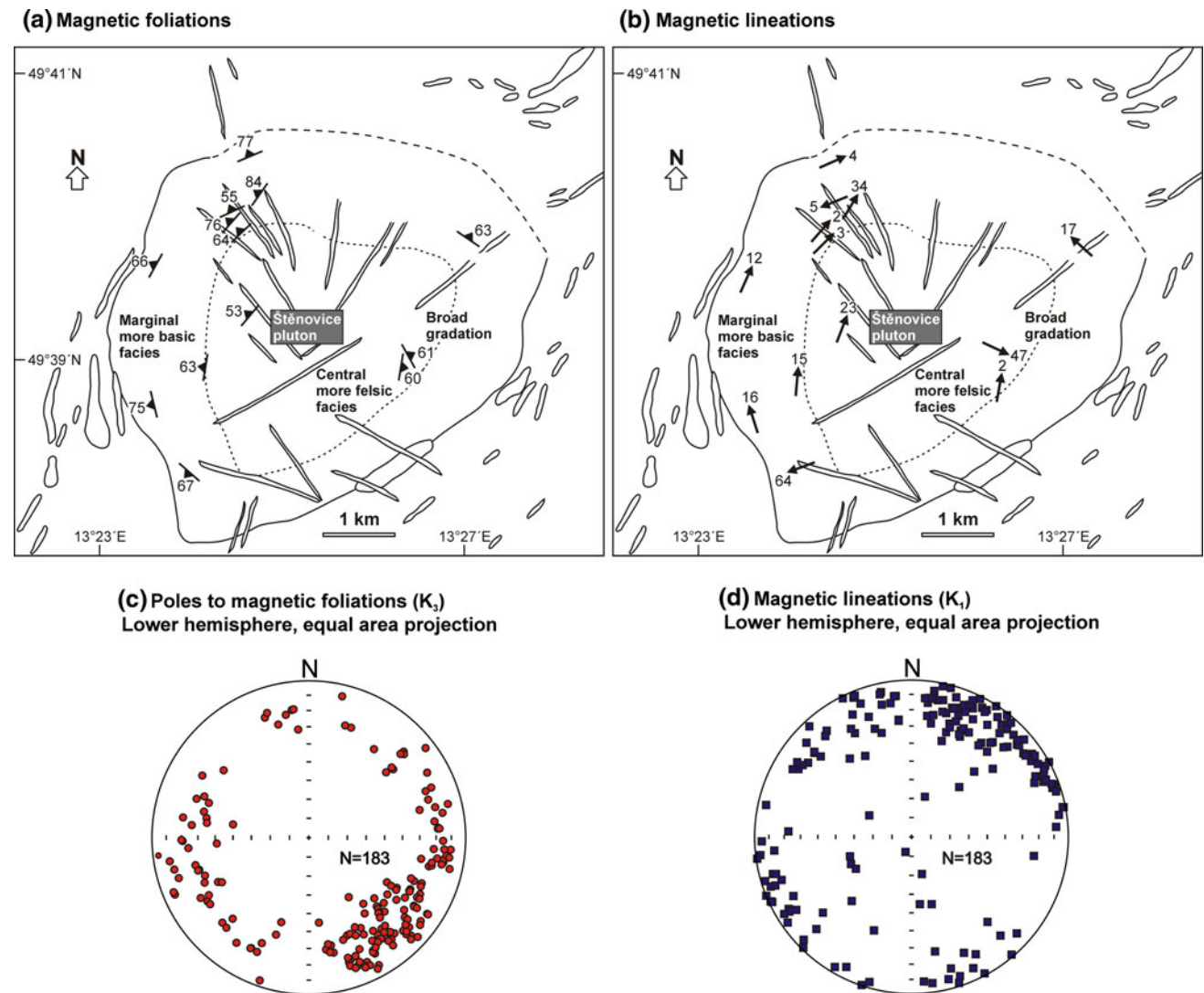


Fig. 10 **a, b** Maps of magnetic foliations and lineations (mean values at each station) in the Štěnovice pluton. Foliations are steep and margin-parallel, lineations plunge shallowly to moderately at variable

foliations (compare Figs. 2 and 10a, c). Both mesoscopic and magnetic foliations define an “onion-skin” pattern. The plunge of magnetic lineations is highly variable ranging from 0° to 82° but most of the lineations plunge shallowly ($0\text{--}40^\circ$; 93% specimens) and trend parallel to the pluton margin (Figs. 9, 10b, d).

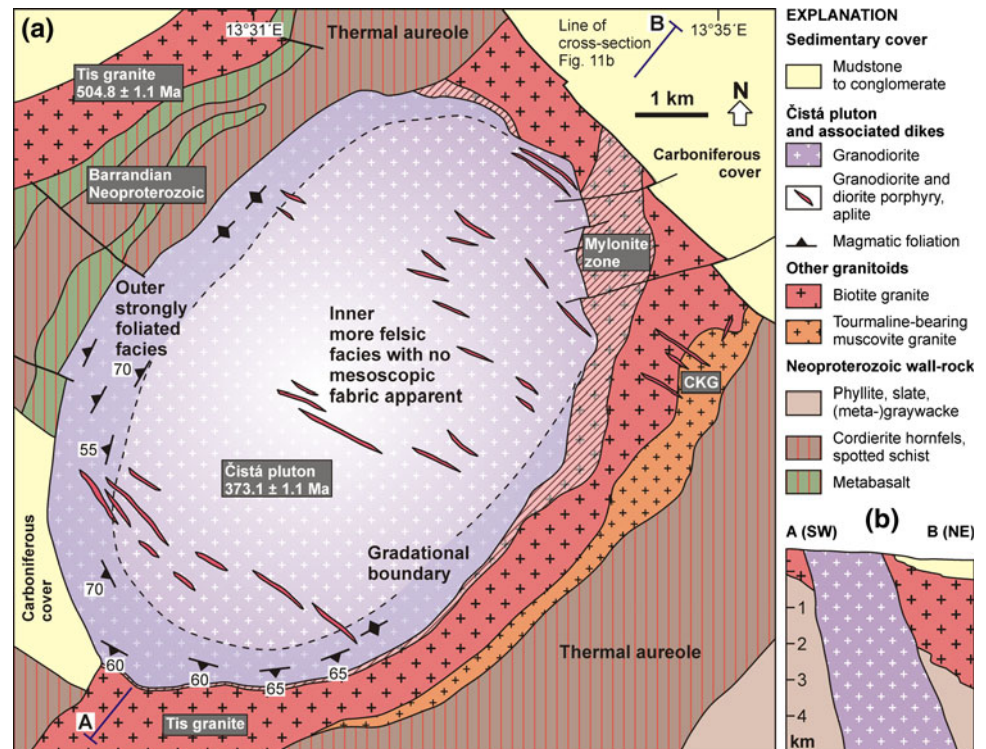
Geologic setting, structure, and magnetic fabric of the Čistá pluton

The Čistá pluton, dated at 373.1 ± 1.1 Ma using the Pb–Pb single zircon evaporation method (Venera et al. 2000), has an elliptical shape in plan view (8.5×6 km, ~ 38 km²) with its long axis oriented \sim NE–SW (Fig. 11a; see Klomínský 1963; Chlupáčová et al. 1975;

trends but in many cases are subparallel to the pluton margin. **c, d** Synoptic stereographic projections (equal area, lower hemisphere) of all magnetic foliations and lineations in the pluton

Kopecný et al. 1997 for other details on regional geology). On the basis of a gravimetric survey verified by several boreholes, the three-dimensional pluton shape at depth is a steeply dipping cylinder (stock) plunging northeast (Fig. 11b; Kopecný et al. 1997). The pluton intruded across the poorly exposed low-grade Neoproterozoic (Ediacaran) phyllites and metabasalts to the northwest and a Cambrian tabular pluton to the southeast (the ~ 505 Ma Tis granite; Venera et al. 2000). The contact of the Čistá pluton against its wall-rock is generally steep and dips inward or outward in different parts of the pluton. The southwestern end of the pluton is concealed beneath the Carboniferous cover, while its northwestern margin is poorly exposed and is parallel to the \sim NE–SW-trending lithologic contacts in the Neoproterozoic host (Fig. 11a). The granodiorite/Tis granite

Fig. 11 a Simplified geologic map of the Čistá pluton. The pluton intrudes the Neoproterozoic meta-sedimentary rocks to the northwest and the Late Cambrian Tis granite to the southeast. Geologic background compiled from the Czech Geological Survey 1:50,000 map (sheets 12–13 Jesenice and 12–31 Plasy), Klomínský (1963), and Kopecký et al. (1997); structural data taken from Klomínský (1963) and Kopecký et al. (1997). Evaporation Pb–Pb zircon ages of Venera et al. (2000) for the Čistá granodiorite and the Tis granite are also shown. **b** Simplified NE–SW cross-section across the pluton and its host rock. Based on geophysical and borehole data the pluton has steeply inclined cylindrical shape; modified from Kopecký et al. (1997)



contact is delineated by a cataclasite–mylonite and associated alkaline-metasomatic (fenite) zone (Fig. 11a).

An up to 3-km wide thermal aureole, characterized by hornfels and spotted schists, is developed in the Neoproterozoic wall/rock southeast of the Tis granite and along the northwestern margin of the Čistá granodiorite (Fig. 11a). As the Čistá granodiorite intruded across the large tabular body of the Tis granite (Kopecký et al. 1997; Fig. 11b), the northwestern segment of the aureole likely reflects superimposed thermal effects on wall-rock from both intrusions.

The Čistá pluton is normally zoned; an outer rim composed of strongly foliated (a complete transition from magmatic to subsolidus foliation was described by Venera et al. 2000) and more mafic amphibole–biotite granodiorite (plagioclase prevails over K-feldspar) with abundant mafic microgranular enclaves grades inward into more felsic, medium- to fine-grained biotite granodiorite with a weak or macroscopically not discernible magmatic fabric. The overall internal structure of the pluton is concentric, defined by steep margin-parallel foliation associated with variably oriented hornblende lineation (see structural map in Fig. 6 in Venera et al. 2000). Late ~NW–SE-trending dikes of granodiorite, diorite porphyry, and aplite cut across the pluton (Fig. 11a), implying that the granodiorite body underwent a post-emplacement brittle extension parallel to the long axis of the pluton (in plan view).

The most in-depth investigation into the internal structure and magnetic (AMS) fabric of the Čistá pluton was

presented by Chlupáčová et al. (1975). Their AMS data corroborate the overall concentric structure of the pluton (Fig. 12) and also indicate a generally oblate shape of the AMS ellipsoids and increasing degree of magnetic anisotropy toward the pluton margin. Similarly to the Štěnovice pluton, the main AMS carrier in the Čistá pluton is magnetite, which particularly near the pluton margin, also grew mimetically enhancing the shape-preferred orientation of biotite flakes (Hrouda et al. 1971, 1972; Chlupáčová et al. 1975).

Except for one station (No. 7 in Fig. 12), magnetic foliations are steep and margin-parallel and magnetic lineations plunge steeply to moderately (Fig. 12). In a synoptic stereonet, magnetic foliation poles thus concentrate near the periphery of the diagram while magnetic lineations define a prominent cluster close to its center passing into a cluster of data points corresponding to lineations plunging moderately to the ~NNE (Fig. 12). The apparent preponderance of the ~NE–SW magnetic foliations is a sampling bias caused by the lack of stations at the NE and SW ends of the pluton.

Interpretation of structure and emplacement of the Štěnovice and Čistá plutons

The following lines of evidence suggest that the Štěnovice and Čistá plutons have characteristics typical of concentrically expanded plutons (CEPs) emplaced via diapirism

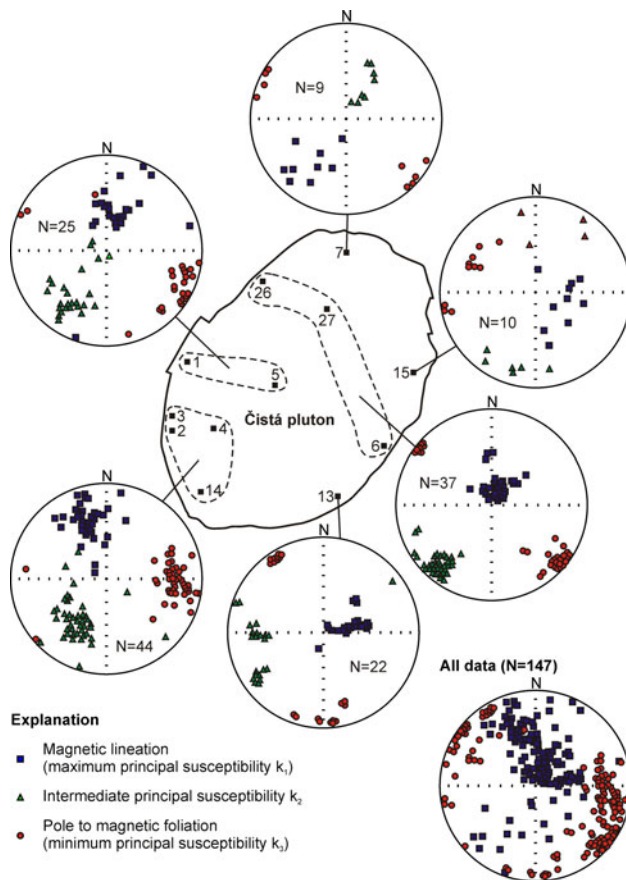


Fig. 12 Simplified map showing orientation of principal susceptibilities at 13 stations in the Čistá pluton (bold outline). All the AMS data from the pluton are also summarized in the synoptic stereonet (stereographic projections are equal area, lower hemisphere). Note the steep, margin-parallel magnetic foliations and steep to NNE-plunging magnetic lineations. The AMS data were taken from Chlupáčová et al. (1975)

and/or in situ lateral expansion (Paterson and Vernon 1995; Dietl and Koyi 2002).

- Both plutons have steep margins and elliptical shapes in plan view. As inferred from gravimetric and borehole data, the Čistá pluton continues downward for at least 5 km as an inclined, steep-sided cylinder (Fig. 11b; Kopecký et al. 1997). Similarly, the Štěnovice pluton has an outward-dipping steep margin near the present-day erosion surface and, on the basis of our gravimetric interpretation, extends down for at least 6–8 km as a downward-narrowing cone with a weakly elliptical cross-section (Fig. 3c).
- Both plutons are surrounded by distinct thermal and structural aureoles. Lithologic contacts and the host-rock structures are notably deflected in a wide zone around the Štěnovice pluton. The width of this aureole corresponds to 1/3 of the pluton radius, which is well comparable to other examples of CEPs (e.g., Paterson

et al. 1991; Paterson and Fowler 1993; Paterson and Vernon 1995; Miller and Paterson 1999). The interpretation of the aureole in the Neoproterozoic host rocks northwest of the Čistá pluton is not so straightforward, as the aureoles of both the Tis and Čistá plutons overlap. Large portions of this margin are poorly exposed and parallel to the trend of regional structures, thus provide no or ambiguous information on the emplacement of the pluton. The contact of the Čistá pluton against the Tis granite is a tens to hundreds meters wide high-temperature mylonite zone (Fig. 11a), which may represent a narrow ductile aureole wherein the host, thermally softened Tis granite (Venera et al. 2000) accommodated strain related to the emplacement of the Čistá pluton.

It has been shown by He et al. (2009) that examining wall-rock structures within aureoles of CEPs is crucial in distinguishing between ballooning (in situ lateral expansion of a pluton producing large flattening strains in the wall-rock) from purely diapiric magma emplacement accommodated by downward return flow of the wall-rock. In the case of both plutons examined here, however, the lack of exposure and scarcity of structural data from the aureoles (particularly in segments at a high angle to regional host-rock structures) preclude rigorous distinction between these two end-member, but commonly closely interlinked, modes of emplacement.

- In both plutons, no internal contacts were found that could be used to define smaller within-pluton intrusive units representing individual magma batches or sheets. Instead, the plutons are normally zoned with the outer more mafic facies passing gradually into a more felsic interior (Klomínský 1963, 1965; Kopecký et al. 1997; Figs. 2, 11a). The gravimetric survey indicates no significant change in rock densities in the deeper sections of the plutons that could possibly reflect the presence of denser bodies of gabbros or diorites or large screens of the Neoproterozoic host rock down to depth of at least ~8 km (Fig. 3c). This, in turn, suggests that even at such depth the plutons are compositionally rather homogeneous like near the present-day surface. We thus interpret that both the Štěnovice and Čistá plutons intruded either as single, coherent magma blobs with sidewall fractional crystallization producing the normal zoning, or as two or just a few coeval, thus not well recognizable, nested somewhat more felsic into less felsic batches (e.g., Chlupáčová et al. 1975).
- In both plutons, the steeply dipping mineral (mesoscopic) foliations define margin-parallel, concentric (“onion-skin”) patterns (Figs. 2, 11a) that are also typical of CEPs (e.g., Ramsay 1989; Paterson and

Fowler 1993; Miller and Paterson 1999; Molyneux and Hutton 2000; Siegesmund and Becker 2000; Galadí-Enríquez et al. 2003; Tahiri et al. 2007; He et al. 2009). This notion is supported by the AMS reflecting the shape anisotropy or mimetic growth of magnetite (Hrouda et al. 1971), as the magnetic foliations in both plutons are margin-parallel and generally mimic the mesoscopic foliations.

In the Čistá pluton, both mineral (hornblende) and magnetic (magnetite) lineations plunge steeply to moderately (Fig. 12), which was interpreted by Chlupáčová et al. (1975) as a result of bulk stretching during diapiric magma ascent through a steep-sided conduit. By contrast, magnetic lineations are margin-parallel (circumferential) and plunge $<40^\circ$ in the Štěnovice pluton (this study, Figs. 9, 10b, d) suggesting that the finite principal stretching in the magma was oriented at a high angle to the presumed steep magma ascent path. With the aid of gravimetric data indicating that the Štěnovice pluton has a downward-narrowing shape at depth (Fig. 3c), we suggest that, upon arrival to the present-day exposure level, the bulk steep magma ascent converted to lateral stretching along walls as the conduit broadened. Perhaps, continuing divergent magma flow or arrival of a new magma surge into the hotter pluton center then caused fairly minor margin-perpendicular flattening and lateral along-wall stretching of the outer, highly crystallized magma carapace. The strain recorded by the magnetite fabric was weak, however, as indicated by the lack of subsolidus deformation in the outer granodiorite and generally low fabric intensity in the pluton. Such a mechanism would explain the concentric magmatic (mineral) foliation intensifying toward the pluton margin, shallowly plunging margin-parallel magnetite lineation, and oblate shape of the AMS ellipsoid.

In short, the inferences developed above suggest that the Štěnovice and Čistá plutons intruded as steep-sided and vertically extensive magma batches (stocks) that pierced and, at least in the case of the Štěnovice pluton, expanded laterally into the upper-crustal host rocks. Hence, both plutons are largely discordant and post-kinematic with respect to the regional ductile structures (cleavage, large-scale folds) in their adjacent host rocks—a point that will become particularly important in the following section.

Discussion

Over the past decade, a vigorous discussion has centered on the location and polarity of possible subduction zones in the Bohemian Massif during the Variscan orogeny (e.g., Konopásek and Schulmann 2005; Medaris et al. 2005; Franke 2000, 2006; Finger et al. 2007; Schulmann et al.

2009; Edel and Schulmann 2009; Dörr and Zulauf 2010). The unresolved issues include the exact number of lithospheric microplates involved (separated by oceanic domains), the deformation styles, kinematics, timing, and duration of subductions and subsequent collisions, as well as the link between subduction and magmatism. We envisage that the Štěnovice and Čistá plutons may help to unravel these questions and provide additional information on the yet poorly understood and in many points controversial early (Mid- to Late-Devonian) stages of the Variscan orogeny in the central Bohemian Massif.

The Late Devonian calc-alkaline plutonism in the Teplá–Barrandian unit

The major- and trace-element whole-rock geochemical characteristics, such as normal calc-alkaline chemistry, prevalence of Na over K, deep troughs in HFSE on NMORB-normalized diagrams accompanied by a strong enrichment of hydrous-fluid mobile LILE (Figs. 4, 5, 6), resemble igneous suites from active continental margin arc settings (e.g. Wilson 1989; Tatsumi and Eggins 1995). However, no analyses of basic rocks are available, and it is a well-known fact that the igneous-arc-like signature in granites can be equivocal. Their chemistry may both reflect the true setting as well as signature inherited from a source through either remelting of meta-igneous arc-related rocks (Arculus 1987), or anatexis of immature psammitic sediments containing arc-derived detritus (Roberts and Clemens 1993; Janoušek et al. 2010a, b). This holds true especially for the syn-collisional and post-collisional uplift settings, when a range of crustal sources is available for melting (Pitcher 1982; Pearce et al. 1984; Bonin 1990; Barbarin 1990; Pearce 1996).

Strikingly geochemically similar but significantly younger are Na-rich granodiorites, tonalites, and quartz diorites of the Sázava suite of the Central Bohemian Plutonic Complex (Fig. 1b; 354 ± 4 Ma, Janoušek et al. 2004a). These plutonic rocks are intimately associated with abundant (olivine, clinopyroxene-) amphibole-bearing gabbros and gabbrodiorites, which had to come from a slightly depleted mantle source modified by slab-derived fluids (Janoušek et al. 2004a, 2010a). Comparison of the whole-rock geochemistry of the Štěnovice and Čistá granitoids with that of the Sázava suite shows that all these plutons belong to one family of calc-alkaline and metaluminous–subaluminous plutonic rocks, having an overlapping range of major- and trace-element compositions as well as the overall shape of the trace-element patterns (Figs. 4, 5). This concerns also the REE patterns, characterized by the presence of a slight positive Eu anomaly. This phenomenon is by no means rare in the Sázava suite and was interpreted as a result of fractionation of

amphibole-dominated assemblage or partial melting of amphibole-bearing sources (Janoušek et al. 2000). Slight differences are observed only in Cs, Pb, Zr, and Sr that seem to be somewhat enriched in the Štěnovice pluton compared to the Sázava suite. On the basis of the above, we conclude that the Štěnovice and Čistá plutons have been generated in an initial continental magmatic arc setting.

The Pb–Pb single zircon age of 373 ± 1 Ma for the Čistá granodiorite (Venera et al. 2000) and the newly determined U–Pb age of 375 ± 2 Ma for the Štěnovice granodiorite also rank these plutons to the oldest vestiges of Variscan arc-related plutonic activity in the Bohemian Massif. The only comparable Late Devonian ages were obtained from the Staré Sedlo and Mirovice orthogneisses in the roof pendants of the Central Bohemian Plutonic Complex (Fig. 1b; 375 ± 5 Ma, 373 ± 5 Ma, 369 ± 4 Ma; Košler et al. 1993) and somewhat younger age from the Teufelsberg diorite at the southernmost tip of the TBU (Fig. 1b; 359 ± 2 Ma; Bues et al. 2002).

Tectonic implications

In the following interpretations, we consider only the Late Devonian to early Carboniferous calc-alkaline plutons, which have intrusive contacts against the TBU and thus are indisputably fixed in their original emplacement position in the upper crust. We exclude other comparable granitoid or meta-granitoid complexes that are allochthonous or have been sheared, displaced, or even buried to and exhumed from greater depths (e.g., Janoušek et al. 2006b; Verner et al. 2009).

The supracrustal TBU is specific in that it hosts the arc-related calc-alkaline plutons while it occupies the hanging-wall position with respect to the neighboring Saxothuringian and Moldanubian units in the center of the Bohemian Massif (Fig. 1a, b). Thus, the TBU is the overriding plate for all the hypothetical subduction zones (Fig. 1a). The question arises whether the Late Devonian to early Carboniferous arc-related magmas were generated by the SE-directed subduction of the narrow Saxothuringian Ocean along the present-day Saxothuringian/Teplá–Barrandian boundary (Fig. 1a; e.g., Zulauf 1997b; O’Brien 2000; Janoušek et al. 2004b; Konopásek and Schulmann 2005; Janoušek and Holub 2007; Machek et al. 2009; Schulmann et al. 2009; Žák et al. 2009), or by the opposite NW-directed subduction of the Gföhl Ocean between the Moldanubian unit and southeastern margin of the TBU now occupied by the Central Bohemian Plutonic Complex (Fig. 1a, b; e.g., Medaris et al. 2005; Franke 2000, 2006), or even by subduction of the Raabs Ocean beneath the Moldanubian unit along the eastern margin of the Bohemian Massif (Finger et al. 2007). We argue that the Štěnovice and Čistá plutons may help to resolve this

conundrum and also complement the existing information to examine the spatial and temporal pattern of Variscan plutonism and regional deformation in the TBU.

The earliest Variscan ~NW–SE shortening related to the subduction and subsequent Saxothuringian/Teplá–Barrandian collision is recorded along the NW margin of the TBU at around 380 Ma (Schäfer et al. 1997; Zulauf 1997a; Timmermann et al. 2006; Dörr and Zulauf 2010). This Givetian/Frasnian shortening led here to the top-to-the-NW thrusting and crustal stacking (Zulauf 1997a, 2001; Dörr et al. 1998), causing syn-collisional exhumation of crustal rocks and surface uplift in the NW segment of the TBU. The uplift and exhumation is also reflected in the mica cooling ages (Fig. 1b) and in the deposition of Givetian flysch in the Barrandian basin with the source area in the western TBU (Strnad and Mihaljevič 2005). The overall shortening of the TBU due to the Saxothuringian ocean subduction and subsequent Saxothuringian/Teplá–Barrandian collision lasted from at least ~380 Ma to ~346 Ma, the upper age limit being now precisely bracketed by the syn-tectonic plutons of the Central Bohemian Plutonic Complex (Žák et al. 2005a, b, 2009; Janoušek et al. 2010a).

The geochronologic data indicate that the Variscan calc-alkaline plutonism in the TBU started at around ~375–373 Ma with the emplacement of the small-volume Štěnovice and Čistá plutons (Fig. 1b). As detailed earlier, these two plutons are largely discordant to the regional ductile structures in their nearby host rocks, in contrast to the ductilely deformed calc-alkaline granitoids emplaced at approximately the same time near the present-day TBU/Moldanubian boundary (the ~380–365 Ma Staré Sedlo and Mirovice complexes in Fig. 1b; the significance of this tectonomagmatic event remains enigmatic). This suggests that while the central part of the TBU was little affected by the pervasive Variscan overprint largely preserving Cadomian structures (Hajná et al. 2010), the TBU margins were deforming during the Late Devonian to early Carboniferous (Fig. 1b; e.g., Zulauf 1997a).

The initial calc-alkaline plutonic activity at ~375–373 Ma in the central TBU was followed by a magmatic “flare-up” from ~354 to ~346 Ma to form the bulk of the Central Bohemian Plutonic Complex, leading to significant localization of the background compressive/transpressional deformation into this thermally softened domain along the entire SE flank of the TBU (Fig. 1b; Holub et al. 1997a; Scheuven and Zulauf 2000; Janoušek et al. 2004a, 2010a; Žák et al. 2005a, b, 2009). The >20 M.y. gap between the closure of the Saxothuringian Ocean by continental collision (~380 Ma) and the ~375 Ma minor and ~354 to ~346 Ma voluminous and increasingly potassic plutons (Janoušek et al. 1995, 2000; Holub et al. 1997b) may represent a time lag needed for the generation of large-volume magmas above a subducting slab and their ascent

to the upper-crustal levels. Such a timing of deformation and plutonism in the TBU thus fits well the general time scales of production of calc-alkaline magmas, which may post-date the termination of subduction by as much as 30–50 My depending on the availability of water (e.g., Bonin 1990).

In any case, the cessation of the arc-related plutonic activity in the TBU seems to coincide with subduction of the Saxothuringian felsic meta-igneous crust, the HP–HT metamorphism of which resulted in the formation of felsic garnet–kyanite granulites at ~340 Ma (Janoušek et al. 2004b; Janoušek and Holub 2007). At ~343–335 Ma, the southeastern edge of the Central Bohemian Plutonic Complex (including the TBU roof pendants; Fig. 1b) and the Moldanubian middle crust were also intruded by (ultra-)potassic melasyenitoids and melagranitoids (Klötzli and Parrish 1996; Holub 1997; Gerdes et al. 2000b; Janoušek and Gerdes 2003; Janoušek and Holub 2007; Verner et al. 2006, 2008; Kusiak et al. 2010; Kotková et al. 2010).

In summary, the older ~375–354 Ma calc-alkaline plutons intruded only the upper-crustal TBU to the ~NW whereas the younger (~346–335 Ma), progressively more potassium-rich plutons to the ~SE are in intrusive contact with both the TBU and mid-crustal rocks of the Moldanubian Unit (Fig. 1b; Holub et al. 1997a, b; Žák et al. 2005a). Such a spatial–temporal–compositional shift of plutonism is consistent with a northwesterly subduction/collision zone located along the Teplá–Barrandian/Saxothuringian boundary as a principal geodynamic cause of the Late Devonian/early Carboniferous arc-related magmatism in the TBU.

Conclusions

The Štěnovice and Čistá granodiorite–tonalite plutons are interpreted as representing the initial Late Devonian stage of subsequent early Carboniferous voluminous plutonism in the upper crust of the central Bohemian Massif. The whole-rock and trace-element geochemical characteristics of the granodiorites–tonalites are consistent with the calc-alkaline magma having been generated in a continental margin arc setting. These two plutons are largely discordant to the regional ductile structures in their nearby host rocks and have characteristics of concentrically expanded plutons (CEPs): elliptical cross-section in plan view, steep contacts, inferred downward-narrowing conical shape, faint normal zoning, and margin-parallel magmatic fabric decoupled from the regional host-rock structures. Combined with the existing geochronologic, geochemical, and tectonic data, the Štěnovice and Čistá plutons indicate an overall shift of plutonic activity from the ~NW to the ~SE in the upper-crustal TBU during Late Devonian

to early Carboniferous, accompanied by a general compositional trend of the magmas from medium-K calc-alkaline to shoshonitic/ultrapotassic. Such a pattern in the plutonic activity is compatible with the SE-directed (in the present-day coordinates) subduction of the Saxothuringian Ocean beneath the Teplá–Barrandian upper plate as a principal cause of the arc-related plutonism.

Acknowledgments We gratefully acknowledge Fritz Finger and Philippe Olivier for their detailed and critical reviews and Associate Editor Marlina Elburg for helpful comments and careful editorial handling of the manuscript. This work also benefited greatly from discussions with František Hrouda, Marta Chlupáčová, František Holub, Kryštof Verner, Václav Kachlík, Gernold Zulauf, and Josef Klomínský on various aspects of Variscan magmatism in the Bohemian Massif. František Veselovský of the Czech Geological Survey is thanked for zircon separations. This research was supported by the Czech Academy of Sciences (Grant No. KJB30012702 to Z. Kratinová), by the Grant Agency of the Czech Republic (Grant No. 205/07/0992 to V. Janoušek), and by the Ministry of Education, Youth and Sports of the Czech Republic Research Plan No. MSM0021620855.

References

- Arculus RJ (1987) The significance of source versus process in the tectonic controls of magma genesis. *J Volcanol Geotherm Res* 32:1–12
- Barbarin B (1990) Granitoids: main petrogenetic classifications in relation to origin and tectonic setting. *Geol J* 25:227–238
- Bartošek J, Chlupáčová M, Štovičková N (1969) Petrogenesis and structural position of small granitoid intrusions in the aspect of geophysical data. *J Geol Sci Appl Geophys* 8:37–65
- Bonin B (1990) From orogenic to anorogenic settings: evolution of granitoid suites after a major orogenesis. *Geol J* 25:261–270
- Bouchez JL (1997) Granite is never isotropic: an introduction to AMS studies of granitic rocks. In: Bouchez JL, Hutton DHW, Stephens WE (eds) *Granite: from segregation of melt to emplacement fabrics*. Kluwer, Amsterdam, pp 95–112
- Boynton WV (1984) Cosmochemistry of the rare earth elements: meteorite studies. In: Henderson P (ed) *Rare earth element geochemistry*. Elsevier, Amsterdam, pp 63–114
- Breiter K, Sokol A (1997) Chemistry of the Bohemian granitoids: geotectonic and metallogenetic implications. *J Geol Sci Econ Geol Mineral* 31:75–96
- Bues C, Dörr W, Fiala J, Vejnar Z, Zulauf G (2002) Emplacement depths and radiometric ages of Paleozoic plutons of the Neukirchen–Kdyně massif: differential uplift and exhumation of Cadomian basement due to Carboniferous orogenic collapse (Bohemian Massif). *Tectonophysics* 352:225–243
- Čadková Z, Jakeš P, Haková M, Mrázek P (1985) Geochemical catalogue of the basic network. In: *Lithochemical Database of the Czech Geological Survey, Prague* (unpublished manuscript)
- Chlupáčová M, Hrouda F, Rejl L (1975) The fabric, genesis, and relative age of the granitic rocks of the Čistá–Jesenice massif (Czechoslovakia), as studied by magnetic anisotropy. *Gerlands Beitr Geophys* 84:487–500
- Dallmeyer RD, Urban M (1998) Variscan vs Cadomian tectonothermal activity in northwestern sectors of the Teplá–Barrandian zone, Czech Republic: constraints from $^{40}\text{Ar}/^{39}\text{Ar}$ ages. *Geol Rundsch* 87:94–106

- Debon F, Le Fort P (1983) A chemical–mineralogical classification of common plutonic rocks and associations. *Trans Roy Soc Edinb Earth Sci* 73:135–149
- Didier J, Barbarin B (eds) (1991) *Enclaves and granite petrology*. Elsevier, Amsterdam
- Dietl C, Koyi HA (2002) Emplacement of nested diapirs: results of centrifuge modelling. *J Virtual Explor* 6:81–88
- Dörr W, Zulauf G (2010) Elevator tectonics and orogenic collapse of a Tibetan-style plateau in the European Variscides: the role of the Bohemian shear zone. *Int J Earth Sci* 99:299–325
- Dörr W, Fiala J, Vejnar Z, Zulauf G (1998) U–Pb zircon ages and structural development of metagranitoids of the Teplá crystalline complex: evidence for pervasive Cambrian plutonism within the Bohemian Massif (Czech Republic). *Geol Rundsch* 87:135–149
- Dunstan LP, Gramlich JW, Barnes IL, Purdy WC (1980) Absolute isotopic abundance and the atomic weight of a reference sample of thallium. *J Res Natl Bureau Stand* 85:1–10
- Edel JB, Schulmann K (2009) Geophysical constraints and model of the “Saxothuringian and Rhenohercynian subductions–magmatic arc system” in NE France and SW Germany. *Bull Soc Geol Fr* 180:545–558
- Finger F, Roberts MP, Haunschmid B, Schermaier A, Steyrer HP (1997) Variscan granitoids of central Europe: their typology, potential sources and tectonothermal relations. *Mineral Petrol* 61:67–96
- Finger F, Gerdes A, Janoušek V, René M, Riegler G (2007) Resolving the Variscan evolution of the Moldanubian sector of the Bohemian Massif: the significance of the Bavarian and the Moravo–Moldanubian tectonometamorphic phases. *J Geosci* 52:9–28
- Finger F, René M, Gerdes A, Riegler G (2009) The Saxo-Danubian granite belt: magmatic response to postcollisional delamination of mantle lithosphere below the southwestern sector of the Bohemian Massif (Variscan orogen). *Geol Carpath* 60:205–212
- Franke W (2000) The mid-European segment of the Variscides: tectonostratigraphic units, terrane boundaries and plate tectonic evolution. In: Franke W, Haak V, Oncken O, Tanner D (eds) *Orogenic processes: quantification and modelling in the Variscan belt*, vol 179. *Geol Soc London Spec Publ*, London, pp 35–61
- Franke W (2006) The Variscan orogen in Central Europe: construction and collapse. In: Gee DG, Stephenson RA (eds) *European lithosphere dynamics*, vol 34. *Geol Soc London Memoirs*, London, pp 333–343
- Galadí-Enríquez E, Galindo-Zaldívar J, Simancas F, Exposito I (2003) Diapiric emplacement in the upper crust of a granitic body: the La Bazana granite (SW Spain). *Tectonophysics* 361:83–96
- Gerdes A (2001) Magma homogenization during anatexis, ascent and/or emplacement? Constraints from the Variscan Weinsberg Granites. *Terra Nova* 13:305–312
- Gerdes A, Wörner G, Henk A (2000a) Post-collisional granite generation and HT–LP metamorphism by radiogenic heating: the Variscan South Bohemian Batholith. *J Geol Soc London* 157:577–587
- Gerdes A, Wörner G, Finger F (2000b) Hybrids, magma mixing and enriched mantle melts in post-collisional Variscan granitoids: the Rastenbergl Pluton, Austria. In: Franke W, Haak V, Oncken O, Tanner D (eds) *Orogenic processes: quantification and modelling in the Variscan belt*, vol 179. *Geol Soc London Spec Publ*, London, pp 415–431
- Gerdes A, Friedl G, Parrish RR, Finger F (2003) High-resolution geochronology of Variscan granite emplacement—the South Bohemian Batholith. *J Czech Geol Soc* 48:53–54
- Glodny J, Grauert B, Fiala J, Vejnar Z, Krohe A (1998) Metapegmatites in the western Bohemian massif: ages of crystallisation and metamorphic overprint, as constrained by U–Pb zircon, monazite, garnet, columbite and Rb–Sr muscovite data. *Geol Rundsch* 87:124–134
- Hajná J, Žák J, Kachlík V, Chadima M (2010) Subduction-driven shortening and differential exhumation in a Cadomian accretionary wedge: the Teplá–Barrandian unit, Bohemian Massif. *Precambrian Res* 176:27–45
- He B, Xu YB, Paterson SR (2009) Magmatic diapirism of the Fangshan pluton, southwest of Beijing, China. *J Struct Geol* 31:615–626
- Hibbard MJ (1991) Textural anatomy of twelve magma-mixed granitoid systems. In: Didier J, Barbarin B (eds) *Enclaves and granite petrology*. Elsevier, Amsterdam, pp 431–444
- Hibbard MJ (1995) *Petrography to petrogenesis*. Prentice Hall, New Jersey
- Holub FV (1997) Ultrapotassic plutonic rocks of the durbachite series in the Bohemian Massif: petrology, geochemistry, and petrogenetic interpretation. *J Geol Sci Econ Geol Mineral* 31:5–26
- Holub FV, Cocherie A, Rossi P (1997a) Radiometric dating of granitic rocks from the Central Bohemian Plutonic Complex: constraints on the chronology of thermal and tectonic events along the Barrandian–Moldanubian boundary. *CR Geosci* 325:19–26
- Holub FV, Machart J, Manová M (1997b) The Central Bohemian Plutonic Complex: geology, chemical composition and genetic interpretation. *J Geol Sci Econ Geol Mineral* 31:27–50
- Horn I, Rudnick RL, McDonough WF (2000) Precise elemental and isotope ratio determination by simultaneous solution nebulization and laser ablation-ICP-MS: application to U–Pb geochronology. *Chem Geol* 164:281–301
- Hoskin PWO, Kinny PD, Wyborn D, Chappell BW (2000) Identifying accessory mineral saturation during differentiation in granitoid magmas: an integral approach. *J Petrol* 41:1365–1396
- Hrouda F, Chlupáčová M, Rejl L (1971) The mimetic fabric of magnetite in some foliated granodiorites, as indicated by magnetic anisotropy. *Earth Planet Sci Lett* 11:381–384
- Hrouda F, Chlupáčová M, Rejl L (1972) Changes in the magnetite content and magnetite fabric during fenitization, as investigated by petromagnetic methods. *N Jb Miner Abh* 177:61–72
- Irvine TM, Baragar WR (1971) A guide to the chemical classification of common volcanic rocks. *Canad J Earth Sci* 8:523–548
- Janoušek V (2006) Saturnin, R language script for application of accessory-mineral saturation models in igneous geochemistry. *Geol Carpath* 57:131–142
- Janoušek V, Gerdes A (2003) Timing the magmatic activity within the Central Bohemian Pluton, Czech Republic: conventional U–Pb ages for the Sázava and Tábora intrusions and their geotectonic significance. *J Czech Geol Soc* 48:70–71
- Janoušek V, Holub F (2007) The causal link between HP–HT metamorphism and ultrapotassic magmatism in collisional orogens: case study from the Moldanubian Zone of the Bohemian Massif. *Proc Geol Assoc* 118:75–86
- Janoušek V, Rogers G, Bowes DR (1995) Sr–Nd isotopic constraints on the petrogenesis of the Central Bohemian Pluton, Czech Republic. *Geol Rundsch* 84:520–534
- Janoušek V, Bowes DR, Rogers G, Farrow CM, Jelínek E (2000) Modelling diverse processes in the petrogenesis of a composite batholith: the Central Bohemian Pluton, Central European Hercynides. *J Petrol* 41:511–543
- Janoušek V, Braithwaite CJR, Bowes DR, Gerdes A (2004a) Magma-mixing in the genesis of Hercynian calc-alkaline granitoids: an integrated petrographic and geochemical study of the Sázava intrusion, Central Bohemian Pluton, Czech Republic. *Lithos* 78:67–99
- Janoušek V, Finger F, Roberts MP, Frýda J, Pin C, Dolejš D (2004b) Deciphering petrogenesis of deeply buried granites: whole-rock geochemical constraints on the origin of largely undepleted

- felsic granulites from the Moldanubian Zone of the Bohemian Massif. *Trans Roy Soc Edinb Earth Sci* 95:141–159
- Janoušek V, Farrow CM, Erban V (2006a) Interpretation of whole-rock geochemical data in igneous geochemistry: introducing Geochemical Data Toolkit (GCDkit). *J Petrol* 47:1255–1259
- Janoušek V, Gerdes A, Vrána S, Finger F, Erban V, Friedl G, Braithwaite CJR (2006b) Low-pressure granulites of the Lišov Massif, southern Bohemia: Viséan metamorphism of Late Devonian plutonic arc rocks. *J Petrol* 47:705–744
- Janoušek V, Wiegand B, Žák J (2010a) Dating the onset of Variscan crustal exhumation in the core of the Bohemian Massif: new U–Pb single zircon ages from the high-K calc-alkaline granodiorites of the Blatná suite, Central Bohemian Plutonic Complex. *J Geol Soc London* 167:347–360
- Janoušek V, Konopásek J, Ulrich S, Erban V, Tajčmanová L, Jeřábek P (2010b) Geochemical character and petrogenesis of Pan-African Amspoort suite of the Boundary Igneous Complex in the Kaoko Belt (NW Namibia). *Gondwana Res*. doi:10.1016/j.gr.2010.02.014 (in press)
- Jelínek V (1981) Characterization of the magnetic fabric of rocks. *Tectonophysics* 79:T63–T67
- Klomínský J (1963) Geology of the Čistá massif. *J Geol Sci Geol* 3:7–27
- Klomínský J (1965) The Štěnovice granodiorite massif. *J Geol Sci Geol* 8:75–98
- Klötzli US, Parrish RR (1996) Zircon U/Pb and Pb/Pb geochronology of the Rastenberg granodiorite, South Bohemian Massif, Austria. *Mineral Petrol* 58:197–214
- Konopásek J, Schulmann K (2005) Contrasting early Carboniferous field geotherms: evidence for accretion of a thickened orogenic root and subducted Saxothuringian crust (Central European Variscides). *J Geol Soc London* 162:463–470
- Kopecný L, Chlupáčová M, Klomínský J, Sokol A (1997) The Čistá–Jesenice pluton in western Bohemia: geochemistry, geology and ore potential. *J Geol Sci Econ Geol Mineral* 31:97–127
- Košler J, Sylvester PJ (2003) Present trends and the future of zircon in geochronology: laser ablation ICP-MS. In: Hanchar JM, Hoskin PWO (eds) *Zircon*. *Rev Mineral Geoch* 53:243–275
- Košler J, Aftalion M, Bowers DR (1993) Mid-late Devonian plutonic activity in the Bohemian Massif: U–Pb zircon isotopic evidence from the Staré Sedlo and Mirovice gneiss complexes, Czech Republic. *N Jb Miner Mh* 9:417–431
- Košler J, Rogers G, Roddick JC, Bowes DR (1995) Temporal association of ductile deformation and granitic plutonism: Rb–Sr and ⁴⁰Ar–³⁹Ar evidence from roof pendants above the Central Bohemian Pluton, Czech Republic. *J Geol* 103:711–717
- Košler J, Bowes DR, Farrow CM, Hopgood AM, Rieder M, Rogers G (1997) Constraints on the timing of events in the multi-episodic history of the Teplá–Barrandian complex, western Bohemia, from integration of deformational sequence and Rb–Sr isotopic data. *N Jb Miner Mh* 5:203–220
- Košler J, Fonneland H, Sylvester P, Tubrett M, Pedersen RB (2002) U–Pb dating of detrital zircons for sediment provenance studies—a comparison of laser ablation ICP-MS and SIMS techniques. *Chem Geol* 182:605–618
- Kotková J, Schaltegger U, Leichmann J (2010) Two types of ultrapotassic plutonic rocks in the Bohemian Massif—coeval intrusions at different crustal levels. *Lithos* 115:163–176
- Kováříková P, Siebel W, Jelínek E, Štemprok M, Kachlík V, Holub F, Blecha V (2007) Petrology, geochemistry and zircon age for redwitzite at Abertamy, NW Bohemian Massif (Czech Republic): tracing the mantle component in Late Variscan intrusions. *Chem Erde* 67:151–174
- Kováříková P, Siebel W, Jelínek E, Štemprok M, Kachlík V, Holub FV, Blecha V (2010) Dioritic intrusions of the Slavkovský les (Kaiserwald), Western Bohemia: their origin and significance in late Variscan granitoid magmatism. *Int J Earth Sci* 99:545–565
- Kusiak MA, Dunkley DJ, Suzuki K, Kachlík V, Kedzior A, Lekki J, Opluštil S (2010) Chemical (non-isotopic) and isotopic dating of Phanerozoic zircon—a case study of durbachite from the Třebíč Pluton, Bohemian Massif. *Gondwana Res* 17:153–161
- Machek M, Ulrich S, Janoušek V (2009) Strain coupling between upper mantle and lower crust: natural example from the Běstvína granulite body, Bohemian Massif. *J Met Geol* 27:721–737
- Maniar PD, Piccoli PM (1989) Tectonic discriminations of granitoids. *Geol Soc Am Bull* 101:635–643
- Medaris G, Wang H, Jelínek E, Mihaljevič M, Jakeš P (2005) Characteristics and origins of diverse Variscan peridotites in the Gföhl Nappe, Bohemian Massif, Czech Republic. *Lithos* 82:1–23
- Miller RB, Paterson SR (1999) In defense of magmatic diapirs. *J Struct Geol* 21:1161–1173
- Miller CF, McDowell SM, Mapes RW (2003) Hot and cold granites? Implications of zircon saturation temperatures and preservation of inheritance. *Geology* 31:529–532
- Molyneux SJ, Hutton DHW (2000) Evidence for significant granite space creation by the ballooning mechanism: the example of the Ardara pluton, Ireland. *Geol Soc Am Bull* 112:1543–1558
- Mrlina J (1993) Gravity field of the West Bohemian Proterozoic formation. *Geol Průzk* 35:326–333 (in Czech)
- Nagata T (1961) *Rock magnetism*. Maruzen, Tokyo
- O'Brien PJ (2000) The fundamental Variscan problem: high-temperature metamorphism at different depths and high-pressure metamorphism at different temperatures. In: Franke W, Haak V, Oncken O, Tanner D (eds) *Orogenic processes: quantification and modelling in the Variscan belt*, vol 179. *Geol Soc London Spec Publ*, London, pp 369–386
- Paterson SR, Fowler TK (1993) Re-examining pluton emplacement processes. *J Struct Geol* 15:191–206
- Paterson SR, Vernon RH (1995) Bursting the bubble of ballooning plutons: a return to nested diapirs emplaced by multiple processes. *Geol Soc Am Bull* 107:1356–1380
- Paterson SR, Vernon RH, Tobisch OT (1989) A review of criteria for identification of magmatic and tectonic foliations in granitoids. *J Struct Geol* 11:349–363
- Paterson SR, Vernon RH, Fowler TK (1991) Aureole tectonics. In: Kerrick DM (ed) *Contact metamorphism*. *Rev Mineral* 26:673–722
- Paterson SR, Fowler TK, Schmidt KL, Yoshinobu AS, Yuan ES, Miller RB (1998) Interpreting magmatic fabric patterns in plutons. *Lithos* 44:53–82
- Pearce JA (1996) Sources and settings of granitic rocks. *Episodes* 19:120–125
- Pearce JA, Parkinson IJ (1993) Trace element models of mantle melting: application to volcanic arc petrogenesis. In: Prichard HM, Alabaster T, Harris NBW, Neary CR (eds) *Magmatic processes and plate tectonics*, vol 76. *Geol Soc London Spec Publ*, London, pp 373–403
- Pearce JA, Harris NW, Tindle AG (1984) Trace element discrimination diagrams for the tectonic interpretation of granitic rocks. *J Petrol* 25:956–983
- Peccerillo A, Taylor SR (1976) Geochemistry of the Eocene calc-alkaline volcanic rocks from the Kastamonu area, northern Turkey. *Contrib Mineral Petrol* 58:63–81
- Pitcher WS (1982) Granite type and tectonic environment. In: Hsü KJ (ed) *Mountain building processes*. Academic Press, London, pp 19–40
- Ramsay JG (1989) Emplacement kinematics of a granite diapir: the Chindamora batholith, Zimbabwe. *J Struct Geol* 11:191–209
- Roberts MP, Clemens JD (1993) Origin of high-potassium, calc-alkaline, I-type granitoids. *Geology* 21:825–828

- Saunders AD, Norry MJ, Tarney J (1991) Fluid influence on the trace element compositions of subduction zone magmas. In: Tarney J, Pickering KT, Knipe RJ, Dewey JF (eds) *The behaviour and influence of fluids in subduction zones*. The Royal Society, London, pp 151–166
- Schäfer J, Neuroth H, Ahrendt H, Dörr W, Franke W (1997) Accretion and exhumation at a Variscan active margin, recorded in the Saxothuringian flysch. *Geol Rundsch* 86:599–611
- Schandl ES, Gorton MP (2002) Application of high field strength elements to discriminate tectonic settings in VMS environments. *Econ Geol* 97:629–642
- Scheuven D, Zulauf G (2000) Exhumation, strain localization, and emplacement of granitoids along the western part of the Central Bohemian shear zone (Bohemian Massif). *Int J Earth Sci* 89:617–630
- Schulmann K, Konopásek J, Janoušek V, Lexa O, Lardeaux JM, Edel JB, Štípská P, Ulrich S (2009) An Andean type Palaeozoic convergence in the Bohemian Massif. *CR Geosci* 341:266–286
- Shand SJ (1943) *Eruptive rocks. Their genesis, composition, classification, and their relation to ore-deposits with a chapter on meteorite*. Wiley, New York
- Siebel W, Trzebski R, Stettner G, Hecht L, Casten U, Höhndorf A, Müller P (1997) Granitoid magmatism of the NW Bohemian massif revealed: gravity data, composition, age relations and phase concept. *Geol Rundsch* 86:S45–S63
- Siebel W, Breiter K, Wendt I, Höhndorf A, Henjes-Kunst F, René M (1999) Petrogenesis of contrasting granitoid plutons in western Bohemia (Czech Republic). *Mineral Petrol* 65:207–235
- Siebel W, Chen F, Satir M (2003) Late-Variscan magmatism revisited: new implications from Pb-evaporation zircon ages on the emplacement of redwitzites and granites in NE Bavaria. *Int J Earth Sci* 92:36–53
- Siebel W, Shang CK, Reitter E, Rohrmüller J, Breiter K (2008) Two distinctive granite suites in the SW Bohemian Massif and their record of emplacement: constraints from geochemistry and zircon $^{207}\text{Pb}/^{206}\text{Pb}$ chronology. *J Petrol* 49:1853–1872
- Siegesmund S, Becker JK (2000) Emplacement of the Ardara pluton (Ireland): new constraints from magnetic fabrics, rock fabrics and age dating. *Int J Earth Sci* 89:307–327
- Slaby E, Martin H (2008) Mafic and felsic magma interaction in granites: the Hercynian Karkonosze pluton (Sudetes, Bohemian Massif). *J Petrol* 49:353–391
- Štemprok M, Holub FV, Novák J (2003) Multiple magmatic pulses of the eastern volcano-plutonic complex, Krušné hory/Erzgebirge batholith, and their phosphorus contents. *Bull Geosci* 78:277–296
- Strnad L, Mihaljevič M (2005) Sedimentary provenance of Mid-Devonian clastic sediments in the Teplá-Barrandian Unit (Bohemian Massif): U–Pb and Pb–Pb geochronology of detrital zircons by laser ablation ICP-MS. *Mineral Petrol* 84:47–68
- Sun SS, McDonough WF (1989) Chemical and isotopic systematics of oceanic basalts: implications for mantle composition and processes. In: Saunders AD, Norry M (eds) *Magmatism in ocean basins*, vol 42. *Geol Soc London Spec Publ*, London, pp 313–345
- Tahiri A, Simancas JF, Azor A, Galindo-Zaldívar J, Lodeiro FG, El Hadi H, Poyatos DM, Ruiz-Constán A (2007) Emplacement of ellipsoid-shaped (diapiric ?) granite: structural and gravimetric analysis of the Oulmes granite (Variscan Meseta, Morocco). *J Afr Earth Sci* 48:301–313
- Tatsumi Y, Eggins S (1995) *Subduction zone magmatism*. *Frontiers in Earth Sciences*. Blackwell, Cambridge, Massachusetts
- Timmerman MJ (2008) Palaeozoic magmatism. In: McCann T (ed) *The geology of Central Europe*. Volume 1: Precambrian and Palaeozoic. Geological Society, London, pp 665–748
- Timmermann H, Dörr W, Krenn E, Finger F, Zulauf G (2006) Conventional and in situ geochronology of the Teplá Crystalline unit, Bohemian Massif: implications for the processes involving monazite formation. *Int J Earth Sci* 95:629–647
- Venera Z, Schulmann K, Kröner A (2000) Intrusion within a transtensional tectonic domain: the Čistá granodiorite (Bohemian Massif)—structure and rheological modelling. *J Struct Geol* 22:1437–1454
- Verner K, Žák J, Hrouda F, Holub F (2006) Magma emplacement during exhumation of the lower- to mid-crustal orogenic root: the Jihlava syenitoid pluton, Moldanubian Unit, Bohemian Massif. *J Struct Geol* 28:1553–1567
- Verner K, Žák J, Nahodilová R, Holub F (2008) Magmatic fabrics and emplacement of the cone-sheet-bearing Knížecí Stolec durbachitic pluton (Moldanubian Unit, Bohemian Massif): implications for mid-crustal reworking of granulitic lower crust in the Central European Variscides. *Int J Earth Sci* 97:19–33
- Verner K, Buriánek D, Vrána S, Vondrovic L, Pertoldová J, Hanžl P, Nahodilová R (2009) Tectonometamorphic features of geological units along the northern periphery of the Moldanubian Zone (Bohemian Massif). *J Geosci* 54:87–100
- Vernon RH (1984) Microgranitoid enclaves in granites—globules of hybrid magma quenched in a plutonic environment. *Nature* 309:438–439
- Vernon RH (2000) Review of microstructural evidence of magmatic and solid-state flow. *El Geosci* 5:1–23
- Watson EB, Harrison TM (1983) Zircon saturation revisited: temperature and composition effects in a variety of crustal magma types. *Earth Planet Sci Lett* 64:95–304
- Wiedenbeck M, Alle P, Corfu F, Griffin WL, Meier M, Oberli F, von Quadt A, Roddick JC, Spiegel W (1995) Three natural zircon standards for U–Th–Pb, Lu–Hf, trace element and REE analyses. *Geostand Newslett* 19:1–23
- Wilson M (1989) *Igneous petrogenesis*. Unwin Hyman, London
- Winchester JA (2002) Palaeozoic amalgamation of Central Europe: new results from recent geological and geophysical investigations. *Tectonophysics* 360:5–21
- Žák J, Holub FV, Verner K (2005a) Tectonic evolution of a continental magmatic arc from transpression in the upper crust to exhumation of mid-crustal orogenic root recorded by episodically emplaced plutons: the Central Bohemian Plutonic Complex (Bohemian Massif). *Int J Earth Sci* 94:385–400
- Žák J, Schulmann K, Hrouda F (2005b) Multiple magmatic fabrics in the Sázava pluton (Bohemian Massif, Czech Republic): a result of superposition of wrench-dominated regional transpression on final emplacement. *J Struct Geol* 27:805–822
- Žák J, Dragoun F, Verner K, Chlupáčová M, Holub FV, Kachlík V (2009) Forearc deformation and strain partitioning during growth of a continental magmatic arc: the northwestern margin of the Central Bohemian Plutonic Complex, Bohemian Massif. *Tectonophysics* 469:93–111
- Zulauf G (1997a) From very low-grade to eclogite-facies metamorphism: tilted crustal sections as a consequence of Cadomian and Variscan orogeny in the Teplá–Barrandian unit (Bohemian Massif). *Geotekt Forsch* 89:1–302
- Zulauf G (1997b) Constriction due to subduction: evidence for slab pull in the Mariánské Lázně Complex (central European Variscides). *Terra Nova* 9:232–236
- Zulauf G (2001) Structural style, deformational mechanisms and paleodifferential stress along an exposed crustal section: constraints on the rheology of quartzofeldspathic rocks at supra- and infrastructural levels (Bohemian Massif). *Tectonophysics* 332:211–237

Original paper

Intrusive and deformation history of the Ševětín Pluton, Moldanubian Batholith: record of polyphase tectonic evolution of the Blanice Graben, Bohemian Massif

Jiří ZACHARIÁŠ^{1*}, Jakub TRUBAČ²

¹ Institute of Geochemistry, Mineralogy and Mineral Resources, Faculty of Science, Charles University in Prague, Albertov 6, 128 43 Prague 2, Czech Republic; jiri.zacharias@natur.cuni.cz

² Czech Geological Survey, Klárov 3, 118 21 Prague 1, Czech Republic

*Corresponding author



The Ševětín Pluton, located *c.* 15 km NNE of České Budějovice, is a small, isolated, petrologically and structurally complex intrusive body that is genetically related to the youngest intrusions of the Moldanubian Batholith. As documented in this study, its overall shape, internal magmatic fabric as well as brittle structures (dikes, veins, joints, faults) are, however, related to the formation and polyphase tectonic evolution of the Blanice Graben, an about 200 km long and 5–15 km wide NNE–SSW-trending, deep-seated fault zone that cuts across the Moldanubian Unit.

In total, one pre-intrusive and three syn- to post-intrusive tectonic phases have been distinguished. The oblique, NW–SE oriented compression controlled both the intrusion of the Ševětín biotite–muscovite granite and the early stage of its brittle deformation. Sigmoidal pattern of magnetic foliations in this pluton documents its mostly solid-state deformation during oblique sinistral movements on the main faults of the Blanice Graben. The subsequent strike-slip phase was characterized by E–W oriented subhorizontal extension and can be correlated with the intrusion of *c.* 270 Ma old microgranodiorite dikes. The last extensional phase was associated with the formation of subeconomic Pb–Zn–(Ag?) quartz–calcite veins at *c.* 265 Ma.

Keywords: Moldanubian Zone, Moldanubian Batholith, Blanice Graben, paleostress analysis, AMS study, Pb–Zn veins

Received: 20 February 2014; **accepted:** 3 October 2014; **handling editor:** J. Žák

The online version of this article (doi: 10.3190/jgeosci.175) contains supplementary electronic material.

1. Introduction

Extensional tectonics associated with late-orogenic evolution of collisional orogens is often coupled with extensive crustal melting and subsequent granitic magma emplacement into the middle to upper crustal levels. Simultaneously, large-scale shear zones are formed in the continental crust to accommodate its stretching (e.g. Malavieille 1993; Faure 1995). At late stages of this scenario, shallow crustal levels are dominated by brittle tectonics and by formation tectonically-controlled sedimentary basins.

Granitic bodies emplaced in tectonically active zones can be used both as passive and active markers of crustal deformation, but also have the potential of dating these processes. Anisotropy of magnetic susceptibility (AMS) is a widely used method for analysis of cryptic magmatic to solid-state deformational fabrics in such granitoid rocks. Moreover, the paleostress orientation and stress ratio can be inferred from examining mode-I fractures (dikes, veins, joints), as well as from interpretation of striations (slickenlines) along fault planes.

This study focuses on the identification of tectonic regimes that controlled the evolution of central and

southern parts of the *c.* 200 km long and NNE–SSW-trending Blanice Graben in the core of the Bohemian Massif. Its formation documents the final stages of orogenic collapse associated with the formation of linear Permo–Carboniferous sedimentary basins, as well as with repeated magmatic and hydrothermal activity. In all these aspects, the Blanice Graben resembles similar tectonic zones of Variscan Europe. Our goal was achieved through a detailed study of the magmatic and solid-state deformational fabrics of the Ševětín Pluton, a small intrusion genetically related to the Moldanubian Batholith.

2. Regional setting

Moldanubian Zone (Fig. 1a) represents a heterogeneous assemblage of medium- to high-grade metamorphic rocks, mainly paragneisses and migmatites, locally with calcareous, graphitic and metabasic intercalations as well as bodies of granulite, eclogite and serpentinite (e.g. Fiala et al. 1995). It is usually subdivided into the lower crustal/upper mantle Gföhl Unit with numerous occurrences of HP–HT granulite (e.g. Racek et al. 2006; Janoušek and

Holub 2007; Franěk et al. 2011) and eclogite (e.g. Medaris et al. 2005) massifs and into the medium-pressure mid-crustal Drosendorf and Ostrong units (Dallmeyer et al. 1995; Franke 2000). Recent structural studies documented that many of the high-pressure lithologies within the Gföhl Unit represent vertical extrusions of lower crustal rocks (e.g. Finger et al. 2007; Franěk et al. 2011; Schulmann et al. 2014). The granulite-facies metamorphism occurred at about 340 Ma (e.g. Friedl et al. 2011), followed by rapid exhumation to mid-crustal levels (c. 338–335 Ma) and subsequent nearly isobaric cooling through $\sim 300^\circ\text{C}$ between c. 320–310 Ma (e.g. Matte et al. 1985).

The Moldanubian Batholith (or South Bohemian; c. 6 000 km²) is the largest Variscan magmatic complex in the Bohemian Massif. It has a horseshoe shape with western (Bavarian) and eastern (Moravo–Moldanubian) branches joining in the Waldviertel area (Austria). The eastern branch forms a NNE–SSW trending domal structure formed by gravity-driven diapiric upwelling of the metapelitic middle crust (Žák et al. 2011; Verner et al. 2014). The Moldanubian Batholith consists of three to four principal intrusive groups (mostly S and S/I types, rarely I-type; e.g. Holub et al. 1995; Klečka and Matějka 1996; Matějka and Janoušek 1998; Gerdes et al. 2000, 2003; Gerdes 2001; Finger et al. 2009; Breiter 2010), ranging in age from c. 330–323 Ma to c. 305–302 Ma (see, e.g., the review of Bankwitz et al. 2004).

The Blanice Graben (also called the Kouřim–Blanice–Kaplice–Rödl fault zone; Fig. 1a) extends from Český Brod E of Prague to Linz in Austria. On a regional scale, it belongs to a set of conjugate sinistral (NE–SW; e.g. Vitis, Rödl, Diendorf) and dextral (NW–SE; e.g. Pfahl, Danube) shear zones in the southern part of the Bohemian Massif, which resulted from late Variscan N–S oriented compression (Brandmayr et al. 1995).

The southernmost (Austrian) part of the Blanice Graben (also referred to as the Rödl shear zone) is a sinistral ductile shear zone with NE–SW-trending, steeply dipping foliation and subhorizontal stretching lineation. Synkinematic mylonitization was dated at around 288–281 Ma (Brandmayr et al. 1995; Ar–Ar method); however, these ages most probably only represent cooling below the muscovite blocking temperature. Paleostress analysis of brittle faults and fractures from the same zone documented their formation in the strike-slip regime under NW–SE and NE–SW oriented subhorizontal maximum principal stress direction (σ_1) and minimum principal stress direction (σ_3), respectively. The authors, however, suggested that the brittle deformation phase and related movements corresponded to Alpine tectonic reactivation of the Rödl shear zone at c. 170–180 Ma.

In the northern (Czech) part of the Rödl fault zone, Vrána and Bártek (2005) found indicators of sinistral displacement ~ 17 km south of Kaplice. The early ductile phase of this deformation is constrained to 303 ± 5 Ma by Ar–Ar dating of hornblende from a quartz diorite porphyry dike (Vrána et al. 2005) that intruded synkinematically during the development of the mylonitic fabric in the fault/shear zone.

A late stage of tectonomagmatic activity in the Blanice Graben is indicated by the 270 ± 2 Ma Ar–Ar age of hornblende from a pyroxene microgranodiorite dike near Dehetník (Fig. 1a; Košler et al. 2001). The parental magma of this dike originated from mixing between remelted lower crustal (Moldanubian) rocks and primary magmas derived from an upper mantle source (Košler et al. 2001; Vrána and Janoušek 2006).

The tectonic activity along the faults of the Blanice Graben can also be inferred from the presence of several discontinuous occurrences (erosional relics) of Permo–Carboniferous (Gzhelian to Cisuralian; c. 300–275 Ma) sedimentary successions (Holub 2001). It is not clear whether these originally formed a continuous sedimentary basin. If so, then it was about 12 km wide and at least 130 km long. The main and late stages of sedimentation were accompanied by movements along the eastern faults of the Blanice Graben. This is indicated by: (i) the location of the axis of maximum subsidence close to the eastern margin of the Blanice Graben, (ii) the presence of proluvial conglomerates exclusively along the eastern marginal fault and (iii) the general dip of the strata to the E (10 – 40°). The maximum thickness of the Permo–Carboniferous strata is at least ~ 700 – 800 m in the northern (near Český Brod) and central relics (near Tábor), but attains only ~ 380 m in the southern relic (near České Budějovice). The most intense subsidence in the Blanice Graben occurred at c. 280–270 Ma.

The tectonic history of the Blanice Graben was also reflected in several episodes of hydrothermal activity: Au–Ag (oldest, c. 300 Ma), Ag–Pb–Zn (most widespread) and U (youngest, c. 260 Ma, subeconomic). The geology, mineralogy and tectonic evolution of the Au–Ag deposits were summarized by Zachariáš et al. (2004, 2009) and Zachariáš and Hübst (2012). The Ag–Pb–Zn, mostly vein-type deposits are characterized by quartz–carbonate gangue, by abundance of galena accompanied by sphalerite and Ag-phases (miargyrite, pyrargyrite, argentite and native silver) and by the scarcity of Fe-sulfides (pyrite, arsenopyrite and pyrrhotite). The most important mining districts from the north to the south are Stříbrná Skalice, Ratibořské Hory–Stará Vožice, and Rudolfov. Similar Pb–Zn-bearing mineralization, however without known Ag-phases, was also identified in the studied Ševětín Pluton (see below).

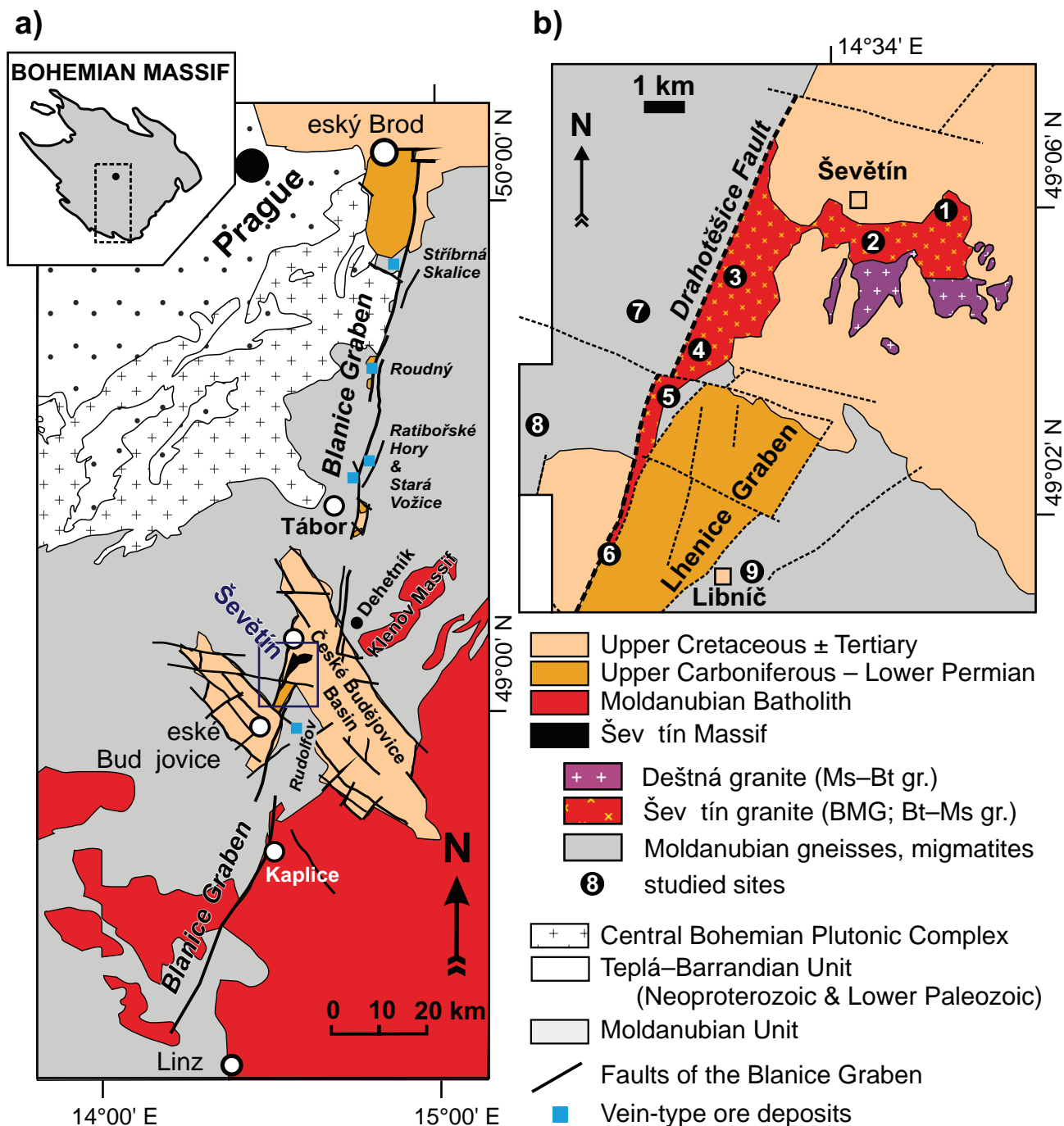


Fig. 1 Simplified geological map of the Blanice Graben (a) and of the Ševětín Pluton (b).

3. Ševětín Pluton

The Ševětín Pluton (SP) forms a small composite body that intruded the southern part of the Moldanubian Zone c. 15 km NNE of České Budějovice (Fig. 1a). To the N and NE, it is overlain by the Upper Cretaceous and Tertiary sedimentary rocks of the České Budějovice Basin. The SP shows a triangular shape, apparently stretched

along the NNW–SSE trending Drahotěšice Fault (Fig. 1b; a western-peripheral fault of the Blanice Graben system). It is not clear whether this contact is tectonic or intrusive. To the south, the SP narrows down to < 300–500 m and is partly overlain in its southern parts by Permian sediments of the Lhenice Graben.

Based on gravimetric survey (Čuta et al. 1975; Kadlec et al. 1978; Šalanský 1981) the SP extends to the N, NE

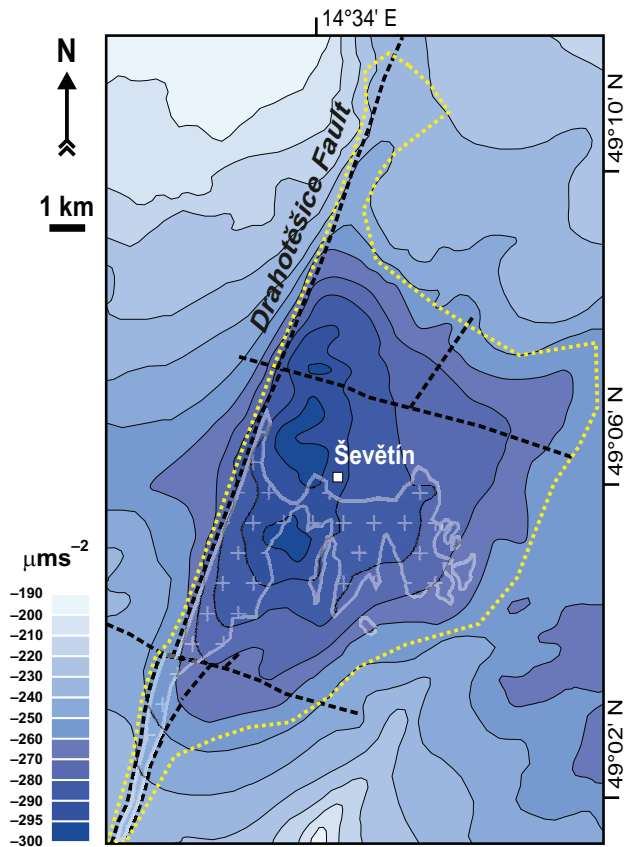


Fig. 2 Bouguer anomaly map of the Ševětín area (after Čuta et al. 1975 and Šalanský 1981). The negative Δg anomaly in the center corresponds to the presence of the Ševětín granite (average density 2620 kg/m^3). The dotted line highlights approximate extent of the Ševětín Pluton, based on interpretation of gravity data and sparse drilling (modified after Kadlec et al. 1978).

and E beneath the sedimentary cover (Fig. 2). The actual size of the Pluton is therefore likely larger than its exposed parts (c. 23 km^2). Its western contact is steeply dipping and parallel with the Drahotěšice Fault, while the eastern is shallowly dipping. The NNE–SSW trending array of local gravity minima, located about 1.0–1.5 km to the E of the Drahotěšice Fault, may indicate a root zone of the SP.

The SP consists of three principal granite units: (i) two-mica cordierite or cordierite–andalusite-bearing Deštná granite (Klečka et al. 1991; René et al. 1999; Matějka et al. 2003); (ii) biotite–muscovite granite (Suk et al. 1978; Matějka 1991; Janoušek et al. 2002) and (iii) fine-grained biotite granite (Janoušek et al. 2002).

The Deštná granite (DG) represents the oldest intrusive phase and crops out only in the central and southeastern parts of the Pluton, being largely covered by Cretaceous and Tertiary sedimentary rocks. It is medium-grained, locally porphyritic (K-feldspar) and rich in muscovite (muscovite > biotite). Cordierite and andalusite form grains up to 1 mm in size (Matějka et al., 2003). Its ab-

solute age is not known but it is believed to belong to the group of “Eisgarn-type” granites (c. 327–328 Ma; Friedl et al. 1996; Gerdes et al. 2003).

The biotite–muscovite granite (BMG) occupies most of the northern and western parts of the Pluton. It is medium- to fine-grained, locally with biotite clots that resulted from replacement of cordierite by muscovite \pm biotite (Janoušek et al. 2002). Biotite granite (BtG) was recently identified only in the Ševětín quarry and its areal extent is small (c. $200 \times 100 \text{ m}$; Janoušek et al. 2002). Both BMG and BtG granites were probably coeval and are also collectively referred to as the Ševětín granite. Their absolute age is unknown. The parental magmas of the BMG and BtG are thought to have represented a mixture of a relatively primitive source (mantle-derived melts or metabasic rocks) and more evolved material geochemically corresponding to mature Moldanubian metasedimentary rocks or to their melts (Janoušek et al. 2002).

The SP was intruded by various dikes: lamprophyre (Ambrož 1935), pyroxene microgranodiorite (Vrána et al. 1993; Košler et al. 2001) and by aplite or leucogranite (this study; Zachariáš and Štrba 2014). The age of the microgranodiorite dike swarm ($270 \pm 3 \text{ Ma}$ ^{39}Ar – ^{40}Ar ; Košler et al. 2001) thus represents the lower age limit for the Ševětín granite intrusion.

Brittle–ductile and brittle deformation of the granites is a conspicuous feature of the SP. Both the DG and BMG are strongly deformed, while the BtG is only weakly deformed or even undeformed (Janoušek et al. 2002). The presence of specific deformation features in quartz grains from Ševětín (Vrána 1987), together with some geochemistry indications (Vrána et al. 1993), led these authors to suppose an impact-related origin of the Ševětín structure. This idea was, however, later abandoned (Cordier et al. 1994; Košler et al. 2001).

Various types of hydrothermal mineralization are known from the SP, associated with the individual stages of brittle deformation of the Pluton. These include quartz–feldspar veins, quartz veins and quartz–carbonate veins (e.g. Čtvrtník and Pavlíček 2002; Welsch and Zikeš 2009 and references therein). The latter are associated with uneconomic Pb–Zn ores, a probable analogue of the Ag–Pb–Zn ores of the Blanice Graben (e.g. Rudolfov and Ratibořské Hory–Stará Vožice ore districts).

4. Methods

This paper is based on three methodological approaches: (i) orientation and kinematic analysis of mesoscopic structures on outcrop scale; (ii) paleostress analysis of fault-slip data and (iii) AMS study of preferred mineral orientation, focused on the identification of relic magmatic fabric and of its solid-state modification.

The study area is relatively flat and outcrops for application of the above methods are scarce. We identified only six suitable localities within, and three outside the Pluton, referred to as SEV1 to SEV9 sites/samples. The most important and also the largest and best exposed site was an active quarry (with dimensions of c. $600 \times 350 \times 50$ m) in the northern part of the Pluton (SEV2), close to the southeastern margin of the Ševětín village. The number of measured data (mostly joints) at the other sites usually varied from 20 to 45 and was thus significantly less than in the Ševětín quarry (over 300). Therefore, some joint systems discernible in the Ševětín quarry may have been missed elsewhere.

Orientation analysis of structural data was performed in the Stereo32 software. All stereoplots represent lower hemisphere equal area projections, except stated otherwise. Paleostress analysis of fault-slip data was done using the numerical Gauss method (Žalohar and Vrabec 2007); the data were processed by the T-Tecto software (version 3.0; author J. Žalohar; http://www2.arnes.si/~jzaloh/t-tecto_homepage.htm).

A total of 16 oriented cores were sampled using a hand-held drill at 7 stations throughout the Pluton. After cutting, these samples yielded 78 standard specimens with a volume of 10 cm^3 . The AMS was measured at low field (450 Am^{-1}) with a MFK1-A Kappabridge instrument in the Laboratory of Rock Magnetism, Institute of Geology and Paleontology, Charles University in Prague. Statistical treatment and analysis of the AMS data were carried out using the ANISOFT 4.2 program package (<http://www.agico.com>). All the measured data and parameters are presented in the Electronic Supplement to this article.

The AMS data are represented by the k_m , P , and T parameters defined as follows: (1) $k_m = (k_1 + k_2 + k_3)/3$; (2) $P = k_1/k_3$ and (3) $T = 2\ln(k_2/k_3)/\ln(k_1/k_3) - 1$; where $k_1 \geq k_2 \geq k_3$ are the principal susceptibilities. Parameter k_m represents the mean bulk magnetic susceptibility, which reflects the proportion and type of magnetic minerals in the analyzed rock. Parameter P (Nagata 1961), the degree of AMS, reflects the eccentricity of the AMS ellipsoid and may thus be related to the intensity of preferred orientation of the magnetic minerals. Parameter T (Jelínek 1981) characterizes the symmetry of the AMS ellipsoid; it varies from -1 (perfectly prolate ellipsoid) through 0 (triaxial ellipsoid) to $+1$ (perfectly oblate ellipsoid). In magnetic fabric studies, the maximum principal susceptibility (k_1) is referred to as the magnetic lineation and the minimum principal susceptibility (k_3) defines a pole to the magnetic foliation; their orientations are presented in stereograms in the geographic (*in situ*) coordinate system. GPS coordinates of drill-cores used in the AMS study as well as of other studied sites are given in the Electronic Supplement. All the data were collected in 2012 and 2013.

5. Results

5.1. Orientation analysis of brittle structures in the Ševětín quarry

5.1.1. Joints

Joints of several generations represent the most ubiquitous mesoscopic phenomena in the Ševětín Pluton. In total, we distinguished six types of joints (referred to as P_1 through P_6) in the quarry with respect to their orientation (Fig. 3).

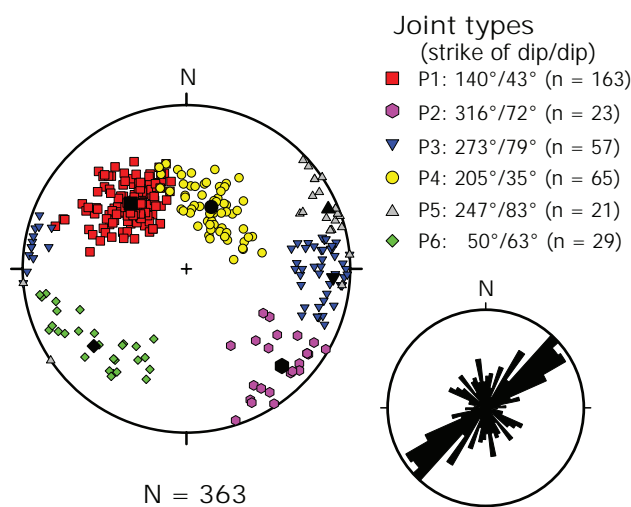


Fig. 3 Summary plot of poles of joints from the active Ševětín quarry and rose diagram of joint strikes. The maxima of the individual joint types given in the legend were converted from the respective eigen-vectors.

P_1 joints represent the most prominent structures in the quarry (Fig. 4a). They strike NE–SW and dip moderately to SE. They are regularly spaced (about 5–20 cm) and represent typical extension joints as indicated by the frequent presence of plumose hackles and rib marks (Fig. 4b). The longitudinal axis of rib marks is roughly identical with the dip line and their shape implies stepward propagation of P_1 joints upward along the dip line. The visibility of ribs and hackles is highlighted by greenish coatings of epidote–chlorite and by even younger scarce coatings of calcite.

P_2 joints are much less frequent than P_1 . Strictly geometrically, they resemble a conjugate system to P_1 joints. However, we found no unambiguous evidence for the presence of a conjugate P_1 – P_2 system.

P_3 joints are steep, N–S trending and locally filled in by veins of greyish quartz. Some of P_3 joints contain hackles and rib marks; however, they are less visible than those at the P_1 joints. Locally, the joints may display systematic down-slip of northern segments (Fig. 4c).

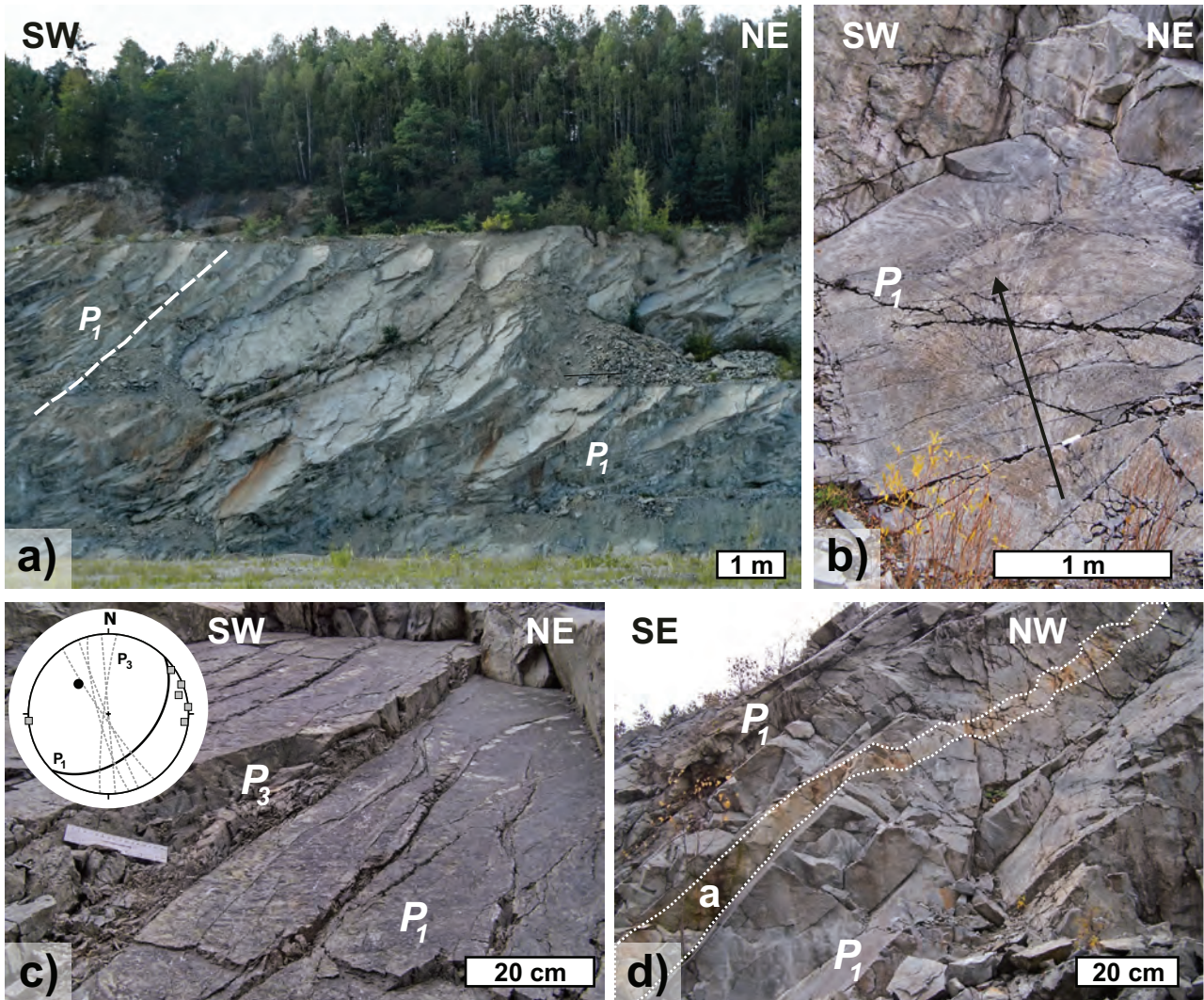
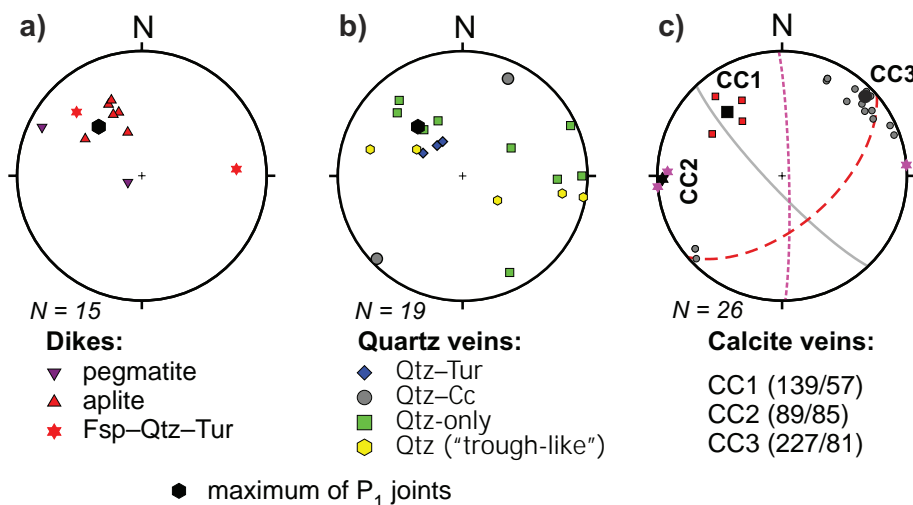


Fig. 4 Photos of P_1 joints at the new Ševětín quarry: **a** – Moderately inclined P_1 joints in the southwestern wall of the quarry. **b** – Detail of plume hackles and rib marks on the surface of a P_1 joint. The arrow indicates the axis of the plume and upward direction of the fracture opening. **c** – P_1 joint crosscut by steep P_3 joints, accompanied by systematic down-throw of the northeastern segments. **d** – Dike of aplite intruding the BMG between two P_1 joints.



Therefore, they represent most probably mixed Mode I-II fractures.

P_4 joints strike mostly NW-SE and dip moderately to the SW. They frequently show evidence for shear movements and usually do not crosscut P_1 joints. Some are rimmed by feldspathic masses (up to 1.5 cm thick), while the others host veins of greyish quartz.

Fig. 5 Summary diagrams for intrusive dikes (a), quartz veins (b) and calcite veins (c) observed in the BMG granite in the Ševětín quarry.

P_5 and P_6 joints are oriented WNW–ESE and dip steeply to the NE to ENE (P_5) or to SE (P_6). Some P_5 joints were filled in by late calcite veins (CC3). Both calcite veins and P_5 joints represent extension fractures (Mode I).

5.1.2. Dikes

We identified several aplite and pegmatitic dikes in the quarry. The largest is a pinkish aplite ~20 cm thick, at least 70–60 m long along its strike, and *c.* 10 m along the dip. It is parallel or subparallel to P_1 joints (Fig. 4d). Other observed aplite dikes are much smaller, mostly less than 5 cm thick, and of a more variable orientation. Most of them, however, are still subparallel with P_1 joints (Fig. 5a).

In addition to aplite, several dikes of leucocratic granite (10 to 50 cm thick) can be found in the southwestern wall of the quarry, but these were not accessible for direct structural measurements. It can be seen in Fig. 6 that these dikes are first parallel to P_1 joints, but later steepen and finally one of them approaches almost vertical orientation at the bottom of the quarry wall. Another felsic but much thicker zone (dike?) is located above these dikes and is also parallel to P_1 joints.

5.1.3. Hydrothermal veins

Several types/generations of hydrothermal veins and of transitional late-magmatic to early hydrothermal products can be identified in the Ševětín quarry. The latter are represented by fractures/veins with feldspathic rims, which may contain quartz, hornblende and/or tourmaline in the core. They are usually less than 2 cm thick and mostly parallel to P_1 joints.

Probably three generations of hydrothermal quartz veins exist in the quarry (Fig. 5b): (i) The undoubtedly

oldest, less than 5 mm thick quartz veinlets with tourmaline, slightly oblique to P_1 joints and locally crosscutting them; (ii) Up to several cm thick veins of greyish quartz (with finely disseminated chlorite and/or pyrite), more or less subparallel to P_4 joints and (iii) Older growth zones in the veins of late calcite (CC3).

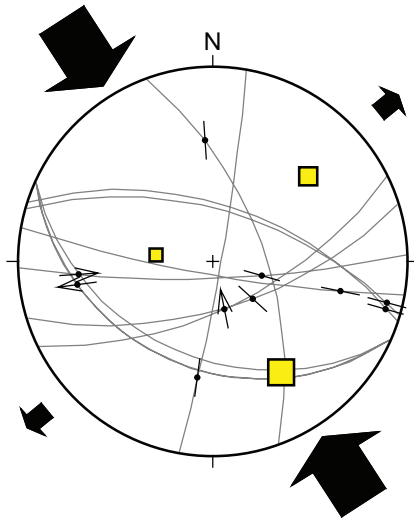
With respect to their orientation, three clusters of calcite veins and veinlets were identified (Fig. 5c) and referred to as CC1, CC2, CC3. Veins of the late calcite (CC3) are the most frequent. They are extensional in nature, as indicated by bilaterally symmetrical growth zones and less frequently by crustiform or breccia textures. We found them associated with P_5 joints, but they may also accompany the main fault (being parallel with it). Čtvrtník and Pavlíček (2002) described about 20 cm thick calcite vein (CC3?) with abundant sphalerite and/or galena spatially associated with the main fault. However, we found only one calcite vein with sparse sphalerite grains. The other two groups (CC2, CC1) may represent two separate and older but volumetrically minor calcite generations. Alternatively, they may have been coeval with the CC3 group as the fluids just reached structures of different orientation.

5.1.4. Faults and fault-slip data

Two major more or less parallel faults (striking NE–SW and inclined 70 to 85° to the SE) crop out in the Ševětín quarry (for details, see Zachariáš and Štrba 2014). They are oblique to the Drahotěšice Fault and are associated with numerous second-order small-scale faults. The fault plane of the western fault is flanked by *c.* 0.5 m wide zone of friable gouge of dark appearance. Rocks in an about 50–80 m wide zone between these two faults are highly fractured. Although both faults probably accumulated most of the brittle deformation, the fault planes themselves are almost free of identifiable striation. Striations

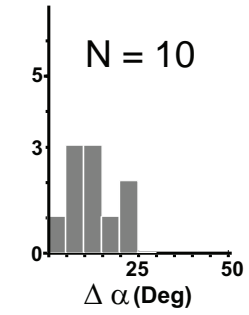
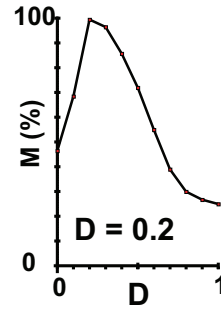


Fig. 6 Parallel dikes of leucocratic granite (highlighted by shading) in the southern wall of the active Ševětín quarry. Note they are initially parallel with P_1 joints, but later become much steeper.

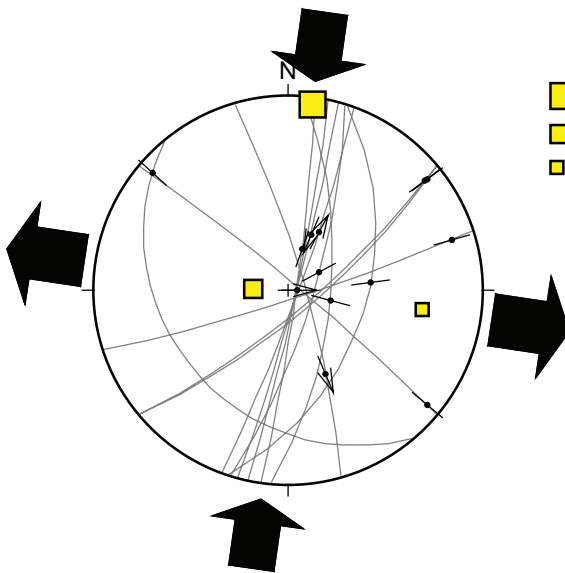


- $\sigma_1 = 148^\circ/22^\circ$
- $\sigma_2 = 48^\circ/23^\circ$
- $\sigma_3 = 277^\circ/57^\circ$

$\sigma_1 : \sigma_2 : \sigma_3$
1.06 : 0.27 : 0.08

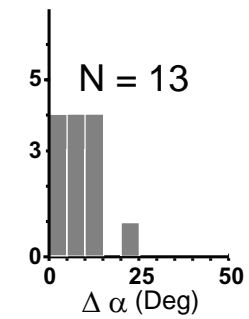
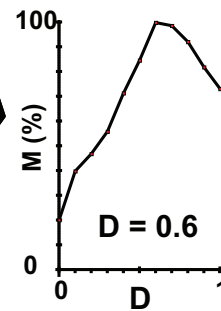


Phase 1

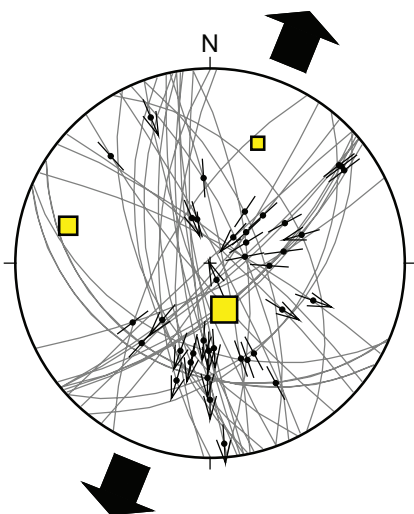


- $\sigma_1 = 8^\circ/2^\circ$
- $\sigma_2 = 272^\circ/70^\circ$
- $\sigma_3 = 98^\circ/20^\circ$

$\sigma_1 : \sigma_2 : \sigma_3$
0.86 : 0.54 : 0.06

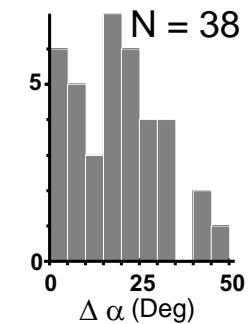
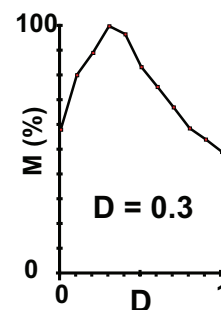


Phase 2



- $\sigma_1 = 163^\circ/62^\circ$
- $\sigma_2 = 285^\circ/16^\circ$
- $\sigma_3 = 22^\circ/23^\circ$

$\sigma_1 : \sigma_2 : \sigma_3$
1.01 : 0.35 : 0.07



Phase 3

are, however, rather frequent within the highly fractured zone. We identified a total of 65 fault planes with slickenlines in the Ševětín quarry that were included in the paleostress analysis. Fault-slip data from other sites were sparse (less than three per locality) and thus excluded.

5.1.5. Paleostress analysis of fault-slip data

Our calculations started with a larger maximum misfit value (50–60°) between the theoretical and real slip vectors and were repeated until lower misfit values (15–20°) and numerically stable solutions were obtained. The analysis resulted in the separation of fault-slip data into three populations representing separate tectonic phases (Fig. 7). They differ in the orientation of the paleostress axes and in the stress ratio [represented by the D parameter, where $D = (\sigma_2 - \sigma_3) / (\sigma_1 - \sigma_3)$].

Phase 1 represented an oblique compression regime, with the maximum principal stress in the NW–SE direction. The minimum principal stress (σ_3) was moderately inclined to the W.

Phase 2 reflected a strike-slip regime, as indicated by subvertical orientation of the intermediate stress axis (σ_2). The maximum principal stress (σ_1) was oriented N–S and the least principal stress (σ_3) E–W.

Phase 3 corresponded to an extensional regime with maximum subhorizontal σ_3 in the NNE–SSW direction.

5.2. Orientation analysis of brittle structures on a regional scale

Three to four dominant joint systems are identified on a regional scale: the P_1 system is best recognizable in the northern part of the SP (Fig. 8; sites 1–3), but is still identifiable across the whole Pluton. At a single locality (site 4), the P_1 system grades into steep joints, similar in orientation to P_3 joints at the Ševětín quarry (site 2). Most localities, and notably the abandoned quarry south of the village of Vitín (site 3; the second largest outcrop after the Ševětín quarry), lack P_4 joints.

5.3. Ductile structures in the surrounding Moldanubian unit

Localities outside the Ševětín Pluton are represented by sillimanite–biotite paragneisses (site 7), migmatites

(site 8) and migmatitic biotite gneisses (site 9). They all show subhorizontal metamorphic foliation (S_1 ; Figs 8 and 9a). Stretching lineation (L_1) is, however, visible only in the paragneiss (site 7), where it is subhorizontal and trends NW–SE (Fig. 9b). At the same locality we also identified open folds with moderately inclined axial planes and with well-developed second-order chevron-like folds in the hinge zones (Fig. 9b). All the folds exhibit the same axis orientation, identical with the strike and dip of the stretching lineation.

5.4. Magnetic fabric parameters and orientation of the Ševětín Pluton

5.4.1. Bulk susceptibility

The bulk magnetic susceptibility of the measured specimens is of the order of 10^{-5} (Fig. 10a; SI units are used throughout this paper), characteristic of paramagnetic granites (e.g., Hrouda and Kahan 1991; Bouchez 1997). A slight increase in the bulk susceptibility can be seen from the sample SEV2b (32×10^{-6} to 39×10^{-6}) through the SEV2c, SEV3, SEV4 (60×10^{-6} to 73×10^{-6}) to the SEV2a, SEV6 and SEV1 (74×10^{-6} to 104×10^{-6}).

5.4.2. P and T parameters

The Ševětín granite is characterized by a low degree of anisotropy not exceeding 1.2 (corresponding to 12% magnetic anisotropy) for most of the analyzed specimens (Fig. 10b).

Sample SEV1 ($P = 1.013$ – 1.054) is the least anisotropic, SEV2b ($P = 1.040$ – 1.058), SEV2c ($P = 1.033$ – 1.069 ; one outlier with $P = 1.263$) and SEV3 ($P = 1.024$ – 1.084) are slightly more so. The degree of anisotropy of samples SEV2a and SEV4 is more widely scattered from 1.044 to 1.085 (Fig. 10b). The highest degree of anisotropy was measured in the SEV6 specimen ($P = 1.072$ – 1.119).

In contrast to the slight differences in the P parameter, the granites exhibit a mutually comparable range of shape parameter from highly prolate (T as low as -0.826) to highly oblate ($T = 0.879$ at most), as well as a distinct trend of concomitantly increasing oblateness and degree of anisotropy (Fig. 10b).

5.4.3. Orientations

In terms of orientation, all the granite samples except SEV3 and SEV6 exhibit N–S to NE–SW trending, steep to moderately dipping magnetic foliation, indicated by clusters of the k_3 axes in the stereonet (Fig. 11a). In

⇐

Fig. 7 Separation of fault-slip data, based on paleostress inversion analysis using the Gauss method (Žalohar and Vrabec 2007), into three stress phases. All stereoplots represent lower hemisphere equal angle projections. Solid arrows indicate orientations of maximum horizontal compression and/or extension. The other diagrams show the confidence of the parameter D estimate and histograms of deviation between the calculated and measured slip vectors.

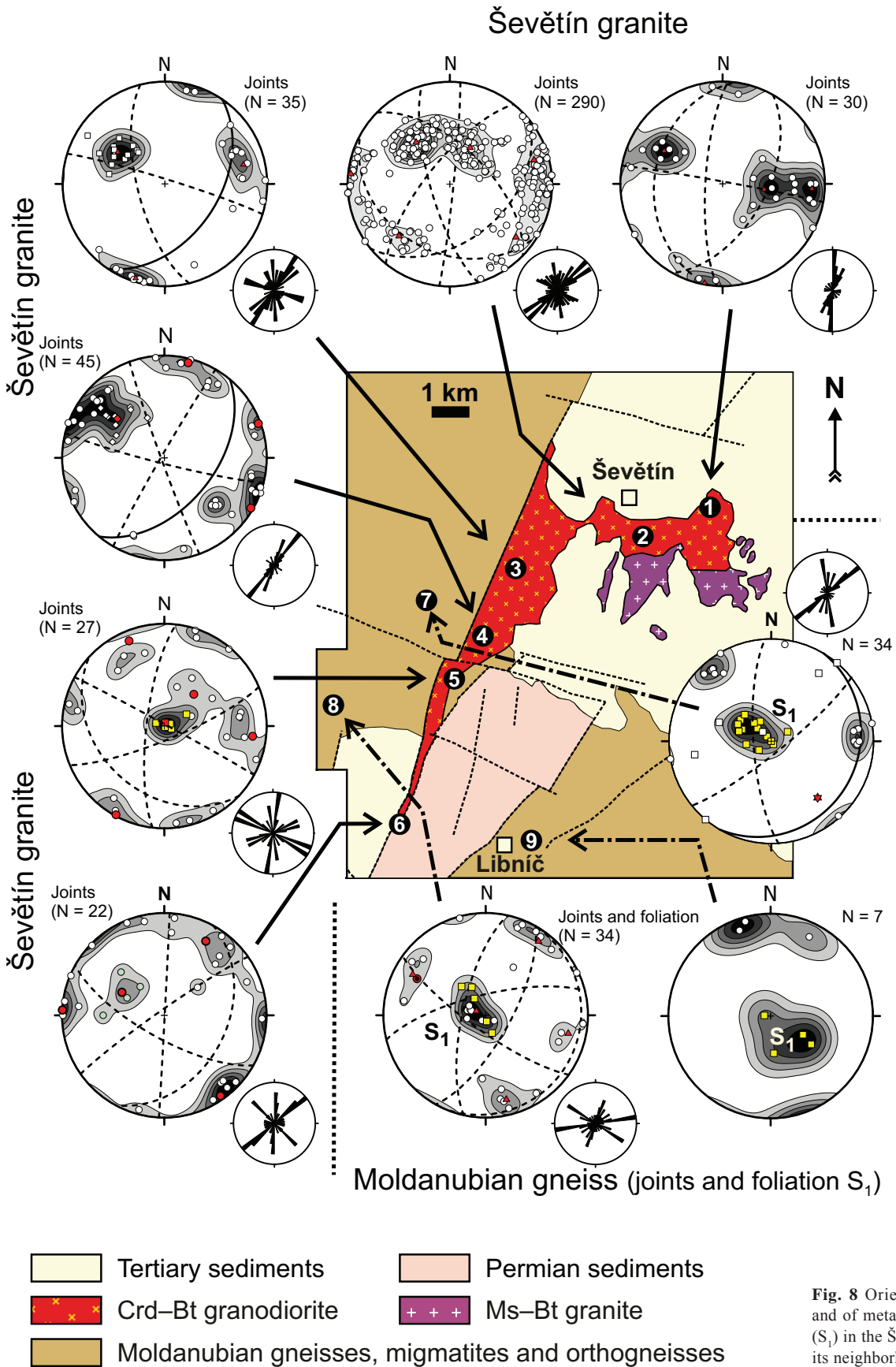


Fig. 8 Orientation of joints and of metamorphic foliation (S_1) in the Ševětín Pluton and its neighborhood.

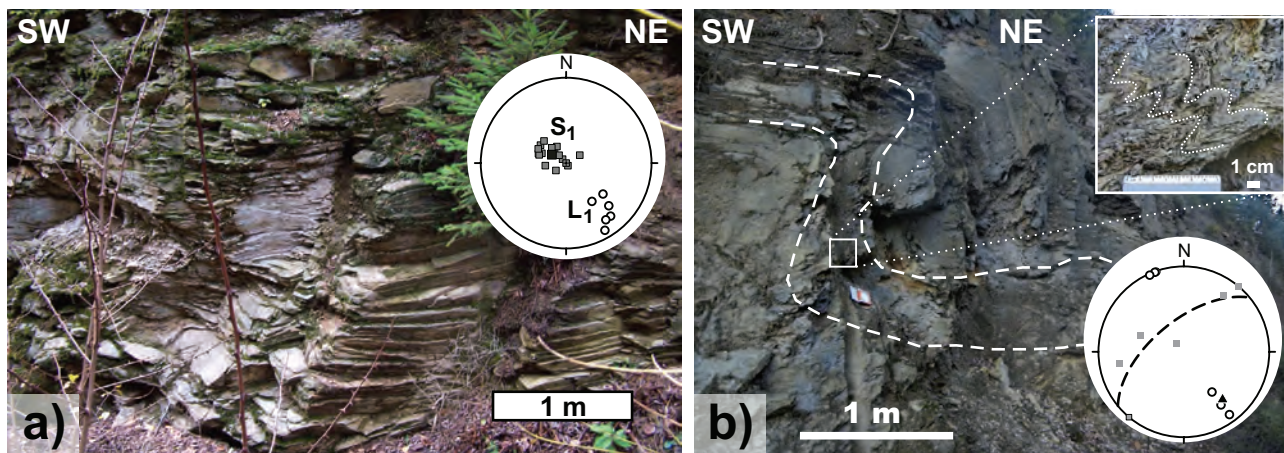


Fig. 9a – Subhorizontal metamorphic foliation (S_1) of biotite paragneiss in the railway cut near Chotýčany (Stop 5). The stereogram shows the orientation of the poles of metamorphic foliation (S_1 ; full squares) and of metamorphic stretching lineation (L_1 ; open circles). **b** – Local development of a small-scale flexure/fold in paragneiss from the same outcrop as the previous photo. The inserted photograph documents second-order chevron-like folds in the hinge zone of the main fold. The stereogram shows the orientation of fold limbs (full squares), of measured fold axes of chevron-like folds (open circles) and of the constructed π -pole (full triangle) and circle (dashed). Note the identical trend and plunge of metamorphic stretching lineation and of fold axes.

sample SEV3, the magnetic foliation is also steep; however, it trends NW–SE. Notably, individual k_3 axes in this sample are broadly scattered along a girdle with a pole located at the maximum magnetic lineation (maximum of the k_1 axes). Magnetic foliation in the sample SEV6 trends E–W.

Magnetic lineations (k_1 axes) are usually well defined and of subhorizontal plunge. They trend N–S to NE–SW, except samples SEV6 (E–W) and SEV3 (NW–SE) and form clusters in the stereonet. The only exception is sample SEV1, where the individual k_1 axes are scattered along a girdle with a pole at the maximum of the k_3 axes.

6. Discussion

6.1. Relative age relationships between joints, dikes and veins

The P_1 joints represent the oldest population of joints because: (i) late magmatic dikes of aplite and leucogranite show similar orientation as P_1 joints (Fig. 4a); (ii) neither the aplite dikes are crosscut by P_1 joints, nor are the P_1 joints cut by the dikes (Fig. 4d) and (iii) P_1 joints are displaced by other types of joints (P_3 , P_4 , P_5 ; see Fig. 4c).

Displacement relationships indicate that P_4 joints are older than P_5 . Late formation of P_5 and P_6 joints can be

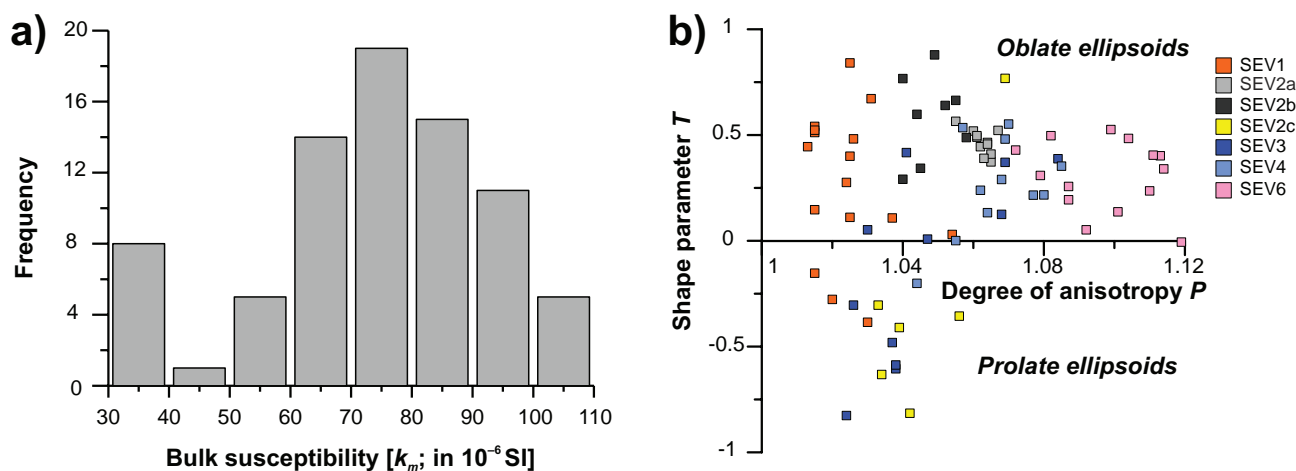


Fig. 10 Magnetic properties for all the studied samples from the Ševětín Pluton: **a** – Summary histogram of the mean magnetic susceptibility; **b** – Magnetic anisotropy P–T plot.

a) AMS fabrics

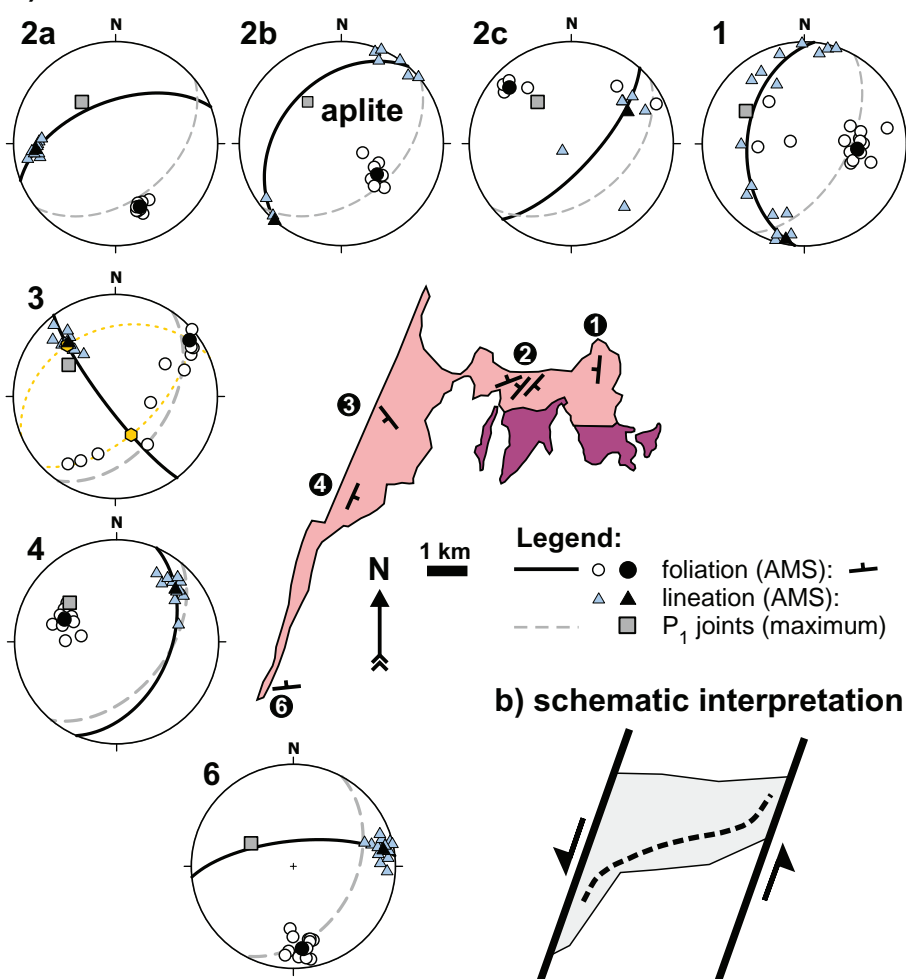


Fig. 11a – Orientation of magnetic foliation (poles represented by the k_3 axes and by the mean plane) and lineations (represented by k_1 axes) at the Ševětín Pluton. The orientation of P_1 joints (mean pole and plane) is also plotted, for comparison with Fig. 8. The apparent inverse orientation of k_1 and k_3 axes at the site 3 (SEV3), compared to other sites, may be due to the presence of cordierite, while the magnetic susceptibility of the other samples is controlled by biotite and muscovite. **b** – Schematic summary of magnetic foliation trends across the Ševětín Pluton. The overall sigmoidal shape of this trend points to mostly solid-state deformation of the Ševětín granite during oblique sinistral movements on the main faults of the Blanice Graben.

deduced indirectly from spatial association of extension veins of late calcite (CC3) with these joints. Relative age of P_2 joints remains questionable. Similar orientation of P_2 joints and of CC2 calcite points to post- P_1 and pre- P_3 nature of P_2 joints.

6.2. Summary of the intrusive and deformational evolution of the Ševětín Pluton

6.2.1. Late metamorphic phase

The metamorphic foliation (S_3 ; this study) in Moldanubian rocks to the W and SE of the SP can be, on regional scale, correlated with the subhorizontal foliation S_4 of Franěk et al. (2011). Its formation was related to the LP–MT stage of deformation of the Moldanubian Unit at *c.* 340 Ma (Franěk et al. 2011). Further to the E of the SP, the metamorphic foliation becomes gradually steeper due to diapiric formation of the Pelhřimov granite–dome Complex (Verner et al. 2014) at *c.* 328–327 Ma. In contrast to the Pelhřimov Com-

plex (Klenov Pluton) the relations between the metamorphic fabrics in the Moldanubian rocks, and the magmatic and solid-state deformation fabrics in the SP are more obscure: (i) the BMG lacks mesoscopically visible magmatic fabrics as well as clear S_1 overprint; (ii) there is no change in the dip of S_1 foliation in the Moldanubian rocks towards the SP; (iii) the magnetic foliation of the SP is much steeper than the metamorphic foliation; (iv) sparse folds in the Moldanubian paragneisses with axial planes trending NW–SE and dipping moderately to SW (Fig. 9b) must have postdated the S_1 foliation and indicate NE–SW oriented local shortening.

6.2.2. Intrusion of the Ševětín Pluton

The SP is volumetrically dominated by two intrusive units: the Deštná granite (DG) and the biotite–muscovite granite (BMG). Their absolute intrusive ages are not known; however, the DG is petrologically and geochemically similar to the Klenov granite that has been recently dated at 328.4 ± 0.2 Ma and 327.1 ± 0.2 Ma (U–Pb monazite; Verner et al. 2014), while the BMG might be similar in age to the Freistadt

granodiorite (302 ± 2 Ma; Friedl et al. 1992), or slightly older. An age of *c.* 305 Ma for BMG would be compatible with the onset of sedimentation in the Blanice Graben, as well as with the oldest dated tectonic and intrusive activity at the Rödl fault zone (Vrána et al. 2005). The two intrusive units also differ in shape: the DG is only slightly elongated in the E–W to ENE–SWS direction, while the BMG is markedly stretched in NNE–SSW direction (Figs 1 and 2), i.e. parallel with the strike of the Blanice Graben. Temporal separation of the BMG and DG intrusions is therefore possible.

The mean magnetic susceptibility of all the studied samples (Fig. 10a) indicates that micas are the main carrier of the susceptibility. This is also reflected in the dominant planar fabric. The BMG almost lacks evidence for ductile deformation; therefore, we consider the planar magnetic fabric to reflect magmatic foliation. The AMS fabric pattern reveals a transition from NNE–SSW trending foliation at the eastern margin of the SP, through NE–SW trending foliations in the center, back to NNE–SSW trends at the western margin. The overall sigmoidal pattern (Fig. 11b) of magnetic foliation across the SP points either to synkinematic intrusion of the BMG during sinistral strike-slip activity on the Blanice Graben fault system or to subsolidus modification of magmatic foliation (trending E–W to NE–SW) during sinistral strike-slip motion. The latter option is supported by moderate gradual increase in the anisotropy of AMS data from the E (site 1) towards the W (sites 4 and 6) that points to higher strain and higher solid-state deformation in the vicinity of the western margin of the Blanice Graben, than along the eastern margin. Importantly, asymmetry of the gravimetric anomaly (Fig. 2) and alignment of gravity minima (NNE–SSW) suggest that the BMG was rooted/intruded along the western margin of the Blanice Graben.

Sample SEV3 is the only exception to the above-described regional trends. Apparent inversion of the k_1 and k_3 maxima might be due to the presence (relics?) of cordierite in the studied sample. The cordierite is known to define an inverse magnetic fabric (Rochette et al. 1992), where k_1 and k_3 represent the pole of magnetic foliation and lineation, respectively. If this is true in our case, then SEV3 defines the same trend of magmatic foliation and lineation as the other samples. Cordierite forms sparse phenocrysts in the DG. Its original presence in the BMG is indicated only by clusters of micas rimming rare cordierite relics (Janoušek et al. 2002). The SEV3 sample may thus represent less altered BMG granite.

The only mesoscopic indication of magmatic foliation we found in the BMG (site SEV2a), where biotite defines weak planar fabric (dip direction/dip: $170^\circ/85^\circ$). This resembles the dip direction of magnetic foliation from site SEV6 ($354^\circ/70^\circ$) and SEV2a ($339^\circ/60^\circ$). There is, however, not enough data to discuss the extent of solid-state modification of the magmatic fabric.

6.2.3. Early brittle deformation phase (oblique compression regime)

Fault-slip data from the BMG at the Ševětín quarry indicate NW–SE oriented subhorizontal compression. The orientation of the minimum principal stress axis (σ_3 : $277^\circ/57^\circ$) is more or less similar to the maximum of the poles of P_1 joints ($320^\circ/47^\circ$), which are extensional in nature. Similarly, most of the late magmatic dikes (aplite, leucogranite or pegmatite) also exhibit poles clustered tightly around the P_1 maximum (Fig. 5a). The same holds for early hydrothermal quartz veins with minor tourmaline. All these data thus unambiguously indicate the long persistency of a minimum stress axis moderately inclined to the NW to W. The orientation of the maximum principal stress axis (slightly inclined to the SE) was favorable for oblique sinistral movements along the main faults of the Blanice Graben (Fig. 12b). Overall persistence of orientation of P_1 joints across the whole studied area, compared to curved trends of magnetic foliations, may indicate that major oblique strike-slip movements along the faults of Blanice Graben occurred before formation of P_1 joints.

6.2.4. Mid-stage brittle deformation phase (strike-slip regime)

This phase, which is mostly indicated by numerical analysis of the fault-slip data, points to subhorizontal N–S oriented compression and subhorizontal E–W oriented extension (Fig. 12c). This is compatible with the orientation of P_3 joints, as well as with the formation of some of the thin aplite dikes or the monomineral quartz veins (free of tourmaline/feldspar). Overall scarcity of hydrothermal veins coupled with this tectonic phase, however, indicates only a short-lived and relatively insignificant hydrothermal activity.

The magmatic activity (270 ± 2 Ma; Košler et al. 2001) ascribed to this phase produced NNE–SSW to N–S trending and steeply dipping dikes of pyroxene-bearing microgranodiorite (Vrána et al. 1993) and quartz monzodiorite (Vrána and Janoušek 2006).

6.2.5. Late brittle deformation phase (extension regime)

Numerous fault-slip data indicate NNE–SSW oriented subhorizontal extension (Fig. 12d). The maximum of poles of late (quartz)–calcite (CC3) tension veins is shifted clockwise by *c.* 20 – 30° ; however, it is still compatible with the stress axes calculated from the fault-slip data. The minor change in the strike of the P_6 relative to the P_5 joints most probably also reflects the clockwise rotation of the σ_1 and σ_3 stress axes. During this phase, the main

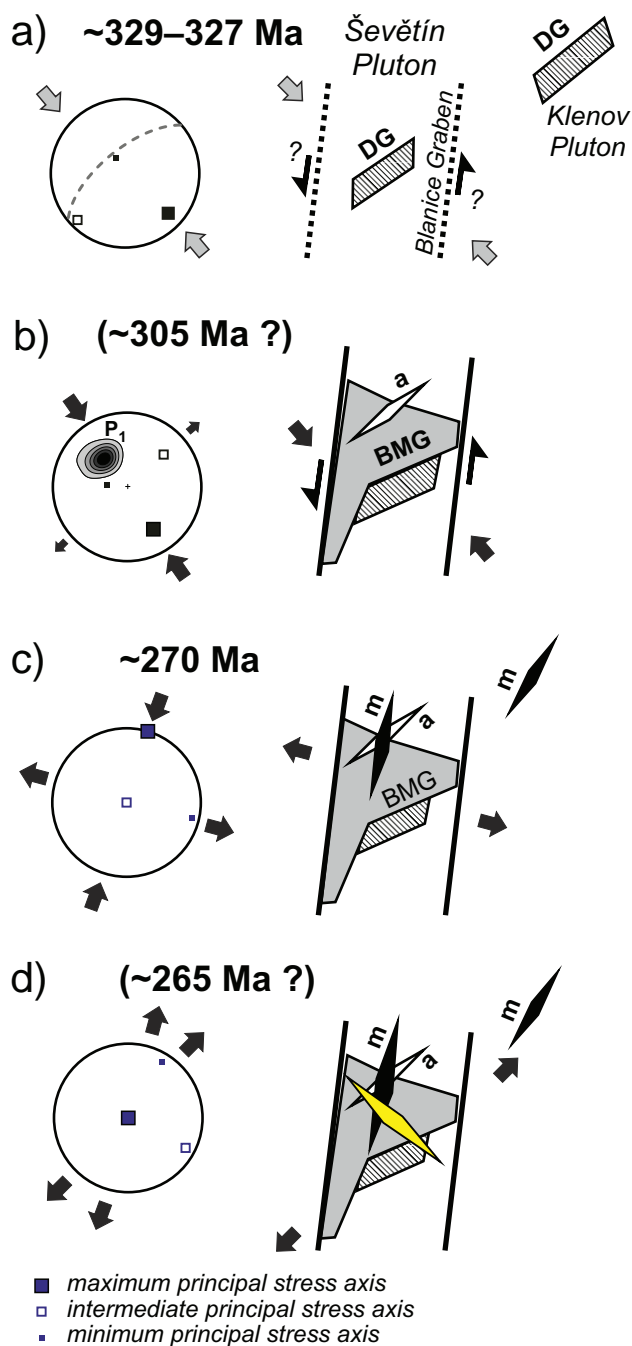


Fig. 12 Schematic model of emplacement of the Ševětín Pluton in the context of evolution of the Blanice Graben: **a** – intrusion of the two-mica Deštná type granite under NW–SE oriented compression; **b** – intrusion of biotite–muscovite granite (BMG), followed by more or less coeval formation of extensional P_1 joints and of aplitic dikes under oblique compression; **c** – strike-slip phase and late intrusion of the 270 Ma old pyroxene microgranodiorite dike into the relatively cool Ševětín Pluton; **d** – late extensional phase coupled with the formation NW–SE trending hydrothermal (quartz)–calcite veins with uneconomic Pb–Zn ores.

stage of late hydrothermal activity occurred within the Blanice Graben, as indicated by the uneconomic Pb–Zn ores (hydrothermal veins).

7. Conclusions

A structural study of the Ševětín Pluton (SP) enabled detailed reconstruction of the Blanice Graben tectonic evolution and of associated magmatic activity:

- The AMS study revealed steeply to moderately dipping planar magnetic fabrics that we interpreted mostly as solid-state in origin, especially in the vicinity of the Drahoštěšice Fault (western margin of the Blanice Graben). Local preservation of original magmatic foliation is possible in the central to eastern parts of the SP. The overall sigmoidal trend of the magnetic fabrics indicates sinistral movements along the Blanice Graben fault systems postdating the intrusion of the biotite–muscovite granite (BTG) of the SP. This is further supported by well-defined subhorizontal magnetic lineation. The magnetic fabric of the SP is thus in sharp contrast to the subhorizontal metamorphic foliation and subhorizontal NW–SE trending stretching lineation in the surrounding Moldanubian host rocks.
- Paleostress and kinematic analysis of brittle structures allowed differentiation of three tectonic phases (oblique compression, strike-slip and extension), which postdated the intrusion of the BMG.
- The oblique compression phase comprised both the emplacement of the BMG and early stages of its brittle deformation. It was accompanied by the formation of NE–SW trending joints (P_1) and dikes (aplite), both dipping moderately to the SE.
- The strike-slip phase indicates more or less E–W trending extension and can be correlated with the intrusion of *c.* 270 Ma microgranodiorite dikes. The orientation of the stress axis was, however, unfavorable for the main movements on the major faults of the Blanice Graben.
- The extension phase was accompanied by the formation of hydrothermal Pb–Zn–(Ag) quartz–carbonate veins and scarce P_5 and P_6 tension joints.

Acknowledgements. This paper was supported by the Grant Agency of Charles University (project No. 151810). We also greatly acknowledge the constructive reviews of P. Pitra and R. Grygar and the editorial comments of J. Žák and V. Janoušek.

Electronic supplementary material. List of the AMS data and of GPS coordinates of all studied sites is available online at the Journal web site (<http://dx.doi.org/10.3190/jgeosci.175>).

References

- AMBROŽ V (1935) Study on the metamorphic rocks between Hluboká and Týn nad Vltavou. Spisy přírodověd Fak Univ Karl 138: 1–44 (in Czech)

- BANKWITZ P, BANKWITZ E, THOMAS R, WEMMER K, KÄMPF H (2004) Age and depth evidence for pre-exhumation joints in granite plutons: fracturing during the early cooling stage of felsic rock. In: COSGROVE JW, ENGELDER T (eds) *The Initiation, Propagation and Arrest of Joints and Other Fractures*. Geological Society of London Special Publications 231: 25–47
- BOUCHEZ JL (1997) Granite is never isotropic: an introduction to AMS studies of granitic rocks. In: BOUCHEZ JL, HUTTON DHW, STEPHENS W (eds) *Granite: From Segregation of Melt to Emplacement Fabrics*. Kluwer Academic Publishers, Dordrecht, pp 95–112
- BRANDMAYR M, DALLMEYER RD, HANDLER R, WALLBRECHER E (1995) Conjugate shear zones in the Southern Bohemian Massif (Austria): implications for Variscan and Alpine tectonothermal activity. *Tectonophysics* 248: 97–116
- BREITER K (2010) Geochemical classification of Variscan granitoids in the Moldanubicum (Czech Republic, Austria). *Abh Geol B-A* 65: 19–25
- CORDIER P, VRÁNA S, DOUKHAN JC (1994) Shock metamorphism in quartz at Ševětín and Sušice (Bohemia)? A T.E.M. investigation. *Meteoritics* 29: 98–99
- ČTVRTNÍK J, PAVLÍČEK V (2002) Occurrence of colored sphalerite at Ševětín. *Minerál* 10: 9–12 (in Czech)
- ČUTA J, MANOVÁ M, ŠALANSKÝ K (1975) Explanations to geophysical map 1:25 000, sheet 22-444 Ševětín. Unpublished report, Geofyzika Brno, Prague, pp 1–22 (in Czech)
- DALLMAYER RD, FRANKE W, WEBER K (eds) (1995) *Pre-Permian Geology of Central and Eastern Europe*. Springer-Verlag, Berlin, pp 1–604
- FAURE M. (1995) Late orogenic Carboniferous extensions in the Variscan French Massif Central. *Tectonics* 14: 132–153
- FIALA J, FUCHS G., WENDT J.I. (1995) VII.C.1 Stratigraphy. In: DALLMAYER RD, FRANKE W, WEBER K (eds) *Pre-Permian Geology of Central and Eastern Europe*. Springer-Verlag, Berlin, pp 417–428
- FINGER F, GERDES A, JANOUŠEK V, RENÉ M, RIEGLER G (2007) Resolving the Variscan evolution of the Moldanubian sector of the Bohemian Massif: the significance of the Bavarian and the Moravo–Moldanubian tectonometamorphic phases. *J Geosci* 52: 9–28
- FINGER F, RENÉ M, GERDES A, RIEGLER G (2009) The Saxo-Danubian Granite Belt: magmatic response to postcollisional delamination of mantle lithosphere below the southwestern sector of the Bohemian Massif (Variscan Orogen). *Geol Carpathica* 60: 205–212
- FRANĚK J, SCHULMANN K, LEXA O, TOMEK C, EDEL JB (2011) Model of syn-convergent extrusion of orogenic lower crust in the core of the Variscan belt: implications for exhumation of high-pressure rocks in large hot orogens. *J Metamorph Geol* 29: 53–78
- FRANKE W (2000) The mid-European segment of the Variscides: tectonostratigraphic units, terrane boundaries and plate tectonic evolution. In: FRANKE W, HAAK V, ONCKEN O, TANNER D (eds) *Orogenic Processes, Quantification and Modelling in the Variscan Belt*. Geological Society of London Special Publications 179: 35–61
- FRIEDL G, VON QUADT A, FRASL G, FINGER F (1992) Neue U/Pb Altersdaten aus der südlichen Böhmisches Masse. *Frankfurter Geowiss Arb A11*: 217–218 (in German)
- FRIEDL G, VON QUADT A, FRASL G, FINGER F (1996) Timing der Intrusionstätigkeit im Südböhmisches Batholith: 6. Symposium Tektonik-Strukturgeologie-Kristallinologie, Salzburg, 10–15 April 1996. Fakultas Universitätsverlag, Vienna, pp 127–130 (in German)
- FRIEDL G, COOKE RA, FINGER F, MCNAUGHTON NJ, FLETCHER IR (2011) Timing of Variscan HP–HT metamorphism in the Moldanubian Zone of the Bohemian Massif: U–Pb SHRIMP dating on multiply zoned zircons from a granulite from the Dunkelsteiner Wald Massif, Lower Austria. *Mineral Petrol* 102: 63–75
- GERDES A (2001) Magma homogenization during anatexis, ascent and/or emplacement? Constraints from the Variscan Weinsberg Granites. *Terra Nova* 13: 305–312
- GERDES A, WÖRNER G, HENK A (2000) Post-collisional granite generation and HT–LP metamorphism by radiogenic heating: the Variscan South Bohemian Batholith. *J Geol Soc, London* 157: 577–587
- GERDES A, FRIEDL G, PARRISH RR, FINGER F (2003) High-resolution geochronology of Variscan granite emplacement – the South Bohemian Batholith. *J Czech Geol Soc* 48: 53–54
- HOLUB V (2001) The occurrences of the Permo–Carboniferous sequences in the Blanice Graben. In: PEŠEK J, HOLUB V, JAROŠ J, MALÝ L, MARTÍNEK K, PROUZA V, SPUDIL J, TÁSLER R (eds) *Geology and Deposits of Upper Paleozoic Limnic Basins of the Czech Republic*. Czech Geological Survey, Prague, pp 197–207 (in Czech)
- HOLUB FV, KLEČKA M, MATĚJKA D (1995) Igneous activity. In: DALLMAYER RD, FRANKE W, WEBER K (eds) *Pre-Permian Geology of Central and Eastern Europe*. Springer-Verlag, Berlin, pp 444–452
- HROUDA F, KAHAN Š (1991) The magnetic fabric relationship between sedimentary and basement nappes in the High Tatra Mountains, N. Slovakia. *J Struct Geol* 13: 431–442
- JANOUŠEK V, HOLUB FV (2007) The causal link between HP–HT metamorphism and ultrapotassic magmatism in collisional orogens: case study from the Moldanubian Zone of the Bohemian Massif. *Proc Geol Assoc* 118: 75–86
- JANOUŠEK V, VRÁNA S, ERBAN V (2002) Petrology, geochemical character and petrogenesis of a Variscan post-orogenic granite: case study from the Ševětín Massif, Moldanubian Batholith, Southern Bohemia. *J Czech Geol Soc* 7: 1–22
- JELÍNEK V (1981) Characterization of the magnetic fabric of rocks. *Tectonophysics* 79: T63–T67
- KADLEC E, ODSTRČIL J, ŠALANSKÝ K (1978) Summary Processing of Geophysical Data from the South-Bohemian Basins Area. Unpublished report, Geofyzika Brno, Prague, pp 1–175 (in Czech)

- KLEČKA M, MATĚJKA D (1996) Moldanubian Batholith – an example of the evolution of the Late Paleozoic granitoid magmatism in the Moldanubian Zone, Bohemian Massif (Central Europe). In: SRIVASTAVA RK, CHANDRA R (eds) *Magmatism in Relation to Diverse Tectonic Settings*. Oxford and IBH Publishing Co., New Delhi, pp 353–373
- KLEČKA M, MATĚJKA D, JALOVEC J, VAŇKOVÁ V (1991) Geochemical research of a granitoid group of the Eisgarn type in the S part of the Central Massif of the Moldanubian Pluton. *Zpr geol výzk v roce 1989*, 109–111 (in Czech)
- KOŠLER J, KELLEY SP, VRÁNA S (2001) $^{40}\text{Ar}/^{39}\text{Ar}$ hornblende dating of a microgranodiorite dyke: implications for early Permian extension in the Moldanubian Zone of the Bohemian Massif. *Int J Earth Sci (Geol Rundsch)* 90: 379–385
- MALAVIELLE J (1993) Late orogenic extension in mountain belts: insights from the Basin and Ranges and the Late Paleozoic Variscan Belt. *Tectonics* 12: 1115–1130
- MATĚJKA D (1991) *Geochemical and Petrological Characteristics of Rocks of the Moldanubian Zone South of Veselí nad Lužnicí: A Relationship Between the Ševětín Granodiorite and Rocks of The Eisgarn Type*. Unpublished Ph.D. thesis, Charles University, Prague, pp 1–148 (in Czech)
- MATĚJKA D, JANOUŠEK V (1998) Whole-rock geochemistry and petrogenesis of granites from the northern part of the Moldanubian Batholith (Czech Republic). *Acta Univ Carol, Geol* 42: 73–79
- MATĚJKA D, NOSEK T, RENÉ M (2003) Petrogenesis of two-mica granites of the Ševětín Massif. *Mitt Österr Miner Ges* 148: 359–371
- MATTE P, MALUSKI H, ECHTLER H (1985) Variscan eastward ductile shearing in the Waldviertel nappes (South eastern Bohemian Massif, Austria) – $^{39}\text{Ar}/^{40}\text{Ar}$ data. *Compt Rend Acad Sci serie II* 301: 721–726
- MEDARIS LG, WANG H, JELÍNEK E, MIHALJEVIČ M, JAKEŠ P (2005) Characteristics and origins of diverse Variscan peridotites in the Gföhl Nappe, Bohemian Massif, Czech Republic. *Lithos* 82: 1–23
- NAGATA T (1961) *Rock Magnetism*. Maruzen, Tokyo, pp 1–350
- RACEK M, ŠTÍPSKÁ P, PITRA P; SCHULMANN K, LEXA O (2006) Metamorphic record of burial and exhumation of orogenic lower and middle crust: a new tectonothermal model for the Drosendorf Window (Bohemian Massif, Austria). *Mineral Petrol* 86: 221–251
- RENÉ M, MATĚJKA D, KLEČKA M (1999) Petrogenesis of granites of the Klenov Massif. *Acta Montana* 113: 107–134
- ROCHETTE P, JACKSON MJ, AUBOURG C (1992) Rock magnetism and the interpretation of anisotropy of magnetic susceptibility. *Rev Geophys* 30: 209–226
- SCHULMANN K, LEXA O, JANOUŠEK V, LARDEAUX JM, EDEL JB (2014) Anatomy of a diffuse cryptic suture zone: an example from the Bohemian Massif, European Variscides. *Geology* 42: 275–278
- SUK M, DORNIČ J, HOKR Z, HOLÁSEK O, HOLUB V, LÍBALOVÁ J, ODEHNAL L, SATTRAN V, ŠALANSKÝ K, ZIMA K, ŽEBERA K (1978) Explanations to the general geological map of the ČSSR 1 : 25 000, sheet 22-444 Ševětín. Czech Geological Survey, Prague, pp 1–65 (in Czech)
- ŠALANSKÝ K (1981) Explanations to geophysical map 1 : 25 000, sheet 22-442 Dolní Bukovsko. Unpublished report, Geofyzika Brno, Prague, pp 1–16 (in Czech)
- VERNER K, ŽÁK J, ŠRÁMEK J, PAČLÍKOVÁ J, ZAVŘELOVÁ A, MACHEK M, FINGER F, JOHNSON K (2014) Formation of elongated granite–migmatite domes as isostatic accommodation structures in collisional orogens. *J Geodyn* 73: 100–117
- VRÁNA S (1987) The Ševětín astrobleme, southern Bohemia, Czechoslovakia. *Geol Rdsch* 76: 505–528
- VRÁNA S, BĀRTEK J (2005) Retrograde metamorphism in a regional shear zone and related chemical changes: the Kaplice Unit of muscovite–biotite gneisses in the Moldanubian Zone of southern Bohemia, Czech Republic. *J Czech Geol Soc* 50: 43–57
- VRÁNA S, JANOUŠEK V (2006) Late-orogenic Variscan magmatism: the case of quartz monzodiorite dykes from the Blanice Graben, southern Bohemia. *J Czech Geol Soc* 51: 231–248
- VRÁNA S, BENDL J, BUZEK F (1993) Pyroxene microgranodiorite dykes from the Ševětín structure, Czech Republic: mineralogical, chemical and isotopic indication of a possible impact melt origin. *J Czech Geol Soc* 38: 129–148
- VRÁNA S, SLABÝ J, BENDL J (2005) The Kaplice dyke swarm of biotite granodiorite porphyry and its relationship to the Freistadt granodiorite, Moldanubian Batholith. *J Czech Geol Soc* 50: 9–17
- WELSER P, ZIKEŠ J (2009) Minerals from the Ševětín quarry. *Minerál* 17: 326–334 (in Czech)
- ZACHARIÁŠ J, HÜBST Z (2012) Structural evolution of the Roudný gold deposit, Bohemian Massif: a combination of paleostress analysis and review of historical documents. *J Geosci* 57: 87–103
- ZACHARIÁŠ J, ŠTRBA M (2014, in print) Evolution of brittle deformations in the granite from the quarry at Ševětín near České Budějovice and their relationship to formation of Pb–Zn ores. *Sbor Jihočes Muz (Čes Budějovice), příř Vědy* 54: (in Czech)
- ZACHARIÁŠ J, FRÝDA J, PATEROVÁ B, MIHALJEVIČ M (2004) Arsenopyrite and As-bearing pyrite from the Roudný deposit, Bohemian Massif. *Mineral Mag* 68: 31–46
- ZACHARIÁŠ J, PATEROVÁ B, PUDILOVÁ M (2009) Mineralogy, fluid inclusion, and stable isotope constraints on the genesis of the Roudný Au–Ag deposit, Bohemian Massif. *Econ Geol* 104: 53–72
- ŽÁK J, VERNER K, FINGER F, FARYAD SW, CHLUPÁČOVÁ M, VESELOVSKÝ F (2011) The generation of voluminous S-type granites in the Moldanubian unit, Bohemian Massif, by rapid isothermal exhumation of the metapelitic middle crust. *Lithos* 121: 25–40
- ŽALOHAR J, VRABEC M (2007) Paleostress analysis of heterogeneous fault-slip data: the Gauss method. *J Struct Geol* 29: 1798–1810

A plate-kinematic model for the assembly of the Bohemian Massif constrained by structural relationships around granitoid plutons

JIRÍ ŽÁK^{1*}, KRYŠTOF VERNER^{2,3}, VOJTĚCH JANOUŠEK^{2,3}, FRANTIŠEK V. HOLUB³,
VÁCLAV KACHLÍK¹, FRITZ FINGER⁴, JAROSLAVA HAJNÁ¹, FILIP TOMEK¹,
LUKÁŠ VONDROVIC^{2,3} & JAKUB TRUBAČ^{1,2,3}

¹*Institute of Geology and Palaeontology, Faculty of Science, Charles University,
Albertov 6, Prague, 12843, Czech Republic*

²*Czech Geological Survey, Klárov 3, Prague, 11821, Czech Republic*

³*Institute of Petrology and Structural Geology, Faculty of Science, Charles University,
Albertov 6, Prague, 12843, Czech Republic*

⁴*Division of Mineralogy, University of Salzburg, Hellbrunnerstraße 34, A-5020 Salzburg, Austria*

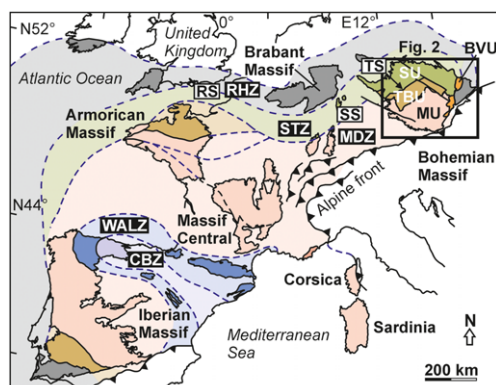
*Corresponding author (e-mail: jirizak@natur.cuni.cz)

Abstract: This paper summarizes the current knowledge on the nature, kinematics and timing of movement along major tectonic boundaries in the Bohemian Massif and demonstrates how the Variscan plutonism and deformation evolved in space and time. Four main episodes are recognized: (1) Late Devonian–early Carboniferous subduction and continental underthrusting of the Saxothuringian Unit beneath the Teplá–Barrandian Unit resulted in the orogen-perpendicular shortening and growth of an inboard magmatic arc during c. 354–346 Ma; (2) the subduction-driven shortening was replaced by collapse of the Teplá–Barrandian upper crust, exhumation of the high-grade (Moldanubian) core of the orogen at c. 346–337 Ma and by dextral strike-slip along orogen-perpendicular NW–SE shear zones; (3) following closure of a Rheohercynian Ocean basin, the Brunia microplate was underthrust beneath the eastern flank of the Saxothuringian/Teplá–Barrandian/Moldanubian ‘assemblage’; this process commenced at c. 346 Ma in the NE and ceased at c. 335 Ma in the SW; and (4) late readjustments within the amalgamated Bohemian Massif included crustal exhumation and mainly S-type granite plutonism along the edge of the Brunia indenter at c. 330–327 Ma, and peripheral tectonothermal activity driven by strike-slip faulting and possibly mantle delamination around the consolidated Bohemian Massif’s interior until late Carboniferous–earliest Permian times.

The Bohemian Massif of central Europe is the largest inlier of the once-continuous but now largely dismembered Ouachita–Appalachian–Variscan orogenic belt (Fig. 1) that formed during the Devonian–Carboniferous closure of the Rheic Ocean and other small oceanic domains by convergence of the Gondwana and Laurussia supercontinents (e.g. Franke 1989; Pin 1990; Matte 2001; Winchester 2002; Winchester *et al.* 2006; Ballèvre *et al.* 2009; Faure *et al.* 2009; Edel *et al.* 2013; Faryad & Kachlík 2013; Kroner & Romer 2013). A characteristic feature of the Variscan Orogeny was the involvement of multiple microplates of Cadomian or Avalonian affinity that were partially extended or entirely detached from the northern margin of Gondwana during late Cambrian–Early Ordovician times (e.g. Pin & Marini 1993; Franke 2000; Matte 2001; Murphy & Nance 2002; Nance & Linnemann 2008; von Raumer & Stampfli 2008; Nance *et al.* 2010, 2012). These microplates were then stuck in a broad collision zone between

Gondwana and Laurussia as the two supercontinents converged, resulting in multiple subduction, accretion and collision events along the margins of the neighbouring microplates.

This style of orogeny is greatly exemplified in the Bohemian Massif, which is a mosaic consisting of several lithotectonic units (Figs 1 & 2). The timing and kinematics of their amalgamation and further development during the Variscan Orogeny have been vigorously debated and summarized in several plate-tectonic reconstructions (e.g. Matte 1986, 1991, 2001; Franke 1989, 2006; Pharaoh 1999; Pitra *et al.* 1999; Franke & Żelaźniewicz 2002; Winchester 2002; Edel *et al.* 2003; Finger *et al.* 2007; Schulmann *et al.* 2009; Kroner & Romer 2013). This short contribution is not meant as a comprehensive review, but rather focuses on granitoid and syenitoid plutons as temporal and strain markers of regional deformation. We utilize modern structural data in combination with geochronology, mainly U–Pb dating on zircon. Below



EUROPEAN VARISCIDES

Tectonic zones

RHZ Rhenohercynian Zone

STZ Saxothuringian Zone

MDZ Moldanubian Zone

WALZ West Asturian–Leonese Zone

CBZ Cantabrian Zone

Principal sutures

RS Rheic suture

SS Saxothuringian suture

TS Teplá suture (continuation of Saxothuringian suture)

Lithotectonic units in the Bohemian Massif

SU Saxothuringian Unit

TBU Teplá–Barrandian Unit

MU Moldanubian Unit

BVU Brunovistulian Unit and other Neoproterozoic terranes of Avalonian affinity in tectonic windows

Fig. 1. Overview geological map showing basement outcrop areas and principal lithotectonic zones and sutures of the Variscan orogenic belt in Europe. The Bohemian Massif is the easternmost inlier of the orogen. Compiled from Winchester (2002), Asch (2003) and Martínez Catalán (2011, 2012).

we first briefly describe the principal lithotectonic units in the interior of the Bohemian Massif and then comment on the nature, kinematics and timing of movements along their boundaries. Based on these datasets, we propose a plate-tectonic model and outline some relevant open questions and possible directions for future research.

Major lithotectonic units in the interior of the Bohemian Massif

Saxothuringian Unit

The northerly and northwesterly Saxothuringian Unit (Fig. 2) consists of late Neoproterozoic volcano-sedimentary successions, interpreted as a back-arc and retro-arc system of the Cadomian orogen, intruded by a voluminous late Neoproterozoic–early Cambrian granitoid plutonic complex (the Lusitan Massif, LM in Fig. 2; Kröner *et al.* 1994, 1995; Linnemann & Romer 2002; Linnemann *et al.* 2000, 2004, 2008; Tichomirowa *et al.* 2012). The Cadomian basement is overlain unconformably by Lower Palaeozoic volcano-sedimentary passive-margin successions (Buschmann *et al.* 2006); both

units host orthogneisses and bimodal metavolcanic rocks of chiefly Cambro-Ordovician and Late Devonian–early Carboniferous protolith ages (Patočka & Smulikowski 2000; Kröner *et al.* 2001; Oberc-Dziedzic *et al.* 2005a, b; Nowak *et al.* 2011). This Neoproterozoic–Early Palaeozoic package was affected by Variscan subduction-related high-pressure–low temperature (HP/LT) greenschist/blueschist to (U)HP/HT metamorphism and was then strongly reworked during nappe stacking and extensional unroofing under MP/MT to greenschist-facies conditions. The latter process was associated with, and followed by, strike-slip movements along major NW–SE-trending faults (Aleksandrowski *et al.* 1997; Marheine *et al.* 2002; Mazur *et al.* 2006). Importantly, relics of blueschist-facies rocks with cooling ages constrained at c. 360 Ma (Cháb & Vrána 1979; Smulikowski 1995; Maluski & Patočka 1997; Marheine *et al.* 2002; Faryad & Kachlík 2013; cf. Žáčková *et al.* 2010), together with diamond-bearing metasedimentary rocks and granulites, delineate the margins of the Saxothuringian Unit (Behr *et al.* 1982; Schmädicke 1991; Schäfer *et al.* 1997; Willner *et al.* 1997, 2002; Kröner & Willner 1998; Kröner *et al.* 1998; Massonne 2001; Mueller & Massonne 2001; Rötzer & Romer 2001; O'Brien & Rötzer 2003; Konopásek & Schulmann 2005; Schmädicke *et al.* 2010; Kotková *et al.* 2011). Indeed, the Saxothuringian Unit has been regarded as a separate collage of terranes in the framework of the Bohemian Massif (e.g. Cymerman *et al.* 1997; Żelaźniewicz 1997; Mazur *et al.* 2006), although uncertainty exists as to how far it travelled from, or whether it remained attached to, the northern margin of Gondwana during the early Palaeozoic Era (Linnemann *et al.* 2004).

During the waning stages of the Variscan Orogeny (c. 330–305 Ma; Fig. 3), the Saxothuringian Unit was intruded by a number of granite plutons of diverse geochemical composition ranging from I-types (e.g. main portion of the Krkonoše–Jizera Plutonic Complex, KJPC in Fig. 2; Słaby & Martin 2008) to strongly peraluminous S- and A-types bearing Sn–W mineralization (most granite units in the Krušné hory/Erzgebirge; Fig. 2; see Förster *et al.* 1999; Štemprok *et al.* 2003; Förster & Romer 2010; Breiter 2012 for reviews). The plutons continue to the SW and cross-cut boundaries between lithotectonic units with no apparent change in composition or age (e.g. Northern Oberpfalz, NOP; Figs 2 & 3).

Teplá–Barrandian Unit

The upper-crustal Teplá–Barrandian Unit in the centre of the Bohemian Massif (Fig. 2) occupies the hanging-wall position with respect to the

neighbouring Saxothuringian and Moldanubian units and is thus the overriding plate for all the hypothetical subduction zones. Moreover, a large central portion of this unit has never been buried to great depths and has therefore escaped the Variscan pervasive metamorphism and ductile deformation (Suchý *et al.* 1996, 2007; Hajná *et al.* 2010, 2011, 2012).

The Teplá–Barrandian Unit consists of generally low-grade Neoproterozoic basement intruded by Cambro-Ordovician plutons and is overlain unconformably by the lower Palaeozoic (lower Cambrian–middle Givetian) passive-margin volcano-sedimentary successions (Fig. 2; Zulauf 1997b; Chlupáč *et al.* 1998; Dörr *et al.* 1998, 2002; Hajná *et al.* 2010, 2011). The largest part of the Teplá–Barrandian Neoproterozoic basement to the south, west and NW of the Lower Palaeozoic overlap successions was interpreted as a Cadomian accretionary wedge with a related volcanic arc preserved along the southeastern flank of the unit, albeit severely reworked by Variscan deformation (Waldhausrová 1984; Sláma *et al.* 2008a; Hajná *et al.* 2010, 2011). Small remnants of Cadomian intra- and back-arc basins also occur close to the Teplá–Barrandian/Moldanubian boundary (Sláma *et al.* 2008a; Hajná *et al.* 2010, 2011).

There are three important features associated with the Teplá–Barrandian Unit. First, as inferred from seismic anisotropy by Babuška & Plomerová (1992, 2001, 2013), Plomerová *et al.* (2005) and Babuška *et al.* (2008, 2010), the Teplá–Barrandian mantle lithosphere exhibits olivine fabric different from that of the neighbouring Saxothuringian and Moldanubian units, perhaps being inherited from the Cadomian accretion and subduction.

Second, its northwestern tip structurally overlies the Mariánské Lázně meta-ophiolite complex (MLC in Fig. 2) which exhibits the earliest Cambrian (*c.* 540 Ma) and Early Ordovician (*c.* 480 Ma) protolith ages (Bowes & Aftalion 1991; Timmermann *et al.* 2004), interpreted as recording attachment of oceanic lithosphere and rifting of the ‘proto-Teplá–Barrandian’ margin, respectively (Timmermann *et al.* 2004; Sláma *et al.* 2008a). The Late Devonian ages (*c.* 380 Ma) in the complex then constrain its Variscan subduction-related eclogite-facies metamorphism (Beard *et al.* 1995; Zulauf 1997b). Taken together, the present-day northwestern margin of the Teplá–Barrandian Unit must have acted repeatedly as an active plate margin with subduction of oceanic crust during both the Cadomian and Variscan orogenies (e.g. Zulauf 1997b; Dörr *et al.* 2002; Dörr & Zulauf 2010).

Third, the Teplá–Barrandian upper crust was intruded by a number of Late Devonian–early Carboniferous calc-alkaline granitoid plutons (Figs 2 & 3) that bear a distinctive geochemical imprint

of subduction (Palivcová 1984; Janoušek *et al.* 1995, 2000, 2004a, 2006; Holub *et al.* 1997b; Verner *et al.* 2009a; Vondrovic *et al.* 2011) and reveal a consistent spatial–temporal–compositional trend (Žák *et al.* 2011a). The earliest Late Devonian (*c.* 375–373 Ma) Čistá and Štěnovice plutons occupy the centre (ČP and ŠP in Fig. 2; Klomínský 1963, 1965; Kopecký *et al.* 1997; Venera *et al.* 2000; Žák *et al.* 2011a) whereas the early Carboniferous (*c.* 354–337 Ma) plutons form a large continental magmatic arc along the southeastern flank of the Teplá–Barrandian Unit (the Central Bohemian Plutonic Complex, CBPC in Fig. 2; Holub *et al.* 1997a, b; Dörr *et al.* 1998; Janoušek *et al.* 2004a, 2010; Dörr & Zulauf 2010). The arc itself shows internal compositional zoning from the older *c.* 354 Ma calc-alkaline intrusions to the north and NW through *c.* 346 Ma high-K calc-alkaline in the centre to *c.* 343–337 Ma ultrapotassic plutons along its southeastern margin (Fig. 2; Janoušek *et al.* 1995; Holub *et al.* 1997a, b; Žák *et al.* 2005a). The exception are the Late Devonian Mirovice and Staré Sedlo orthogneisses (MC and SSC in Fig. 2; *c.* 380–365 Ma; Košler *et al.* 1993) which also exhibit calc-alkaline arc-related geochemical signature (Košler & Farrow 1994) but occur in the roof of the central part of the plutonic complex (Fig. 2). They were deformed prior to emplacement of at least 20 myr younger high-K calc-alkaline and even younger ultrapotassic plutons. Interestingly, dismembered and reworked parts of comparable arc-related rocks can also be found in the Moldanubian Unit (the Lišov granulite, LI in Fig. 2; Janoušek *et al.* 2006).

The Moldanubian Unit

In contrast to the above, the Moldanubian Unit *s.s.* (Fig. 2; considered here without the metamorphic complexes along its northeastern margin; Pertoldová *et al.* 2010) is deeply eroded middle–lower crust characterized by a complex Variscan tectono-metamorphic history (e.g. Vrána *et al.* 1995; Finger *et al.* 2007; Faryad *et al.* 2010; Franěk *et al.* 2011). It has recently been interpreted as representing an orogenic root (Schulmann *et al.* 2005, 2008, 2009). Except for rare Palaeoproterozoic (*c.* 2.1 Ga) meta-igneous rocks (Wendt *et al.* 1993), large portions of the Moldanubian Unit have Neoproterozoic–early Palaeozoic igneous and siliciclastic protoliths, the latter now represented by the LP/HT commonly sillimanite- and cordierite-bearing and migmatitic biotite paragneisses (‘the Monotonous Series’). On the other hand, other meta-sedimentary complexes contain abundant lenses of marble, amphibolite and quartzite (‘the Variegated Series’; Fuchs & Matura 1976; Kröner *et al.* 1988; Fiala *et al.* 1995; Linner 1996) and are, at least partly, Early Palaeozoic in

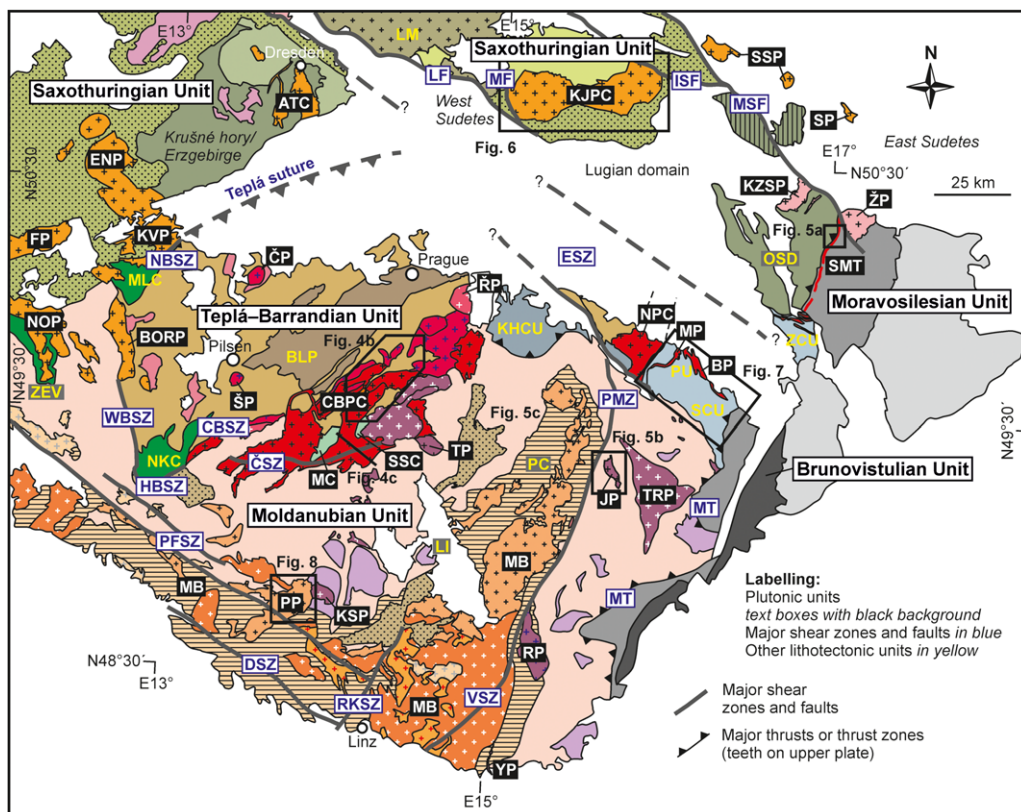









Fig. 2. Greatly simplified geological map of the interior Bohemian Massif emphasizing geological units and tectonic features discussed in the text. Compiled from Fusán *et al.* (1967) and Cháb *et al.* (2007). Plutonic units: ATC, Altenberg–Teplice caldera; BOPR, Bor Pluton; BP, Budislav Pluton; CBPC, Central Bohemian Plutonic Complex; ČP, Čistá Pluton; ENP, Eibenstock–Nejdek Pluton; FP, Fichtelgebirge (Srnčiny) Pluton; JP, Jihlava Pluton; KJPC, Krkonoše–Jizera Plutonic Complex; KSP, Knížecí Stolec Pluton; KVP, Karlovy Vary Pluton; KZSP, Kłodzko–Złoty Stok Pluton; MB, Moldanubian Batholith; MC, Mirotice Complex; MP, Mířetín Pluton; NOP, Northern Oberpfalz Pluton; NPC, Nasavrky Plutonic Complex; PP, Plechý Pluton; RP, Rastenberg Pluton; ŘP, Říčany Pluton; SMT, Staré Město tonalite sill; SP, Strzelín Pluton; ŠP, Štěnovice Pluton; SSC, Staré Sedlo Complex; SSP, Strzegom–Sobótka Pluton; TP, Tábor Pluton; TRP, Třebíč Pluton; YP, Ybbs Pluton; ŽP, Žulová Pluton. Shear zones and faults: CBSZ, Central Bohemian Shear Zone; ČSZ, Červená Shear Zone; DSZ, Danube Shear Zone; ESZ, Elbe Shear Zone; HBSZ, Hoher Bogen Shear Zone; ISF, Intra-Sudetic Fault; LF, Lusatian Fault; MF, Machnín Fault; MSF, Marginal-Sudetic Fault; MT, Moldanubian thrust; NBSZ, North Bohemian Shear Zone; PFSZ, Pfahl Shear Zone; PMZ, Příbyslav Mylonite Zone; RKSZ, Rodl–Kaplice Shear Zone; VSZ, Vitis Shear Zone; WBSZ, West Bohemian Shear Zone. Other geological units: BLP, Barrandian Lower Palaeozoic successions; KHCU, Kutná Hora Crystalline Unit; LI, Lišov granulite; LM, Lusatian Massif; MLC, Mariánské Lázně Complex; NKC, Neukirchen–Kdyně Complex; OSD, Orlica–Sněžník Dome; PC, Pelhřimov Complex; PU, Polička Crystalline Unit; SCU, Svatka Crystalline Unit; ZEV, Erbendorf–Vohenstrauß Zone; ZCU, Zábřeh Crystalline Unit.

age (Janoušek *et al.* 2008). The Moldanubian Unit also contains intercalations and relics of Neoproterozoic and Cambro-Ordovician orthogneisses (e.g. Friedl *et al.* 2004) as well as (U)HP eclogite-to granulite-facies and mantle rocks (Becker & Altherr 1992; Becker 1997; Kotková *et al.* 1997; Vrána & Frýda 2003; Nakamura *et al.* 2004; Medaris *et al.* 2005, 2006; Naemura *et al.* 2009, 2011). Together with various types of migmatites







and migmatized granite gneisses, these rocks have been collectively termed ‘the Gföhl assemblage’ (see Petrakakis 1997; Franke 2000; Finger *et al.* 2007; Faryad 2011 for detailed reviews and terminology) and interpreted in previous studies as parts of a single nappe (‘the Gföhl nappe’; e.g. Tollmann 1982, 1995; Franke 1999, 2006). This view has been challenged in favour of vertical ‘forceful’ exhumation along separate channel-like domains in

KEY

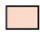



Saxothuringian Unit

-  Neoproterozoic to Lower Palaeozoic metasedimentary and metaigneous rocks with Variscan greenschist facies overprint and relics of HP–LT blueschist facies rocks
-  Neoproterozoic basement with MP–MT Variscan overprint
-  Neoproterozoic to lower Cambrian granitoids
-  Upper Cambrian to Lower Ordovician (meta-)granitoids and orthogneisses
-  High-grade units with (U)HP rocks with tectonically intercalated relics of HP–LT rocks re-equilibrated under greenschist to amphibolite facies conditions
-  High-grade rocks in Góry Sowie (migmatite, minor granulite and garnet peridotite inclusions)
-  Granulites and associated (U)HP rocks



Teplá–Barrandian Unit

-  Neoproterozoic to lower Cambrian volcano-sedimentary successions,
-  Neoproterozoic and Lower Palaeozoic rocks in roof pendants of Variscan plutons, and comparable rocks along the northeastern margin of the Moldanubian Unit (undivided)
-  Neoproterozoic to Cambro–Ordovician basic to ultrabasic (meta-)igneous rocks
-  Cambrian granitoids and orthogneisses
-  Lower Palaeozoic volcano-sedimentary overlap successions
-  Upper Devonian orthogneisses in roof pendants




Moldanubian Unit

-  Heterogeneous assemblages dominated by paragneisses and migmatites with minor bodies of orthogneisses, marble, amphibolite, quartzite, and eclogite (Monotonous and Variegated "Series", Gföhl assemblage, undivided)
-  Mica schists and retrogressed rocks
-  Major bodies of granulites and associated (U)HP rocks including mantle peridotites and eclogites
-  Migmatites in association with granite plutons

Metamorphic complexes along the northeastern margin of the Moldanubian Unit


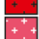

-  Orthogneisses and mica schists with (U)HP rocks
-  Low-grade to medium-grade metamorphic rocks

Moravosilesian and Brunovistulian units




-  Neoproterozoic basement (Brunia)
-  Moravian Zone (strongly reworked and imbricated Neoproterozoic basement with inverted Variscan metamorphic zonation)
-  Devonian pre-flysch succession and Upper Devonian to Lower Carboniferous siliciclastic sedimentary rocks (Variscan flysch)

VARISCAN PLUTONIC ROCKS

Early-orogenic (syn-collisional) arc-related granitoids


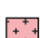
-  Medium-K calc-alkaline Sázava suite and related rocks
-  High-K calc-alkaline Blatná suite and related rocks
-  Other suites (undifferentiated)

(Ultra-)potassic melasyenitoids and melagranitoids

-  Melasyenites to melagranites (durbachite suite)
-  Two-pyroxene melasyenites
-  Granodiorites, melagranites, quartz monzonites, quartz diorites

Late-orogenic (post-collisional) "peripheral" granitoids

Saxothuringian granitoids and plutons in the East Sudetes

-  Various biotite and two-mica granites, commonly porphyritic, minor diorites to granodiorites (redwitzites)
-  Compositionally diverse intrusions including granodiorite (dominant), tonalite, syenite, and diorite

Moldanubian Batholith





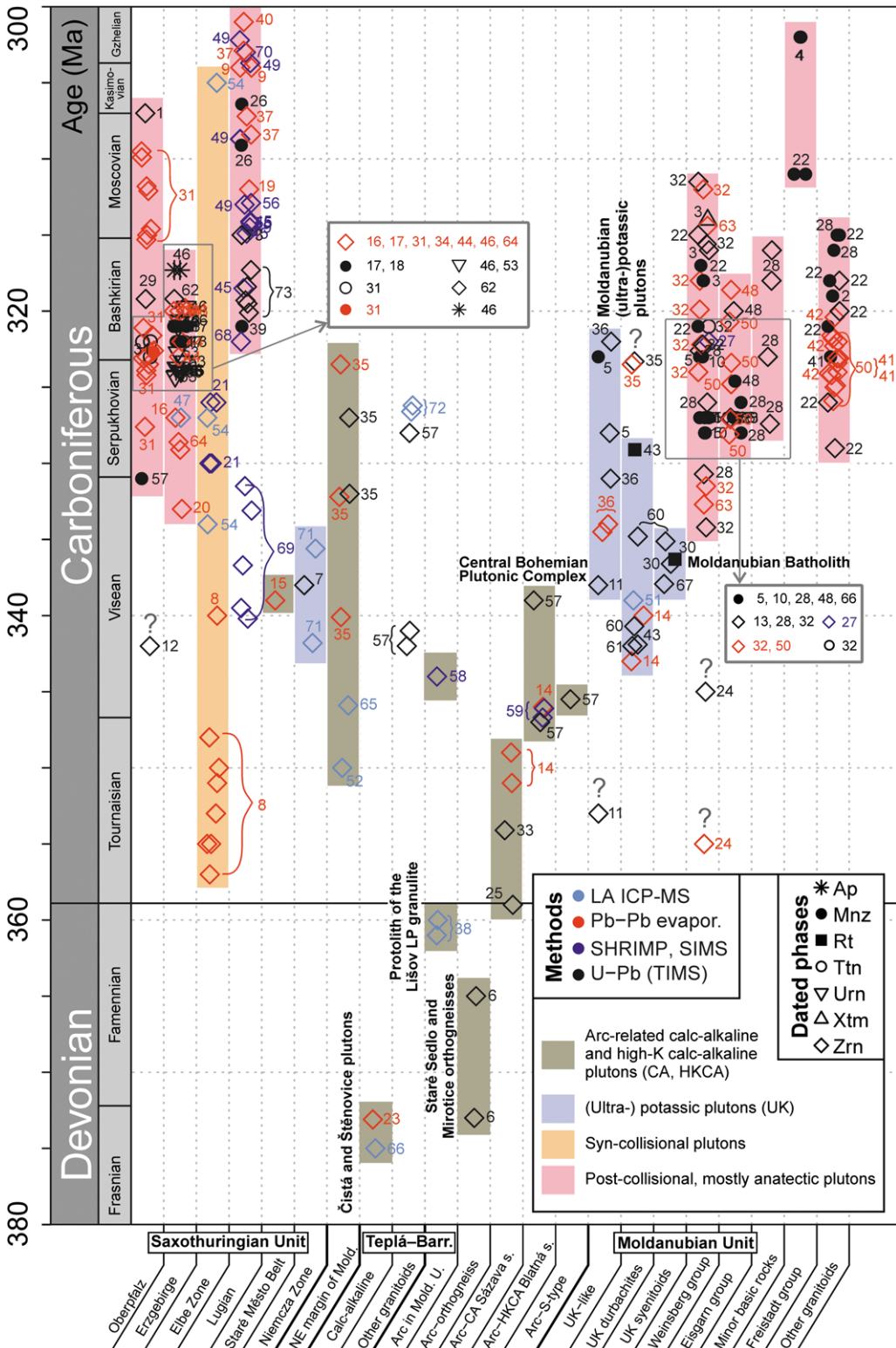
-  "Weinsberg" granite
-  "Eisgarn" granite
-  Freistadt granodiorite
-  Other granitoids (undivided)

Fig. 2. Continued.

response to buoyancy forces and crustal shortening (Franěk *et al.* 2006, 2011; Maierová *et al.* 2012). Although exceptions do occur, the inferred ages of the granulite-facies metamorphism concentrate at *c.* 340 Ma throughout the Moldanubian Unit (van Breemen *et al.* 1982; Aftalion *et al.* 1989; Wendt *et al.* 1994; Kröner *et al.* 2000; Janoušek *et al.* 2006; Kotková 2007; Sláma *et al.* 2008*b*; Tajčmanová *et al.* 2010; Friedl *et al.* 2011). Latest findings point, however, to a more complex pre-340 Ma burial and exhumation history of the (U)HP rocks within the Moldanubian Unit (Prince *et al.* 2000; Faryad *et al.* 2009, 2010, 2013; Friedl *et al.* 2011).

The Moldanubian Unit hosts several plutonic suites (Figs 2 & 3). An older, rather specific one is

represented by ultrapotassic melagranitoids to melasyenitoids ('durbachites' and related rocks) with U–Pb zircon ages ranging from *c.* 343 to *c.* 335 Ma (Holub 1997; Holub *et al.* 1997*a*, 2012; Janoušek & Gerdes 2003; Janoušek & Holub 2007; Verner *et al.* 2008; Kotková *et al.* 2010; Kusiak *et al.* 2010). The 'durbachites' also intruded the upper-crustal rocks along the southeastern flank of the Teplá–Barrandian Unit and the high-K calc-alkaline granitoids of the Central Bohemian Plutonic Complex (Fig. 2). Recent petrogenetic interpretations suggest that the primary (ultra-)potassic magmas were derived from anomalous lithospheric mantle strongly enriched in large ion lithophile elements (LILE) and light rare earth elements (LREE) and subsequently mixed with



anatctic melts (Janoušek *et al.* 1995, 2000; Holub 1997; Wenzel *et al.* 1997; Becker *et al.* 1999; Gerdes *et al.* 2000a; von Raumer *et al.* 2013). Furthermore, Janoušek & Holub (2007) and Lexa *et al.* (2011) explained the temporal and spatial link between the ultrapotassic plutons and HP granulites (Fig. 2) as a result of contamination of the local mantle by subducted/re-laminated Ordovician felsic meta-igneous rocks of Saxothuringian provenance, the presumed protolith to the Moldanubian granulites (Janoušek *et al.* 2004b).

The other suites of crustally derived granitoids include coarse-grained I- to S-type K-feldsparphyric biotite granites dated at *c.* 331–323 Ma ('the Weinsberg granite'; Figs 2 & 3) and peraluminous S-type two-mica granites dated at *c.* 330–327 Ma ('the Eisgarn granite'; Fig. 2; U–Pb zircon ages according to Gerdes *et al.* 2003). Together with intrusions of the Freistadt biotite granodiorite (Figs 2 & 3), late highly fractionated granites and minor basic bodies, these two suites compose the Moldanubian Batholith (MB in Fig. 2), the largest plutonic body in the entire Variscan belt (Liew *et al.* 1989; Vellmer & Wedepohl 1994; Holub *et al.* 1995; Klečka & Matějka 1996; Klötzli & Parrish 1996; Finger *et al.* 1997, 2009; Gerdes *et al.* 2000a, b, 2003; Gerdes 2001; Klötzli *et al.* 2001; Breiter 2010; Žák *et al.* 2011b). In the map view, the individual intrusive units of the batholith are clustered in two nearly perpendicular segments oriented *c.* WNW–ESE and *c.* NNE–SSW (Fig. 2). The former is defined by a number of separate smaller plutons that involve both 'Eisgarn' and 'Weinsberg' granites whereas the latter, hosted by a complex of cordierite-bearing migmatites and migmatized paragneisses, is chiefly made up of the 'Eisgarn granite' (the Pelhřimov Complex, PC in Fig. 2; Žák *et al.* 2011b).

Brunovistulian Unit

In contrast to the above units that share the Cadomian or 'West African' affinity (e.g. Drost *et al.* 2004; Linnemann *et al.* 2004; Drost *et al.* 2011), the Brunovistulian Unit (Fig. 2; 'Brunia') underlying the eastern margin of the Bohemian Massif is an exotic terrane of problematic provenance more akin to Avalonia (Friedl *et al.* 2000; Kalvoda *et al.* 2008). Its pre-Variscan evolution was therefore rather different from that of the remainder of the Bohemian Massif and involved late Neoproterozoic terrane accretion followed by extensive post-collisional plutonism at *c.* 595–585 Ma and deposition of Neoproterozoic–early Palaeozoic successions on to the welded terranes (van Breemen *et al.* 1982; Dudek 1980; Finger *et al.* 1989, 2000a, b; Jelínek & Dudek 1993; Finger & Steyrer 1995; Fritz *et al.* 1996; Schulmann & Gayer 2000; Leichmann & Höck 2008).

Key observations on the nature, timing and kinematics along major tectonic boundaries in the Bohemian Massif and their relation to granitoid plutonism

Orogen-parallel NE–SW-trending boundaries

The Teplá suture. The Saxothuringian/Teplá–Barandian boundary, referred to as the Teplá suture (TS in Fig. 1), is in fact a broad zone consisting of an imbricated stack of NW-directed nappes. It involves portions of both subducted oceanic lithosphere and crust from the overriding margin of the

Fig. 3. Overview of the U–Pb and Pb/Pb ages from Late Devonian–late Carboniferous plutonic rocks of the Bohemian Massif. The stratigraphic table is based on International Stratigraphic Chart, version 2013/1 (<http://www.stratigraphy.org/ICSChart/ChronostratChart2013-01.pdf>). Mineral abbreviations after Kretz (1983). References: 1, Wendt *et al.* (1986); 2, Frasl & Finger (1991); 3, von Quadt & Finger (1991); 4, Friedl *et al.* (1992); 5, Friedl *et al.* (1993); 6, Košler *et al.* (1993); 7, Oliver *et al.* (1993); 8, Wenzel *et al.* (1993); 9, Kröner *et al.* (1994); 10, Friedl *et al.* (1996); 11, Klötzli & Parrish (1996); 12, Köhler & Hölzl (1996); 13, Finger *et al.* (1997); 14, Holub *et al.* (1997a); 15, Parry *et al.* (1997); 16, Tichomirowa (1997); 17, Förster (1998); 18, Förster *et al.* (2009); 19, Hammer *et al.* (1999); 20, Kempe *et al.* (1999); 21, Nasdala *et al.* (1999); 22, Propach *et al.* (2000); 23, Venera *et al.* (2000); 24, Klötzli *et al.* (2001); 25, Bues *et al.* (2002); 26, Turniak & Bröcker (2002); 27, Finger *et al.* (2003); 28, Gerdes *et al.* (2003); 29, Chen *et al.* (2003); 30, Janoušek & Gerdes (2003); 31, Siebel *et al.* (2003); 32, Chen & Siebel (2004); 33, Janoušek *et al.* (2004a); 34, Kempe *et al.* (2004); 35, Schulmann *et al.* (2005); 36, Siebel *et al.* (2005); 37, Turniak *et al.* (2005); 38, Janoušek *et al.* (2006); 39, Klomínský *et al.* (2007); 40, Turniak *et al.* (2006); 41, Siebel *et al.* (2006a); 42, Siebel *et al.* (2006b); 43, Kotková *et al.* (2007); 44, Kovaříková *et al.* (2007); 45, Machowiak & Armstrong (2007); 46, Romer *et al.* (2007); 47, Hofmann *et al.* (2008); 48, Klein *et al.* (2008); 49, Kusiak *et al.* (2008); 50, Siebel *et al.* (2008); 51, unpublished data cited in Verner *et al.* (2008); 52, Vondrovic & Verner (2008); 53, Förster *et al.* (2009); 54, Hofmann *et al.* (2009); 55, Kusiak *et al.* (2009); 56, Awdankiewicz *et al.* (2010); 57, Dörr & Zulauf (2010); 58, Finger *et al.* (2010); 59, Janoušek *et al.* (2010); 60, Kotková *et al.* (2010); 61, Kusiak *et al.* (2010); 62, Romer *et al.* (2010); 63, Siebel *et al.* (2010); 64, Tichomirowa & Leonhardt (2010); 65, Vondrovic *et al.* (2011); 66, Žák *et al.* (2011a); 67, Holub *et al.* (2012); 68, Kryza *et al.* (2012); 69, Mikulski *et al.* (2013); 70, Oberc-Dziedzic *et al.* (2013); 71, Pietranik *et al.* (2013); 72, Trubač *et al.* (2013); 73, Žák *et al.* (2013).

Teplá–Barrandian Unit that were exhumed from the suture and thrust over the Saxothuringian foreland (Fig. 2; Behr *et al.* 1982; Franke 1989; Kachlík 1993; Schäfer *et al.* 1997; Mazur & Alexandrowski 2001). Relics of these nappes also extend as a series of klippen further to the west and NW (Erbendorf–Vohenstrauss Zone, ZEV in Fig. 2, Münchberg, Frankenbergr and Wildenfels nappes). The suture formed initially by SE-directed subduction and closure of the Saxothuringian Ocean, welding the Saxothuringian and Teplá–Barrandian units at *c.* 380 Ma (Franke 1989; Beard *et al.* 1995; Schäfer *et al.* 1997; Zulauf 1997*b*). As proposed by O'Brien (2000), Janoušek *et al.* (2004*b*), Konopásek & Schulmann (2005), Janoušek & Holub (2007) and Lexa *et al.* (2011), the Saxothuringian subduction continued in continental underthrusting until *c.* 340 Ma; its waning stages therefore broadly overlapped with the onset of normal movements and collapse of the Teplá–Barrandian Unit at *c.* 346 Ma (Zulauf 1994; Scheuvens & Zulauf 2000; Zulauf *et al.* 2002; Žák *et al.* 2005*a*; Dörr & Zulauf 2010; Janoušek *et al.* 2010).

In detail, recent structural work suggests that the deformation resulting from the Saxothuringian/Teplá–Barrandian convergence was rather complex in the overriding Teplá–Barrandian plate (Fig. 4). The deformation was partitioned into pure shear-dominated domains that accommodated orogen-perpendicular WNW–ESE shortening alternating with narrow orogen-parallel high-strain zones that recorded dextral transpression or lateral extrusion (Fig. 4*a*; Hajná *et al.* 2012). The orogen-parallel zones were localized along pre-existing lithological boundaries or in the softened thermal aureoles of the arc plutons (Fig. 4*b*; Žák *et al.* 2005*b*; Macheck *et al.* 2009; Hajná *et al.* 2012). As with the arc-related plutonism, these zones indicate younging of deformation in the overriding Teplá–Barrandian plate from *c.* 370–380 in the NW to *c.* 346 Ma in the SE (Hajná *et al.* 2011; Žák *et al.* 2011*a*).

The Teplá–Barrandian/Moldanubian boundary.

This boundary (variously referred to as 'the Central Bohemian suture', 'Central Bohemian Shear Zone' or 'Gföhl suture') is one of the most intriguing tectonic features of the Bohemian Massif, unique in that every possible sense of movement was invoked to explain its kinematic evolution (Tollmann 1982; Rajlich 1987, 1988; Matte *et al.* 1990; Košler *et al.* 1995; Pitra *et al.* 1999; Franke 2000; Scheuvens & Zulauf 2000; Franke & Żelaźniewicz 2002; Medaris *et al.* 2005; Žák *et al.* 2005*a, b*, 2009*a*, 2012; Dörr & Zulauf 2010).

The earliest record of the Variscan Orogeny along the Teplá–Barrandian/Moldanubian boundary is preserved in the Lower–Middle Devonian siliciclastic successions (Chlupáč 1989) and in the

Late Devonian (*c.* 380–365 Ma) Mirovice and Staré Sedlo orthogneisses (Figs 2 & 3). The latter meta-granitoids are sheeted, exhibit subhorizontal intrusive contacts, flat-lying solid-state foliation and NE–SW subhorizontal stretching lineation and are commonly characterized by a prolate fabric ellipsoid (Tomek 2011; Tomek & Žák 2011). A different structural pattern is observed in the earliest *c.* 354 Ma calc-alkaline intrusions (Sázava suite) of the Central Bohemian Plutonic Complex, which were syntectonic with partitioned regional dextral transpression characterized by the WNW–ESE arc-perpendicular shortening and arc-parallel horizontal stretching (Fig. 4*b*; Žák *et al.* 2005*a, b*, 2009*a*; Hajná *et al.* 2012). This transpressive deformation lasted until *c.* 346 Ma when it was replaced by ductile normal shearing along the Červená Shear Zone (ČSZ in Fig. 2) associated with exhumation of the high-grade core of the orogen, the Moldanubian Unit (Fig. 4*c*; Holub *et al.* 1997*b*; Žák *et al.* 2005*a*, 2012; Janoušek *et al.* 2010). The cessation of ductile deformation along the Teplá–Barrandian/Moldanubian boundary is bracketed by the *c.* 336 Ma post-tectonic Říčany Pluton in the NE (ŘP in Fig. 2; Janoušek *et al.* 1997; Trubač *et al.* 2009) and by undeformed melasyenites including *c.* 338 Ma dykes (Holub *et al.* 2012) and *c.* 337 Ma Tábor Pluton (TP in Fig. 2) that intruded discordantly the Moldanubian gneisses to the SE of the shear zone (Janoušek & Gerdes 2003; Žák *et al.* 2005*a*).

The Moldanubian thrust system. Along the eastern margin of the Bohemian Massif, the Moldanubian Unit has been thrust over the Brunia microplate (MT in Fig. 2; e.g. Suess 1912; Dudek 1980; Schulmann *et al.* 1991, 2005, 2008; Fritz & Neubauer 1993; Štípská & Schulmann 1995; Fritz *et al.* 1996; Racek *et al.* 2006; Finger *et al.* 2007; Kalvoda *et al.* 2008). The highly oblique top-to-the-NNE Saxothuringian–Moldanubian/Brunia collision presumably commenced prior to 346 Ma in the NE (Schulmann & Gayer 2000; Jastrzębski 2009; Chopin *et al.* 2012), also constrained by the syntectonic Staré Město tonalite sill (SMT in Figs 2 & 5*a*; Parry *et al.* 1997, dated at 344.5 ± 1.1 Ma and 339.4 ± 1.1 Ma by Štípská *et al.* 2004). The Brunia underthrusting resulted in a NNE–SSW-trending belt of imbricated nappe stacks along the whole eastern margin of the Bohemian Massif (the Moravosilesian Unit; Fig. 2). Geophysical data indicate that the Brunia microplate, exposed in tectonic windows of the Moravian nappes, continues *c.* 70 km westwards beneath the Moldanubian rocks (Mísař 1994; Schulmann *et al.* 2008; Guy *et al.* 2011; Verner *et al.* 2014). The inferred westernmost edge of the Brunia microplate at depth coincides with the Příbyslav Mylonite Zone at the

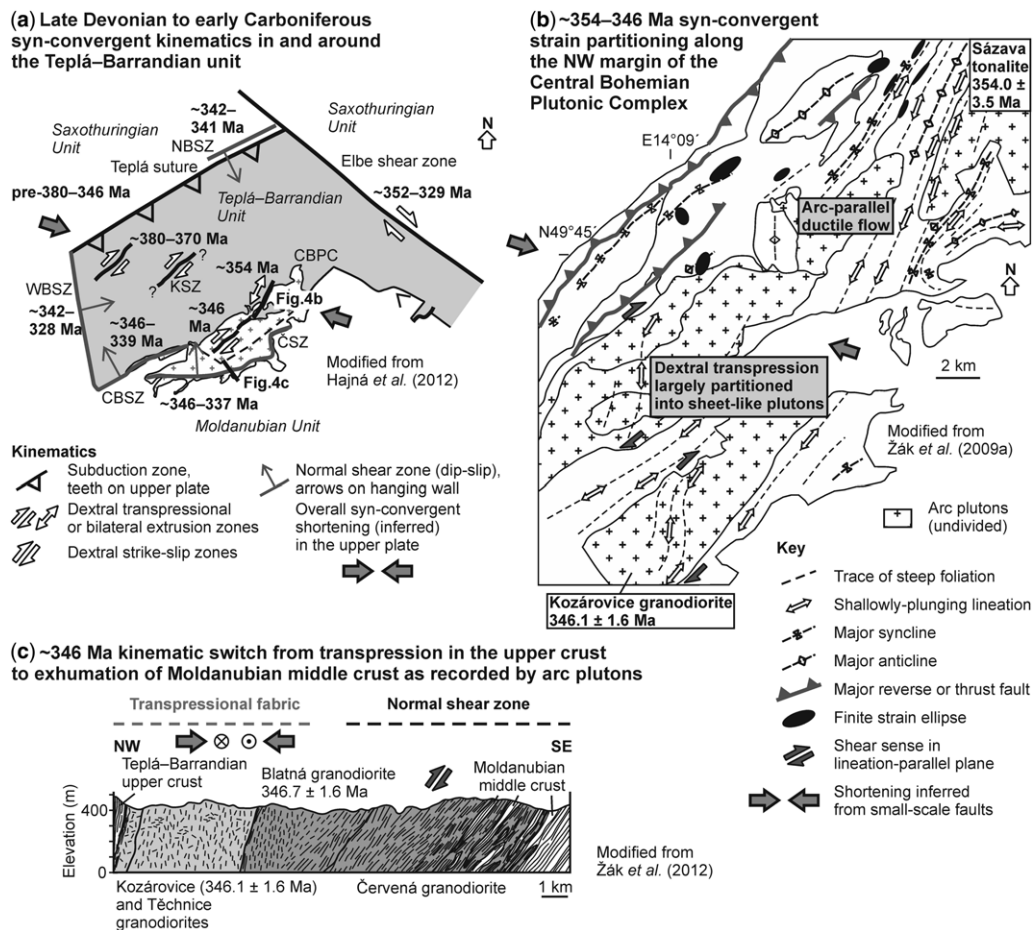


Fig. 4. Structural sketches summarizing deformation, kinematics and plutonism during prolonged Late Devonian–early Carboniferous convergence of the Saxothuringian and Teplá–Barrandian units. **(a)** Map of major shear zones inside and around the Teplá–Barrandian Unit showing overall WNW–ESE shortening in the upper crust replaced by normal movements and onset of exhumation of the Moldanubian Unit from *c.* 346 Ma onwards. See Hajná *et al.* (2012) for details. CBPC, Central Bohemian Plutonic Complex; CBSZ, Central Bohemian Shear Zone; ČSZ, Červená Shear Zone; KSZ, Krakovec Shear Zone; NBSZ, North Bohemian Shear Zone; WBSZ, West Bohemian Shear Zone. **(b)** Close-up of the northwestern margin of the Central Bohemian Plutonic Complex. The background WNW–ESE shortening was partitioned into arc-parallel ductile flow or dextral transpression depending on the orientation of syntectonic plutons. See Žák *et al.* (2009a) for details. **(c)** A kinematic switch from transpression to ductile normal shearing is recorded in the *c.* 346 Ma Blatná and Červená granodiorites of the Central Bohemian Plutonic Complex. This change marks the onset of exhumation of the southeasterly high-grade Moldanubian Unit. See Žák *et al.* (2005a, 2012) and Janoušek *et al.* (2010) for details.

present-day erosional level (PMZ in Fig. 2). This zone was recognized as an important crustal-scale geophysical and tectonic boundary that cuts across the entire Moldanubian Unit along the NNE–SSW direction and was associated with oblique-slip (dextral, west-side-up) movements initiated at *c.* 335 Ma (Fig. 5b; Verner *et al.* 2006; Kotková *et al.* 2010) and renewed at *c.* 330–327 Ma (Fig. 5c; Žák *et al.* 2011b; Verner *et al.* 2014).

Orogen-perpendicular NW–SE-trending boundaries

The Sudetic fault system. The northeasternmost margin of the Bohemian Massif ('the Sudetes') is cut by a series of major faults (Fig. 2; Lusatian, Machnín, Intra-Sudetic, Marginal-Sudetic; e.g. Aleksandrowski *et al.* 1997; Danišik *et al.* 2012), referred to as the Sudetic fault system here. The

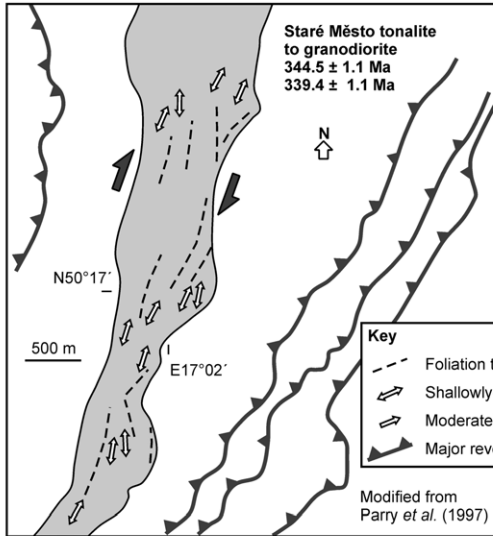
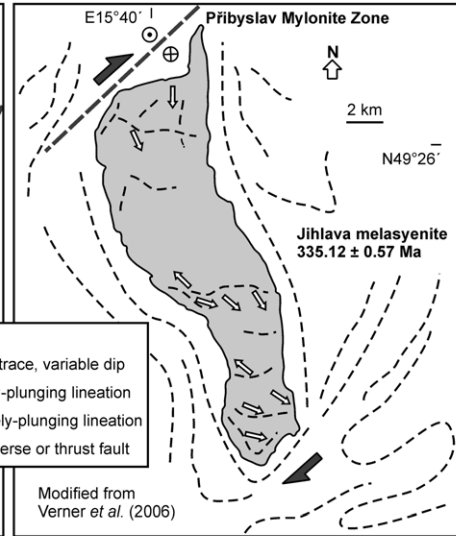
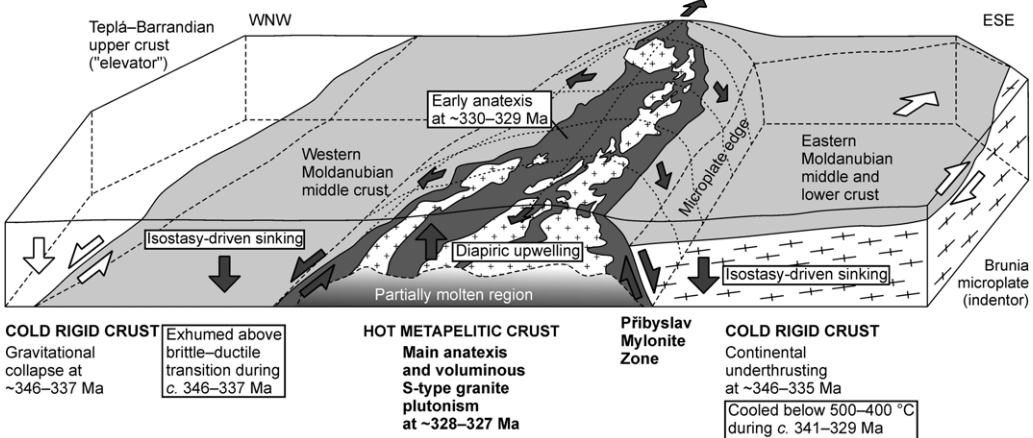
(a) Emplacement of the Staré Město sill during dextral transpression related to underthrusting of the Brunia microplate**(b)** Emplacement of the Jihlava Pluton during dextral transtension along the Přebyslav Mylonite Zone related to underthrusting of the Brunia microplate**(c)** ~330–327 Ma post-collisional diapiric upwelling of hot middle crust along the edge of the underthrust Brunia microplate

Fig. 5. Examples of syntectonic plutons emplaced during and after underthrusting of the Brunia microplate along the eastern margin of the Bohemian Massif. **(a)** The Staré Město sill records synmagmatic dextral transpression resulting from early stages of the continental underthrusting in the NE. See Parry *et al.* (1997) for details. **(b)** Sigmoidal-shaped Jihlava melasyenite was emplaced later (c. 335 Ma) during the same process in which the Brunia microplate proceeded further to the SSW. See Verner *et al.* (2006) for details. **(c)** Subsequently, the microplate edge acted as a rigid backstop that localized large-scale diapiric upwelling of a granite–migmatite dome, referred to as the Pelhřimov Complex, at c. 330–327 Ma. See Žák *et al.* (2011b) and Verner *et al.* (2014) for details.

fault-bounded blocks host several granitoid plutons (Fig. 2; e.g. Strzegom–Sobótka, Strzelin, Klodzko–Złoty Stok, Žulová; see Mazur *et al.* 2007; Mikulski *et al.* 2013; Oberc-Dziedzic *et al.* 2013 for reviews) that are largely concealed and their internal fabrics and structural relations are

yet to be examined in detail. The exception is the shallow-level Krkonoše–Jizera Plutonic Complex (KJPC in Fig. 2; e.g. Klomínský 1969; Mierzejewski 2002; Slaby & Martin 2008; Žák *et al.* 2009b), a classic area of granite geology that has become world-famous through the pioneering

work of Cloos (1925). Existing radiometric ages of granites in this plutonic complex scatter widely from 329 ± 17 Ma (Rb–Sr; Pin *et al.* 1987) to 304 ± 14 Ma (U–Pb; Kröner *et al.* 2001; see Awdankiewicz *et al.* 2010 for review); however, recent U–Pb zircon ages point to a more restricted time span from 322 ± 3 Ma (porphyritic biotite granite; Kryza *et al.* 2012) to 313 ± 3 Ma (dykes cutting the granite; Awdankiewicz *et al.* 2010). The plutonic complex intruded into already cold crust and post-dated both the blueschist (>360 Ma) and greenschist (*c.* 340 Ma) facies tectonometamorphic events in its host rocks (Maluski & Patočka 1997; Marheine *et al.* 2002; Mazur *et al.* 2006). The granite generation and emplacement was therefore presumably controlled by extensional unroofing and dextral displacement along the Sudetic fault system (Fig. 6; Aleksandrowski *et al.* 1997; Žák *et al.* 2013). The early ductile shearing commenced at *c.* 337–335 Ma and was also associated with the opening of a middle Viséan molasse basin (Turnau *et al.* 2002). Magnetic fabric analysis by Diot *et al.* (1995) and Žák *et al.* (2013) indicates that the plutonic complex recorded WNW–ESE horizontal stretching and was also syntectonic with dextral movements along the Intra-Sudetic Fault (Fig. 6).

The Elbe Shear Zone. The more southerly Elbe Shear Zone (ESZ in Fig. 2), which runs across the northern portion of the Bohemian Massif, is a broad zone of dextral shearing with prolonged kinematic history which has caused significant dextral offset of the amalgamated Saxothuringian/Teplá–Barrandian units. The earliest ductile movements were recorded within a *c.* 50–100 km wide belt of the middle–upper-crustal rocks between the southwesterly Moldanubian and northeasterly Saxothuringian units (Fig. 2). The dominant ductile deformation is characterized here by the NW–SE metamorphic foliation, subhorizontal NW–SE stretching lineation and dextral strike-slip kinematics (Fig. 7; Synek & Oliveriová 1993; Kachlík 1999; Scheck *et al.* 2002; Verner *et al.* 2009*a*; Vondrovič *et al.* 2011). The broad Elbe Shear Zone hosts several syntectonic calc-alkaline granodiorite-dominated intrusions emplaced at various stages of deformation. These include the Nasavrky Plutonic Complex (NPC in Fig. 2; Hroudá *et al.* 1999) and Budislav and Miřetín plutons (BP and MP in Fig. 2; Verner *et al.* 2009*a*; Vondrovič & Verner 2010; Vondrovič *et al.* 2011). The latter two intrusions were dated at 350 ± 5 Ma (Vondrovič & Verner 2010) and 346 ± 5 Ma (Vondrovič *et al.* 2011), respectively, and are comparable to

Strike-slip-related emplacement and syn-magmatic deformation of the Krkonoše–Jizera Plutonic Complex, Saxothuringian Unit

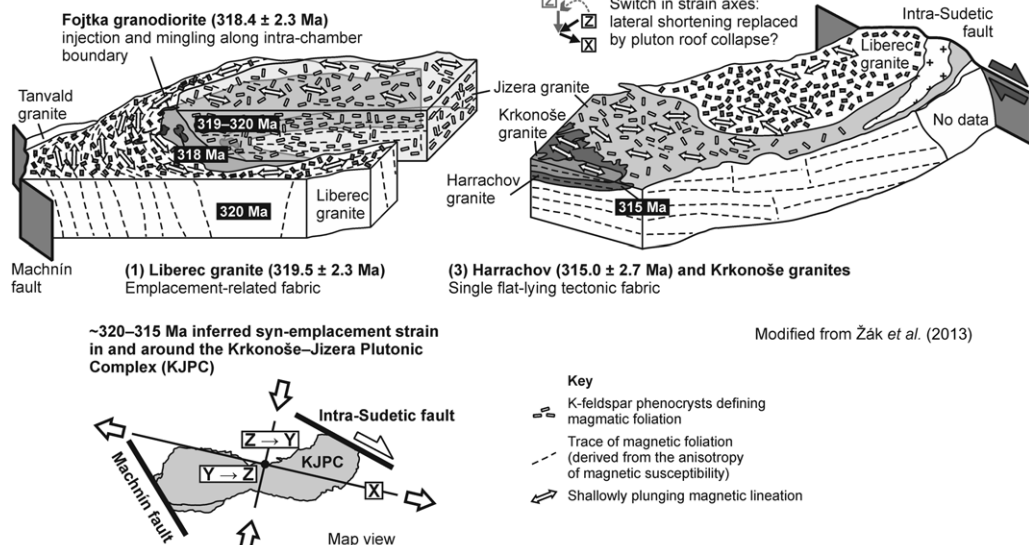


Fig. 6. Schematic block diagram showing the inferred inwards- and upwards-younging emplacement sequence and fabric evolution recorded in the *c.* 320–315 Ma Krkonoše–Jizera Plutonic Complex. Magmatic fabrics evolve from outer margin-parallel to those recording strain related to strike-slip movements along the major pluton-bounding faults. See Žák *et al.* (2013) for details.

Successive syn-tectonic emplacement of calc-alkaline plutons into the broad ductile Elbe shear zone

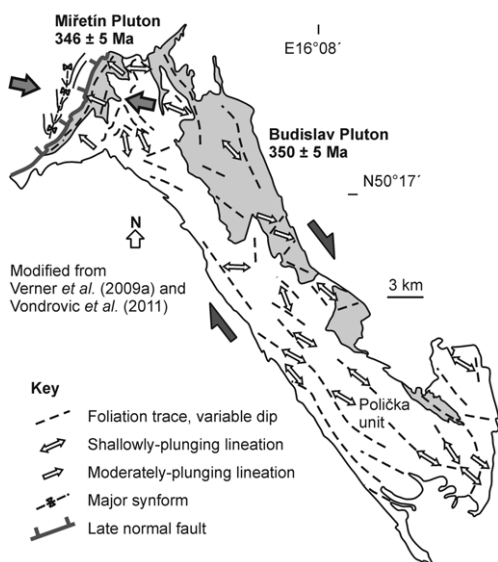


Fig. 7. Fabric patterns of syntectonic calc-alkaline plutons emplaced during early stages of ductile movements along the Elbe Shear Zone at *c.* 350–345 Ma. See Verner *et al.* (2009a) and Vondrovič *et al.* (2011) for details.

the arc-related granitoids of the Central Bohemian Plutonic Complex (Vondrovič *et al.* 2011). The Budislav Pluton was coeval with ductile dextral shearing along the Elbe Shear Zone whereas the Miřetín Pluton records WNW–ESE transpression that post-dated the dextral movements (Fig. 7; Per-toldová *et al.* 2010; Vondrovič *et al.* 2011; cf.

Pitra *et al.* 1994; Pitra 2012). Subsequently, the Elbe Shear Zone was multiply reactivated in the brittle–ductile and brittle regime during early Carboniferous time (e.g. Wenzel *et al.* 1997; Hofmann *et al.* 2009; Verner *et al.* 2009a).

The Pfahl Shear Zone. The Pfahl Shear Zone (PSZ in Fig. 2) extends for more than 150 km along-strike and, together with the subparallel southwesterly Danube Shear Zone (DSZ in Fig. 2), is a major tectonic feature of the southwestern Bohemian Massif (e.g. Peucker-Ehrenbrink & Behr 1993; Brandmayr *et al.* 1995; Büttner & Kruhl 1997; Büttner 2007). The existing U–Pb and Pb–Pb ages and structural relations of granitoid rocks associated with the shear zone indicate the initial stages of dextral shearing at *c.* 342–327 Ma and mylonitic deformation coeval with granite emplacement during *c.* 331–321 Ma (Fig. 8; Chen & Siebel 2004; Siebel *et al.* 2005, 2006b; Verner *et al.* 2009b). Slip along the Pfahl Shear Zone continued after emplacement of the *c.* 322–323 Ma Patersdorf granite, which is truncated by the shear zone (Siebel *et al.* 2006b). Conflicting views exist on whether the shear zone separates two different basement terranes or just intersects the otherwise continuous southwestern Moldanubian Unit (Finger *et al.* 2007, 2010; Siebel *et al.* 2008, 2009; Finger & René 2009).

A tentative model linking the Variscan orogenic deformation with plutonism in the Bohemian Massif

The Variscan Orogeny in the Bohemian Massif was accompanied by episodic granitoid plutonism with

Strike-slip-related emplacement and syn-magmatic deformation of the Eisgarn-type granites along the Pfahl shear zone

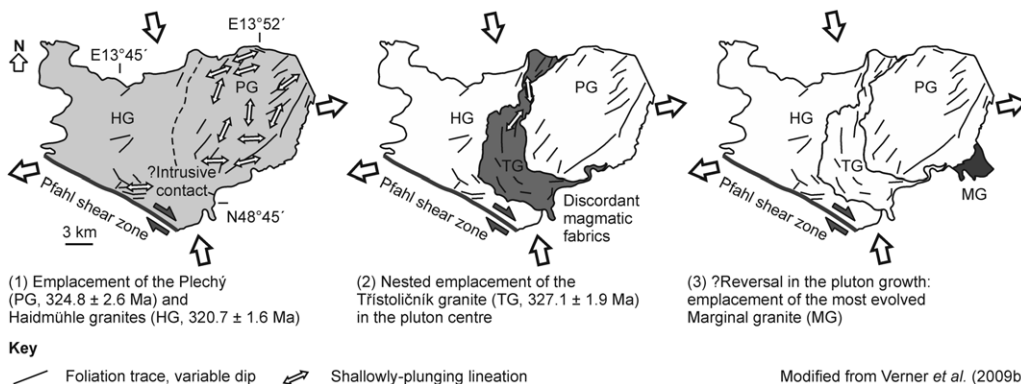


Fig. 8. Magmatic fabric pattern and syntectonic emplacement of the 'Eisgarn-type' granites along the dextral Pfahl Shear Zone as exemplified by the Plechý Pluton. See Verner *et al.* (2009b) for details.

several peaks of the plutonic activity that are now well constrained by geochronological data. As opposed to an outdated view of granites in the Bohemian Massif as post-tectonic (e.g. Franke 2000, 2006), it has been shown that most of the plutons are in fact syntectonic and play a key role in constraining the timing, regime and kinematics of Variscan orogenic deformations (Figs 4–8; e.g. Diot *et al.* 1995; Büttner & Kruhl 1997; Parry *et al.* 1997; Scheuven & Zulauf 2000; Venera *et al.* 2000; Žák *et al.* 2005a, b, 2009a, 2011a, b; Verner *et al.* 2006, 2008, 2009a, b; Vondrovic *et al.* 2011; Hajná *et al.* 2012; this study).

The earliest Variscan orogenic deformation in the interior of the Bohemian Massif is recorded by a dramatic change in sedimentation from carbonates to Givetian siliciclastic flysch successions (c. 388–383 Ma; e.g. Chlupáč 1989; Chlupáč *et al.* 1998; Strnad & Mihaljevič 2005). This event may be linked to the onset of the SE-directed frontal subduction of the Saxothuringian Ocean (Fig. 9a), leading to exhumation of (U)HP rocks, uplift and cooling along the western margin of the Teplá–Barrandian Unit (c. 387–365 Ma; Kachlík 1993; Kotková *et al.* 1995; Zulauf 1997a; Dallmeyer & Urban 1998; Konopásek & Schulmann 2005; Strnad & Mihaljevič 2005; Hajná *et al.* 2012). At approximately the same time, the opposite southeastern flank of the Teplá–Barrandian Unit was intruded by the c. 380–365 Ma protolith to Mirovice and Staré Sedlo orthogneisses (Fig. 9a; Košler *et al.* 1993), interpreted as a sill complex emplaced during previously unrecognized but still enigmatic transtensional event (Tomek 2011). All in all, the Late Devonian oceanic subduction resulted in suturing the Saxothuringian and Teplá–Barrandian units at c. 380 Ma (Schäfer *et al.* 1997; Zulauf 1997a) and presumably continued in underthrusting of the Saxothuringian passive margin until the high-grade metamorphism at c. 340 Ma (O'Brien 2000; Konopásek & Schulmann 2005; Schulmann *et al.* 2009).

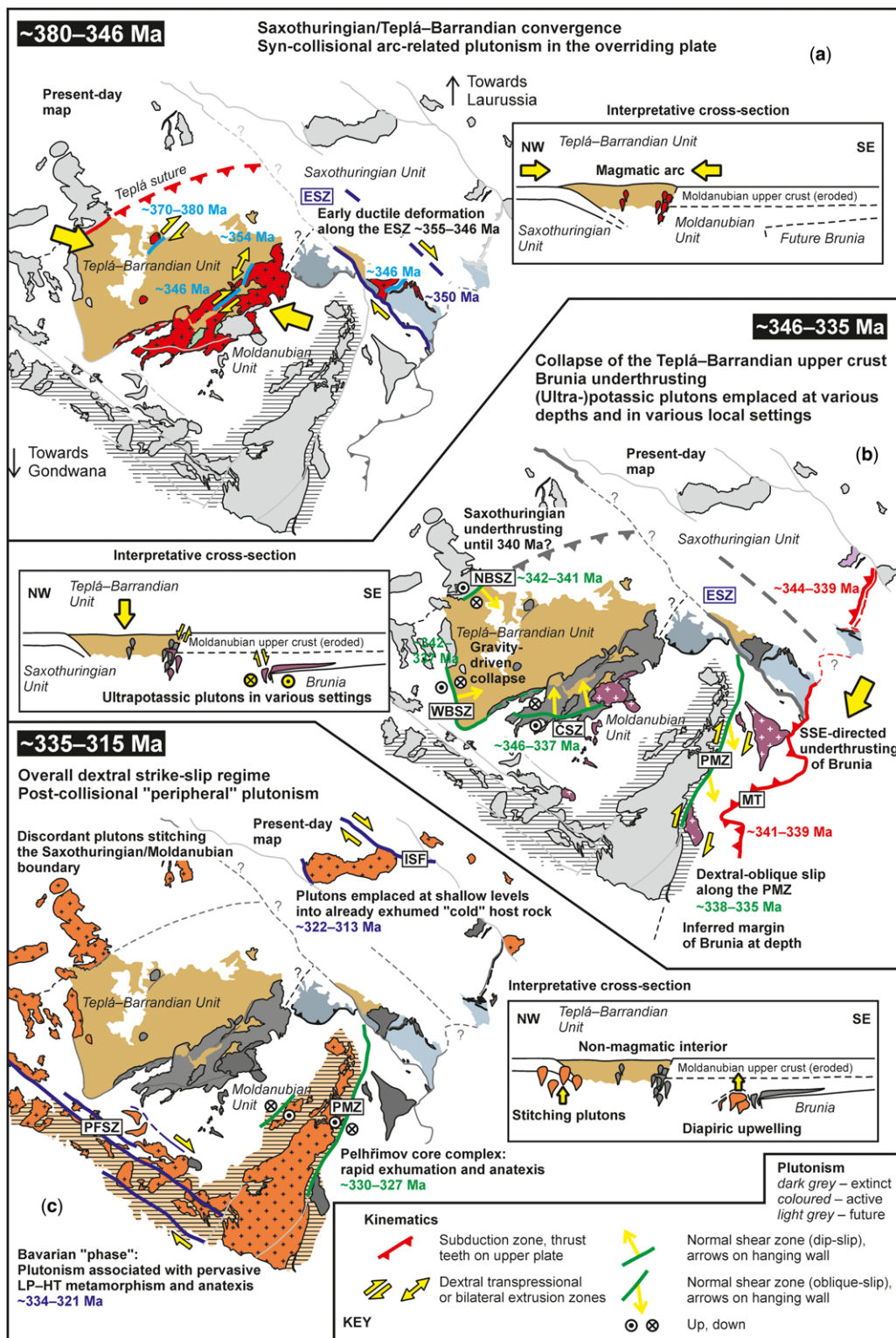
In one view, the Saxothuringian oceanic subduction produced the minor c. 373–375 Ma Štěnovice and Čistá granodiorite plutons in the central Teplá–Barrandian Unit (Fig. 9a; Žák *et al.* 2011a) and culminated in the development of a large magmatic arc along its southeastern flank at c. 354–346 Ma (Figs 3, 4 & 9a; Konopásek & Schulmann 2005; Žák *et al.* 2005a, 2009a, 2011a, 2012; Janoušek & Holub 2007; Schulmann *et al.* 2009). The associated SE-migrating transpressional deformation (from the Teplá suture towards the interior of the orogen) is well recorded in the arc granitoids and is characterized by orogen-perpendicular WNW–ESE to NW–SE shortening and orogen-parallel stretching (Figs 4a, 4b & 9a; Zulauf 1997a; Žák *et al.* 2009a; Hajná *et al.* 2012). In

alternative hypotheses, the Staré Sedlo and Mirovice orthogneisses and the Central Bohemian Plutonic Complex are linked to opposite, westward subduction of either the Gföhl or Raabs oceans (Franke 1999, 2006; Kachlík 1999; Finger *et al.* 2007; Babuška & Plomerová 2013).

The convergent stage was terminated by a rapid gravity-driven collapse of the thickened Teplá–Barrandian upper crust (Fig. 9b). The main phase of ductile normal shearing lasted from c. 346 to c. 337 Ma (Fig. 4c; Scheuven & Zulauf 2000; Žák *et al.* 2005a, 2012; Dörr & Zulauf 2010; Janoušek *et al.* 2010; Franěk *et al.* 2011; Holub *et al.* 2012) and was associated with exhumation of the adjacent high-grade core of the orogen and the Moldanubian Unit including the granulite-facies rocks (Franěk *et al.* 2006, 2011), and with emplacement of (ultra-)potassic ‘durbachite’ plutons (Fig. 9a; Wenzel *et al.* 1997; Janoušek & Holub 2007; Verner *et al.* 2008).

It is interesting to note that the upper crustal collapse broadly overlapped with the inferred timing of the earliest ductile movements along the orogen-perpendicular c. NW–SE-trending dextral strike-slip shear zones. The northeastern portion of the amalgamated Saxothuringian/Teplá–Barrandian/Moldanubian block has been truncated and dextrally displaced along the Sudetic and Elbe fault zones that parallel the southeastern margin of Baltica (Franke & Żelazniewicz 2002); movements started from c. 355–346 Ma (Fig. 7; Verner *et al.* 2009a) and lasted until at least c. 315 Ma (Wenzel *et al.* 1997; Hofmann *et al.* 2009; Pertoldová *et al.* 2010; Vondrovic *et al.* 2011). In turn, this suggests that the orogenic processes governed by the prolonged frontal Saxothuringian subduction/underthrusting including the internal deformation of the Teplá–Barrandian overriding plate, were abruptly replaced by gravity-driven collapse (Figs 4c & 9b; e.g. Zulauf 1994; Zulauf *et al.* 2002; Dörr & Zulauf 2010; Franěk *et al.* 2011; Žák *et al.* 2012) and by dextral strike-slip movements (Fig. 9c), which could have been caused by the overall westward motion of Gondwana with respect to Laurussia since c. 345 Ma (e.g. Martínez Catalán 2011).

Subsequently, while most of the orogenic ductile deformation and exhumation was completed in the central Bohemian Massif in the vicinity of the Teplá–Barrandian Unit by c. 339–337 Ma (Žák *et al.* 2012), the eastern part of the Moldanubian Unit was still involved in an underthrusting/collision with the Brunia microplate, closing oceanic domains correlative with the Rhenohercynian Ocean as witnessed by several fragments of oceanic crust (Finger & Von Quadt 1995; Höck *et al.* 1997; Soejono *et al.* 2010). Continental underthrusting led to extrusion of the Moldanubian rocks over the top of Brunia, nappe emplacement at



c. 341–339 Ma (Štípská & Schulmann 1995) and propagation of the microplate edge as far west as the Příbyslav Mylonite Zone (Fig. 9b). Our structural data around the Jihlava Pluton suggest that this process overlapped with, and was followed by, dextral west-side-up shearing along the Příbyslav Mylonite Zone at c. 338–335 Ma (Fig. 5b; Verner *et al.* 2006) and most likely terminated prior to c. 330 Ma when the Moldanubian rocks were unroofed and exposed to erosion (Štípská & Schulmann 1995; Scharbert *et al.* 1997; Vrána & Novák 2000; Hartley & Otava 2001; Kotková *et al.* 2007). Later on, Brunia acted as a ‘passive’ rigid backstop localizing extensive migmatization and rapid exhumation of the Moldanubian metasedimentary rocks along its edge to produce vast volumes of S-type granitoids at c. 330–327 Ma (Figs 5c & 9c; the Pelhřimov Complex; Bell *et al.* 2011; Žák *et al.* 2011b; Verner *et al.* 2014).

The waning stages of the Variscan Orogeny were characterized by tectonothermal activity on the periphery around the ‘stable’ core of the Bohemian Massif (Fig. 9c). They included emplacement of huge volumes of the northerly and westerly granitoids in the Saxothuringian Zone and Northern Oberpfalz (e.g. Hecht *et al.* 1997; Siebel *et al.* 1997; Förster *et al.* 1999; Förster & Romer 2010; Breiter 2012) and c. 334–321 Ma LP/HT metamorphism, crustal anatexis and associated plutonism in the southwestern Moldanubian Unit (Fig. 9c; e.g. Kalt *et al.* 1999, 2000; Tropper *et al.* 2006; Klein *et al.* 2008; Finger *et al.* 2009). These late-stage events affected already-exhumed crust at shallow levels and were linked to continuing movements along the NW–SE strike-slip faults (e.g. the Krkonoše–Jizera Plutonic Complex, Aleksandrowski *et al.* 1997; Plechý Pluton, Verner *et al.* 2009b; Figs 6 & 8) or reflected high heat flux caused by mantle delamination as proposed by Henk *et al.* (2000) and Finger *et al.* (2009). Alternatively, Verner *et al.* (2014) proposed that at least some of these granites, commonly in association with migmatites, may represent large-scale diapir-type instabilities accommodating vertical isostatic re-equilibration of the orogen after the microplate convergence. Later destruction of the orogenic belt, post-orogenic igneous activity, intracontinental

basin development and multiple reactivations along the inherited basement fault zones are another part of the story and are not dealt with in detail here.

Concluding remarks and open questions

The above overview is, of course, far from being conclusive and complete. At the very least, however, it clearly demonstrates how the orogenic processes and related deformation and plutonism evolved in space and time. As a consequence of overall convergence of Gondwana and Laurussia, four main episodes can be recognized in the interior Bohemian Massif as follows.

- (1) Microplate attachment by prolonged, nearly frontal oceanic subduction and continental underthrusting of the Saxothuringian Unit beneath the Teplá–Barrandian Unit resulted in the orogen-perpendicular shortening and orogen-parallel extension in the overriding plate (Fig. 9a). The plate convergence was crowned by the emplacement of huge volumes of calc-alkaline magmatic-arc granitoids at c. 354–346 Ma (the Central Bohemian Plutonic Complex).
- (2) The subduction-driven shortening was replaced by dextral strike-slip along the orogen-perpendicular shear zones as the convergence of intervening microplates became increasingly overridden by the overall westward motion of Gondwana with respect to Laurussia during early Carboniferous times. This was broadly contemporaneous with the collapse of the Teplá–Barrandian upper crust, (ultra-)potassic plutonism and the exhumation of the high-grade (Moldanubian) core of the orogen at c. 346–335 Ma (Fig. 9b).
- (3) Following the subduction and closure of the easterly Rheohercynian Ocean basins, an Avalonian-type Brunia microplate was underthrust to the SSW beneath the eastern flank of the Saxothuringian/Teplá–Barrandian/Moldanubian ‘assemblage’ (c. 346–335 Ma). This was a dominant process that shaped the eastern margin of the Bohemian Massif and

Fig. 9. Greatly idealized sketch emphasizing spatial, temporal and compositional pattern of Variscan plutonism in the Bohemian Massif. The plutonism is also linked to kinematics and timing of movement along principal tectonic boundaries as inferred from geochronological and structural data. See text for details and references. Note that the scheme portrays kinematics on the present-day geological background; the exact amount of shortening and of displacement along each shear zone or fault is difficult to reconstruct during relevant time intervals. Also note that Variscan deformations were typically three-dimensional and complex along each boundary. Shear zones and faults: ČSZ, Červená Shear Zone; ESZ, Elbe Shear Zone; ISF, Intra-Sudetic Fault; MT, Moldanubian Thrust; NBSZ, North Bohemian Shear Zone; PFSZ, Pfahl Shear Zone; PMZ, Příbyslav Mylonite Zone; WBSZ, West Bohemian Shear Zone.

its waning stages were also accompanied by emplacement of the (ultra-)potassic plutons (Fig. 9b).

- (4) Late readjustments within the amalgamated Bohemian Massif included rapid exhumation and voluminous c. 327–330 Ma S-type-dominated granite plutonism and tectonothermal activity on the periphery around the consolidated orogen's core (Fig. 9c), followed by the destruction of the orogenic belt, post-orogenic igneous activity, continental basin development and multiple reactivations along the inherited basement fault zones.

Finally, we close our overview by pointing out some of the open issues that we find most controversial or least understood and that could be potential goals for future research, namely: (1) the existence of the 'Gföhl suture' between the Teplá–Barrandian and Moldanubian units, that is, whether these two represent once-separate microplates surrounded by oceanic lithosphere or are just variously reworked segments of a single microplate; (2) the role of easterly, west-directed subduction zones in generating arc-magmatism in the central Bohemian Massif; (3) amounts of both vertical and horizontal displacements and crustal shortening within the orogen during any of the above four episodes; (4) exact age(s) of the (U)HP metamorphic peak in eclogite–granulite-facies rocks and mechanisms and timing of their exhumation; (5) sense, timing and amounts of relative microplate rotations in course of the Variscan Orogeny; (6) the evolution of Variscan palaeotopography and possible orogenic plateaux in space and time; (7) the role of mantle delamination in driving granitoid plutonism and related tectonothermal activity; and (8) the nature of forces leading to destruction of the orogenic belt.

We gratefully acknowledge two anonymous reviewers for their constructive comments regarding the original manuscript and K. Schulmann for careful editorial handling. Our research into granites was supported from the Grant Agency of the Czech Republic through grant nos P210/11/1168 (to J. Žák) and 205/09/0630 (to F. Holub) as well as from the Ministry of Education, Youth and Sports of the Czech Republic (grant no. LK11202, Research Plans no. MSM0021620855 and SVV261203) and Charles University in Prague Research Program PRVOUK P44. This study incorporates PhD research by J. Trubač, L. Vondrovic and F. Tomek.

References

AFTALION, M., BOWES, D. R. & VRÁNA, S. 1989. Early Carboniferous U–Pb zircon age of garnetiferous, perpotassic granulites, Blanský les massif, Czechoslovakia. *Neues Jahrbuch für Mineralogie, Monatshefte*, **4**, 145–152.

- ALEKSANDROWSKI, P., KRYZA, R., MAZUR, S. & ŽÁBA, J. 1997. Kinematic data on major Variscan strike-slip faults and shear zones in the Polish Sudetes, north-east Bohemian Massif. *Geological Magazine*, **134**, 727–739.
- ASCH, K. 2003. *The 1:5 million international geological map of Europe and adjacent areas: development and implementation of a GIS-enabled concept*. Geologisches Jahrbuch, Sonderhefte, **A3**. E. Schweizerbart, Stuttgart.
- AWDANKIEWICZ, M., AWDANKIEWICZ, H., KRYZA, R. & RODIONOV, N. 2010. SHRIMP zircon study of a micromonzodiorite dyke in the Karkonosze Granite, Sudetes (SW Poland): age constraints for late Variscan magmatism in Central Europe. *Geological Magazine*, **147**, 77–85.
- BABUŠKA, V. & PLOMEROVÁ, J. 1992. The lithosphere in central Europe – seismological and petrological aspects. *Tectonophysics*, **207**, 141–163.
- BABUŠKA, V. & PLOMEROVÁ, J. 2001. Subcrustal lithosphere around the Saxothuringian–Moldanubian Suture Zone – a model derived from anisotropy of seismic wave velocities. *Tectonophysics*, **332**, 185–199.
- BABUŠKA, V. & PLOMEROVÁ, J. 2013. Boundaries of mantle-lithosphere domains in the Bohemian Massif as extinct exhumation channels for high-pressure rocks. *Gondwana Research*, **23**, 973–987.
- BABUŠKA, V., PLOMEROVÁ, J. & VECSEY, L. 2008. Mantle fabric of western Bohemian Massif (central Europe) constrained by 3D seismic P and S anisotropy. *Tectonophysics*, **462**, 149–163.
- BABUŠKA, V., FIALA, J. & PLOMEROVÁ, J. 2010. Bottom to top lithosphere structure and evolution of western Eger Rift (Central Europe). *International Journal of Earth Sciences*, **99**, 891–907.
- BALLÉVRE, M., BOSSE, V., DUCASSOU, C. & PITRA, P. 2009. Palaeozoic history of the Armorican Massif: models for the tectonic evolution of the suture zones. *Comptes Rendus Geoscience*, **341**, 174–201.
- BEARD, B. L., MEDARIS, L. G., JOHNSON, C. M., JELÍNEK, E., TONIKA, J. & RICIPUTI, L. R. 1995. Geochronology and geochemistry of eclogites from the Mariánské Lázně Complex, Czech Republic: implications for Variscan orogenesis. *Geologische Rundschau*, **84**, 552–567.
- BECKER, H. 1997. Petrological constraints on the cooling history of high-temperature garnet peridotite massifs in lower Austria. *Contributions to Mineralogy and Petrology*, **128**, 272–286.
- BECKER, H. & ALTHERR, R. 1992. Evidence from ultra-high-pressure marbles for recycling of sediments into the mantle. *Nature*, **358**, 745–748.
- BECKER, H., WENZEL, T. & VOLKER, F. 1999. Geochemistry of glimmerite veins in peridotites from Lower Austria – implications for the origin of K-rich magmas in collision zones. *Journal of Petrology*, **40**, 315–338.
- BEHR, H. J., ENGEL, W. & FRANKE, W. 1982. Variscan wildflysch and nappe tectonics in the Saxothuringian Zone (Northeast Bavaria, West Germany). *American Journal of Science*, **282**, 1438–1470.
- BELL, B., JOHNSON, K., ŽÁK, J., VERNER, K. & SCHWARTZ, J. J. 2011. Migmatization and melt generation in the Monotonous Unit, Moldanubian Batholith, Czech

- Republic: implications of zircon Pb/U (SHRIMP-RG) ages and Hf isotope compositions. *Geological Society of America Abstracts with Programs*, **43**, 66.
- BOWES, D. R. & AFTALION, M. 1991. U–Pb zircon isotopic evidence for early Ordovician and late Proterozoic units in the Mariánské Lázně Complex, Central European Hercynides. *Neues Jahrbuch für Mineralogie, Monatshefte*, **7**, 315–326.
- BRANDMAYR, M., DALLMEYER, R. D., HANDLER, R. & WALLBRECHER, E. 1995. Conjugate shear zones in the Southern Bohemian Massif (Austria): implications for Variscan and Alpine tectonothermal activity. *Tectonophysics*, **248**, 97–116.
- BREITER, K. 2010. Geochemical classification of Variscan granitoids in the Moldanubicum (Czech Republic, Austria). *Abhandlungen der Geologischen Bundesanstalt*, **65**, 19–25.
- BREITER, K. 2012. Nearly contemporaneous evolution of the A- and S-type fractionated granites in the Krušné hory/Erzgebirge Mts., Central Europe. *Lithos*, **151**, 105–121.
- BUES, C., DÖRR, W., FIALA, J., VEJNAR, Z. & ZULAUF, G. 2002. Emplacement depths and radiometric ages of Paleozoic plutons of the Neukirchen–Kdyně Massif: differential uplift and exhumation of Cadomian basement due to Carboniferous orogenic collapse (Bohemian Massif). *Tectonophysics*, **352**, 225–243.
- BUSCHMANN, B., ELICKI, O. & JONAS, P. 2006. The Cadomian unconformity in the Saxo-Thuringian Zone, Germany: palaeogeographic affinities of Ediacaran (terminal Neoproterozoic) and Cambrian strata. *Precambrian Research*, **147**, 387–403.
- BÜTTNER, S. H. 2007. Late Variscan stress-field rotation initiating escape tectonics in the south-western Bohemian Massif: a far field response to late-orogenic extension. *Journal of Geosciences*, **52**, 29–43.
- BÜTTNER, S. H. & KRÜHL, J. H. 1997. The evolution of a late-Variscan high-T/low-P region: the southeastern margin of the Bohemian Massif. *Geologische Rundschau*, **86**, 21–38.
- CHÁB, J. & VRÁNA, S. 1979. Crossite–actinolite amphiboles of the Krkonoše–Jizera Crystalline Complex and their geological significance. *Bulletin of the Central Geological Survey*, **56**, 143–150.
- CHÁB, J., STRÁNÍK, Z. & ELIÁŠ, M. 2007. *Geological Map of the Czech Republic 1:500,000*. Czech Geological Survey, Prague.
- CHEN, F. K. & SIEBEL, W. 2004. Zircon and titanite geochronology of the Fürstenstein granite massif, Bavarian Forest, NW Bohemian Massif: pulses of the late Variscan magmatic activity. *European Journal of Mineralogy*, **16**, 777–788.
- CHEN, F., SIEBEL, W. & SATIR, M. 2003. Geochemical and isotopic composition and inherited zircon ages as evidence for lower crustal origin of two Variscan S-type granites in the NW Bohemian Massif. *International Journal of Earth Sciences*, **92**, 173–184.
- CHLUPÁČ, I. 1989. Stratigraphy of the Sedlčany–Krásná Hora metamorphic 'Islet' in Bohemia (Proterozoic? to Devonian). *Journal for Mineralogy and Geology*, **34**, 1–16.
- CHLUPÁČ, I., HAVLÍČEK, V., KRÍŽ, J., KUKAL, Z. & ŠTORCH, P. 1998. *Paleozoic of the Barrandian (Cambrian to Devonian)*. Czech Geological Survey, Prague.
- CHOPIN, F., SCHULMANN, K. ET AL. 2012. Crustal influx, indentation, ductile thinning and gravity redistribution in a continental wedge: building a Moldanubian mantled gneiss dome with underthrust Saxothuringian material (European Variscan belt). *Tectonics*, **31**, <http://dx.doi.org/10.1029/2011TC002951>
- CLOOS, H. 1925. *Einführung in die Tektonische Behandlung Magmatischer Erscheinungen (Granittektonik)*. I. Das Riesengebirge in Schlesien. Gebrüder Bornträger, Berlin.
- CYMERMAN, Z., PIASECKI, M. A. J. & SESTON, R. 1997. Terranes and terrane boundaries in the Sudetes, north-east Bohemian Massif. *Geological Magazine*, **134**, 717–725.
- DALLMEYER, R. D. & URBAN, M. 1998. Variscan vs Cadomian tectonothermal activity in northwestern sectors of the Teplá–Barrandian Zone, Czech Republic: constraints from $^{40}\text{Ar}/^{39}\text{Ar}$ ages. *Geologische Rundschau*, **87**, 94–106.
- DANIŠÍK, M., ŠTĚPANČÍKOVÁ, P. & EVANS, N. J. 2012. Constraining long-term denudation and faulting history in intraplate regions by multisystem thermochronology: an example of the Sudetic Marginal Fault (Bohemian Massif, central Europe). *Tectonics*, **31**, <http://dx.doi.org/10.1029/2011TC003012>
- DIOT, H., MAZUR, S. & PIN, C. 1995. Karkonosze Batholith (NE Bohemian Massif): the evidence for pluton emplacement during transtensional–extensional collapse. *Journal of the Czech Geological Society*, **43**, 62.
- DÖRR, W. & ZULAUF, G. 2010. Elevator tectonics and orogenic collapse of a Tibetan-style plateau in the European Variscides: the role of the Bohemian shear zone. *International Journal of Earth Sciences*, **99**, 299–325.
- DÖRR, W., FIALA, J., VEJNAR, Z. & ZULAUF, G. 1998. U–Pb zircon ages and structural development of metagranitoids of the Teplá Crystalline Complex: evidence for pervasive Cambrian plutonism within the Bohemian Massif (Czech Republic). *Geologische Rundschau*, **87**, 135–149.
- DÖRR, W., ZULAUF, G., FIALA, J., FRANKE, W. & VEJNAR, Z. 2002. Neoproterozoic to Early Cambrian history of an active plate margin in the Teplá–Barrandian Unit: a correlation of U–Pb isotopic-dilution-TIMS ages (Bohemia, Czech Republic). *Tectonophysics*, **352**, 65–85.
- DROST, K., LINNEMANN, U. ET AL. 2004. New data on the Neoproterozoic–Cambrian geotectonic setting of the Teplá–Barrandian volcano-sedimentary successions: geochemistry, U–Pb zircon ages, and provenance (Bohemian Massif, Czech Republic). *International Journal of Earth Sciences*, **93**, 742–757.
- DROST, K., GERDES, A., JEFFRIES, T., LINNEMANN, U. & STOREY, C. 2011. Provenance of Neoproterozoic and early Paleozoic siliciclastic rocks of the Teplá–Barrandian unit (Bohemian Massif): evidence from U–Pb detrital zircon ages. *Gondwana Research*, **19**, 213–231.
- DUDEK, A. 1980. The crystalline basement block of the Outer Carpathians in Moravia: Brunovistulicum. *Transactions of the Czechoslovak Academy of Sciences, Mathematical and Natural Science Series*, **90**, 3–85.
- EDEL, J. B., SCHULMANN, K. & HOLUB, F. V. 2003. Anticlockwise and clockwise rotations of the Eastern

- Variscides accommodated by dextral lithospheric wrenching: palaeomagnetic and structural evidence. *Journal of the Geological Society, London*, **160**, 209–218.
- EDEL, J. B., SCHULMANN, K., SKRZYPEK, E. & COCHERIE, A. 2013. Tectonic evolution of the European Variscan belt constrained by palaeomagnetic, structural and anisotropy of magnetic susceptibility data from the Northern Vosges magmatic arc (eastern France). *Journal of the Geological Society, London*, **170**, 785–804.
- FARYAD, S. W. 2011. Distribution and geological position of high-/ultrahigh-pressure units within the European Variscan belt: a review. In: DOBRZHINETSAYA, L. F., FARYAD, S. W., WALLIS, S. & CUTHBERT, S. (eds) *Ultrahigh-Pressure Metamorphism: 25 Years After the Discovery of Coesite and Diamond*. Elsevier, Amsterdam, 361–397.
- FARYAD, S. W. & KACHLÍK, V. 2013. New evidence of blueschist facies rocks and their geotectonic implication for Variscan suture(s) in the Bohemian Massif. *Journal of Metamorphic Geology*, **31**, 63–82.
- FARYAD, S. W., DOLEJŠ, D. & MACHEK, M. 2009. Garnet exsolution in pyroxene from clinopyroxenites in the Moldanubian zone: constraining the early pre-convergence history of ultramafic rocks in the Variscan orogen. *Journal of Metamorphic Geology*, **27**, 655–671.
- FARYAD, S. W., NAHODILOVÁ, R. & DOLEJŠ, D. 2010. Incipient eclogite facies metamorphism in the Moldanubian granulites revealed by mineral inclusions in garnet. *Lithos*, **114**, 54–69.
- FARYAD, S. W., JEDLIČKA, R. & ETTINGER, K. 2013. Subduction of lithospheric upper mantle recorded by solid phase inclusions and compositional zoning in garnet: example from the Bohemian Massif. *Gondwana Research*, **23**, 944–955.
- FAURE, M., LARDEAUX, J. M. & LEDRU, P. 2009. A review of the pre-Permian geology of the Variscan French Massif Central. *Comptes Rendus Geoscience*, **341**, 202–213.
- FIALA, J., FUCHS, G. & WENDT, J. I. 1995. Moldanubian Zone – stratigraphy. In: DALLMEYER, R. D., FRANKE, W. & WEBER, K. (eds) *Pre-Permian Geology of Central and Eastern Europe*. Springer, Berlin, 417–428.
- FINGER, F. & RENÉ, M. 2009. A comment on ‘Two distinctive granite suites in the SW Bohemian Massif and their record of emplacement: constraints from geochemistry and zircon $^{207}\text{Pb}/^{206}\text{Pb}$ chronology’ by Siebel *et al.* (Journal of Petrology, 49, 1853–1872). *Journal of Petrology*, **50**, 591–593.
- FINGER, F. & STEYRER, H. P. 1995. A tectonic model for the eastern Variscides: indications from a chemical study of amphibolites in the south-eastern Bohemian Massif. *Geologica Carpathica*, **46**, 137–150.
- FINGER, F. & VON QUADT, A. 1995. U/Pb ages of zircons from a plagiogranite-gneiss in the southeastern Bohemian Massif, Austria – further evidence for an important early Paleozoic rifting episode in the eastern Variscides. *Schweizerische Mineralogische und Petrographische Mitteilungen*, **75**, 265–270.
- FINGER, F., FRASL, G., HÖCK, V. & STEYRER, H. P. 1989. The granitoids of the Moravian Zone of northeastern Austria: products of Cadomian active continental margin? *Precambrian Research*, **45**, 235–245.
- FINGER, F., ROBERTS, M. P., HAUNSCHMID, B., SCHERMAIER, A. & STEYRER, H. P. 1997. Variscan granitoids of central Europe: their typology, potential sources and tectonothermal relations. *Mineralogy and Petrology*, **61**, 67–96.
- FINGER, F., HANŽL, P., PIN, C., VON QUADT, A. & STEYRER, H. P. 2000a. The Brunovistulian: Avalonian Precambrian sequence at the eastern end of the Central European Variscides? In: FRANKE, W., HAAK, V., ONCKEN, O. & TANNER, D. (eds) *Orogenic Processes: Quantification and Modelling in the Variscan Belt*. Geological Society, London, Special Publications, **179**, 103–112.
- FINGER, F., TICHOMIROVA, M., PIN, C. & HANŽL, P. 2000b. Relics of early-Panafrican metabasite-metarhyolite formation in the Brno Massif, Moravia, Czech Republic. *International Journal of Earth Sciences*, **89**, 328–335.
- FINGER, F., DOBLMAYR, P., FRIEDL, G., GERDES, A., KRENN, E. & VON QUADT, A. 2003. Petrology of the Weinsberg granite in the South Bohemian Batholith: new data from the mafic end members. *Journal of the Czech Geological Society*, **48**, 46–47.
- FINGER, F., GERDES, A., JANOUŠEK, V., RENÉ, M. & RIEGLER, G. 2007. Resolving the Variscan evolution of the Moldanubian sector of the Bohemian Massif: the significance of the Bavarian and the Moravo-Moldanubian tectonometamorphic phases. *Journal of Geosciences*, **52**, 9–28.
- FINGER, F., GERDES, A., RENÉ, M. & RIEGLER, G. 2009. The Saxo-Danubian Granite Belt: magmatic response to post-collisional delamination of mantle lithosphere below the south-western sector of the Bohemian Massif (Variscan orogen). *Geologica Carpathica*, **60**, 205–212.
- FINGER, F., DUNKLEY, D. J. & RENÉ, M. 2010. Remnants of Early Carboniferous I-type granodiorite plutons in the Bavarian Forest and their bearing on the tectonic interpretation of the south-western sector of the Bohemian Massif (Bavarian Zone). *Journal of Geosciences*, **55**, 321–332.
- FÖRSTER, H. J. 1998. The chemical composition of REE–Y–Th–U-rich accessory minerals in peraluminous granites of the Erzgebirge–Fichtelgebirge region, Germany: part I, the monazite-(Ce)–brabantite solid solution series. *American Mineralogist*, **83**, 259–272.
- FÖRSTER, H. J. & ROMER, R. L. 2010. Carboniferous magmatism. In: LINNEMANN, U. & ROMER, R. L. (eds) *Pre-Mesozoic Geology of Saxo-Thuringia – from the Cadomian Active Margin to the Variscan Orogen*. E. Schweizerbart, Stuttgart, 287–308.
- FÖRSTER, H. J., TISCHENDORF, G., TRUMBULL, R. B. & GOTTESMANN, B. 1999. Late-collisional granites in the Variscan Erzgebirge, Germany. *Journal of Petrology*, **40**, 1613–1645.
- FÖRSTER, H. J., ROMER, R. L., GOTTESMANN, B., TISCHENDORF, G. & RHEDE, D. 2009. Are the granites of the Aue–Schwarzenberg Zone (Erzgebirge, Germany) a major source for metalliferous ore deposits? A geochemical, Sr–Nd–Pb isotopic, and geochronological study. *Neues Jahrbuch für Mineralogie, Abhandlungen*, **186**, 163–184.
- FRANĚK, J., SCHULMANN, K. & LEXA, O. 2006. Kinematic and rheological model of exhumation of high pressure

- granulites in the Variscan orogenic root: example of the Blanský les granulite, Bohemian Massif, Czech Republic. *Mineralogy and Petrology*, **86**, 253–276.
- FRANĚK, J., SCHULMANN, K., LEXA, O., TOMEK, Č. & EDEL, J. B. 2011. Model of syn-convergent extrusion of orogenic lower crust in the core of the Variscan belt: implications for exhumation of high-pressure rocks in large hot orogens. *Journal of Metamorphic Geology*, **29**, 53–78.
- FRANKE, W. 1989. Variscan plate tectonics in Central Europe – current ideas and open questions. *Tectonophysics*, **169**, 221–228.
- FRANKE, W. 1999. Tectonic and plate tectonic units at the north Gondwana margin: evidence from the central European Variscides. *Abhandlungen der Geologischen Bundesanstalt*, **54**, 7–14.
- FRANKE, W. 2000. The mid-European segment of the Variscides: tectonostratigraphic units, terrane boundaries and plate tectonic evolution. In: FRANKE, W., HAAK, V., ONCKEN, O. & TANNER, D. (eds) *Orogenic Processes: Quantification and Modelling in the Variscan Belt*. Geological Society, London, Special Publications, **179**, 35–61.
- FRANKE, W. 2006. The Variscan orogen in Central Europe: construction and collapse. In: GEE, D. G. & STEPHENSON, R. A. (eds) *European Lithosphere Dynamics*. Geological Society, London, Memoirs, **32**, 333–343.
- FRANKE, W. & ŽELAZNIEWICZ, A. 2002. Structure and evolution of the Bohemian Arc. In: WINCHESTER, J. A., PHAROAH, T. C. & VERNIERS, J. (eds) *Palaeozoic Amalgamation of Central Europe*. Geological Society, London, Special Publications, **201**, 279–293.
- FRASL, G. & FINGER, F. 1991. Geologisch-petrographische Exkursion in den österreichischen Teil des Südböhmischen Batholiths. *Beihfte European Journal of Mineralogy*, **3**, 23–40.
- FRIEDL, G., VON QUADT, A., FRASL, G. & FINGER, F. 1992. Neue U/Pb Altersdaten aus der südlichen Böhmisches Masse. *Frankfurter Geowissenschaftliche Arbeiten Serie A. Geologie-Paläontologie*, **A11**, 217–218.
- FRIEDL, G., VON QUADT, A., OCHSNER, A. & FINGER, F. 1993. Timing of the Variscan Orogeny in the southern Bohemian Massif (NE-Austria) deduced from new U–Pb zircon and monazite dating. *Terra Abstracts*, **5**, 235–236.
- FRIEDL, G., VON QUADT, A. & FINGER, F. 1996. Timing der Intrusionstätigkeit im Südböhmischen Batholith. In: *Symposium Tektonik–Strukturgeologie–Kristallineologie, Salzburg, 10–15 April 1996, Book of Abstracts*. Fakultas Universitätsverlag, Vienna, 127–130.
- FRIEDL, G., FINGER, F., MCNAUGHTON, N. J. & FLETCHER, I. R. 2000. Deducing the ancestry of terranes: SHRIMP evidence for South America-derived Gondwana fragments in central Europe. *Geology*, **28**, 1035–1038.
- FRIEDL, G., FINGER, F., PAQUETTE, J. L., VON QUADT, A., MCNAUGHTON, N. J. & FLETCHER, I. R. 2004. Pre-Variscan geological events in the Austrian part of the Bohemian Massif deduced from U/Pb zircon ages. *International Journal of Earth Sciences*, **93**, 802–823.
- FRIEDL, G., COOKE, R., FINGER, F., MCNAUGHTON, N. & FLETCHER, I. 2011. Timing of Variscan HP–HT metamorphism in the Moldanubian Zone of the Bohemian Massif: U–Pb SHRIMP dating on multiply zoned zircons from a granulite from the Dunkelsteiner Wald Massif, Lower Austria. *Mineralogy and Petrology*, **102**, 63–75.
- FRITZ, H. & NEUBAUER, F. 1993. Kinematics of crustal stacking and dispersion in the south-eastern Bohemian Massif. *International Journal of Earth Sciences*, **82**, 556–565.
- FRITZ, H., DALLMEYER, R. D. & NEUBAUER, F. 1996. Thick-skinned versus thin-skinned thrusting: rheology controlled thrust propagation in the Variscan collisional belt (the southeastern Bohemian Massif, Czech Republic–Austria). *Tectonics*, **15**, 1389–1413.
- FUCHS, G. & MATURA, A. 1976. Zur Geologie des Kristallins der südlichen Böhmisches Masse. *Jahrbuch der Geologischen Bundesanstalt*, **119**, 1–43.
- FUSÁN, O., KODYM, O., MATĚJKA, A. & URBÁNEK, L. 1967. *Geological Map of Czechoslovakia 1:500,000*. Central Geological Survey, Prague.
- GERDES, A. 2001. Magma homogenization during anatexis, ascent and/or emplacement? Constraints from the Variscan Weinsberg granites. *Terra Nova*, **13**, 305–312.
- GERDES, A., WÖRNER, G. & FINGER, F. 2000a. Hybrids, magma mixing and enriched mantle melts in post-collisional Variscan granitoids: the Rastenberg Pluton, Austria. In: FRANKE, W., HAAK, V., ONCKEN, O. & TANNER, D. (eds) *Orogenic Processes: Quantification and Modelling in the Variscan Belt*. Geological Society, London, Special Publications, **179**, 415–431.
- GERDES, A., WÖRNER, G. & HENK, A. 2000b. Post-collisional granite generation and HT–LP metamorphism by radiogenic heating: the Variscan South Bohemian Batholith. *Journal of the Geological Society, London*, **157**, 577–587.
- GERDES, A., FRIEDL, G., PARRISH, R. R. & FINGER, F. 2003. High-resolution geochronology of Variscan granite emplacement – the South Bohemian Batholith. *Journal of the Czech Geological Society*, **48**, 53–54.
- GUY, A., EDEL, J. B., SCHULMANN, K., TOMEK, Č. & LEXA, O. 2011. A geophysical model of the Variscan orogenic root (Bohemian Massif): implications for modern collisional orogens. *Lithos*, **124**, 144–157.
- HAJNÁ, J., ŽÁK, J., KACHLÍK, V. & CHADIMA, M. 2010. Subduction-driven shortening and differential exhumation in a Cadomian accretionary wedge: the Teplá–Barrandian Unit, Bohemian Massif. *Precambrian Research*, **176**, 27–45.
- HAJNÁ, J., ŽÁK, J. & KACHLÍK, V. 2011. Structure and stratigraphy of the Teplá–Barrandian Neoproterozoic, Bohemian Massif: a new plate-tectonic reinterpretation. *Gondwana Research*, **19**, 495–508.
- HAJNÁ, J., ŽÁK, J., KACHLÍK, V. & CHADIMA, M. 2012. Deciphering the Variscan tectonothermal overprint and deformation partitioning in the Cadomian basement of the Teplá–Barrandian Unit, Bohemian Massif. *International Journal of Earth Sciences*, **101**, 1855–1873.
- HAMMER, J., EIDAM, J., RÖBER, B. & EHLING, C. 1999. Prä-variszischer und variszischer granitoider Magmatismus am NE-Rand des Böhmisches Massivs – Geochemie und Petrogenese. *Zeitschrift für Geologische Wissenschaften*, **27**, 401–415.
- HARTLEY, A. J. & OTAVA, J. 2001. Sediment provenance and dispersal in a deep marine foreland basin: the

- Lower Carboniferous Culm Basin, Czech Republic. *Journal of the Geological Society, London*, **158**, 137–150.
- HECHT, L., VIGNERESSE, J. L. & MORTEANI, G. 1997. Constraints on the origin of zonation of the granite complexes in the Fichtelgebirge (Germany and Czech Republic): evidence from a gravity and geochemical study. *Geologische Rundschau*, **86**, S93–S109.
- HENK, A., VON BLANCKENBURG, F., FINGER, F., SCHALTEGGER, U. & ZULAUF, G. 2000. Syn-convergent high-temperature metamorphism and magmatism in the Variscides: a discussion of potential heat sources. In: FRANKE, W., HAAK, V., ONCKEN, O. & TANNER, D. (eds) *Orogenic Processes: Quantification and Modelling in the Variscan Belt*. Geological Society, London, Special Publications, **179**, 387–399.
- HÖCK, V., MONTAG, O. & LEICHMANN, J. 1997. Ophiolite remnants at the eastern margin of the Bohemian Massif and their bearing on the tectonic evolution. *Mineralogy and Petrology*, **60**, 267–287.
- HOFMANN, M., LINNEMANN, U., GERDES, A. & ULLRICH, B. 2008. Closure of the Rheic Ocean and the final pulse of the Variscan Orogeny in the Bohemian Massif – timing of large-scale strike-slip processes and basement exhumation by LA-ICP-MS U–Pb zircon dating from the Elbe Zone (Saxo-Thuringian Zone, Germany). In: KÖNIGSHOF, P. & LINNEMANN, U. (eds) *From Gondwana and Laurussia to Pangaea: Dynamics of Oceans and Supercontinents*. Final Meeting of IGCP 497 and IGCP 499, 20th International Senckenberg-Conference & 2nd Geinitz-Conference, Abstracts and Programme, 53.
- HOFMANN, M., LINNEMANN, U., GERDES, A., ULLRICH, B. & SCHAUER, M. 2009. Timing of dextral strike-slip processes and basement exhumation in the Elbe Zone (Saxo-Thuringian Zone): the final pulse of the Variscan Orogeny in the Bohemian Massif constrained by LA-SF-ICP-MS U–Pb zircon data. In: MURPHY, J. B., KEPPIE, J. D. & HYNES, A. J. (eds) *Ancient Orogens and Modern Analogues*. Geological Society, London, Special Publications, **327**, 197–214.
- HOLUB, F. V. 1997. Ultrapotassic plutonic rocks of the durbachite series in the Bohemian Massif: petrology, geochemistry and petrogenetic interpretation. *Journal of Geological Sciences, Economic Geology, Mineralogy*, **31**, 5–26.
- HOLUB, F. V., KLEČKA, M. & MATĚJKA, D. 1995. Igneous activity. In: DALLMEYER, R. D., FRANKE, W. & WEBER, K. (eds) *Pre-Permian Geology of Central and Eastern Europe*. Springer Verlag, Berlin, 444–452.
- HOLUB, F. V., COCHÉRIE, A. & ROSSI, P. 1997a. Radiometric dating of granitic rocks from the Central Bohemian Plutonic Complex (Czech Republic): constraints on the chronology of thermal and tectonic events along the Moldanubian-Barrandian boundary. *Comptes Rendus de l'Académie de Sciences – Serie IIa: Sciences de la Terre et des Planètes*, **325**, 19–26.
- HOLUB, F. V., MACHART, J. & MANOVÁ, M. 1997b. The Central Bohemian Plutonic Complex: geology, chemical composition and genetic interpretation. *Journal of Geological Sciences, Economic Geology, Mineralogy*, **31**, 27–50.
- HOLUB, F. V., VERNER, K. & SCHMITZ, M. D. 2012. Temporal relations of melagranite porphyry dikes and durbachitic plutons in South Bohemia. *Geoscience Research Reports for 2011*, 23–25.
- HROUDA, F., TÁBORSKÁ, Š., SCHULMANN, K., JEŽEK, J. & DOLEJŠ, D. 1999. Magnetic fabric and rheology of co-mingled magmas in the Nasavrky Plutonic Complex (E Bohemia): implications for intrusive strain and emplacement mechanism. *Tectonophysics*, **307**, 98–111.
- JANOŮŠEK, V. & GERDES, A. 2003. Timing the magmatic activity within the Central Bohemian Pluton, Czech Republic: conventional U–Pb ages for the Sázava and Tábora intrusions and their geotectonic significance. *Journal of the Czech Geological Society*, **48**, 70–71.
- JANOŮŠEK, V. & HOLUB, F. V. 2007. The causal link between HP–HT metamorphism and ultrapotassic magmatism in collisional orogens: case study from the Moldanubian Zone of the Bohemian Massif. *Proceedings of the Geologists' Association*, **118**, 75–86.
- JANOŮŠEK, V., ROGERS, G. & BOWES, D. R. 1995. Sr–Nd isotopic constraints on the petrogenesis of the Central Bohemian Pluton, Czech Republic. *Geologische Rundschau*, **84**, 520–534.
- JANOŮŠEK, V., ROGERS, G., BOWES, D. R. & VAŇKOVÁ, V. 1997. Cryptic trace-element variation as an indicator of reverse zoning in a granitic pluton: the Říčany granite, Czech Republic. *Journal of the Geological Society, London*, **154**, 807–815.
- JANOŮŠEK, V., BOWES, D. R., ROGERS, G., FARROW, C. M. & JELÍNEK, E. 2000. Modelling diverse processes in the petrogenesis of a composite batholith: the Central Bohemian Pluton, Central European Hercynides. *Journal of Petrology*, **41**, 511–543.
- JANOŮŠEK, V., BRAITHWAITE, C. J. R., BOWES, D. R. & GERDES, A. 2004a. Magma-mixing in the genesis of Hercynian calc-alkaline granitoids: an integrated petrographic and geochemical study of the Sázava intrusion, Central Bohemian Pluton, Czech Republic. *Lithos*, **78**, 67–99.
- JANOŮŠEK, V., FINGER, F., ROBERTS, M. P., FRÝDA, J., PIN, C. & DOLEJŠ, D. 2004b. Deciphering the petrogenesis of deeply buried granites: whole-rock geochemical constraints on the origin of largely undepleted felsic granulites from the Moldanubian Zone of the Bohemian Massif. *Transactions of the Royal Society of Edinburgh, Earth Sciences*, **95**, 141–159.
- JANOŮŠEK, V., GERDES, A., VRÁNA, S., FINGER, F., ERBAN, V., FRIEDL, G. & BRAITHWAITE, C. J. R. 2006. Low-pressure granulites of the Lišov Massif, Southern Bohemia: Viséan metamorphism of Late Devonian plutonic arc rocks. *Journal of Petrology*, **47**, 705–744.
- JANOŮŠEK, V., VRÁNA, S., ERBAN, V., VOKURKA, K. & DRÁBEK, M. 2008. Metabasic rocks in the Varied Group of the Moldanubian Zone, southern Bohemia – their petrology, geochemical character and possible petrogenesis. *Journal of Geosciences*, **53**, 31–64.
- JANOŮŠEK, V., WIEGAND, B. & ŽÁK, J. 2010. Dating the onset of Variscan crustal exhumation in the core of the Bohemian Massif: new U–Pb single zircon ages from the high-K calc-alkaline granodiorites of the Blatná suite, Central Bohemian Plutonic Complex. *Journal of the Geological Society, London*, **167**, 347–360.
- JASTRZĘBSKI, M. 2009. A Variscan continental collision of the West Sudetes and the Brunovistulian Terrane: a

- contribution from structural and metamorphic record of the Stronie Formation, the Orlica–Śnieżnik Dome, SW Poland. *International Journal of Earth Sciences*, **98**, 1901–1923.
- JELÍNEK, E. & DUDEK, A. 1993. Geochemistry of the subsurface Precambrian plutonic rocks from the Brunovistulian Complex in the Bohemian Massif, Czechoslovakia. *Precambrian Research*, **62**, 103–125.
- KACHLÍK, V. 1993. The evidence for late Variscan nappe thrusting of the Mariánské Lázně Complex over the Saxothuringian Terrane (west Bohemia). *Journal of the Czech Geological Society*, **38**, 43–58.
- KACHLÍK, V. 1999. Relationship between Moldanubicum, the Kutná Hora Crystalline Unit and Bohemicum (Central Bohemia, Czech Republic): a result of poly-phase Variscan nappe tectonics. *Journal of the Czech Geological Society*, **44**, 201–291.
- KALT, A., BERGER, A. & BLÜMEL, P. 1999. Metamorphic evolution of cordierite-bearing migmatites from the Bayerische Wald (Variscan Belt, Germany). *Journal of Petrology*, **40**, 601–627.
- KALT, A., CORFU, F. & WILBRANS, J. R. 2000. Time calibration of a P–T path from a Variscan high-temperature low-pressure metamorphic complex (Bayerischer Wald, Germany), and the detection of inherited monazite. *Contributions to Mineralogy and Petrology*, **138**, 143–163.
- KALVODA, J., BÁBEK, O., FATKA, O., LEICHMANN, J., MELICHAR, R., NEHYBA, S. & ŠPAČEK, P. 2008. Brunovistulian Terrane (Bohemian Massif, Central Europe) from late Proterozoic to late Paleozoic: a review. *International Journal of Earth Sciences*, **97**, 497–518.
- KEMPE, U., WOLF, D., EBERMANN, U. & BOMBACH, K. 1999. 330 Ma Pb/Pb single zircon evaporation ages for the Altenberg Granite Porphyry, Eastern Erzgebirge (Germany): implications for Hercynian granite magmatism and tin mineralisation. *Zeitschrift für Geologische Wissenschaften*, **27**, 385–400.
- KEMPE, U., BOMBACH, K., SCHLOTHAUER, T., HUTSCHENREUTER, J., WOLF, D., MATUKOV, D. & SERGEEV, S. 2004. Pb/Pb and U/Pb zircon dating of subvolcanic rhyolite as a time marker for Hercynian granite magmatism and Sn mineralisation in the Eibensstock granite, Erzgebirge, Germany: considering effects of zircon alteration. *Mineralium Deposita*, **39**, 646–669.
- KLEČKA, M. & MATĚJKA, D. 1996. Moldanubian Batholith – an example of the evolution of the Late Palaeozoic granitoid magmatism in the Moldanubian Zone, Bohemian Massif (Central Europe). In: SRIVASTAVA, R. K. & CHANDRA, R. (eds) *Magmatism in Relation to Diverse Tectonic Settings*. Oxford & IBH Publishing Co., New Delhi, 353–373.
- KLEIN, T., KIEHM, S., SIEBEL, W., SHANG, C. K., ROHRMÜLLER, J., DÖRR, W. & ZULAUFG, G. 2008. Age and emplacement of late-Variscan granites of the western Bohemian Massif with main focus on the Hauzenberg granitoids (European Variscides, Germany). *Lithos*, **102**, 478–507.
- KLOMÍNSKÝ, J. 1963. Geology of the Čistá massif. *Journal of Geological Sciences, Geology*, **3**, 7–27.
- KLOMÍNSKÝ, J. 1965. The Štěnovice granodiorite massif. *Journal of Geological Sciences, Geology*, **8**, 75–98.
- KLOMÍNSKÝ, J. 1969. The Krkonoše–Jizera granitoid massif. *Journal of Geological Sciences, Geology*, **15**, 1–134.
- KLOMÍNSKÝ, J., SCHOVÁNEK, P., JARCHOVSKÝ, T., SULOVSÝ, P. & TOUŽIMSKÝ, M. 2007. Contact of the Tanvald and Liberec granites near Jablonec nad Nisou. *Geoscience Research Reports for 2006*, 24–29.
- KLÖTZLI, U. S. & PARRISH, R. R. 1996. Zircon U/Pb and Pb/Pb geochronology of the Rastenberg granodiorite, South Bohemian Massif, Austria. *Mineralogy and Petrology*, **58**, 197–214.
- KLÖTZLI, U. S., KOLLER, F., SCHARBERT, H. G. & HÖCK, V. 2001. Cadomian lower-crustal contributions to Variscan granite petrogenesis (South Bohemian Pluton, Austria): constraints from zircon topology and geochronology, whole-rock, and feldspar Pb–Sr isotope systematics. *Journal of Petrology*, **42**, 1621–1642.
- KONOPÁSEK, J. & SCHULMANN, K. 2005. Contrasting Early Carboniferous field geotherms: evidence for accretion of a thickened orogenic root and subducted Saxothuringian crust (Central European Variscides). *Journal of the Geological Society, London*, **162**, 463–470.
- KOPECKÝ, L., CHLUPÁČOVÁ, M., KLOMÍNSKÝ, J. & SOKOL, A. 1997. The Čistá–Jesenice pluton in western Bohemia: geochemistry, geology and ore potential. *Journal of Geological Sciences, Economic Geology, Mineralogy*, **31**, 97–127.
- KOŠLER, J. & FARROW, C. M. 1994. Mid-late Devonian arc-type magmatism in the Bohemian Massif: Sr and Nd isotope and trace element evidence from the Staré Sedlo and Mirovice gneiss complexes, Czech Republic. *Journal of the Czech Geological Society*, **39**, 56–58.
- KOŠLER, J., AFTALION, M. & BOWES, D. R. 1993. Mid-late Devonian plutonic activity in the Bohemian Massif: U–Pb zircon isotopic evidence from the Staré Sedlo and Mirovice gneiss complexes, Czech Republic. *Neues Jahrbuch für Mineralogie, Monatshefte*, **1993**, 417–431.
- KOŠLER, J., ROGERS, G., RODDICK, J. C. & BOWES, D. R. 1995. Temporal association of ductile deformation and granitic plutonism: Rb–Sr and ⁴⁰Ar–³⁹Ar evidence from roof pendants above the Central Bohemian Pluton, Czech Republic. *Journal of Geology*, **103**, 711–717.
- KOTKOVÁ, J., KRÖNER, A., TODT, W. & FIALA, J. 1995. Zircon dating of north Bohemian granulites, Czech Republic: further evidence for the Lower Carboniferous high-pressure event in the Bohemian Massif. *Geologische Rundschau*, **85**, 154–161.
- KOTKOVÁ, J., HARLEY, S. L. & FIŠERA, M. 1997. A vestige of very high-pressure (c. 28 kbar) metamorphism in the Variscan Bohemian Massif, Czech Republic. *European Journal of Mineralogy*, **9**, 1017–1033.
- KOTKOVÁ, J., GERDES, A., PARRISH, R. R. & NOVÁK, M. 2007. Clasts of Variscan high-grade rocks within Upper Visean conglomerates – constraints on exhumation history from petrology and U–Pb chronology. *Journal of Metamorphic Geology*, **25**, 781–801.
- KOTKOVÁ, J., SCHALTEGGER, U. & LEICHMANN, J. 2010. Two types of ultrapotassic plutonic rocks in the Bohemian Massif – coeval intrusions at different crustal levels. *Lithos*, **115**, 163–176.
- KOTKOVÁ, J., O'BRIEN, P. J. & ZIEMANN, M. A. 2011. Diamond and coesite discovered in Saxony-type

- granulite: solution to the Variscan garnet peridotite enigma. *Geology*, **39**, 667–670.
- KOVARÍKOVÁ, P., SIEBEL, W., JELÍNEK, E., ŠTEMPROK, M., KACHLÍK, V., HOLUB, F. V. & BLECHA, V. 2007. Petrology, geochemistry and zircon age for redwitzite at Abertamy, NW Bohemian Massif (Czech Republic): tracing the mantle component in Late Variscan intrusions. *Chemie der Erde – Geochemistry*, **67**, 151–174.
- KÖHLER, H. & HÖLZL, S. 1996. The age of the Leuchtenberg granite (NE Bavaria, Germany). A revision on account of new U–Pb zircon ages. *Neues Jahrbuch für Mineralogie, Monatshefte*, **5**, 212–222.
- KRETZ, R. 1983. Symbols for rock-forming minerals. *American Mineralogist*, **68**, 277–279.
- KRÖNER, A. & WILLNER, A. P. 1998. Time of formation and peak of Variscan HP–HT metamorphism of quartz-feldspar rocks in the Central Erzgebirge, Saxony, Germany. *Contributions to Mineralogy and Petrology*, **132**, 1–20.
- KRÖNER, A., WENDT, I. ET AL. 1988. U–Pb zircon and Sm–Nd model ages of high-grade Moldanubian metasediments, Bohemian Massif, Czechoslovakia. *Contributions to Mineralogy and Petrology*, **99**, 257–266.
- KRÖNER, A., HEGNER, E., HAMMER, J., HAASE, G., BIELICKI, K. H., KRAUSS, M. & EIDAM, J. 1994. Geochronology and Nd–Sr systematics of Lusatian granulites – significance for the evolution of the Variscan orogen in east-central Europe. *Geologische Rundschau*, **83**, 357–376.
- KRÖNER, A., WILLNER, A. P., HEGNER, E., FRISCHBUTTER, A., HOFMANN, J. & BERGNER, R. 1995. Latest Precambrian (Cadomian) zircon ages, Nd isotopic systematics and P–T evolution of granulitoid orthogneisses of the Erzgebirge, Saxony and Czech Republic. *Geologische Rundschau*, **84**, 437–456.
- KRÖNER, A., JAECKEL, P., REISCHMANN, T. & KRONER, U. 1998. Further evidence for an early Carboniferous (c. 340 Ma) age of high-grade metamorphism in the Saxonian granulite complex. *Geologische Rundschau*, **86**, 751–766.
- KRÖNER, A., O'BRIEN, P. J., NEMCHIN, A. A. & PIDGEON, R. T. 2000. Zircon ages for high pressure granulites from South Bohemia, Czech Republic, and their connection to Carboniferous high temperature processes. *Contributions to Mineralogy and Petrology*, **138**, 127–142.
- KRÖNER, A., JAECKEL, P., HEGNER, E. & OPLETAL, M. 2001. Single zircon ages and whole rock Nd isotopic systematics of early Palaeozoic granulitoid gneisses from the Czech and Polish Sudetes (Jizerské hory, Krkonoše Mountains and Orlice–Sněžník Complex). *International Journal of Earth Sciences*, **90**, 304–324.
- KRONER, U. & ROMER, R. L. 2013. Two plates – many subduction zones: the Variscan orogeny reconsidered. *Gondwana Research*, **24**, 298–329.
- KRYZA, R., CROWLEY, Q. G., LARIONOV, A., PIN, C., OBERC-DZIEDZIC, T. & MOCHNACKA, K. 2012. Chemical abrasion applied to SHRIMP zircon geochronology: an example from the Variscan Karkonosze Granite (Sudetes, SW Poland). *Gondwana Research*, **21**, 757–767.
- KUSIAK, M. A., SUZUKI, K., DUNKLEY, D. J., LEKKI, J., BAKUN-CZUBAROW, N., PASZKOWSKI, M. & BUDZYŃ, B. 2008. EPMA and PIXE dating of monazite in granulites from Stary Gieraltów, NE Bohemian Massif, Poland. *Gondwana Research*, **14**, 675–685.
- KUSIAK, M. A., DUNKLEY, D. J., SŁABY, E., MARTIN, H. & BUDZYŃ, B. 2009. Sensitive high-resolution ion microprobe analysis of zircon reequilibrated by late magmatic fluids in a hybridized pluton. *Geology*, **37**, 1063–1066.
- KUSIAK, M. A., DUNKLEY, D. J., SUZUKI, K., KACHLÍK, V., KEDZIOR, A., LEKKI, J. & OPLUŠTIL, S. 2010. Chemical (non-isotopic) and isotopic dating of Phanerozoic zircon – a case study of durbachite from the Třebíč Pluton, Bohemian Massif. *Gondwana Research*, **17**, 153–161.
- LEICHMANN, J. & HÖCK, V. 2008. The Brno Batholith: an insight into the magmatic and metamorphic evolution of the Cadomian Brunovistulian Unit, eastern margin of the Bohemian Massif. *Journal of Geosciences*, **53**, 281–305.
- LEXA, O., SCHULMANN, K., JANOUŠEK, V., ŠTÍPŠKÁ, P., GUY, A. & RACEK, M. 2011. Heat sources and trigger mechanisms of exhumation of HP granulites in Variscan orogenic root. *Journal of Metamorphic Geology*, **29**, 79–102.
- LIEW, T. C., FINGER, F. & HÖCK, V. 1989. The Moldanubian granulitoid plutons in Austria: chemical and isotopic studies bearing on their environmental setting. *Chemical Geology*, **76**, 41–55.
- LINNEMANN, U. & ROMER, R. L. 2002. The Cadomian Orogeny in Saxo-Thuringia, Germany: geochemical and Nd–Sr–Pb isotopic characterization of marginal basins with constraints to geotectonic setting and provenance. *Tectonophysics*, **352**, 33–64.
- LINNEMANN, U., GEHLICH, M. ET AL. 2000. From Cadomian subduction to Early Palaeozoic rifting: the evolution of Saxo-Thuringia at the margin of Gondwana in the light of single zircon geochronology and basin development (Central European Variscides, Germany). In: FRANKE, W., HAAK, V., ONCKEN, O. & TANNER, D. (eds) *Orogenic Processes: Quantification and Modelling in the Variscan Belt*. Geological Society, London, Special Publications, **179**, 131–153.
- LINNEMANN, U., MCNAUGHTON, N. J., ROMER, R. L., GEHLICH, M., DROST, K. & TONK, C. 2004. West African provenance for Saxo-Thuringia (Bohemian Massif): did Armorica ever leave pre-Pangean Gondwana? U/Pb-SHRIMP zircon evidence and the Nd-isotopic record. *International Journal of Earth Sciences*, **93**, 683–705.
- LINNEMANN, U., PEREIRA, F., JEFFRIES, T. E., DROST, K. & GERDE, A. 2008. The Cadomian orogeny and the opening of the Rheic Ocean: the diachrony of geotectonic processes constrained by LA-ICP-MS U–Pb zircon dating (Ossa-Morena and Saxo-Thuringian Zones, Iberian and Bohemian massifs). *Tectonophysics*, **461**, 21–43.
- LINNER, M. 1996. Metamorphism and partial melting of paragneisses of the Monotonous Group, SE Moldanubicum (Austria). *Mineralogy and Petrology*, **58**, 215–234.
- MACHEK, M., ULRICH, S. & JANOUŠEK, V. 2009. Strain coupling between upper mantle and lower crust: natural example from the Běstvína granulite body,

- Bohemian Massif. *Journal of Metamorphic Geology*, **27**, 721–737.
- MACHOWIAK, K. & ARMSTRONG, R. 2007. SHRIMP U–Pb zircon age from the Karkonosze granite. *Mineralogica Polonica Special Papers*, **31**, 193–196.
- MAIEROVÁ, P., ČADEK, O., LEXA, O. & SCHULMANN, K. 2012. A numerical model of exhumation of the orogenic lower crust in the Bohemian Massif during the Variscan orogeny. *Studia Geophysica et Geodaetica*, **56**, 595–619.
- MALUSKI, H. & PATOČKA, F. 1997. Geochemistry and $^{40}\text{Ar}/^{39}\text{Ar}$ geochronology of the mafic metavolcanic rocks from the Rýchorý Mountains complex (west Sudetes, Bohemian Massif): palaeotectonic significance. *Geological Magazine*, **134**, 703–716.
- MARHEINE, D., MALUSKI, H., KACHLÍK, V., PATOČKA, F. & ŽELAŽNIEWICZ, A. 2002. The $^{40}\text{Ar}/^{39}\text{Ar}$ ages from the West Sudetes (NE Bohemian Massif): constraints on the Variscan polyphase tectonothermal development. In: WINCHESTER, J. A., PHAROAH, T. C. & VERNIERS, J. (eds) *Palaeozoic Amalgamation of Central Europe*. Geological Society, London, Special Publications, **201**, 133–155.
- MARTÍNEZ CATALÁN, J. R. 2011. Are the oroclinal belts of the Variscan belt related to late Variscan strike-slip tectonics? *Terra Nova*, **23**, 241–247.
- MARTÍNEZ CATALÁN, J. R. 2012. The Central Iberian arc, an orocline centered in the Iberian Massif and some implications for the Variscan belt. *International Journal of Earth Sciences*, **101**, 1299–1314.
- MASSONNE, H. J. 2001. First find of coesite in the ultrahigh-pressure metamorphic area of the central Erzgebirge, Germany. *European Journal of Mineralogy*, **13**, 565–570.
- MATTE, P. 1986. Tectonics and plate tectonics model for the Variscan belt of Europe. *Tectonophysics*, **126**, 329–374.
- MATTE, P. 1991. Accretionary history and crustal evolution of the Variscan belt in Western Europe. *Tectonophysics*, **196**, 309–337.
- MATTE, P. 2001. The Variscan collage and orogeny (480–290 Ma) and the tectonic definition of the Armorica microplate: a review. *Terra Nova*, **13**, 122–128.
- MATTE, P., MALUSKI, H., RAJLICH, P. & FRANKE, W. 1990. Terrane boundaries in the Bohemian Massif: result of large-scale Variscan shearing. *Tectonophysics*, **177**, 151–170.
- MAZUR, S. & ALEXANDROWSKI, P. 2001. The Tepla(?) / Saxothuringian suture in the Karkonosze–Izera Massif, western Sudetes, central European Variscides. *International Journal of Earth Sciences*, **90**, 341–360.
- MAZUR, S., ALEKSANDROWSKI, P., KRYZA, R. & OBERCZIEDZIC, T. 2006. The Variscan Orogen in Poland. *Geological Quarterly*, **50**, 89–118.
- MAZUR, S., ALEKSANDROWSKI, P., TURNIAK, K. & AWDANKIEWICZ, M. 2007. Geology, tectonic evolution and Late Palaeozoic magmatism of Sudetes – an overview. In: KOZŁOWSKI, A. & WISZNIEWSKA, J. (eds) *Granitoids in Poland*. Archivum Mineralogiae Monograph, **1**, Warsaw University and the Polish Academy of Sciences, Warsaw, 59–87.
- MEDARIS, L. G., WANG, H., JELÍNEK, E., MIHALJEVIČ, M. & JAKEŠ, P. 2005. Characteristics and origins of diverse Variscan peridotites in the Gföhl Nappe, Bohemian Massif, Czech Republic. *Lithos*, **82**, 1–23.
- MEDARIS, L. G., BEARD, B. L. & JELÍNEK, E. 2006. Mantle-derived, UHP garnet pyroxenite and eclogite in the Moldanubian Gföhl nappe, Bohemian Massif: a geochemical review, new P–T determinations, and tectonic interpretation. *International Geology Review*, **48**, 765–777.
- MIERZEJEWSKI, M. P. 2002. Additional data and remarks to Hans Cloos' work in the Karkonosze Mts (Riesengebirge). *Zeitschrift der Geologischen Wissenschaften*, **30**, 37–48.
- MIKULSKI, S. Z., WILLIAMS, I. S. & BAGIŃSKI, B. 2013. Early Carboniferous (Viséan) emplacement of the collisional Klodzko–Złoty Stok granulitoids (Sudetes, SW Poland): constraints from geochemical data and zircon U–Pb ages. *International Journal of Earth Sciences*, **102**, 1007–1027.
- MÍŠAŘ, Z. 1994. Terranes of eastern Bohemian Massif: tectonostratigraphic and lithological units of the Moravicum and Moldanubicum. *Journal of the Czech Geological Society*, **39**, 71–73.
- MUELLER, H. J. & MASSONNE, H. J. 2001. Experimental high pressure investigation of partial melting in natural rocks and their influence on V_p and V_s . *Physics and Chemistry of the Earth, Part A: Solid Earth and Geodesy*, **26**, 325–332.
- MURPHY, J. B. & NANCE, R. D. 2002. Sm–Nd isotopic systematics as tectonic tracers: an example from West Avalonia in the Canadian Appalachians. *Earth-Science Reviews*, **59**, 77–100.
- NAEMURA, K., HIRAJIMA, T. & SVOJTKA, M. 2009. The pressure–temperature path and the origin of phlogopite in spinel–garnet peridotites from the Blanský les Massif of the Moldanubian Zone, Czech Republic. *Journal of Petrology*, **50**, 1795–1827.
- NAEMURA, K., IKUTA, D. ET AL. 2011. Diamond and other possible ultradeep evidence discovered in the orogenic spinel–garnet peridotite from the Moldanubian Zone of the Bohemian Massif, Czech Republic. In: DOBRZHINETSAYA, L. F., FARYAD, S. W., WALLIS, S. & CUTHBERT, S. (eds) *Ultrahigh-Pressure Metamorphism: 25 Years after the Discovery of Coesite and Diamond*. Elsevier, Amsterdam, 78–111.
- NAKAMURA, D., SVOJTKA, M., NAEMURA, K. & HIRAJIMA, T. 2004. Very high-pressure (>4 GPa) eclogite associated with the Moldanubian Zone garnet peridotite (Nové Dvory, Czech Republic). *Journal of Metamorphic Geology*, **22**, 593–603.
- NANCE, R. D. & LINNEMANN, U. 2008. The Rheic Ocean: origin, evolution, and significance. *GSA Today*, **18**, 4–12.
- NANCE, R. D., GUTIÉRREZ-ALONSO, G. ET AL. 2010. Evolution of the Rheic Ocean. *Gondwana Research*, **17**, 194–222.
- NANCE, R. D., GUTIÉRREZ-ALONSO, G. ET AL. 2012. A brief history of the Rheic Ocean. *Geoscience Frontiers*, **3**, 125–135.
- NASDALA, L., WENZEL, T., PIDGEON, R. T. & KRONZ, A. 1999. Internal structures and dating of complex zircons from Meissen Massif monzonites, Saxony. *Chemical Geology*, **156**, 331–341.
- NOWAK, I., ŽELAŽNIEWICZ, A., DÖRR, W., FRANKE, W. & LARIONOV, A. N. 2011. The Izera metabasites, West

- Sudetes, Poland: geologic and isotopic U–Pb zircon evidence of Devonian extension in the Saxothuringian Terrane. *Lithos*, **126**, 435–454.
- O'BRIEN, P. J. 2000. The fundamental Variscan problem: high-temperature metamorphism at different depths and high-pressure metamorphism at different temperatures. In: FRANKE, W., HAAK, V., ONCKEN, O. & TANNER, D. (eds) *Orogenic Processes: Quantification and Modelling in the Variscan Belt*. Geological Society, London, Special Publications, **179**, 369–386.
- O'BRIEN, P. J. & RÖTZLER, J. 2003. High-pressure granulites: formation, recovery of peak conditions and implications for tectonics. *Journal of Metamorphic Geology*, **21**, 3–20.
- OBERC-DZIEDZIC, T., KRYZA, R., KLIMAS, K., FANNING, M. C. & MADEJ, S. 2005a. Gneiss protolith ages and tectonic boundaries in the NE part of the Bohemian Massif (Fore-Sudetic Block, SW Poland). *Geological Quarterly*, **49**, 363–378.
- OBERC-DZIEDZIC, T., PIN, C. & KRYZA, R. 2005b. Early Palaeozoic crustal melting in an extensional setting: petrological and Sm–Nd evidence from the Iżera granite-gneisses, Polish Sudetes. *International Journal of Earth Sciences*, **94**, 354–368.
- OBERC-DZIEDZIC, T., KRYZA, R., PIN, C. & MADEJ, S. 2013. Sequential granite emplacement: a structural study of the late Variscan Strzelin intrusion, SW Poland. *International Journal of Earth Sciences*, **102**, 1289–1304.
- OLIVER, G. J. H., CORFU, F. & KROGH, T. E. 1993. U–Pb ages from SW Poland: evidence for a Caledonian suture zone between Baltica and Gondwana. *Journal of the Geological Society, London*, **150**, 355–369.
- PALIVCOVÁ, M. 1984. Basic series of an 'Andinotype' batholithic association in the Variscan Central Bohemian Pluton. *Geologica Carpathica*, **35**, 39–60.
- PARRY, M., ŠTÍPSKÁ, P., SCHULMANN, K., HROUDA, F., JEŽEK, J. & KRÖNER, A. 1997. Tonalite sill emplacement at an oblique plate boundary: northeastern margin of the Bohemian Massif. *Tectonophysics*, **280**, 61–81.
- PATOČKA, F. & SMULIKOWSKI, W. 2000. Early Palaeozoic intracontinental rifting and incipient oceanic spreading in the Czech/Polish East Krkonoše/Karkonosze Complex, West Sudetes (NE Bohemian Massif). *Geologia Suetica*, **33**, 1–15.
- PERTOLDOVÁ, J., VERNER, K., VRÁNA, S., BURIÁNEK, D., ŠTĚDRÁ, V. & VONDROVIC, L. 2010. Comparison of lithology and tectonometamorphic evolution of units at the northern margin of the Moldanubian Zone: implications for geodynamic evolution in the northeastern part of the Bohemian Massif. *Journal of Geosciences*, **55**, 299–319.
- PETRAKAKIS, K. 1997. Evolution of Moldanubian rocks in Austria: review and synthesis. *Journal of Metamorphic Geology*, **15**, 203–222.
- PEUCKER-EHRENBRINK, B. & BEHR, H. J. 1993. Chemistry of hydrothermal quartz in the post-Variscan 'Bavarian Pfahl' system, F.R. Germany. *Chemical Geology*, **103**, 85–102.
- PHARAOH, T. C. 1999. Palaeozoic terranes and their lithospheric boundaries within the Trans-European Suture Zone (TESZ): a review. *Tectonophysics*, **314**, 17–41.
- PIETRANIK, A., STOREY, C. & KIERCZAK, J. 2013. The Niemcza diorites and monzodiorites (Sudetes, SW Poland): a record of changing geotectonic setting at ca. 340 Ma. *Geological Quarterly*, **57**, 325–334.
- PIN, C. 1990. Variscan oceans: ages, origins and geodynamic implications inferred from geochemical and radiometric data. *Tectonophysics*, **177**, 215–227.
- PIN, C. & MARINI, F. 1993. Early Ordovician continental break-up in Variscan Europe: Nd–Sr isotope and trace element evidence from bimodal igneous associations of the Southern Massif Central, France. *Lithos*, **29**, 177–196.
- PIN, C., MIERZEJEWSKI, M. & DUTHOU, J. L. 1987. Rb–Sr isochron age of the Karkonosze granite from the Sklarska Poreba Huta quarry and the determination of initial $^{87}\text{Sr}/^{86}\text{Sr}$ ratio in this granite. *Przegląd Geologiczny*, **10**, 512–517.
- PITRA, P. 2012. Emplacement, structural and P–T evolution of the ~346 Ma Mifetín Pluton (eastern Teplá–Barrandian Zone, Bohemian Massif): implications for regional transpressional tectonics – Discussion. *Journal of Geosciences*, **57**, 189–191.
- PITRA, P., BURG, J. P., SCHULMANN, K. & LEDRU, P. 1994. Late orogenic extension in the Bohemian Massif: petrostructural evidence in the Hlinsko region. *Geodynamica Acta*, **7**, 15–30.
- PITRA, P., BURG, J. P. & GUIRAUD, M. 1999. Late Variscan strike-slip tectonics between the Teplá–Barrandian and Moldanubian terranes (Czech Bohemian Massif). *Journal of the Geological Society, London*, **156**, 1003–1020.
- PLOMEROVÁ, J., VECSEY, L., BABUŠKA, V., GRANET, M. & ACHAUER, U. 2005. Passive seismic experiment mosaic – a pilot study of mantle lithosphere anisotropy of the Bohemian Massif. *Studia Geophysica et Geodaetica*, **49**, 541–560.
- PRINCE, C. I., KOŠLER, J., VANCE, D. & GÜNTHER, D. 2000. Comparison of laser ablation ICP-MS and isotope dilution REE analyses – implications for Sm–Nd garnet geochronology. *Chemical Geology*, **168**, 255–274.
- PROPACH, G., BAUMANN, A., SCHULZ-SCHMALSCHLAGER, M. & GRAUERT, B. 2000. Zircon and monazite U–Pb ages of Variscan granitoid rocks and gneisses in the Moldanubian Zone of eastern Bavaria, Germany. *Neues Jahrbuch für Geologie und Paläontologie, Monatshefte*, **6**, 345–377.
- RACEK, M., ŠTÍPSKÁ, P., PITRA, P., SCHULMANN, K. & LEXA, O. 2006. Metamorphic record of burial and exhumation of orogenic lower and middle crust: a new tectonothermal model for the Drosendorf Window (Bohemian Massif, Austria). *Mineralogy and Petrology*, **86**, 221–251.
- RAJLICH, P. 1987. Variszische duktile Tektonik im Böhmischem Massiv. *Geologische Rundschau*, **76**, 755–786.
- RAJLICH, P. 1988. Variscan shearing kinematics in the Bohemian Massif: Moldanubian and Moravo–Silesian junction. *Acta Universitatis Carolinae, Geologica*, **1988**, 387–400.
- ROMER, R. L., THOMAS, R., STEIN, H. J. & RHEDE, D. 2007. Dating multiply overprinted Sn-mineralized

- granites – examples from the Erzgebirge, Germany. *Mineralium Deposita*, **42**, 337–359.
- ROMER, R. L., FÖRSTER, H. J. & ŠTEMPROK, M. 2010. Age constraints for the late-Variscan magmatism in the Altenberg–Teplce Caldera (Eastern Erzgebirge/Krušné hory). *Neues Jahrbuch für Mineralogie, Abhandlungen*, **187**, 289–305.
- RÖTZLER, J. & ROMER, R. L. 2001. P–T–t evolution of ultrahigh-temperature granulites from the Saxon Granulite Massif, Germany. Part I: petrology. *Journal of Petrology*, **42**, 1995–2013.
- SCHÄFER, J., NEUROTH, H., AHRENDT, H., DÖRR, W. & FRANKE, W. 1997. Accretion and exhumation at a Variscan active margin, recorded in the Saxothuringian flysch. *Geologische Rundschau*, **86**, 599–611.
- SCHARBERT, S., BREITER, K. & FRANK, W. 1997. The cooling history of the southern Bohemian Massif. *Journal of the Czech Geological Society*, **42**, 24.
- SHECKE, M., BAYER, U., OTTO, V., LAMARCHE, J., BANKA, D. & PHARAOH, T. 2002. The Elbe Fault System in North Central Europe – a basement controlled zone of crustal weakness. *Tectonophysics*, **360**, 281–299.
- SCHUEVENS, D. & ZULAU, G. 2000. Exhumation, strain localization, and emplacement of granulites along the western part of the Central Bohemian shear zone (Bohemian Massif). *International Journal of Earth Sciences*, **89**, 617–630.
- SCHMÄDICKE, E. 1991. Quartz pseudomorphs after coesite in eclogites from the Saxonian Erzgebirge. *European Journal of Mineralogy*, **3**, 231–238.
- SCHMÄDICKE, E., GOSE, J. & WILL, T. M. 2010. The P–T evolution of ultra high temperature garnet-bearing ultramafic rocks from the Saxonian Granulitgebirge Core Complex, Bohemian Massif. *Journal of Metamorphic Geology*, **28**, 489–508.
- SCHULMANN, K. & GAYER, R. 2000. A model for continental accretionary wedge developed by oblique collision: the NE Bohemian Massif. *Journal of the Geological Society, London*, **157**, 401–416.
- SCHULMANN, K., LEDRU, P., AUTRAN, A., MELKA, R., LARDEAUX, J. M., URBAN, M. & LOBKOWICZ, M. 1991. Evolution of nappes in the eastern margin of the Bohemian Massif: a kinematic interpretation. *Geologische Rundschau*, **80**, 73–92.
- SCHULMANN, K., KRÖNER, A., HEGNER, E., WENDT, I., KONOPÁSEK, J., LEXA, O. & ŠTÍPSKÁ, P. 2005. Chronological constraints on the pre-orogenic history, burial and exhumation of deep-seated rocks along the eastern margin of the Variscan orogen, Bohemian Massif, Czech Republic. *American Journal of Science*, **305**, 407–448.
- SCHULMANN, K., LEXA, O. ET AL. 2008. Vertical extrusion and horizontal channel flow of orogenic lower crust: key exhumation mechanisms in large hot orogens? *Journal of Metamorphic Geology*, **26**, 273–297.
- SCHULMANN, K., KONOPÁSEK, J. ET AL. 2009. An Andean type Palaeozoic convergence in the Bohemian Massif. *Comptes Rendus Geoscience*, **341**, 266–286.
- SIEBEL, W., TRZEBSKI, R., STETTNER, G., HECHT, L., CASTEN, U., HÖHNDORF, A. & MÜLLER, P. 1997. Granitoid magmatism of the NW Bohemian Massif revealed: gravity data, composition, age relations and phase concept. *Geologische Rundschau*, **86**, S45–S63.
- SIEBEL, W., CHEN, F. & SATIR, M. 2003. Late-Variscan magmatism revisited: new implications from Pb–evaporation zircon ages on the emplacement of redwitzites and granites in NE Bavaria. *International Journal of Earth Sciences*, **92**, 36–53.
- SIEBEL, W., BLAHA, U., CHEN, F. & ROHRMÜLLER, J. 2005. Geochronology and geochemistry of a dyke-host rock association and implications for the formation of the Bavarian Pfahl shear zone, Bohemian Massif. *International Journal of Earth Sciences*, **94**, 8–23.
- SIEBEL, W., HANN, H. P., SHANG, C. K., ROHRMÜLLER, J. & CHEN, F. 2006a. Coeval late-Variscan emplacement of granitic rocks: an example from the Regensburg Forest, NE Bavaria. *Neues Jahrbuch für Mineralogie, Abhandlungen*, **183**, 13–26.
- SIEBEL, W., THIEL, M. & CHEN, F. 2006b. Zircon geochronology and compositional record of late- to post-kinematic granulites associated with the Bavarian Pfahl zone (Bavarian Forest). *Mineralogy and Petrology*, **8**, 45–62.
- SIEBEL, W., SHANG, C. K., REITTER, E., ROHRMÜLLER, J. & BREITER, K. 2008. Two distinctive granite suites in the SW Bohemian Massif and their record of emplacement: constraints from geochemistry and zircon $^{207}\text{Pb}/^{206}\text{Pb}$ chronology. *Journal of Petrology*, **49**, 1853–1872.
- SIEBEL, W., SHANG, C. K., REITTER, E., ROHRMÜLLER, J. & BREITER, K. 2009. Two distinctive granite suites in the southwestern Bohemian Massif: reply to F. Finger and M. René. *Journal of Petrology*, **50**, 595–599.
- SIEBEL, W., HANN, H. ET AL. 2010. Age constraints on faulting and fault reactivation: a multi-chronological approach. *International Journal of Earth Sciences*, **99**, 1187–1197.
- SŁABY, E. & MARTIN, H. 2008. Mafic and felsic magma interaction in granites: the Hercynian Karkonosze Pluton (Sudetes, Bohemian Massif). *Journal of Petrology*, **49**, 353–391.
- SLÁMA, J., DUNKLEY, D. J., KACHLÍK, V. & KUSIAK, M. A. 2008a. Transition from island-arc to passive setting on the continental margin of Gondwana: U–Pb zircon dating of Neoproterozoic metaconglomerates from the SE margin of the Teplá–Barrandian Unit, Bohemian Massif. *Tectonophysics*, **461**, 44–59.
- SLÁMA, J., KOŠLER, J. ET AL. 2008b. Plešovice zircon – a new natural reference material for U–Pb and Hf isotopic microanalysis. *Chemical Geology*, **249**, 1–35.
- SMULIKOWSKI, W. 1995. Evidence of glaucophane-schist facies metamorphism in the East Karkonosze Complex, West Sudetes, Poland. *Geologische Rundschau*, **84**, 720–737.
- SOEJONO, I., ŽÁČKOVÁ, E., JANOUŠEK, V., MACHEK, M. & KOŠLER, J. 2010. Vestige of an Early Cambrian incipient oceanic crust incorporated in the Variscan orogen: Letovice Complex, Bohemian Massif. *Journal of the Geological Society, London*, **167**, 1113–1130.
- ŠTEMPROK, M., HOLUB, F. V. & NOVÁK, J. 2003. Multiple magmatic pulses of the Eastern Volcano-Plutonic Complex, Krušné hory/Erzgebirge batholith, and their phosphorus contents. *Bulletin of Geosciences*, **78**, 277–296.

- ŠTÍPSKÁ, P. & SCHULMANN, K. 1995. Inverted metamorphic zonation in a basement-derived nappe sequence, eastern margin of the Bohemian Massif. *Geological Journal*, **30**, 385–413.
- ŠTÍPSKÁ, P., SCHULMANN, K. & KRÖNER, A. 2004. Vertical extrusion and middle crustal spreading of omphacite granulite: a model of syn-convergent exhumation (Bohemian Massif, Czech Republic). *Journal of Metamorphic Geology*, **22**, 179–198.
- STRNAD, L. & MIHALJEVIČ, M. 2005. Sedimentary provenance of Mid-Devonian clastic sediments in the Teplá–Barrandian Unit (Bohemian Massif): U–Pb and Pb–Pb geochronology of detrital zircons by laser ablation ICP-MS. *Mineralogy and Petrology*, **84**, 47–68.
- SUCHÝ, V., ROZKOŠNÝ, I., ŽÁK, K. & FRANČŮ, J. 1996. Epigenetic dolomitization of the Pířdolí formation (Upper Silurian), the Barrandian basin, Czech Republic: implications for burial history of the Lower Paleozoic strata. *Geologische Rundschau*, **85**, 264–277.
- SUCHÝ, V., SÝKOROVÁ, I., MELKA, K., FILIP, J. & MACHOVIČ, V. 2007. Illite ‘crystallinity’, maturation of organic matter and microstructural development associated with lowest-grade metamorphism of Neoproterozoic sediments in the Teplá–Barrandian unit, Czech Republic. *Clay Minerals*, **42**, 503–526.
- SUESS, F. E. 1912. Die moravische Fenster und ihre Beziehung zum Grundgebirge des Hohen Gesenkes. *Denkschriften Österreichische Akademie der Wissenschaften, Mathematisch-naturwissenschaftliche Klasse*, **88**, 541–631.
- SYNEK, J. & OLIVERIOVÁ, D. 1993. Terrane character of the north-east margin of the Moldanubian Zone: the Kutná Hora Crystalline Complex, Bohemian Massif. *Geologische Rundschau*, **82**, 566–582.
- TAJČMANOVÁ, L., SOEJONO, I., KONOPÁSEK, J., KOŠLER, J. & KLÖTZLI, U. 2010. Structural position of high-pressure felsic to intermediate granulites from NE Moldanubian domain (Bohemian Massif). *Journal of the Geological Society, London*, **167**, 329–345.
- TICHOMIROVA, M. 1997. $^{207}\text{Pb}/^{206}\text{Pb}$ -Einzelzircondatierungen zur Bestimmung des Intrusionsalters des Niederbobritzcher Granites. *Terra Nostra*, **8**, 183–184.
- TICHOMIROVA, M. & LEONHARDT, D. 2010. New age determinations (Pb/Pb zircon evaporation, Rb/Sr) on the granites from Aue-Schwarzenberg and Eibenstock, Western Erzgebirge, Germany. *Zeitschrift für Geologische Wissenschaften*, **38**, 99–123.
- TICHOMIROVA, M., SERGEEV, S. A., BERGER, H. J. & LEONHARDT, D. 2012. Inferring protoliths of high-grade metamorphic gneisses of the Erzgebirge using zirconology, geochemistry and comparison with lower-grade rocks from Lusatia (Saxothuringia, Germany). *Contributions to Mineralogy and Petrology*, **164**, 375–396.
- TIMMERMANN, H., ŠTĚDRÁ, V., GERDES, A., NOBLE, S. R., PARRISH, R. R. & DÖRR, W. 2004. The problem of dating high-pressure metamorphism: a U–Pb isotope and geochemical study on eclogites and related rocks of the Mariánské Lázně Complex, Czech Republic. *Journal of Petrology*, **45**, 1311–1338.
- TOLLMANN, A. 1982. Großräumiger variszischer Deckenbau im Moldanubikum und neue Gedanken zum Variszikum Europas. *Geotektonische Forschungen*, **64**, 1–91.
- TOLLMANN, A. 1995. Das Ausmass des variszischer Deckbaues im Moldanubikum. *Krystalinikum*, **18**, 117–132.
- TOMEK, F. 2011. *The Late Devonian to Early Carboniferous kinematic evolution of the Teplá–Barrandian/Moldanubian boundary*. Diploma thesis, Charles University in Prague.
- TOMEK, F. & ŽÁK, J. 2011. The Late Devonian to early Carboniferous kinematic evolution of the Teplá–Barrandian/Moldanubian boundary. In: *Proceedings of the 2nd Congress of the Czech and Slovak Geological Societies*, Czech Geological Society, Prague, 94.
- TROPPEL, P., DEIBL, I., FINGER, F. & KAINDL, R. 2006. P–T–t evolution of spinel–cordierite–garnet gneisses from the Sauwald Zone (Southern Bohemian Massif, Upper Austria): is there evidence for two independent late-Variscan low-P/high-T events in the Moldanubian Unit? *International Journal of Earth Sciences*, **95**, 1019–1037.
- TRUBAČ, J., ŽÁK, J., CHLUPÁČOVÁ, M. & JANOUŠEK, V. 2009. Magnetic fabric of the Řičany granite, Bohemian Massif: a record of helical magma flow? *Journal of Volcanology and Geothermal Research*, **181**, 25–34.
- TRUBAČ, J., JANOUŠEK, V., ŽÁK, J. & GERDES, A. 2013. Geochemistry and petrogenesis of a nested granite intrusion – the Sedmihof composite Stock (Bohemian Massif). *Mineralogical Magazine*, **77**, 2360.
- TURNAU, E., ZELAŹNIEWICZ, A. & FRANKE, W. 2002. Middle to early late Viséan onset of late orogenic sedimentation in the Intra-Sudetic Basin, West Sudetes: miospore evidence and tectonic implication. *Geologia Sudetica*, **34**, 9–16.
- TURNIAK, K. & BRÖCKER, M. 2002. Age of the two-mica granite from the Strzegom–Sobótka Massif: new data from U/Pb monazite and xenotime study. *Mineralogical Society of Poland – Special Papers*, **20**, 211–213.
- TURNIAK, K., TICHOMIROVA, M. & BOMBACH, K. 2005. Zircon Pb–evaporation ages of granitoids from the Strzegom–Sobótka Massif (SW Poland). *Mineralogical Society of Poland – Special Papers*, **25**, 241–245.
- TURNIAK, K., TICHOMIROVA, M. & BOMBACH, K. 2006. Pb–evaporation zircon ages of post-tectonic granitoids from the Strzelin Massif (SW Poland). *Mineralogia Polonica – Special Papers*, **29**, 212–215.
- VAN BREEMEN, O., AFTALION, M., BOWES, D. R., DUDEK, A., MÍSAŘ, Z., POVONDRÁ, P. & VRÁNA, S. 1982. Geochronological studies of the Bohemian Massif, Czechoslovakia, and their significance in the evolution of Central Europe. *Transactions of the Royal Society of Edinburgh, Earth Sciences*, **73**, 89–108.
- VELLMER, C. & WEDEPOHL, K. H. 1994. Geochemical characterization and origin of granitoids from the South Bohemian Batholith in Lower Austria. *Contributions to Mineralogy and Petrology*, **118**, 13–32.
- VENERA, Z., SCHULMANN, K. & KRÖNER, A. 2000. Intrusion within a transensional tectonic domain: the Čistá granodiorite (Bohemian Massif) – structure and rheological modelling. *Journal of Structural Geology*, **22**, 1437–1454.
- VERNER, K., ŽÁK, J., HROUDA, F. & HOLUB, F. V. 2006. Magma emplacement during exhumation of the

- lower- to mid-crustal orogenic root: the Jihlava syenitoid pluton, Moldanubian Unit, Bohemian Massif. *Journal of Structural Geology*, **28**, 1553–1567.
- VERNER, K., ŽÁK, J., NAHODILOVÁ, R. & HOLUB, F. 2008. Magmatic fabrics and emplacement of the cone-sheet-bearing Knížecí Stolec durbachitic pluton (Moldanubian Unit, Bohemian Massif): implications for mid-crustal reworking of granulitic lower crust in the Central European Variscides. *International Journal of Earth Sciences*, **97**, 19–33.
- VERNER, K., BURIÁNEK, D., VRÁNA, S., VONDROVIC, L., PERTOLDOVÁ, J., HANŽL, P. & NAHODILOVÁ, R. 2009a. Tectonometamorphic features of geological units along the northern periphery of the Moldanubian Zone. *Journal of Geosciences*, **54**, 87–100.
- VERNER, K., ŽÁK, J., PERTOLDOVÁ, J., ŠRÁMEK, J., SEDLÁK, J., TRUBAČ, J. & TÝCOVÁ, P. 2009b. Magmatic history and geophysical signature of a post-collisional intrusive center emplaced near a crustal-scale shear zone: the Plechý granite pluton (Moldanubian batholith, Bohemian Massif). *International Journal of Earth Sciences*, **98**, 517–532.
- VERNER, K., ŽÁK, J. ET AL. 2014. Formation of elongated granite–migmatite domes as isostatic accommodation structures in collisional orogens. *Journal of Geodynamics*, **73**, 100–117.
- VONDROVIC, L. & VERNER, K. 2008. The record of structural evolution and U–Pb zircon dating of the tonalite intrusions (Polička Crystalline Unit, Bohemian Massif). In: POBLET, J., MEDINA, M. G., PEDREIRA, D. & FERNÁNDEZ, C. L. (eds) *International Meeting of Young Researchers in Structural Geology and Tectonics – Programme and Extended Abstracts*. University of Oviedo, Spain, 369–373.
- VONDROVIC, L. & VERNER, K. 2010. The record of structural evolution and U–Pb zircon dating of the tonalite intrusions (Polička Crystalline Unit, Bohemian Massif). *Trabajos de Geología*, **30**, 316–321.
- VONDROVIC, L., VERNER, K., BURIÁNEK, D., HALODOVÁ, P., KACHLÍK, V. & MÍKOVÁ, J. 2011. Emplacement, structural and P–T evolution of the ~346 Ma Miřetín Pluton (eastern Teplá–Barrandian Zone, Bohemian Massif): implications for regional tectonopressional tectonics. *Journal of Geosciences*, **56**, 343–357.
- VON QUADT, A. & FINGER, F. 1991. Geochronologische Untersuchungen im österreichischen Teil des Südböhmischen Batholiths: U–Pb Datierungen an Zirkonen, Monaziten und Xenotimen des Weinsberger Granits. *Beihefte European Journal of Mineralogy*, **1**, 281.
- VON RAUMER, J. F. & STAMPFLI, G. M. 2008. The birth of the Rheic Ocean – Early Palaeozoic subsidence patterns and subsequent tectonic plate scenarios. *Tectonophysics*, **461**, 9–20.
- VON RAUMER, J. F., FINGER, F., VESELÁ, P. & STAMPFLI, G. M. 2013. Durbachites–vaugnerites – a geodynamic marker in the central European Variscan orogen. *Terra Nova*, <http://dx.doi.org/10.1111/ter.12071>
- VRÁNA, S. & FRÝDA, J. 2003. Ultrahigh-pressure grossular-rich garnetite from the Moldanubian Zone, Czech Republic. *European Journal of Mineralogy*, **15**, 43–54.
- VRÁNA, S. & NOVÁK, M. 2000. Petrology and geochemistry of granulite clasts in the Visean Luleč conglomerate, Kulm in central Moravia, Czech Republic. *Bulletin of the Czech Geological Survey*, **75**, 405–413.
- VRÁNA, S., BLÜMEL, P. & PETRAKAKIS, K. 1995. Moldanubian Zone – metamorphic evolution. In: DALLMEYER, R. D., FRANKE, W. & WEBER, K. (eds) *Pre-Permian Geology of Central and Eastern Europe*. Springer, Berlin, 453–468.
- WALDHAUSROVÁ, J. 1984. Proterozoic volcanics and intrusive rocks of the Jílové Zone (Central Bohemia). *Krytalinikum*, **17**, 77–97.
- WENDT, I., LENZ, H. & DELISLE, G. 1986. Gesamtgesteins- und Mineraldatierungen des Falkenberger Granits. *Geologisches Jahrbuch*, **E34**, 1–85.
- WENDT, J. I., KRÖNER, A., FIALA, J. & TODT, W. 1993. Evidence from zircon dating for existence of approximately 2.1 Ga old crystalline basement in southern Bohemia, Czech Republic. *Geologische Rundschau*, **82**, 42–50.
- WENDT, J. I., KRÖNER, A., FIALA, J. & TODT, W. 1994. U–Pb zircon and Sm–Nd dating of Moldanubian HP/HT granulites from south Bohemia, Czech Republic. *Journal of the Geological Society, London*, **151**, 83–90.
- WENZEL, T., HENGST, M. & PILOT, J. 1993. The plutonic rocks of the Elbe Valley-Zone (Germany): evidence for the magmatic development from single-zircon evaporation and K–Ar age determinations. *Chemical Geology*, **104**, 75–92.
- WENZEL, T., MERTZ, D. F., OBERHÄNSLI, R., BECKER, T. & RENNE, P. R. 1997. Age, geodynamic setting, and mantle enrichment processes of a K-rich intrusion from the Meissen Massif (northern Bohemian Massif) and implications for related occurrences from the mid-European Hercynian. *Geologische Rundschau*, **86**, 556–570.
- WILLNER, A. P., RÖTZLER, K. & MARESC, W. V. 1997. Pressure–temperature and fluid evolution of quartzofeldspathic metamorphic rocks with a relic high-pressure, granulite-facies history from the central Erzgebirge (Saxony, Germany). *Journal of Petrology*, **38**, 307–336.
- WILLNER, A. P., SEBZUNGU, E., GERYA, T. V., MARESC, W. V. & KROHE, A. 2002. Numerical modelling of PT-paths related to rapid exhumation of high-pressure rocks from the crustal root in the Variscan Erzgebirge Dome (Saxony/Germany). *Journal of Geodynamics*, **33**, 281–314.
- WINCHESTER, J. A. 2002. Palaeozoic amalgamation of Central Europe: new results from recent geological and geophysical investigations. *Tectonophysics*, **360**, 5–21.
- WINCHESTER, J. A., PHARAOH, T. C., VERNIERS, J., IOANE, D. & SEGHEDI, A. 2006. Palaeozoic accretion of Gondwana-derived terranes to the East European Craton: recognition of detached terrane fragments dispersed after collision with promontories. In: GEE, D. G. & STEPHENSON, R. A. (eds) *European Lithosphere Dynamics*. Geological Society, London, Memoirs, **32**, 232–332.
- ŽÁČKOVÁ, E., KONOPÁSEK, J., JEŘÁBEK, P., FINGER, F. & KOŠLER, J. 2010. Early Carboniferous blueschist facies metamorphism in metapelites of the West Sudetes (Northern Saxothuringian Domain,

- Bohemian Massif). *Journal of Metamorphic Geology*, **28**, 361–379.
- ŽÁK, J., HOLUB, F. V. & VERNER, K. 2005a. Tectonic evolution of a continental magmatic arc from transpression in the upper crust to exhumation of mid-crustal orogenic root recorded by episodically emplaced plutons: the Central Bohemian Plutonic Complex (Bohemian Massif). *International Journal of Earth Sciences*, **94**, 385–400.
- ŽÁK, J., SCHULMANN, K. & HROUDA, F. 2005b. Multiple magmatic fabrics in the Sázava pluton (Bohemian Massif, Czech Republic): a result of superposition of wrench-dominated regional transpression on final emplacement. *Journal of Structural Geology*, **27**, 805–822.
- ŽÁK, J., DRAGON, F., VERNER, K., CHLUPÁČOVÁ, M., HOLUB, F. V. & KACHLÍK, V. 2009a. Forearc deformation and strain partitioning during growth of a continental magmatic arc: the northwestern margin of the Central Bohemian Plutonic Complex, Bohemian Massif. *Tectonophysics*, **469**, 93–111.
- ŽÁK, J., VERNER, K., KLOMÍNSKÝ, J. & CHLUPÁČOVÁ, M. 2009b. 'Granite tectonics' revisited: insights from comparison of K-feldspar shape-fabric, anisotropy of magnetic susceptibility (AMS), and brittle fractures in the Jizera granite, Bohemian Massif. *International Journal of Earth Sciences*, **98**, 949–967.
- ŽÁK, J., KRATINOVÁ, Z., TRUBAČ, J., JANOUŠEK, V., SLÁMA, J. & MRLINA, J. 2011a. Structure, emplacement, and tectonic setting of Late Devonian granitoid plutons in the Teplá–Barrandian unit, Bohemian Massif. *International Journal of Earth Sciences*, **100**, 1477–1495.
- ŽÁK, J., VERNER, K., FINGER, F., FARYAD, S. W., CHLUPÁČOVÁ, M. & VESELOVSKÝ, F. 2011b. The generation of voluminous S-type granites in the Moldanubian Unit, Bohemian Massif, by rapid isothermal exhumation of the metapelitic middle crust. *Lithos*, **121**, 25–40.
- ŽÁK, J., VERNER, K., HOLUB, F. V., KABELE, P., CHLUPÁČOVÁ, M. & HALODOVÁ, P. 2012. Magmatic to solid state fabrics in syntectonic granitoids recording early Carboniferous orogenic collapse in the Bohemian Massif. *Journal of Structural Geology*, **36**, 27–42.
- ŽÁK, J., VERNER, K., SLÁMA, J., KACHLÍK, V. & CHLUPÁČOVÁ, M. 2013. Multistage magma emplacement and progressive strain accumulation in the shallow-level Krkonoše–Jizera plutonic complex, Bohemian Massif. *Tectonics*, **32**, 1493–1512.
- ŽELAŽNIEWICZ, A. 1997. The Sudetes as a Palaeozoic orogen in central Europe. *Geological Magazine*, **134**, 691–702.
- ZULAUF, G. 1994. Ductile normal faulting along the West Bohemian Shear Zone (Moldanubian/Teplá–Barrandian boundary): evidence for late Variscan extensional collapse in the Variscan Internides. *Geologische Rundschau*, **83**, 276–292.
- ZULAUF, G. 1997a. Constriction due to subduction: evidence for slab pull in the Mariánské Lázně Complex (central European Variscides). *Terra Nova*, **9**, 232–236.
- ZULAUF, G. 1997b. From very low-grade to eclogite-facies metamorphism: tilted crustal sections as a consequence of Cadomian and Variscan orogeny in the Teplá–Barrandian unit (Bohemian Massif). *Geotektonische Forschungen*, **89**, 1–302.
- ZULAUF, G., BUES, C., DÖRR, W. & VEJNAR, Z. 2002. 10 km minimum throw along the West Bohemian shear zone: evidence for dramatic crustal thickening and high topography in the Bohemian Massif (European Variscides). *International Journal of Earth Sciences*, **91**, 850–864.